GLACIER FLUCTUATIONS

GLOBAL TEMPERATURE AND SEA-LEVEL CHANGE

Paul Willem Leclercq

Beoordelingscommissie: Prof. dr. M.R. van den Broeke
Prof. dr. W. Haeberli
Prof. dr. B.J.J.M. van den Hurk
Prof. dr. C. Schneider

ISBN: 978-90-393-5717-0
printing: Ipskamp

Institute for Marine and Atmospheric research Utrecht (IMAU)
Department of Physics and Astronomy
Faculty of Science
Universiteit Utrecht

Financial support was provided by the Netherlands Organisation for Scientific Research NWO through research grant 816.01.016.

Cover: false colour Landsat image of Sukkertoppen, West Greenland. Courtesy of USGS.

GLACIER FLUCTUATIONS

GLOBAL TEMPERATURE AND SEA-LEVEL CHANGE

GLETSJER FLUCTUATIES,
MONDIALE TEMPERATUUR EN ZEESPIEGEL VERANDERING
(met een samenvatting in het Nederlands)

PROEFSCHRIFT

ter verkrijging van de graad van doctor aan de
Universiteit Utrecht op gezag van de rector magnificus,
prof. dr. G.J. van der Zwaan, ingevolge het besluit van
het college voor promoties in het openbaar te
verdedigen op woensdag 8 februari 2012 des middags
te 12.45 uur

door

Paul Willem Leclercq

geboren op 17 juli 1979 te Tilburg

Promotor: Prof. dr. J. Oerlemans

Contents

Summary

The current world-wide glacier retreat is a clear sign of global warming. In addition, glaciers contribute to sea-level rise as a consequence of the current retreat. In this thesis we use records of past glacier fluctuations to reconstruct past climate variations and the glacier contribution to sea-level change.

Firstly, a coherent data set of world-wide glacier fluctuations over the past centuries is compiled. Most available information of glacier fluctuations concerns fluctuations in glacier length. There is currently a large number of sources available, varying from field observations, satellite images and aerial photography to reconstructions from historical documents and geological evidence. The data set, resulting from the compilation of available data, contains 374 length records of glaciers from all continents. All records start before 1950 and the longest record has its first data point in 1534. The data set is described in Chapter 2.

In Chapter 3, a climatic interpretation of the length fluctuations of Glaciar Frías is presented. This glacier in North Patagonia has the longest detailed length record in southern South America. Analysis of the Glaciar Frías fluctuations can provide insight in the fluctuations of North Patagonian climate. The glacier behaviour is modelled with a simplified mass balance model that is coupled with a flow line model. A warming of North Patagonian climate with 1.16 °C since the mid 17th century, or a decrease in precipitation of 34%, would best explain the observed retreat since 1639. In addition, the glacier model is forced with existing climate reconstructions. It appears that the length fluctuations are mainly driven by variations in temperature rather than variations in precipitation. The modelled glacier lengths serve as a test for the climate reconstructions. The translation in glacier length shows that the uncertainties in the reconstructions are rather large.

The development of such detailed models is not feasible for all glaciers in the length fluctuations data set. In the next chapter a simplified approach is used to reconstruct global and hemispheric temperature for the period 1600–2000 from world-wide glacier length fluctuations. The reconstructions show that global temperature was more or less constant from 1600 until the middle of the 19th century. Since then, temperature rises until 2000, with a period of slight cooling from 1940 to 1970. Glacier-based reconstructions are completely independent from both other proxy-based reconstructions and the instrumental record. Still, the reconstructed temperature agrees well with the instrumental record of the 20th century and it is in broad agreement with existing temperature reconstructions. However, according to the glacier length reconstruction the global warming starts in the middle of the 19th century instead of in the beginning of the 20th century, as indicated by several other reconstructions.

The data set of glacier length changes can also be used to estimate the glacier contribution to sea-level change. In Chapter 5, a global glacier length signal is calculated from the available glacier length records. The global length signal is scaled to global volume change, which is calibrated on mass balance and geodetic observations of the period 1950–2005. The reconstructed glacier contribution is 8.4 ± 2.1 cm for the period 1800–2005 and 9.1 ± 2.3 cm for the period 1850–2005. These estimates are significantly higher than earlier estimates. Glacier retreat accounts for half the observed sea-level rise since the middle of the 19$^{\text{th}}$ century.

Due to the dynamic response of glaciers to changes in the climatic forcing, the conventional surface mass balance is not a good indicator of climate variations on time scales of the glacier response time. Instead, the reference-surface mass balance should be used to account for the changes in glacier geometry. In the last chapter, a first-order estimate is made of the difference between the conventional mass balance and the reference-surface mass balance in the specific case of twelve Swiss glaciers for the period 1908–2008. To obtain this estimate we made use of the observed length fluctuations.

Knowledge of historical glacier length fluctuations provides insight in the interaction between glaciers and climate. Moreover, the compilation of world-wide data set of glacier length records provides a means to reconstruct the climatic fluctuations over the last four centuries independently from other reconstructions. This reconstruction confirms that the current global warming of 0.94 °C since the middle of the 19$^{\text{th}}$ is exceptional in the last four centuries at least. With the glacier length records it also is possible to estimate the glacier contribution to sea-level since the beginning of the 19$^{\text{th}}$ century, extending the record based on direct observations of glacier volume.

1

Introduction and conclusions

Glaciers have retreated world-wide over the last century, and this retreat is continuing at present. The general retreat of glaciers is an evident sign of global warming. Observations of glacier fluctuations over the past centuries can be used to learn more about past climate, and, in addition, can help us to explain the sea-level rise observed over the last 200 years. World-wide observations of glacier length changes over the last four centuries are the topic of this thesis.

This thesis is a compilation of research articles included in Chapters 2–6. These articles can be read independently from each other. Chapter 2 presents a global data set of glacier length records, which is used in the subsequent chapters. In Chapter 3 and 4, the observed glacier length fluctuations are used for the reconstruction of North Patagonian and global climate over the last four centuries. In Chapter 5, an estimate of the glacier contribution to sea-level rise is given, again based on the glacier length changes. The last chapter explores the effect of changes in the glacier geometry on the glacier mass balance using glacier length changes.

This first chapter introduces these topics. The first parts provide a general introduction to climate reconstructions and the main glaciological processes. In the following sections, the topics of the next chapters are introduced with some background information, and a summary of the main results and conclusions is presented along with an outlook for future research.

1.1 Reconstructing climate of the past

Knowledge of past climate variations is one of the keys to the understanding of the climate system. As our climate is not a repeatable experiment, knowledge of the past is needed to validate climate models. The record of past climate should preferably cover a long period, such that many different types of the (global) climate variations are included. A larger range in observed states of the climate improves the testing of climate models, which are calibrated on measurements of the present climate. Validation of models outside the range given by the present climate is of particular importance for models that are used in projections of future climate. In the near future, the climate is expected to have a very different forcing due to the projected enhanced greenhouse effect. Furthermore, the climate system incorporates many slow processes. The modelling of these processes can only be tested if the record used for validation is of considerable length.

However, the period of measurements is rather short. The instrumental temperature record is the longest and starts around the middle of the 19th century. Before this period, there is no global coverage of the instrumental record, although some longer records of observations exist, mainly in Europe [e.g. *Auer et al.*, 2007]. Fortunately, it is very well possible to reconstruct past climate fluctuations. Variations in climate have an impact on a many processes on Earth, like the growing and dissemination of organisms, erosion and sediment transport, and changes in the cryosphere. Some of these processes act as natural archives, logging the impact of climatic change. The most frequently used natural archives are tree ring chronologies; the ring width and wood density are a proxy for variations in temperature or precipitation. But many other biological proxies exist (e.g. pollen, corals), as well as physical proxies (such as the chemical composition of ice, varved lake sediments, ground temperature), and historical sources (harvest dates and other documentary evidence of climatic change), each having its own advantages and disadvantages.

Over recent decades, much progress has been made and an increasing amount of records of past climate has become available [*Jansen et al.*, 2007]. As an example, a compilation of several reconstructions of Northern Hemisphere temperature over the last 1300 years is shown in Figure 1.1. The proxy-based ensemble shows that it is very likely that the recent decades were the warmest in the past millennium. Most of these reconstructions make use of several different proxies and except for *Oerlemans* [2005] and *Pollack and Smerdon* [2004] all reconstructions include tree-ring data.

There are several problems to overcome when making climate reconstructions from indirect evidence. Most proxies are not dependent on just one climate parameter (e.g. temperature or precipitation), and the proxy signal has to be disentangled. Furthermore, many proxies are only part of the year sensitive to fluctuations of the climate parameters, or in some seasons more than in others. The spatial coverage is limited for most of the proxies. For example, it is only possible to drill ice cores on the ice sheets and on a limited number of high-altitude glacier basins [e.g. *Thompson et al.*, 2003]. The Southern Hemisphere and in particular the

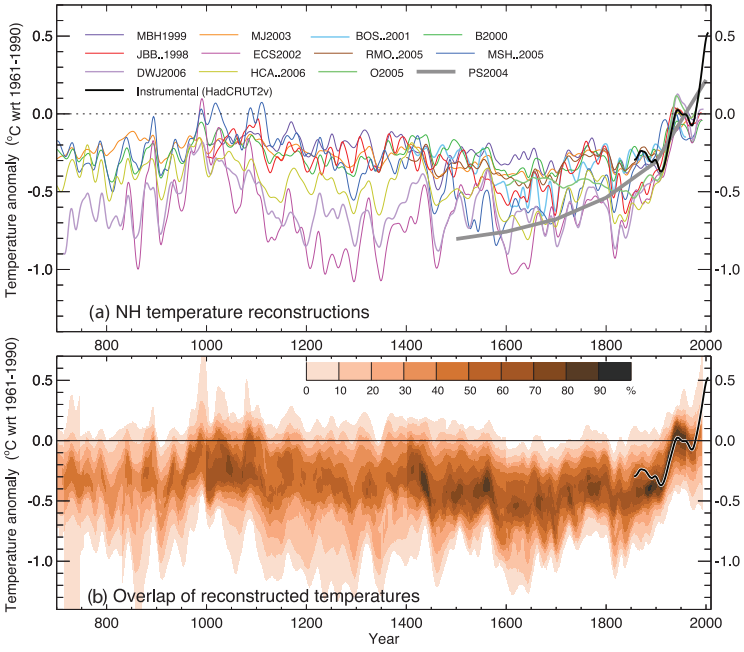

Figure 1.1: *NH temperature records, smoothed with a 30 year Gaussian filter.* ***a)*** *Reconstructions using multiple climate proxy records [Jones et al., 1998; Mann and Bradley, 1999; Briffa, 2000; Briffa et al., 2001; Esper et al., 2002; Mann and Jones, 2003; Pollack and Smerdon, 2004; Rutherford et al., 2005; Moberg et al., 2005; Oerlemans, 2005; D' Arrigo et al., 2006; Hegerl et al., 2006].* ***b)*** *Overlap of the published multi-decadal time scale uncertainty ranges of all temperature reconstructions shown above, indicating the probability of past temperatures. In both Figures, the instrumental HadCRUT2v record is shown in black. Figure taken from Jansen et al. [2007].*

tropics are poorly covered by proxies. To conclude, for most of the above mentioned proxies the provided information is not directly transferable into quantitative variations in the connected climate parameter. There exists, for instance, no theory that directly relates the thickness of a tree ring in a specific year to the temperature of that year. Instead, an index is derived from the proxy observations. Subsequently, this index is correlated with the observed climate variable to find a transfer function. The transfer function is applied to the proxy index in the period before the instrumental record. This method requires a substantial period of overlap between the proxy record and a reliable instrumental record, and that the relation between the climate parameter and the proxy evidence remains constant in time. Most of the differences between the reconstructions in Figure 1.1a are caused by different choices in the procedure of calibration to the instrumental record [*Jansen et al.*, 2007].

The uncertainties are different for the different proxies. Therefore, it is desirable to use as many independent proxies as possible, in order to reduce the combined uncertainty (Figure

1.1b). From this perspective it is useful to explore the potentials of observed glacier length fluctuations. Glacier fluctuations are an attractive proxy for the study of past climatic change. Glaciers convert the climate variations into large and therefore easily observable length fluctuations. The glacier length fluctuations have a direct link with climate variations through the surface mass balance, as will be discussed in Section 1.2. Therefore, they are considered to be good climate indicators. Glacier fluctuations are a physical proxy: the relation between climate and length fluctuations can be calculated quantitatively from glacier models. The results do not have to be calibrated on measured climate, and thus the instrumental record can be used as independent validation. The glacier records can also complement the early instrumental record (and other reconstructions) as glaciers are in general on higher altitudes than observations, and often located in remote areas were meteorological observations are sparse. And, to conclude, glacier length changes are completely independent of other proxies.

Before we proceed with the climate reconstructions presented in this thesis, the most important glaciological processes are described briefly in the next Section, and the available information on glacier fluctuations is discussed in Section 1.3.

1.2 Glaciers

1.2.1 Global distribution of glaciers

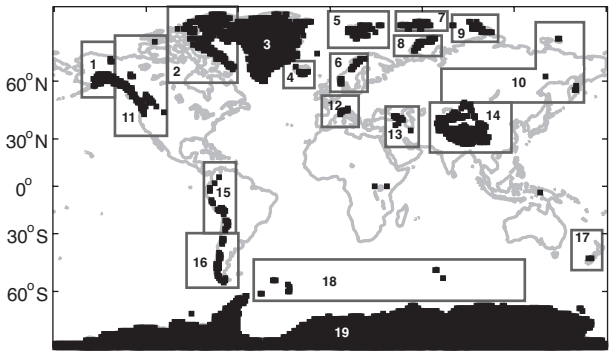

Figure 1.2: *Global distribution of ice covered area. The black dots depict the 1°x1° grid cells that contain ice covered area. Data originate from Cogley [2003]. The boxes indicate the regions as defined by Radić and Hock [2010], for which the area covered by glaciers and ice caps is given in Figure 1.3.*

Almost 10% of the world's land surface is covered by ice [*Paterson*, 1994]. Most of the world's ice can be found at high latitudes in the Arctic and Antarctic regions (Figure 1.2). In addition, ice is found along high mountain ranges, such as the Andes, the Himalayas, the Rocky Mountains, and the Coastal Mountains of North West America. Of all the ice mass

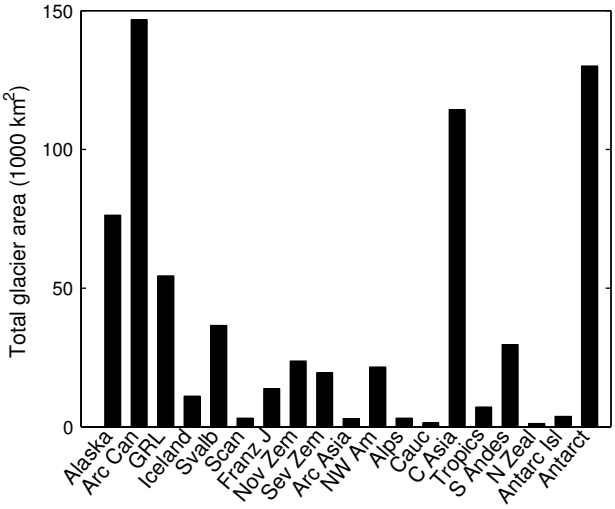

Figure 1.3: *Area covered by glaciers and ice caps. The global glacier area is divided into 19 regions (see Figure 1.2), Only ice that is not part of the ice sheets of Greenland and Antarctica is included. Data originate from Radić and Hock [2010] except for the area of local glaciers on Antarctica, where the estimate of Hock et al. [2009] is followed.*

presently on Earth, more than 99% of the volume is stored in the ice sheets of Antarctica and Greenland. Less than 1% of the global ice volume is distributed over the more than 200,000 glaciers and ice caps. The area of these glaciers and ice caps, which constitute all ice bodies not part of the two ice sheets (and hereafter referred to as glaciers), is estimated to be 700,000 – 760,000 km^2 [*Cogley*, 2003; *Hock et al.*, 2009; *Radić and Hock*, 2010]. Most of the glacier area is located in the polar regions and the Canadian Arctic is the region with the largest glacier cover (Figure 1.3). Glaciers in alpine mountain ranges such as the Alps, the Causasus and Scandinavia represent only a small portion of the global glacier area. Still, glaciers can be found at virtually all latitudes and at all continents. There are numerous glaciers in the mid-latitudes, in both hemispheres. Also in the tropics glaciers can be found, as for instance in the tropical parts of Central Asia, the region with the third largest glacierised area. In central Africa and Indonesia there are a few small tropical glaciers. These are not displayed in Figure 1.3. Because their area is so small, they are not included in the dataset of *Radić and Hock* [2010].

1.2.2 Glaciers and climate

Glaciers and ice caps are located in those places where the annual amount of snowfall exceeds the amount of annual snow melt. The accumulated snow transforms into ice under its own

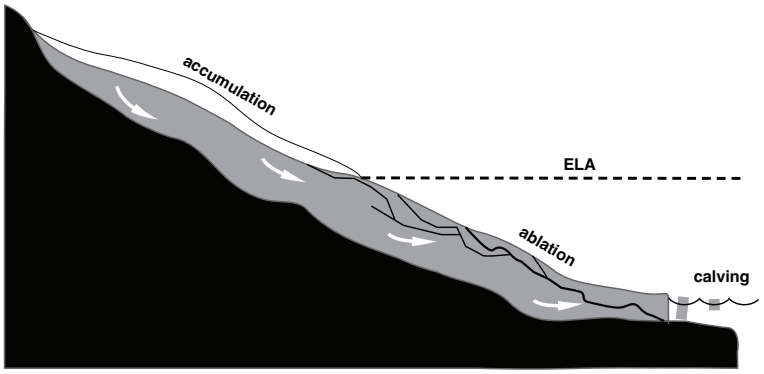

Figure 1.4: *Schematic picture of a glacier. Indicated are the bed (black) on which ice (grey) flows downward (white arrows). The equilibrium line altitude (ELA) is indicated by a dashed line, above which there is net accumulation of snow (white) and below which there is ablation in the form of surface melt and iceberg calving at the terminus.*

weight, a process that can take years to decades depending on the temperature of the snow [*Ligtenberg et al.*, 2011, and references therein]. Forced by gravity, ice flows downslope, where eventually melt exceeds the amount of snowfall and ice is lost (Figure 1.4). Meltwater penetrates through the glacier to the glacier bed via crevasses and moulins. It then finds its way towards the glacier terminus along the glacier bed through a system of cavities and channels in the ice. The area where the annual snowfall exceeds the melt and the glaciers gains mass, is called the accumulation area. The region where the melt exceeds snowfall and ice is lost is called ablation area. The altitude of the transition between the accumulation area and the ablation area is called the equilibrium line altitude (ELA). At the ELA annual melt equals annual snowfall and the net mass gain is zero. When the amount of melt below the ELA cannot compensate for the amount of accumulation upstream before the flow of ice reaches a water body, either a lake or the sea, ice breaks off in the form of icebergs, a process called calving.

In the case of mountain glaciers, the transition from accumulation to ablation area is governed by altitude, because, in general, temperature decreases with increasing altitude. Snow accumulates higher up the mountain and ice flows downward, where higher teperatures will melt the ice. For the much larger ice sheets, also latitude can play a role; the ice flows from the cold high latitudes near the poles towards the equator. From here on we will focus on mountain glaciers and ice caps, the topic of this thesis.

In a constant climate, which implies a constant ELA, a balance will establish between the amount of snow accumulation in the accumulation area and the amount of ice loss in the ablation area. The glacier will then have a constant geometry, while the glacier ice is flowing and thus transports mass from the accumulation area to the ablation area. However, in reality

climate is never constant. The ELA fluctuates, and glaciers respond to the climate changes by advancing and retreating. In periods in which a glacier gains mass, through reduced melt or increased snowfall, this surplus of mass makes the glacier grow. As ice flows downward, the increased glacier extent mainly increases the ablation area. Hence, the total ablation increases and the glacier reaches an equilibrium with the new climate. In the case of mass loss (higher ablation or less snowfall), the opposite occurs. The loss of ice is highest at the terminus of the glacier where the ablation is highest. The glacier tongue melts away and the glacier retreats upslope, which decreases the ablation area and therefore the total ablation. Because the response takes time, the adjustment of the glacier geometry lags the changes in climate. In general, glaciers are in imbalance with the current climate.

The change in glacier geometry as response to a change in climate is described by the *climate sensitivity* and the *response time* of the glacier. The climate sensitivity is defined as the difference in geometry (e.g. length or volume) between two equilibrium states before and after a perturbation in climate, divided by the magnitude of the perturbation. This geometrical adjustment takes time, determined by the response time of the glacier in question. The response time is defined as an e-folding response time: the time needed to reach $(1-e^{-1})$ of the final adjustment after a stepwise perturbation of a glacier in equilibrium. Both the response time and the climate sensitivity are dependent of the glacier geometry and the local climate (see Section 1.2.6).

Most mountain glaciers and the outlet glaciers of ice caps have a well-defined direction of flow, confined by valley walls. Therefore, the changes in geometry can be well represented by the change in glacier length. For changes in length that are small in relation to the total glacier length, the change of the glacier length ΔL as a response to climate change can be described by a linear first-order differential equation [e.g. *Oerlemans*, 2007]. When the climate change is represented by a shift in the equilibrium line altitude ΔELA, the rate of glacier length change is given by:

$$\frac{\partial L}{\partial t} = \frac{1}{\tau}\left(c_L \Delta ELA - \Delta L\right) \tag{1.1}$$

where the constants τ and c_L are the response time and the climate sensitivity ($c_L < 0$), respectively. Starting from an equilibrium state, the rate of length change is at a maximum directly after the change in climate, and then declines when the length change ΔL compensates for the climatic imbalance, with a time-scale determined by the response time. Eventually, when the length change ΔL reaches the new equilibrium value $c_L \Delta ELA$, the rate of length change is zero. However, the converse is in general not true: in a continuously varying climate the glacier is not necessarily in equilibrium when the terminus position is stable, i.e. when $\frac{\partial L}{\partial t} = 0$.

Figure 1.5: ***a)*** *Accumulation measurements in a snowpit by Anders Sirevaag on Hardangerjøkulen, Norway. The holes in the side of the snowpit result from snow density measurements. Photo by Carita Knudsen.* ***b)*** *Ablation measurement with a stake drilled in the ice at the tongue of Sulztalferner, Austria. Photo by Marc Olefs.*

1.2.3 Glacier mass balance

The mass balance of a glacier is the net mass gain (or mass loss when the balance is negative) of the glacier over a defined period. It is determined by the sum of all processes that add mass to, and remove mass from, the glacier. In practice, the accumulation and ablation at the glacier surface, and the ablation through calving, are the most relevant contributors to the glacier mass balance. The mass change induced at the glacier surface, the surface mass balance, is the direct link between climate and the glacier mass budget. The calving rate is mainly a function of water depth at the glacier terminus [*Pelto and Warren*, 1991; *van der Veen*, 1996]. Hence, the bed topography is the primary agent in the ablation through calving after small perturbations in the terminus position [*Vieli and Nick*, 2011]. As we are interested in the climatic response of glaciers, we will focus on the surface mass balance.

Mostly, the mass balance is measured and calculated for one hydrological year, running from the beginning of the accumulation season until the end of the ablation season. At any point on a glacier surface, the surface mass balance is the annual sum of the amount of solid precipitation (snow), refrozen meltwater and rain, minus sublimation and melt. For most glaciers, solid precipitation and melt are the most important components [*Oerlemans et al.*, 1999;

Greuell and Smeets, 2001]. The amount of solid precipitation is determined by the amount of precipitation and the temperature at which this precipitation falls. The amount of melt is determined by the surface energy balance, which is treated in the next Section.

Glacier surface mass balance is measured with several methods. Accumulation is mostly measured by digging snow pits at the end of the accumulation season (Figure 1.5a). From the snow pit the depth and the density of the accumulated snow can be measured. Stakes are drilled into the ice to measure the ablation. The loss of ice volume is measured by the difference in stake height above the surface between beginning and end of the year (Figure 1.5b). These basic methods give the change in mass, but the temporal resolution is low and they do not give insight in the contributions of the different fluxes of the surface energy balance. More advanced measurements involve the use of weather stations, preferably automatic such that year-round operation is feasible [*Oerlemans and Knap*, 1998]. By measuring incoming and reflected solar radiation, incoming and outgoing longwave radiation, temperature, and windspeed, the complete energy budget can be calculated (see next Section). In addition, the change in surface altitude can be measured almost continuously with a sonic ranger mounted on a stake.

The first mass balance measurements were point measurements, and started around the beginning of the 20th century in Switzerland [*Huss et al.*, 2008]. Starting in 1946, Störglaciären in Sweden has been the first glacier where the mass balance was measured for the entire glacier. Since then, the mass balance of 226 glaciers has been measured for at least one year. The number of long mass balance records is small. Only 30 records have continuous measurements since 1976 [*WGMS*, 2008]. When the mass balance of a glacier is measured over several years, the average mass balance profile, i.e. the average annual balance as a function of height, can be determined. In Figure 1.6, the mass balance profiles of 8 glaciers are shown. The profiles are different, as the glaciers are not in the same climate, but some similarities are evident. Below the ELA, the balance gradient is approximately constant, which means that the mass balance profile is a linear function of altitude. For some glaciers this also holds above ELA, but often the balance gradient is decreasing with altitude above the ELA. Normally, precipitation increases with altitude, but for many glaciers accumulation in the upper regions is limited by snow drift.

1.2.4 Surface energy balance

The melt of snow and ice is governed by the surface energy balance. The surface energy balance is the sum of the energy fluxes between the glacier surface, the atmosphere above, and the snow and ice layers below the surface. An imbalance in the energy budget affects the temperature of the glacier surface. If the glacier surface is at the melting point (0 °C), excess of heat transferred towards the glacier surface results in the melt of ice or snow. On mountain glaciers, the most important components of the energy balance are incoming (S_{in})

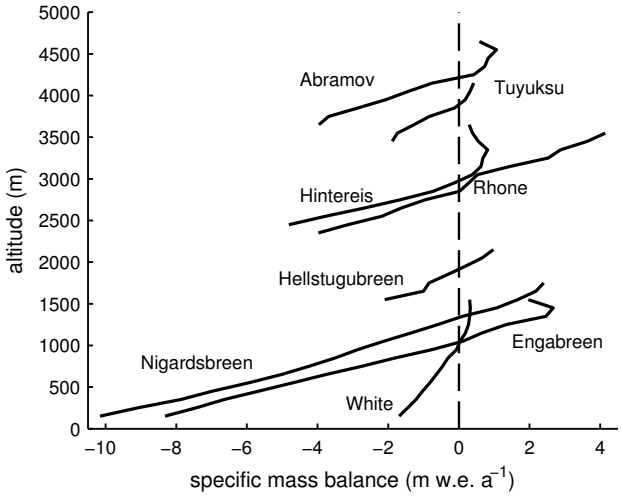

Figure 1.6: *Multi-year averaged observed profile of the annual mass balance for 8 glaciers in different climates. Data source: WGMS.*

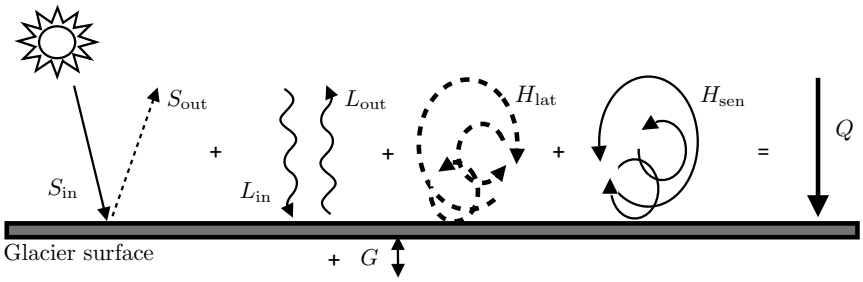

Figure 1.7: *Schematic picture of the surface energy components, symbols are explained in the text. Q is the sum of all components, and is positive when heat is transported towards the glacier surface.*

and reflected (S_{out}) solar radiation, incoming (L_{in}) and outgoing (L_{out}) long wave radiation, sensible heat flux (H_{sen}), latent heat flux (H_{lat}), and the subsurface heat flux (G) (Figure 1.7).

The incoming solar radiation S_{in} has a daily cycle, and varies with the time of year, depending of the latitude of the glacier. Part of the solar radiation that comes in at the top of the atmosphere is absorbed or reflected by the atmosphere, e.g. by clouds and aerosols. Furthermore, the exposure (slope and orientation) of the glacier surface to the sun influences the intensity of the incoming radiation: a steep north facing glacier receives far less sun than a glacier orientated towards the south (on the Northern Hemisphere, on the Southern Hemisphere it is the

opposite). Part of the incoming solar radiation is reflected by the glacier surface. The fraction of the incoming solar radiation that is reflected by the surface is called the albedo. The albedo of a glacier surface has a large range: freshly fallen snow has an albedo of 0.90, whereas the albedo of glacier ice can go down to 0.25. This means that the reflected solar radiation (S_{out}) can vary from 25 to 90% of S_{in}. We will see later that this has large consequences for the climate sensitivity of glaciers.

The emitted longwave radiation is determined by the temperature. The temperature of the glacier surface cannot exceed the melting point and thus the emitted longwave radiation has an upper bound. Still, the annual mean longwave budget is negative, i.e. the glacier surface is cooled by the net longwave radiation, because snow and ice are effective radiators in this part of the spectrum [e.g. *Brock et al.*, 2007; *Giesen et al.*, 2008]. Only during warm and cloudy days, the longwave radiation flux is zero or positive.

The sensible and latent heat fluxes do not exchange heat between the atmosphere and the glacier surface by radiation, but by turbulence. They depend on temperature differences and wind speed. The sensible heat flux transports heat to the surface when the air above it is warmer, and away from the surface when the atmosphere is cooler. The latent heat flux transports heat by transporting water vapour. Where the water vapour condenses, heat is released. As both fluxes are turbulent, they increase with higher wind speeds.

To conclude, heat is exchanged between the surface and the underlying snow and ice. Directly, due to temperature differences between surface layer and the deeper layers, but also by the heat that is transported downward by percolating meltwater. If the sum of all these energy fluxes (Q) is positive, the glacier surface heats up. When the glacier surface is at melting point, positive Q is the energy that is used for melting snow or ice.

1.2.5 Feedbacks in the glacier response to climate change

There are a few interesting feedback mechanisms that enhance the response of glaciers to climate change. First, we will discuss the albedo feedback on melt. In a period of melt due to high temperatures or high incoming radiation, the albedo of snow decreases because the grain size of the snow increases [*Wiscombe and Warren*, 1980; *Kuipers Munneke et al.*, 2008]. When the albedo decreases, the absorbed fraction of S_{in} increases, which leads to more melt and a lower albedo. In a second albedo feedback for retreating glaciers, the albedo of the glacier tongue will lower due to the increased amount of dust on the ice surface. The glacier forefield and lateral moraines, ice free after the retreat, provide dust that is blown onto the glacier surface. In addition, the thinning of the glacier tongue leads to melt-out of dust, that subsequently accumulates on the surface. Due to the lower albedo, melt increases and the glacier retreat is accelerated [*Oerlemans et al.*, 2009].

Secondly, glacier thickness depends on glacier size, which leads to the mass balance-altitude feedback. When the mass balance is positive as a consequence of climatic change, the glacier

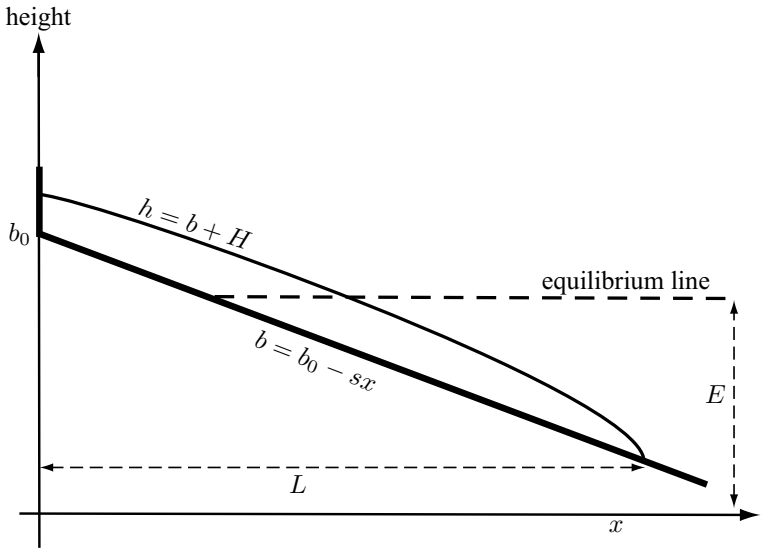

Figure 1.8: *Simple glacier with length L, constant width, on a bed with constant slope s ($s > 0$).*

advances and it also becomes thicker. Thus, the glacier surface is at a higher altitude, which again increases the mass balance. On the other hand, the surface of a retreating glacier will lower and thus melt will be enhanced, accelerating the retreat. For ice caps which have a large, but flat, accumulation area, this feedback can be very important. The surface lowering from a small climate perturbation can lead to an irreversible decay of the ice cap [e.g. *Giesen and Oerlemans*, 2010].

1.2.6 Glacier models

Simple glacier model

Glacier models have been developed to understand and describe the glaciological processes discussed above. The simplest glacier model describes a glacier with constant width on a bed with a constant slope (Figure 1.8), and a linear balance gradient [*Oerlemans*, 2001]. This is a crude simplification of the real geometry and balance gradient of the majority of glaciers, but this simple model will give several useful insights in the dynamics of glaciers, that will be used in Chapter 4.

Because of the constant slope, the height of the glacier bed can be described with:

$$b(x) = b_0 - sx \tag{1.2}$$

where x is the distance along the flow line, b_0 (m) is the height of the glacier bed at $x = 0$ and the slope s is positive. The balance rate $\dot{b}(x)$ (mass balance per unit of time) is given by:

$$\dot{b}(x) = \beta\,(h(x) - E) \tag{1.3}$$

where β (m w.e. $a^{-1}m^{-1}$) is the constant balance gradient, h (m) is the height of the glacier surface, the sum of the height of the bed $b(x)$ (m) and the thickness of the glacier $H(x)$ (m), and E (m) is short for ELA.

The mass balance of the glacier per unit of time is given by the balance rate integrated over the entire glacier surface. Because the glacier width is constant, this is just the integral of the balance rate over the glacier length, multiplied with the constant width. By conservation of mass, the mass balance must be zero in an equilibrium state of the glacier:

$$\int_0^L \dot{b}(x)dx = \int_0^L \beta\,(H(x) + b_0 - sx - E)\,dx = 0 \tag{1.4}$$

Solving for the length of the glacier gives the equilibrium length L_{eq} of the glacier in the climate characterised by the ELA:

$$L_{\text{eq}} = \frac{2\,(b_0 + H_m - E)}{s} \tag{1.5}$$

where H_m is the mean glacier thickness. The length of the glacier is therefore not only determined by the climate (the ELA) and the height of the mountain, but also by the slope of the bed and the mean glacier thickness. It is even possible to have a glacier in equilibrium with non-zero length when the ELA is higher than the highest point of the bed. The sensitivity of the glacier length to changes in the equilibrium line altitude is

$$\frac{dL}{dE} = -\frac{2}{s} \tag{1.6}$$

In this simple model, the sensitivity of glaciers to changes in climate is solely determined by the slope of the glacier bed. Under the assumption that the change in ELA is dependent on changes in the annual average temperature, the minimal glacier model gives the temperature sensitivity c_{T}

$$c_{\text{T}} \equiv \frac{dL}{dT} = -\frac{c_1}{s} \tag{1.7}$$

This result will be used in Chapter 4, where the constant c_1 is calibrated to the results of numerical models.

The simple model can not only be used to estimate the climate sensitivity of a glacier, it also provides an expression for the response time. Because the length response time is a measure for how fast a perturbation of the mass balance transfers down to the glacier tongue, a meaningful expression for the response time would depend on the glacier length L and a

characteristic ice velocity $\tilde{u}$ [*Oerlemans*, 2001]

$$\tau = c_\tau \frac{L}{\tilde{u}} \tag{1.8}$$

where c_τ is a dimensionless constant. The ice velocity at the equilibrium line is taken to be the characteristic ice velocity: $\tilde{u} = u_{ELA}$. The flux at the equilibrium line is the total mass turnover of the glacier: all accumulated ice flows from the accumulation area to the ablation area and passes the equilibrium line. For the simple glacier that has a constant width and a constant balance gradient, the equilibrium line is at $x = L/2$ if the glacier is in an equilibrium state. The flux at the equilibrium line is given by

$$H_{ELA} u_{ELA} = \int_0^{\frac{L}{2}} \beta \left(H(x) - sx + b_0 - E \right) dx \tag{1.9}$$

which gives

$$H_{ELA} u_{ELA} = \frac{\beta L}{2} \left(\bar{H}_{ACC} + b_0 - E - \frac{sL}{4} \right) \tag{1.10}$$

where $\bar{H}_{ACC}$ is the mean ice thickness of the accumulation area. Assuming that the mean thickness of the accumulation area equals the mean thickness of the whole glacier, we can use Eq. 1.5 to eliminate the mean ice thickness of the accumulation zone. The ice velocity at the equilibrium line is then given by

$$u_{ELA} = \frac{\beta s L^2}{8 H_{ELA}} \tag{1.11}$$

It is reasonable to assume that the ice thickness at the equilibrium line is proportional to the overall mean ice thickness $H_{ELA} = c_{\mathrm{H}} H_m$. To conclude, the relation between mean ice thickness, glacier slope and glacier length, $H_m = \sqrt{\frac{\mu L}{1+20s}}$ as was suggested by *Oerlemans* [2001] based on experiments with a numerical model, can be used to get an expression for the response time τ in terms of glacier length, slope, balance gradient only

$$\tau = c_2 \frac{1}{\beta s \sqrt{1+20s} \sqrt{L}} \tag{1.12}$$

This indicates that steep glaciers and glaciers with a large balance gradient have a short response time. It does not show that large glaciers react slowly to changes in climate. On the contrary, at first sight the length reduces the response time. However, because the glacier length is inversely proportional to the glacier slope (Eq. 1.5), the influence of the glacier length on the response time is very small.

These results from the simple model give useful insights in the basic properties of glaciers in relation to their response to changes in climate. Moreover, these relations for the response time and climate sensitivity require limited input data and can be applied to glaciers of which

the exact geometry is not known. This will prove to be of great benefit in the temperature reconstructions from glacier changes, described in Chapter 4.

More advanced models

To describe the behaviour of a specific glacier in detail, a model that combines the mass balance and the ice dynamics in more detail is a better tool than the simple model described above. Both the mass balance and the ice dynamics depend on the specific geometry of a glacier. For example, the effects of shading by the surrounding mountains and the orientation of the glacier surface influence the incoming solar radiation, and many glaciers have a wide accumulation area and a narrow tongue. These geometrical effects make the glacier longer, extending to lower elevations. Also the flow velocity and ice thickness are effected by variations in the bed slope and steepness of the valley walls. All these effects influence the reaction of glaciers to fluctuations in climate, but are not accounted for by the simple model.

In the ideal case, the constant balance gradient in the simple model is replaced by a mass balance model that calculates the different components of the energy flux explicitly for the entire glacier surface (Figure 1.7). However, the required meteorological input is often not available. This lack of input data has lead to the development of simplifications of the mass balance calculations. The methods vary from simplifications in description of some of the fluxes [e.g. *Machgut et al.*, 2006], to empirically derived relations between melt and temperature [see *Hock*, 2003, 2005, for an overview]. In order to capture the sensitivity of the mass balance to changes in precipitation and temperature correctly, the model should at least make a distinction between the energy received from solar radiation and the energy fluxes related to temperature. In this approach, it is important to capture the albedo well. Most of the energy for melt comes from solar radiation, but the albedo of the glacier surface reduces the absorbed radiation to 10 to 70% of the incoming radiation. Bare ice absorbs up to seven times more solar energy than freshly fallen snow.

The glacier motion consists of two parts: sliding of the glacier over its bed, and deformation of the ice. Sliding is a complex process, that is governed by the steepness of the bed, the ice load, and the friction at the base of the ice. It is difficult to make a good estimate of this friction. It depends on the water pressure, possible variations in the hydraulic system, and the rheology and structure of the bed. Sliding is not fully understood yet. The deformation of ice is the consequence of internal stresses. Gravity pulls down the ice, while the friction at the bed and at the sides of the glacier tend to keep the ice in place. By deforming, the ice minimizes the internal stresses. When despite deformation the internal stresses are too high, the material fails: the ice breaks and crevasses are formed. The calculation of the deformation velocity of ice is complicated by the non-linear rheology of ice. Although glacier models exist that completely solve the full set of deformation equations (so-called Full Stokes models), these are computationally expensive. In most glacier studies, assumptions are made that simplify the problem, like the shallow ice approximation (SIA). Furthermore, the spatial

Figure 1.9: *Repeat photography of Gaisbergferner, Austria: photographed in 1872 (left) and in 2009 (right). On the right photo, two frontal moraine ridges are visible in the glacier forefield. Source: J. Alean and M. Hambrey, Glaciers Online (www.swisseduc.ch/glaciers).*

dimension of the ice flow can be reduced to the main flow line of the glacier. This is reasonable in the study of the relation between climatic change and glaciers. The interest is not in small scale processes (e.g. crevassing, ice avalanches etc.) and period of interest typically covers a centennial period where the response is mainly determined by conservation of mass. Typically, the calculated mass balance has a much larger contribution to the uncertainties than the simplified description of ice dynamics.

1.3 Observed glacier length fluctuations

There is a wealth of information on historical length changes of glaciers over the world. Glaciers, especially the larger valley glaciers that descend into habitable area, have been noted for their beauty and their hazards (Figure 1.9). Furthermore, glaciers have a large eroding capacity that leaves prominent traces in the landscape, witnessed by many fjords and glacial valleys. The eroded material is partly deposited along the sides of the glaciers in the form of moraines. Combining historical information shows us that glaciers have changed considerably over the last decades and centuries. These records of historical glacier length

fluctuations are useful in the study of glacier dynamics and can provide insight in past climate fluctuations.

For many glaciers, length measurements have been taken on a regular basis during the 20th century, and for some even at the end of the 19th century. These measurements are the result of field work as well as the interpretation of aerial and satellite images. Furthermore, there exist numerous reconstructions of glacier length variations from before the measurement period. There are many different sources for these reconstructions. The most common are historical documents and geological evidence. Historical information consists of paintings, official documents, and expedition reports or sketches from pioneers. The most abundant geomorphological evidences are moraines that can be dated, overridden or damaged trees, and variations in glacial sediment. For most glaciers, the available information is a combination of several types of sources. As an example, two length records are discussed shortly. In Figure 1.10 the reconstructed length fluctuations of Glaciar Frías, Argentina are shown. During the past centuries Glaciar Frías descended below the tree line, which makes it now possible to date former glacier stands by the age of regrown trees. The length record is a compilation of dated moraines, aerial photography, satellite images, field measurements and ground photography. The combination of all these sources provides a length record which covers the period 1639–2009 with a considerable detail. Two historical images of the Mer de Glace, France, are shown in Figure 1.11. This glacier descended into the valley of Chamonix, which became a renowned tourist destination as early as the 18th century. Therefore, there exist numerous historical sources in the form of paintings, descriptions, and photographs of the glacier terminus. Since the end of the 19th century, regular length change measurements were taken. A thorough compilation of this material makes this record one of the most detailed glacier length records at present [*Nussbaumer et al.*, 2007].

The mixture of information on glacier length changes implies a large variety of sources. Most measurements are reported to, and published by, the World Glacier Monitoring Service (WGMS) [*WGMS*, 2008 and earlier volumes]. However, until recently the WGMS did not collect length reconstructions [*Zemp et al.*, 2011]. Reconstructed length changes can be found in regular scientific publications, complemented by field reports, websites of glacier monitoring programs and personal communication. To use the information of world-wide glacier fluctuations, all this information has to be put together in one coherent way. In Chapter 2 a global data set of glacier length records is described. This data set is an extension of the data set used in *Oerlemans* [2005] and *Oerlemans et al.* [2007] and contains at present 374 records.

The data set is compiled to study the glacier fluctuations in relation to climatic change. Since the response of glaciers is rather slow, a length record has to cover at least several decades. Therefore, only records that start before 1950 and cover at least 40 years are included. Furthermore, glaciers whose length fluctuations are not directly related to climate should be excluded. For example, glaciers known to be surging are not included as the length fluctuations of surge-type glaciers are not climate driven. Surging is a spectacular cyclic behaviour

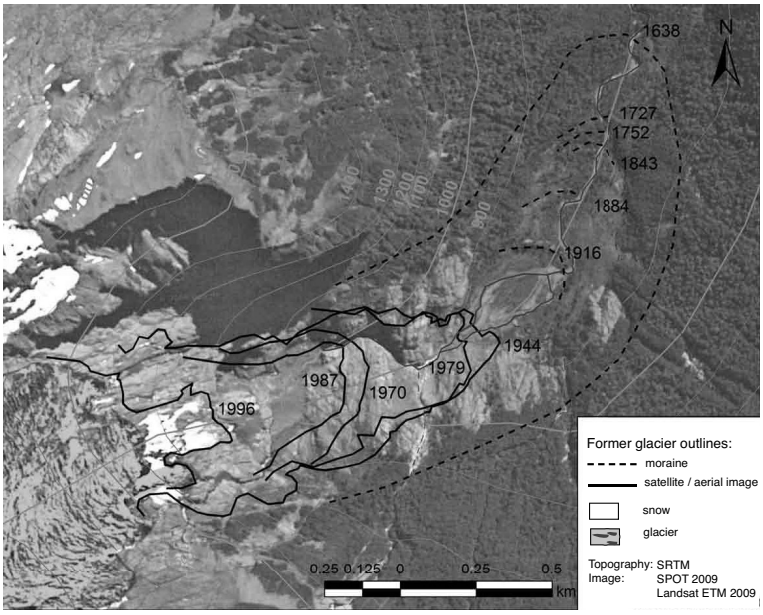

Figure 1.10: *Satellite image of the glacier terminus (lower left) and glacier forefield with the reconstructed length changes of Glaciar Frías, Argentina. The dotted outlines represent maximum extents derived from moraines dated with dendrochronology. The black lines indicate glacier outlines derived from different aerial and satellite images. In addition to these images, annual field measurements of the glacier length are available for 1976 to 1985 (not shown).*

which make some glaciers suddenly advance over several kilometres due to a change in the ice dynamics. The advances are followed by a retreat in the so-called quiescent phase. The data set does include the length record of 21 tidewater glaciers and 17 glaciers calving in fresh water, as the data set is also used for the reconstruction of the glacier contribution to sea-level rise (Chapter 5). Besides the length change, the location, altitude range, area, length, and climatological precipitation are also included for each glacier. The data set spans the period 1534–2009, although most records start in the 19th century. The data set includes length records of glaciers on all continents and on virtually all latitudes. However, several regions with a large area covered by glaciers, such as the Canadian and Russian Arctic and glaciers around the Antarctic ice sheet, are not represented in the data set.

While reading this thesis it is important to keep in mind that the data set with glacier length fluctuations has been extended continuously. For this reason, the results described in this thesis are not all based on the same data set and the number of available records is different in Chapters 2, 4, and 5. The latest version of the data set, as described in Chapter 2, is available online (www.staff.science.uu.nl/∼lecle102/data) and will be submitted to the WGMS.

Figure 1.11: *Examples of historical material used in the reconstruction of the Mer de Glace [Nussbaumer et al., 2007].* ***a)*** Aiguille Verte with the Glacier du Bois and the village Les Prats, Savoie*, painted by Samuel Birmann in 1823 (Kunstmuseum Basel, Kupferstichkabinett, Inv. Bi. 30.125, photographed by Martin P. Bühler).* ***b)*** Glacier des Bois and Aiguille Verte*, photograph from 1862 by Alphonse Braun (CAH Annecy, Collection Paul Payot; photographed by H.J. Zumbühl).*

1.4 Climate reconstructions from glacier length fluctuations

In this thesis, two studies are presented that use glacier length records as a climate proxy. In Chapter 3, climate variations in Northern Patagonia are reconstructed from the length fluctuations of Glaciar Frías (Figure 1.10). This glacier is modelled in detail with a coupled mass balance - dynamical model. In Chapter 4, global and hemispheric temperature variations since 1600 are reconstructed with the use of the glacier length data set.

In Section 1.1, we have indicated several reasons why glacier length fluctuations are a valuable proxy for past climate variations. However, there are also some disadvantages to the use of glaciers as a climate proxy that have to be accounted for: *i)* The fluctuations are a function of variations in both temperature and precipitation, although, in general, glaciers are more sensitive to the typical variations in temperature than to those in precipitation. *ii)* There is a varying seasonality in the sensitivity. Glaciers in cold regions are mainly sensitive to summer temperature variations, while glaciers in the tropics and in a maritime climate are sensitive to temperature variations in a much larger part of the year. *iii)* The climate response involves complex dynamical and meteorological processes that in principle should be captured by an appropriate model. *iv)* The temporal resolution is limited by the dynamical response of glaciers. The latter is only a disadvantage when one is interested in yearly variations. For the study of climate, by definition the average over a period of several decades, it can be of advantage that glaciers integrate the short-term weather fluctuations into a long-term signal, which is easy to measure.

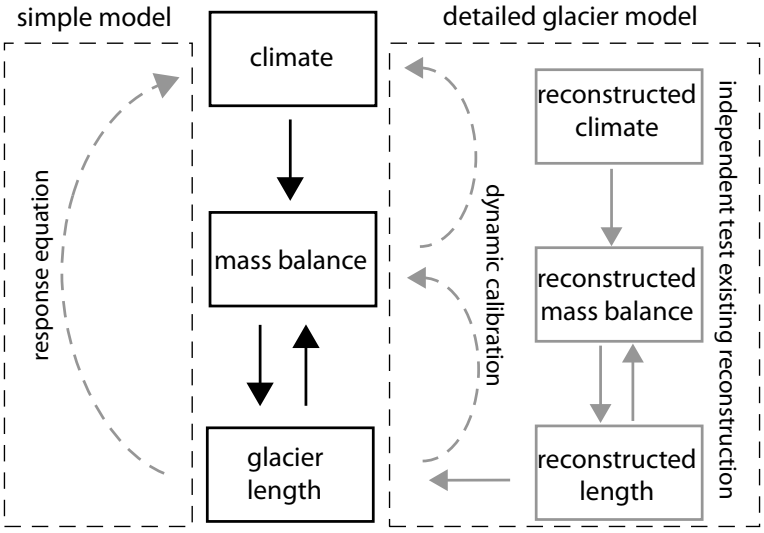

Figure 1.12: *Schematic display of the model approaches used to extract a climate signal from glacier length records. In black, the glaciological processes are schematically shown: the climate forces the mass balance, and, together with the ice dynamics, the mass balance determines the glacier geometry. Changes in geometry have a feedback on the mass balance. In grey the approaches to extract climatic information from glacier length are given. To the left the approach for large-scale reconstructions (Section 1.4.2), to the right the two approaches with the detailed glacier model (Section 1.4.1).*

1.4.1 North Patagonian climate reconstruction

Meteorological observations are rather sparse in southern South America. There are no long, detailed measurement series like in Europe. Even at present, the observational network is mainly limited to low-altitude urbanized regions [*Rosenblüth et al.*, 1997]. Therefore, knowledge of long-term climate variations depends on reconstructions based on proxies. Over the last three decades, the number of tree ring records has increased significantly [*Boninsegna et al.*, 2009], and they are complemented by documentary evidence, lake sediments and ice cores. However, it is often difficult to calibrate the biogenic proxy records, because the meteorological information is sparse [*Neukom et al.*, 2011]. The climatic information that can be derived from the South American glacier length records can be a valuable addition to the existing proxies.

The length record of Glaciar Frías, North Patagonia, is long and fairly detailed. It covers the period 1639–2009, and consists of a compilation of field measurements, satellite observations, aerial photography, historical documents, and moraines dated with dendrochronology [*Villalba et al.*, 1990]. The glacier mass balance is calculated with a simplified mass balance model [*Oerlemans*, 2010], in which the surface energy balance is described with only two terms. The first term describes the absorbed short-wave radiation, the second combines the

temperature dependent fluxes ($L_{\text{in,out}}$, H_{lat}, and H_{sen}) in one parameterization. The model is forced with ERA re-analysis data. The ice dynamics are described with a flowline model, using the shallow ice approximation. Unfortunately, there exist no mass balance measurements of Glaciar Frías. Instead, the modelled mass-balance is calibrated to measurements on glaciers 130 and 190 km north of Glaciar Frías [*Rivera et al.*, 2005; *Bown et al.*, 2007; *Brock et al.*, 2007]. The modelled mass balance is validated by comparing the modelled glacier length with the observed glacier length.

The combination of the historical length record and the glacier model can be used in two ways to reconstruct past North Patagonian climate (see the *detailed glacier model* box in Figure 1.12). Firstly, we can use dynamic calibration of the mass balance profile to find a history of perturbations which reproduces the observed length record [*Oerlemans*, 1997a]. These mass balance profile perturbations can be converted into a climate record with the mass balance sensitivity. With this method it is not possible to separate the contributions of precipitation fluctuations and variations in temperature. The dynamic calibration shows that in the middle of the 17th century, temperature must have been 1.16 °C lower, or precipitation must have been 34% higher, than the 1980-2009 average to explain the observed length changes. Secondly, the glacier model can be forced with existing temperature and precipitation reconstructions. The match between the modelled and observed length change gives an idea of the accurateness of the reconstructions. The model of Glaciar Frías is forced with the multi-proxy precipitation and temperature reconstructions of *Neukom et al.* [2010] and *Neukom et al.* [2011] and with the independent *Villalba et al.* [2003] temperature proxy, which is based on tree rings. The uncertainties in these reconstructions are large, up to 2 km when translated into glacier length. Nevertheless, some interesting conclusions can be derived. The variations in precipitation seem to be of minor importance; the modelled length fluctuations are dominated by the reconstructed temperature variations. And in the beginning of the 19th century, both temperature reconstructions are ~ 0.7 °C too warm to explain the glacier length observations.

The uncertainties in the climate reconstruction from the length fluctuations are probably substantial, but they are hard to quantify. At present, there are no measurements of the mass balance of Glaciar Frías, so it is impossible to calibrate the mass balance model accurately. Without measurements it is also difficult to estimate the uncertainty in the calculations. Therefore, the North Patagonian climate reconstruction from the glacier length record of Glaciar Frías could greatly benefit from mass balance and meteorological measurements on this glacier.

1.4.2 Global and hemispheric temperature reconstruction

The data set of global glacier length changes can be used for a global climate reconstruction for the period 1600–2000. However, it is very difficult to model each of the more than 300 glaciers in detail, as was done for Glaciar Frías. For most of the glaciers in the data set there are no mass balance measurements and a detailed glacier geometry is not known. For the

global and hemispheric reconstructions a different approach is chosen, that exploits the large sample of glaciers and the large spatial scale of the reconstructions.

It can be argued that temperature is the only relevant climate parameter for hemispheric and global glacier length fluctuations. From mass balance studies it is clear that for individual glaciers, fluctuations in temperature are the main driver of mass balance fluctuations on decadal time-scales. This is again confirmed by the reconstruction of the glacier length fluctuations of Glaciar Frías. Secondly, the variations in precipitation have a much shorter spatial correlation distance than temperature variations. Hence, the small influence that precipitation has on the glacier length fluctuations will average out in large-scale reconstructions. The global and hemispheric climate reconstruction is the reconstruction of the temperature variations that best explain the observed global, or hemispherical, glacier length fluctuations.

This temperature is calculated directly from the length variations with the linear differential equation (Eq. 1.1, the climate variations ΔELA are characterized by ΔT, Figure 1.12). Thus, mass balance calculations for every glacier in the data set are circumvented. The temperature variations are a function of length change, climate sensitivity, and response time only. The expressions of the simple glacier model, described in Section 1.2.6, are used to calculate the response time and the climate sensitivity. The constants c_1 and c_2 are calibrated to the results of numerical models. The expressions will not be very accurate for individual glaciers, but the average result will be reliable if the sample of the numerical models used in the calibration is representative. A temperature reconstruction is derived from each glacier length record. The reconstructed temperature records are averaged to hemispheric and global mean temperature anomalies for the period 1600–2000. The averaging procedure takes the spatial distribution of the length records into account.

The temperature anomalies reconstructed from glacier length fluctuations reproduce the instrumental record of the 20th century very well for the global, the Northern and the Southern Hemisphere average. This validates the approach. The pattern of all three reconstructions is very comparable: more or less constant temperature for the period 1600–1850, followed by a continuous rise in temperature from 1850 until 1945. There is a short decline in temperature from 1945 to 1970, that is followed by a temperature increase until 2000. Global mean temperature rose by 0.94 ± 0.31 °C over the period 1830–2000. The high global temperatures in the period 1980–2000 are unprecedented in the whole period of reconstruction, and also the rate of global temperature increase in this period is the highest since 1600. The warming over the period 1850–2000 is 0.82 ± 0.27 °C and 1.27 ± 0.76 °C for the NH and SH, respectively. To conclude, the reconstructions are in broad agreement with existing multi-proxy evidence [*Mann et al.*, 2008]. However, the glacier reconstruction shows a global warming since the middle on the 19th century, which is in contrast with the instrumental record and the reconstruction of *Mann et al.* [2008] (which follows the instrumental record from 1850 onwards). The instrumental record does not show a clear warming trend until the beginning of the 20th century.

Analysis on the sources of uncertainty in the reconstruction show that improvement of the calculation of the climate sensitivity and further extension of the data set would reduce the uncertainty most effectively. The extension of the data set should not only include new records. Gaps in the existing records should be filled where possible, and records that end before 2000 should be updated. The calculation of the climate sensitivity could be improved by taking the glacier geometry better into account.

1.5 Glacier contribution to sea-level rise

In the past, sea level has changed substantially due to the growth and decline of ice sheets during the glacial cycles. During the last glacial maximum global mean sea level was about 120 m lower than today. At present, glaciers and ice sheets store a large volume of water on land, equivalent to a global mean sea-level rise of almost 65 m [*Lemke et al.*, 2007]. Sea level has been rising in the past two centuries with 15–20 cm [*Jevrejeva et al.*, 2006; *Church and White*, 2011, Figure 1.13], and it is expected to continue to rise in the next century as a consequence of continued global warming. Because a substantial sea-level rise could threaten the millions of people living in coastal areas, it is important to be able to predict future sea-level changes. However, confidence in future predictions is determined by the ability to understand past sea-level changes. To understand the historical sea-level rise, the different processes that contribute to it must be well understood.

Recently, *Church et al.* [2011] have been able to close the sea-level budget for the period 1971-2008, which means that for this period the sum of the different contributions to sea-level change is equal to the observed sea-level change. The most important contributors to sea-level rise are mass changes of the Greenland and Antarctic ice sheets, combined mass changes of all glaciers and ice caps, thermal expansion of the ocean water, and changes in terrestrial water storage. Since 1972, thermal expansion and glaciers and ice caps were the largest contributors, comparable in size, followed by the Antarctic and Greenland ice sheets. In *Church et al.* [2011], the terrestrial storage was a negative contributor, following *Konikow* [2011]. However, according to *Wada et al.* [2010] changes in terrestrial water storage contributed to sea-level rise, due to groundwater depletion.

Combining the glaciers and ice sheets, the cryosphere is the largest contributor to sea-level rise. As the total ice volume of glaciers is much smaller than that of the ice sheets, the relative volume loss of glaciers is much larger than that of the ice sheets. This can be explained by the shorter response time of glaciers, and a larger climate sensitivity due to the fact that most glaciers are located in a milder, wetter climate than most parts of the ice sheets [*Oerlemans and Fortuin*, 1992]. However, the mass loss of the ice sheets is accelerating at the moment. If this acceleration continues, the contribution of the ice sheets will likely catch up with that of the glaciers and ice caps in the 21st century [*Rignot et al.*, 2011].

Before 1970, the sea-level budget has not been closed yet. Estimates indicate that over the first half of the 20th century the contributions of thermal expansion and changes in terrestrial storage are relatively small. Although there are large uncertainties in the contribution of the ice sheets due to a lack of measurements, the glacier contribution to sea-level rise over the past century is estimated to be larger than the ice sheet contribution [*Church et al.*, 2001] (Figure 1.13). To estimate the glacier contribution to sea-level rise over the 20th century, two different approaches are used. The first uses modelled climate sensitivity of the glacier mass balance in combination with a temperature forcing, either measured or modelled. Estimates resulting from this method vary from 20–30 mm for the period 1865–1990 [*Zuo and Oerlemans*, 1997a; *Gregory and Oerlemans*, 1998] to 28 $\pm$ 16 mm for the period 1900–1961 [*Meier*, 1984]. These results strongly depend on the precipitation estimates, the key factor in determining the climate sensitivity, and the choice of the imbalance between the glaciers and the air temperature anomaly at the start of the reconstruction [*Zuo and Oerlemans*, 1997a]. The alternative approach is to use observations: observed volume changes from mass balance and geodetic measurements, or volume changes deduced from observed glacier length changes. Mass balance measurements are limited to the second half of the 20th century, and provide an estimate of 16 mm for 1961–2004 and over 30 mm for 1951–2008 [*Dyurgerov and Meier*, 2005; *Cogley*, 2009a, respectively]. The calculation based on glacier length changes results in a contribution to sea-level rise of 45 $\pm$ 7 mm for the period 1900–2000 [*Oerlemans et al.*, 2007]. These estimates of the glacier contribution over the 20th century are not sufficient to close the sea-level budget. However, it should be noted that there is a general trend to higher estimates in later studies.

Projections for the 21st century are necessarily based on modelled mass balance sensitivities in combination with projected temperature and precipitation changes. Estimates of glacier contribution to sea-level rise for the 21st century are in the range of 100–250 mm [*Meier et al.*, 2007; *Radic and Hock*, 2011; *Slangen and van de Wal*, 2011].

In Chapter 5 we describe a new estimate of the glacier contribution to sea-level rise for the 19th and 20th century that is based on the data set of world-wide glacier length changes. Since the earlier results of *Oerlemans et al.* [2007], the glacier length data set has been extended substantially, especially in regions with a large glacier cover (Alaska, Arctic, Himalaya, Patagonia). In addition, a new data set of glacier mass balance and volume change from geodetic measurements has become available [*Cogley*, 2009a], which improves the calibration of the length signal to volume change. The resulting new estimates for the glacier contribution to global mean sea-level are 84 $\pm$ 21 mm for the period 1800–2005, 91 $\pm$ 23 mm for the period 1850–2005, and 69 $\pm$ 17 mm for 1900–2005 (Figure 1.13). These estimates are significantly larger than earlier results, which helps to close the budget of global sea-level rise. We also find that there is no indication that the contribution during the second half of the 20th century is significantly larger than that in the first half of the 20th century, despite the fact that the global mean temperature in the second half of the 20th century was higher.

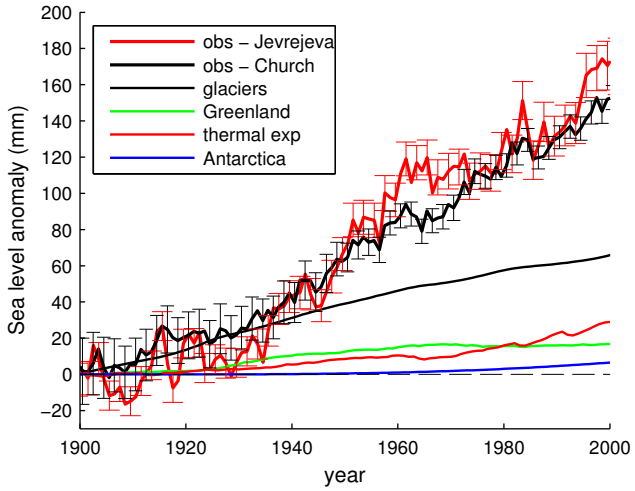

Figure 1.13: *Global mean sea-level change as observed during the 20th century from Jevrejeva et al. [2006] (red) and Church and White [2011] (black); and the main contributors to the sea-level change over the 20th century as compiled by Huitzing [2011]: black: glaciers and ice caps [from Leclercq et al., 2011, see Chapter 5], green: Greenland [from Fettweis et al., 2008], red: thermal expansion from the oceans (CMIP3, J. Gregory pers. com.), blue: Antarctica [from Huybrechts et al., 2004; Lemke et al., 2007].*

Sensitivity experiments show that the estimate mainly depends on variations in the used data sets, and that the result is hardly sensitive to the parameters used for scaling length change to volume change. It appears that the differences between the calculations presented in this thesis and the earlier results of *Oerlemans et al.* [2007] are almost entirely due to the different glacier mass balance data sets used as calibration. The glacier length changes presented in this thesis show a world-wide consistent picture in the period 1900–2005. Going back before 1900, the number of records reduces, especially in the regions which represent a large glacier area. The leads to a larger uncertainty in the global length signal before 1900, caused by the increasing dependency of the global mean on the averaging method.

To reduce the relatively large uncertainty in the glacier contribution to sea-level, data sets of both the mass balance measurements and the length fluctuations need to be expanded and improved in the future. At the moment the overlap between the two data sets is limited: many of the glaciers with known length fluctuations have no mass balance observations and vice versa. With the help of geodetic volume change estimates it might be possible to increase the overlap between both data sets. Furthermore, the data set with glacier length changes should be extended to include more records from the regions where most of the glacier ice is located.

1.6 Climate versus mass balance – the influence of adjustment of the glacier geometry

In the last chapter, glacier length changes are used to make a first estimate of the effect of glacier retreat on the glacier mass balance. The glacier mass balance in a specific period in time is dependent on the climate of that period *and* the glacier geometry. The latter is determined by the history of the glacier and climate. It is thus not straightforward to link the variations in mass balance to climate fluctuations on timescales where the changes in glacier geometry are non-negligible.

Huss et al. [2010a] have reconstructed the mass balance history for 30 Swiss glaciers over the period 1908-2008. They have used a temperature-index model that is calibrated on mass balance measurements and changes in glacier volume derived from geodetic measurements (i.e. by comparing topographic maps and digital elevation models from different years). The decadal mean of the reconstructed mass balance fluctuations is approximated with a combination of a linear trend over the century and a 60-year period sinusoidal (Figure 1.14). The sinusoidal gives the fluctuations in the mass balance on decadal time scale. *Huss et al.* [2010a] link these fluctuations to the Atlantic Multidecadal Oscillation (AMO). They conclude that the natural variations caused by the AMO account for half of the glacier mass loss in the Swiss Alps in the period 2000–2008. However, the changes in glacier geometry over the 20th century were not accounted for.

In a comment to *Huss et al.* [2010a], the glacier length changes of 12 of the 30 glaciers in the sample were used to get a first-order estimate of the influence of the glacier retreat on the mass balance. Based on this estimate, the glacier retreat has significantly reduced the imbalance between glaciers and the current climate. Therefore, we argue that the geometric change should be included for a proper interpretation of the relative importance of short-scale fluctuations in climate. This result might be connected to the conclusion that the rate of sea-level rise from the melt of glaciers did not change much over the 20th century, while global averaged temperatures in the last decades were higher than in any of the previous decades in the 20th century. If the ice loss were simply related to the temperature, the rate of glacier contribution to sea-level rise would have increased over the century. Apparently, the glacier retreat over the last century should be taken into account, also when looking at a global scale.

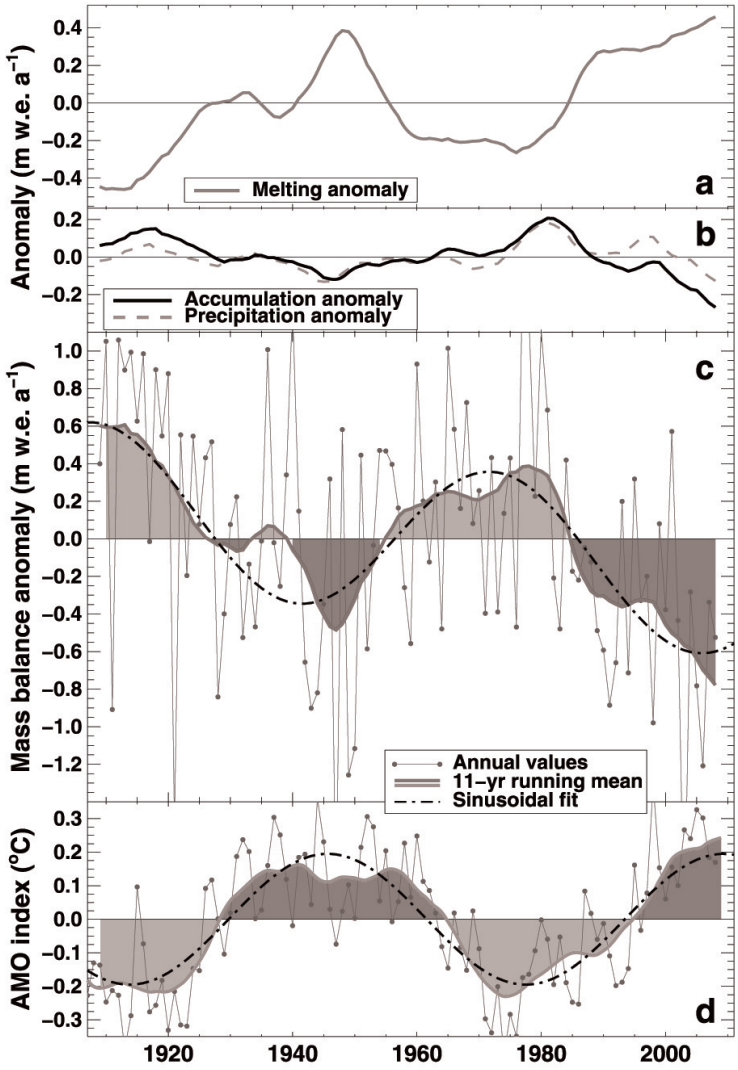

Figure 1.14: *Figure 3 from Huss et al. [2010a] showing their most important results:* ***a)*** *11-year running mean of the annual glacier melt anomaly averaged over the 30 glaciers, and* ***b)*** *annual accumulation and precipitation anomaly (deviations from the 1908–2008 average).* ***c)*** *Annual mass balance anomaly. A sinusoid superimposed on a linear trend is shown.* ***d)*** *Atlantic Multidecadal Oscillation index [Enfield et al., 2001]. Parameters of the sine function in Figures 3c and 3d are based on least square fits.*

A way to do so, is to calculate the so-called reference-surface mass balance [*Elsberg et al.*, 2001]. The reference-surface mass balance for different years is the mass balance calculated

for the same glacier geometry, the reference surface. In a reply to the comment, *Huss et al.* [2010b] have acknowledged that they should have used the reference-surface mass balance for their climatic interpretation. They calculated the reference-surface mass balance for the 30 glaciers in their study. The difference between the specific mass balance and the reference-surface mass balance are substantial for individual glaciers, but according to their calculations there is no general trend: both negative and positive deviations occur. Therefore, the mean of the calculated reference-surface mass balance anomaly is not very different from the mean specific mass balance anomaly, and their final results are not affected much by using the reference-surface mass balance.

1.7 Main conclusions

- The retreat of Glaciar Frías since 1639 can be best explained by an increase in North Patagonian temperature of 1.16 °C or a decrease in precipitation by 34%. Most of this climate change occured since the end of the 19th century.
- Climate reconstructions of North Patagonia have a rather large uncertainty, and the two tested reconstructions were $\sim$ 0.7 °C too warm in the beginning of the 19th century and diverge in the first half of the 20th century.
- Glacier length fluctuations are a reliable proxy for global and hemispheric temperature, reproducing the instrumental record of the 20th century very well.
- According to the glacier length fluctuations, the present global warming started in the middle of the 19th century. Over the period 1830–2000, global mean temperature has risen by 0.94 $\pm$ 0.31 °C. Over the period 1850–2000, Northern and Southern Hemisphere average temperatures have risen by 0.82 $\pm$ 0.27 °C and 1.27 $\pm$ 0.76 °C, respectively.
- The contribution of glaciers and ice caps to sea-level rise is estimated to be 84 $\pm$ 21 mm for the entire period of reconstruction 1800–2005 and 91 $\pm$ 23 mm for the period 1850–2005. The 20th century (1900–2005) glacier contribution to sea-level rise is 69 $\pm$ 17 mm.

1.8 Discussion and outlook

The glaciological approach used in the reconstruction of the climate of northern Patagonia can be applied elsewhere. Even for regions with little meteorological and mass balance measurements, it is possible to construct a glacier model. The simplified mass balance model appears to be applicable in different climatic settings [*Giesen and Oerlemans*, 2011], although it is

recommended to have some observations for calibration of the model parameters. A glacier model, in combination with a long and relatively detailed glacier length record, can be used to explore the possible deficiencies in the long-term trends of other proxy climate records.

The global and hemispheric temperature reconstructions based on glacier length fluctuations provide a completely independent confirmation of existing proxy reconstructions. In the future, it would be worthwhile to examine if the glacier length reconstruction can be included in multi-proxy temperature reconstructions. This is not straightforward, as the temperature records derived from the individual length records are not very reliable. Partly, this is due to the fact that the climate sensitivity is not very accurate, something that could be resolved. More fundamentally, the individual records are also influenced by precipitation and radiation variability. Only the average on large spatial scales can be assumed to solely represent temperature fluctuations.

The new estimate of the glacier contribution to sea-level rise over the past two centuries shows that this contribution is significantly higher than previously assumed. This should help in attempts to close the sea-level budget of the entire 20th, and maybe even the 19th, century.

However, the uncertainty in the reconstructions of climate and sea-level are quite substantial. The origin of these uncertainties lies for a large part in the limitations of the available data. The climate reconstruction from the length fluctuations of Glaciar Frías is limited by the lack of mass balance observations, which makes it difficult to calibrate and validate the mass balance model for this specific glacier. The uncertainty in the global and hemispheric temperature reconstructions would reduce when longer and more detailed glacier length records and a better expression for the climate sensitivity were used. For the latter, more detailed information of the glacier geometry is needed. For a better calibration of the sea-level estimate, the mass balance data set could be extended in time and the overlap between the mass balance and glacier length data sets should be increased. And to conclude, the estimate of the glacier contribution to sea-level rise would improve if the Arctic region is better covered by the glacier length data set.

There are several possibilities to improve the current data set on glacier length fluctuations. First of all, data should be added from regions with little or no coverage: northern Asia and Kamchatka, New Zealand, sub-Antarctic Islands, Arctic regions of Canada, etc. Since the publication of the paper that is the basis for Chapter 5, a start has been made by adding records from Alaska and Greenland (see Chapter 2). It will be a challenge to find usable glacier length data from the Canadian and Russian Arctic, although there might be possibilities in Novaya Zemlya.

Secondly, it is very likely that there exists more information on glacier length fluctuations, than is included in the current data set. We might have overlooked available information, and some data are not (easily) publicly accessible. In addition, there are publications on glacier fluctuations, in which historical maximum positions are dated but the length changes are not put into a comprehensive length change record or are not quantified at all [e.g. *Wiles et al.*,

1999, but several others exist]. That is simply a missed opportunity. In this perspective, it is promising that the WGMS has started to collect glacier length reconstructions through their network of correspondents. However, it is not very likely that the global temperature reconstruction based on glacier length changes can be extended further back than the 17th century. Prior to 1600, information on glacier length changes is sparse and fragmentary.

To conclude, the data set could be linked to modern glacier inventories, like the GLIMS and Globglacier projects. This would make it possible to include a more detailed glacier geometry than the basic information that is currently included, and open up possibilities to include a more sophisticated calculation of the climate sensitivity.

2

A data set of world-wide glacier length fluctuations

Summary

In this thesis, historical glacier length fluctuations are used to reconstruct past climate, and to estimate the glacier contribution to sea-level rise. Hence, the data set of the glacier length records, described in this chapter, is the heart of this thesis. The data set is a compilation of available information on glacier length changes world-wide, including measurements as well as reconstructed glacier length fluctuations. This compilation started a decade ago and earlier versions have been used in several studies.

At present, 374 records are included. All records start before 1950 and cover at least four decades. The number of records changes in time. The longest record starts in 1534 and from this year the number of available records increases gradually in time. In the second half of the 19th century the number of available records increases sharply, from 90 in 1850 to 275 in 1900. After 1962, the number of records decreases again.

Whereas the earlier versions of the data set had a strong bias to European glaciers (in 2005, more than half of the records came from the European Alps), the current data set has improved the global coverage. There are records from all continents. However, the Canadian and Russian Arctic and the glaciers around the Antarctic ice sheet are not represented in the data set.

Beside the glacier length fluctuations, information on the glacier location and geometry is included in the data set, which is needed for the calculations done in Chapters 4 and 5.

2.1 Introduction

Information on glacier changes in the past is useful for several reasons. The change in ice volume of glaciers has a direct impact on the global sea level. Glaciers are one of the main contributors to the sea-level change of the last century [*Bindoff et al.*, 2007]. Moreover, glaciers respond to changes in climate, translating the climatic signal into clearly observable changes in the landscape. Quantitative information on glacier fluctuations over the past centuries can therefore be used to reconstruct climatic change, which is valuable to put the observed global warming over the last decades into perspective.

Of the possible glacier properties that can be measured to quantify glacier fluctuations (i.e. mass balance, volume, area, and length), information of glacier length fluctuations is the most abundant if we go further back in time [*Cogley*, 2009a; *Oerlemans*, 2005; *WGMS*, 2008 and earlier volumes]. Measurement programs were started as early as the 19th century [e.g. *Swiss glacier monitoring network*, 1881-2009], and for many glaciers around the world the length changes prior to the start of measurements can be derived from historical (e.g. paintings, documents) and geological (e.g. moraines, overridden trees) evidence. Of the former, there is a wealth of examples in Europe [e.g. *Nussbaumer et al.*, 2011; *Zumbühl*, 1980] leading to very detailed and long glacier length records. Geological evidence is found at glaciers everywhere around the world, especially in maritime climates, where the glacier terminus descents well below the tree line [e.g. *Villalba et al.*, 1990; *Wiles and Calkin*, 1994].

The combination of all these different sources of information on glacier length fluctuations across the globe has a large potential for the reconstruction of a world-wide picture of glacier changes in the past. It is challenging to combine all the difference sources of information in one coherent data set. In this Chapter we describe a data set of glacier length fluctuations that has been constructed over the course of several years and that, although probably far from complete, contains as much as possible of the world-wide information of glacier length changes in an uniform format.

2.2 Included data

2.2.1 Glacier length fluctuations

At present the data set includes the length record of 374 glaciers (Figure 2.1). With the term glaciers all glaciers and ice caps outside the large ice sheets of Greenland and Antarctica are meant. This definition includes all types of ice bodies varying from small cirque glaciers, valley glaciers, to the outlets of large ice caps and ice fields. Also included are the glaciers and ice caps on Greenland and Antarctica, which are not part of, or attached to, the main ice sheets. Because the main goal of the data set is the study of glacier fluctuations on centennial time-scales, we have only included length records that start before, or in, 1945 and extent over

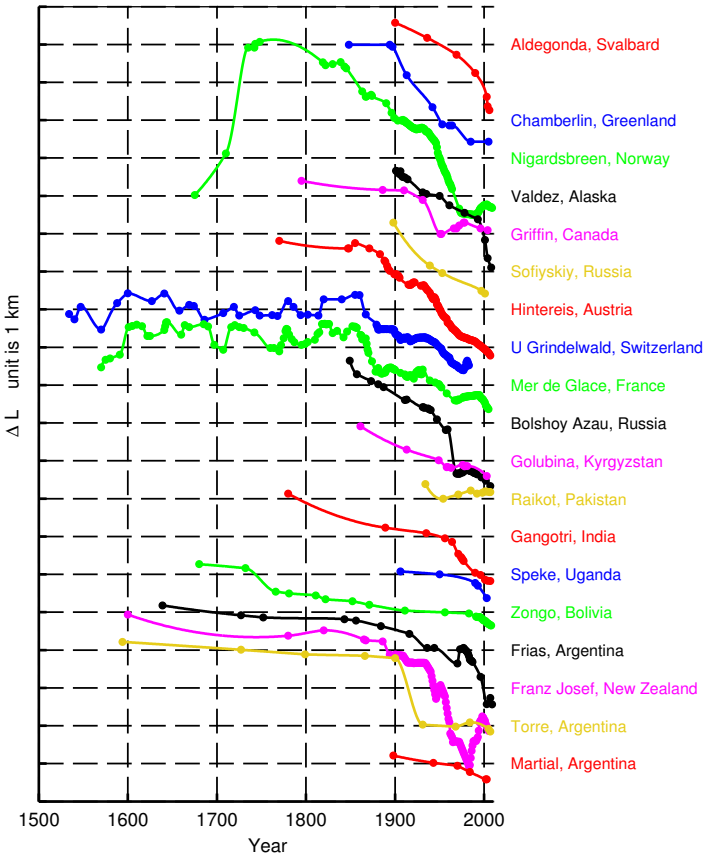

Figure 2.1: *Examples of glacier length records from different parts of the world. Each dot represents a data point (for each of the records the references are given in Appendix A). Data points are connected with Stineman interpolation.*

at least several decades. The shortest length record in the data set covers 40 years, the longest 450 years. The records of glaciers known to be surging are excluded, as these length changes are not climate driven and not representative for a larger sample of glaciers [*Kamb et al.*, 1985; *Yde and Knudsen*, 2005]. To a lesser extent, this is also the case for calving glaciers. In particular for large tidewater glaciers, the glacier bed topography is of major influence in the glacier response to climate [e.g. *Nick*, 2006; *Vieli and Nick*, 2011]. The original goal of the data set was the reconstruction of climate [*Klok and Oerlemans*, 2004; *Oerlemans*, 2005], hence only a few calving glaciers were included. However, the recorded glacier length changes can be used to reconstruct the glacier contribution to sea-level rise [*Oerlemans et al.*,

2007; *Leclercq et al.*, 2011]. The retreat of calving glaciers forms a substantial part of the glacier contribution [*Cogley*, 2009a] and therefore, the length records of calving glaciers are included in the data set. At present, the data set contains 22 tidewater glaciers and 17 glaciers calving in fresh water (most of them are part of the Patagonian Icefields).

The back bone of this data set is formed by the measurements of frontal positions published by the World Glacier Monitoring Service in the Fluctuations of Glaciers [*WGMS*, 2008 and earlier volumes, www.wgms.ch]. The WGMS has a scientific collaboration network consisting of more than 30 national correspondents, who report the glacier observations in their country. These observations vary from annual to decadal front position changes. The measurement methods vary from field measurements, often done by volunteers, to observations based on remote sensing.

Unfortunately, not all available information is included in the WGMS data base. Some observations were simply not reported. Moreover, the WGMS has not started to include reconstructions of frontal positions until last year. Our knowledge of glacier fluctuations before the measurement programs were started, i.e. before 1850 at best, fully consists of reconstructions from historical and geomorphological evidence. Therefore, we have extended the WGMS data set with relevant (quantitative) information of glacier length changes. Additional information can be found in numerous scientific articles and is complemented by annual reports, expedition reports, websites of glacier monitoring programs and personal communication. See Appendix A for details on the individual records and references.

The reconstructions are based on a variety of sources, mainly of historical and geomorphological nature. Historical sources can be both pictures, i.e. paintings, sketches, early photographs, as well as written documents, such as the documented advances of Glacier des Bossons and Nigardsbreen over farmland [*Nussbaumer and Zumbühl*, 2011; *Bogen et al.*, 1989]. For the European glaciers there is a wealth of documents, resulting in long and detailed glacier length records [e.g. *Zumbühl*, 1980; *Nussbaumer et al.*, 2007, 2011]. Historical information is less abundant in other regions of the world, but for example early military maps and accounts from pioneers form a valuable addition to other sources [e.g. *Panov*, 1993; *Araneda et al.*, 2009]. The accuracy of the interpretation of these historical sources depends on the accuracy of descriptions and drawings. It also depends on the landscape around the glacier terminus. Some distinct features in the landscape are needed to connect the historical position to the present-day geometry. The typical uncertainty range of glacier length changes based on historical evidence is 100–200 m.

Glaciers have a high impact on the local landscape, which is subjected to glacial erosion. This leads to geomorphological evidence of former glacier stands. The most frequently used are the lateral and terminal moraines, which are often preserved and indicate a former maximum glacier extent. These moraines can be dated, mostly with dendrochronology or lichenometry. In general, the uncertainty in glacier length reconstructions based on geomorphological evidence is due to the inaccuracy in the dating rather than uncertainty in the position. When

using dendrochronology, the age of trees growing on moraines is measured from the tree rings. For living trees the age is simply measured by counting the tree rings. In the case of dead remains the ring profile can be matched to a regional chronology. The estimated tree age gives the minimal age of the moraine, to which an estimate of the time needed for a tree to start growing has to be added to get the actual age of the moraine. This so-called excesis time is the main source of uncertainty of the dendrochronological dating, typically in the range of 20-40 year [e.g. *Villalba et al.*, 1990; *Koch and Kilian*, 2005]. In addition to the dating of moraines, sporadically trees can be found that are overridden or damaged during a glacier advance [*Wiles and Calkin*, 1994; *Nesje et al.*, 2008]. In the case of lichenometry the age of a moraine is estimated from the size of lichens growing on the boulders on the moraine, in combination with a typical growth rate [e.g. *Evison et al.*, 1996; *Rabatel et al.*, 2005; *Solomina et al.*, 2010]. This dating is in general less accurate than dendrochronology with an uncertainty of 25–60 years. Occasionally, other geological evidence, in combination with other dating methods, are used, e.g. the influence of glacial run-off on peat in the glacier forefield with a chronology based on carbon dating [*Espizúa and Pitte*, 2009].

We include the method of data acquisition for each data point of the glacier length fluctuations. Because of the large variety in methods, we use a bulk method of categories:

1. direct measurements
2. historical sources
3. dendrochronological dating
4. other dating methods.

The category of direct measurements of the glacier terminus position includes field measurements, with or without GPS, (aerial) photography, when designed for the purpose, and satellite observations. The category of historical sources contains all data points derived from historical documents such as sketched maps from pioneers, pictures, paintings, written descriptions, etcetera. Glacier stands derived from geomorphological evidence, dated with dendrochronology are put in the third category. The fourth category includes geomorphological and other geological evidence dated with other, less accurate, methods, e.g. lichenometry and radiocarbon dating. A fifth category covers all data points for which the method is unknown.

2.2.2 Additional information

As can be seen in the examples of the glacier length records in Figure 2.1, there are hardly any records with annual resolution from the first to the last data point. In order to get annual values for the entire period covered by the record, All records are interpolated with Stineman interpolation [*Stineman*, 1980; *Johannesson et al.*, 2009]. The interpolated values are calculated from the values of the data points and the slopes at the given points. The slope at

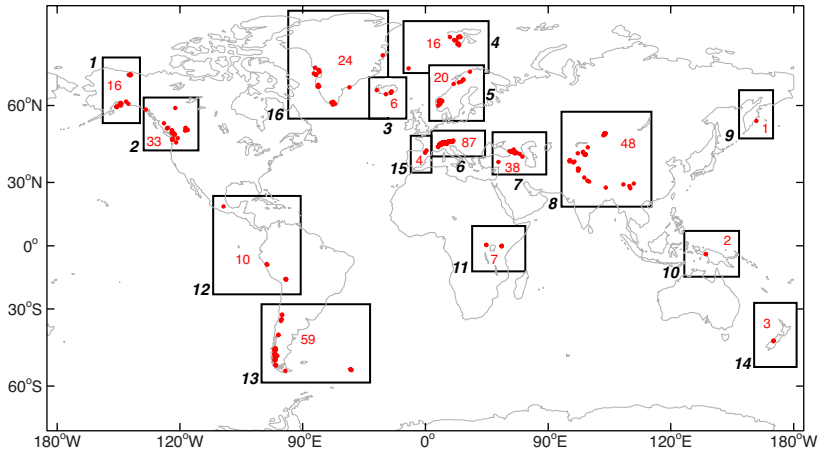

Figure 2.2: *Distribution of records over the world. In many cases the distance between the glaciers is so small that the dots overlap. The boxes indicate the 16 regions, the red number inside the box gives the number of records in the region, the black number outside the box gives the number of the region (cf. Table 2.1).*

a point is calculated from the circle passing through the point itself, and the point before and the point after it. This method works well for series with uneven spacing between the data points, as is the case with the glacier length records. Moreover, it has the advantage that it produces no spurious minima or maxima not prescribed by the data.

Besides the length record, additional information of the glaciers is included in the data set. Included are: the glacier name; the maximum, minimum and, if available, the median elevations; the length of the main flowline in reference year 1950; the glacier area; the glacier position in latitude-longitude; and the average annual precipitation on the glacier.

The data on the glacier geometry and position are in general available from either the same source as the length changes, or from the WGMS and the World Glacier Inventory [*National Snow and Ice Data Center*, 1999, update 2009, http://nsidc.org/data/g01130.html]. The latitude and longitude are given in degrees with a precision of two decimals, but they are not always very accurate. The geometry of a glacier changes in time and measurements are made in different years for different glaciers. For the glacier length this is taken into account. For all glaciers, the glacier length in 1950 (L_{1950}) is calculated from the measured glacier length and the length change between 1950 and the year of measurement. If the record has no data point in 1950, the length change in 1950 is calculated from the interpolated length record. The glacier area is not adjusted.

For the precipitation, we use the climatological annual precipitation at the mean altitude of the glacier. When in situ measurements are lacking, values are estimated from climatologies [e.g. *Zuo and Oerlemans*, 1997a] or nearby weather stations. The majority of the weather stations

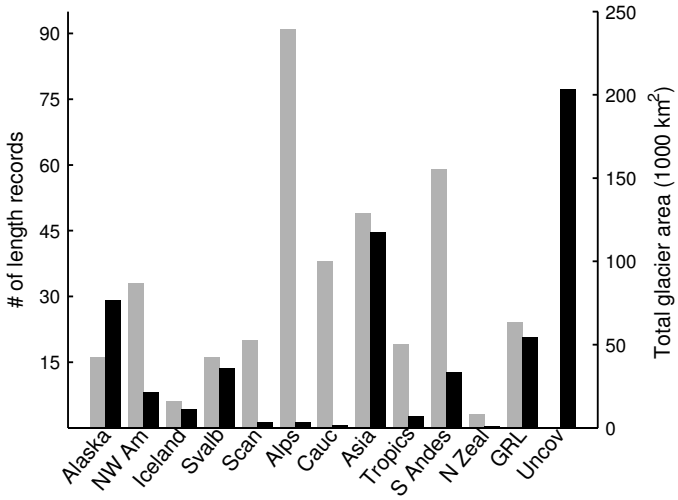

Figure 2.3: *Number of glacier length records per region (grey) vs the total area covered by ice in this region, as given by Radić and Hock [2010] (black). The regions correspond to Figure 2.2 and Table 2.1, except for the regions:* Alps*, to which the* Pyrenees *were added;* Asia*, where regions 8 and 9 are merged; and* Tropics*, where regions 10–12 are merged.* Uncov *gives the glacier-covered area in the Canadian and Russian arctic (regions 4, 5 , 6 and 12 in Radić and Hock [2010]), which is not represented in the glacier length data set. The area of local glaciers on Antarctica is not included in this Figure. Estimates vary between 131000 and 169000 km^2 and should be added to the* Uncov *area.*

are situated at lower elevations than the elevation of the glacier. Therefore, an estimate of the surplus precipitation at the glacier altitude is added to the measurements.

2.3 Data set descriptives

2.3.1 Spatial and temporal coverage

Figure 2.2 shows the global distribution of the 374 glacier length records. Records can be found on all continents and virtually all latitudes. The records are, not surprisingly, strongly clustered in the major mountainous regions. The glacier length records are divided into 16 regions (Figure 2.2, Table 2.1). The data set covers many of the glacierised regions on earth. However, there are relatively few records from regions where much ice is found (Alaska, islands of the Arctic Ocean, Antarctica). There are no records from Antarctica or the Arctic regions of Canada and Russia. In contrast, southern Europe (Pyrenees, Alps, Caucasus) has many records. This point is further illustrated in Figure 2.3, where we have compared the global distribution of the records with the distribution of the area covered by glaciers.

The glacier area is taken from *Radić and Hock* [2010], who give the global area covered by glaciers and ice caps distributed over 19 regions. The two data sets can be matched by combining some of the regions. The local glaciers on Antarctica are excluded; there are no records in Antarctica and there are different values for the area of local glaciers in Antarctica in the literature [cf. *Hock et al.*, 2009]. European glaciers (in Scandinavia, Alps, and Caucasus) are very well represented in the data set, while these regions contain only a small fraction of the global glacier area. Also the tropics, North West America, and the southern Andes are overrepresented in terms of their relative glacier-covered area. A substantial part of the global glaciers is not represented by the length change data set. This is due to the lack of glacier length records in the Russian and Canadian arctic.

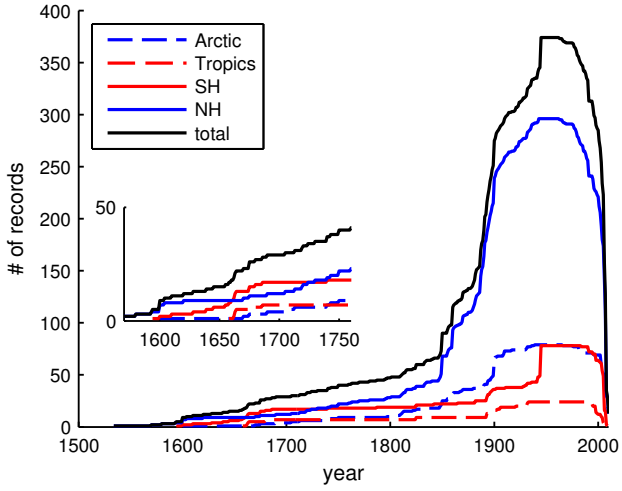

Figure 2.4: *Total number of glacier length records in time (black); number of records on the Southern Hemisphere (red) and Northern Hemisphere (blue). The number of records in the tropics (30°S – 30°N) and the arctic (≥ 60°N) are given in dashed red and blue, respectively. The inset enlarges the period 1570–1760.*

As shown by the record examples (Figure 2.1), there is a large variety in the length of the different records. Consequently, the number of available records changes strongly in time, as shown in Figure 2.4. The majority of the records starts in the 19th century. This leads to a sharp increase in the available number of records from 90 in 1850 to 275 in 1900. Going further back in time, the number of records decreases. Only 29 records start before 1700, and none go further back then 1534. The maximum of 374 records is reached between 1945, when the first aerial photography of the Patagonian Ice Fields became available [*López et al.*, 2010], and 1962. After 1962 the number of records decreases again. A few times, a record ends because of the (nearly) disappearance of the glacier. More often, more recent data are

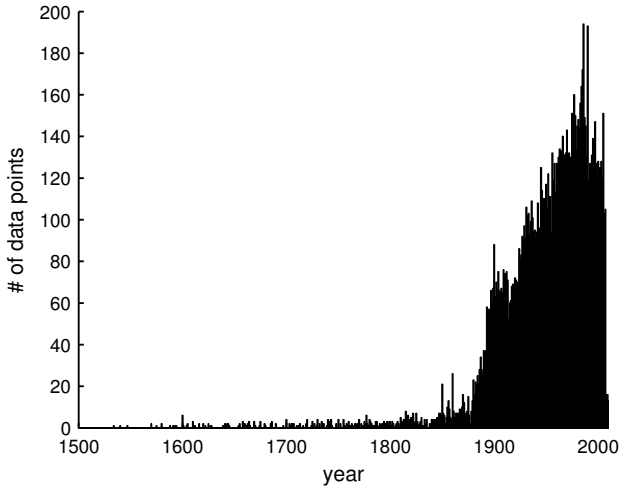

Figure 2.5: *Number of glacier length data points for each year in the period 1500–2010.*

not available because measurements are not continued or not reported. In 1990, many of the records in the former Soviet Union end, which leads to a notable drop of the available records. Of the 374 records, 285 continue up to 2000 at least, and 223 up to 2005.

Figure 2.4 also shows that prior to 1750 the number of available records on the Southern Hemisphere (SH) is comparable to that on the Northern Hemisphere (NH), although the total of records in the data set on the NH is much larger. During the 20th century, there is an appreciable number of records in the arctic ($\geq$60 °N). However, prior to the mid-19th century information is limited, especially in view of the relatively large part of the global ice-covered area located at these high latitudes. Despite the limited amount of glacier covered area in the Tropics, a substantial number of long records is available. Some owing to the reports of early explorers, others to the dating of numerous terminal moraines [*Rabatel et al.*, 2008].

Going back in time, not only the number of records decreases. Also the resolution of the remaining records becomes lower, as can be seen from the examples in Figure 2.1. Several length records in regions like Iceland, Norway, the Alps, and New Zealand have annual resolution in the 20th century. Before 1880, no record has annual data. In this period, length changes are mostly based on reconstructions rather than measurements. For European glaciers there is plenty of historical information, resulting in some detailed records [e.g. *Zumbühl*, 1980; *Nussbaumer et al.*, 2007, 2011]. But most records have sparse data before 1900. From 1900 onwards, there is more information available worldwide, which is evident from Figure 2.5. Whereas before 1800 the number of available glacier length data points in one year never exceeds 6, this number sharply increases around 1900, peaking at 194 in 1986.

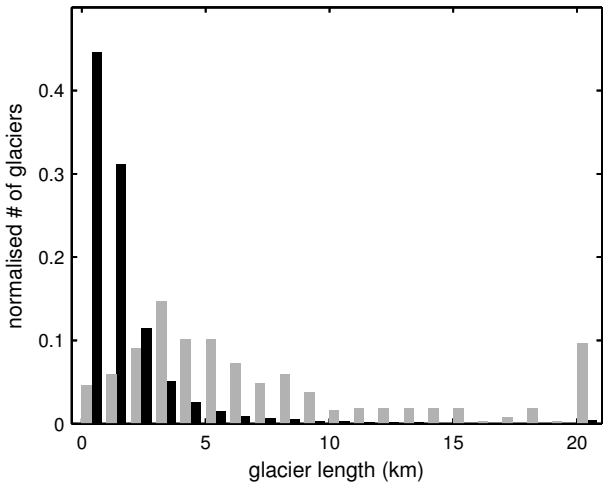

Figure 2.6: *Normalised distribution of glacier length in the glacier length fluctuations data set (grey) and the WGI-XF (black). The right-most bar of both data sets gives the number of glaciers with a length larger than 20 km.*

In Figure 2.6 the normalised distribution of glacier length (L_{1950}) of the glaciers in the glacier length change data set is shown. Most of the glaciers are relatively small, 44% of the glaciers are shorter than 5 km, but the data set also contains several large glaciers: almost 10% of the glaciers is longer than 20 km. Compared to the length distribution of glaciers in the extended format of the World Glacier Inventory (WGI-XF) [*Cogley*, 2009b], the glacier length data set has a bias toward larger (longer) glaciers. At present, the WGI-XF is the most complete glacier inventory, and it contains the glacier length of more than 70,000 glaciers world wide. Of the glaciers in the WGI-XF, 95% is shorter than 5 km and only 0.36 % is larger than 20 km. Apparently, the length fluctuations of the larger glaciers are observed and reconstructed. This is comparable with the available glacier mass balance measurements [*Cogley and Adams*, 1998].

2.3.2 Glacier length changes

Figure 2.7 shows the average rate of length change of all glaciers in the data set for six 40-year periods between 1760–2000. In the periods 1760–1800 and 1801–1840, moderate retreats and advances occur to nearly the same extent. Since the middle of the 19th century, there is a global retreat of glaciers. The number of advancing glaciers is much smaller than the number of retreating glaciers, as indicated by the moderately to strongly negative median

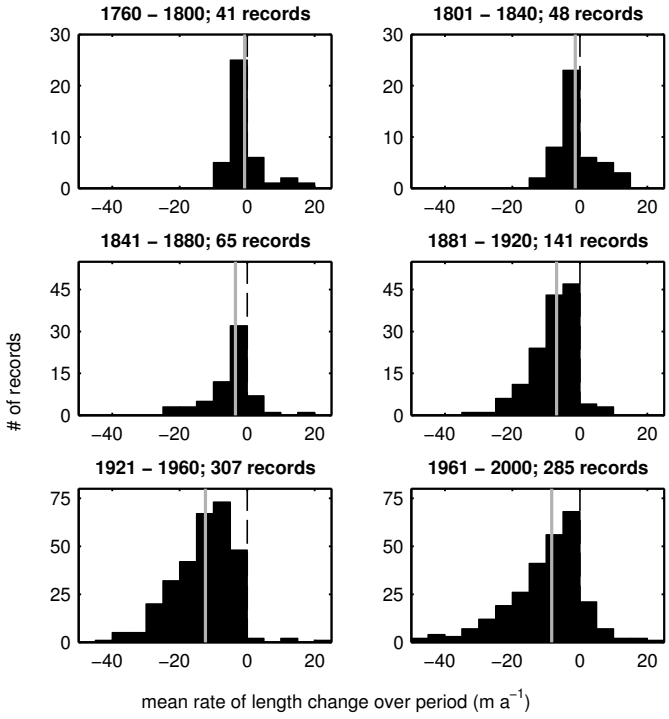

Figure 2.7: *Mean rate of length change (m a^{-1}) of the available glacier length records for six 40-year periods between 1760 and 2000. The median rate of length change of all glaciers in that period is given by a grey line. Note the changing number of glacier length records for the different periods.*

glacier length change. The global retreat is strongest in the period 1921–1960, with a median retreat rate of 12.6 ma^{-1}.

The response of glaciers to changes in climate depends on its climatic setting and the glacier geometry [*Oerlemans*, 2001]. According to the theory, the surface slope of the glacier is the most important geometrical factor: steep glaciers are less sensitive to climate change than flat glaciers (see the simple model results in Chapter 1.2.6). This is supported by the observed glacier length changes in our data set. Figure 2.8 shows the 20th century glacier length change of all glaciers in the data set that cover this period as a function of the mean slope. The spread is large, as glacier slope is not the only relevant parameter, but it is clear that there is a relation between slope and retreat. A large retreat is rare for steep glaciers.

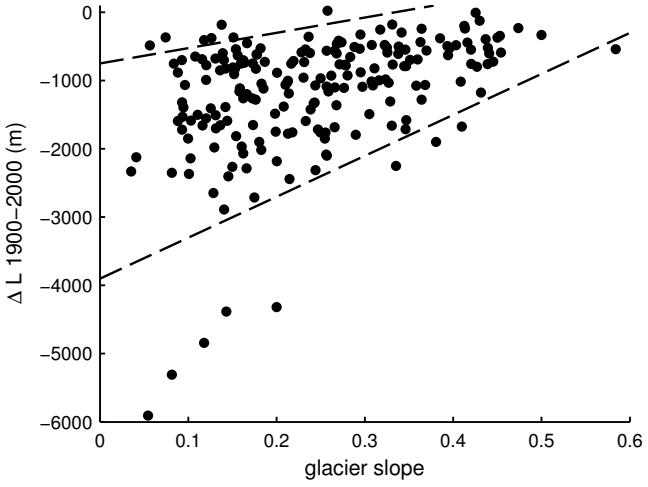

Figure 2.8: *Glacier length change (m) over the period 1900–2000 as a function of the mean slope* $(h_{\max} - h_{\min})/L_{1950}$ *of the glacier. The length change is only shown for the 211 records that entirely cover the period 1900–2000. 92% of the points lie in between the dashed lines.*

2.3.3 Regional differentiation

The origin of the records and the time evolution of the available records is different for each region (Figure 2.9, Table 2.1). Below, we will shortly discuss the most important regional characteristics of the data set.

There are no records with annual data in Alaska. The data set includes records from the arctic Brooks Ranges, as well as from glaciers along the southern coast. The records are mainly based on geomorphological reconstructions extended with some data points from maps, aerial photography, and satellite images since the mid- 20th century [e.g. *Wiles et al.*, 1999; *Evison et al.*, 1996]. Therefore, the average number of data points per record is relatively low, despite the fact that some of the records have considerable length.

There is a substantial amount of information from the Rocky and Coastal Mountains in North-West America. There are quite a few ongoing measurement programs and recent updates [e.g. *Koutnik*, 2009; *Koch et al.*, 2009], However, not all records in this region are up to date. Half of the records ends between 1965 and 1985. On average, the records in this region end earlier than the records in any other region of the data set (Table 2.1).

Annual measurements throughout the 20th century exist in Iceland, the Alps, Scandinavia, and New Zealand [*WGMS*, 2008 and earlier volumes; *Sigurðsson*, 1998; *Andreassen et al.*, 2005]. These regions have a high resolution characterized by the high average number of data

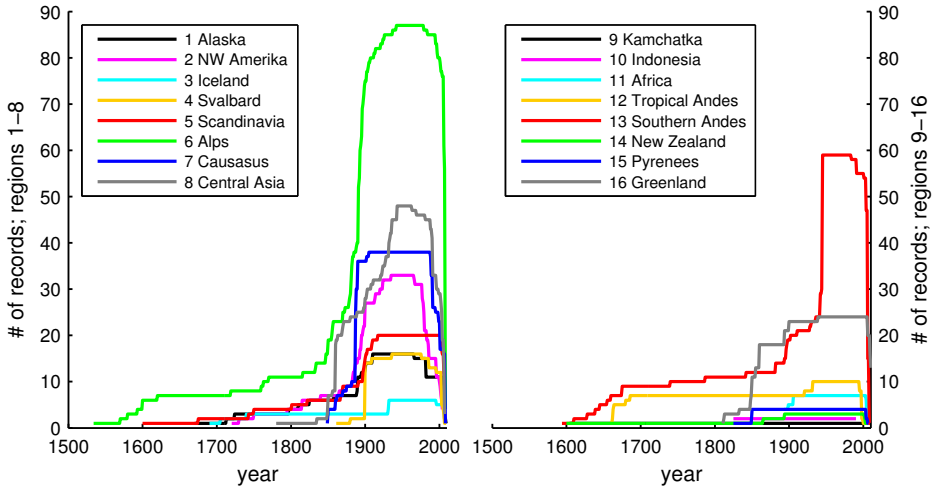

Figure 2.9: *Number of available glacier length records per region in time. The 16 regions are shown in two figures for clarity.*

points per record. For the Alps and Scandinavia, there are also records with a high resolution prior to the 20th century, owing to the large amount of available historical information in these regions [e.g. *Zumbühl*, 1980; *Zumbühl and Holzhauser*, 1988; *Nussbaumer et al.*, 2007, 2011]. The Alps have by far the most length records, but prior to 1800 the number of available records is comparable to the regions in South America.

The Caucasus has records that are fairly detailed with regular measurements since the Geophysical Year 1957 and additions from earlier historical sources as for example military maps from the 19th century [*Panov*, 1993]. The region includes one record from Turkey [*Sarikaya et al.*, 2009]. In Central Asia the number of records is limited compared to the large glacierization of the Himalayas, Tien Shan, Pamirs, Altai, and other mountain ranges. Also the covered period in time is limited in this region. Most of the records start after 1850 and the longest record does not start until 1780. Kamchatka is a region with only one record [*Sawaguchi et al.*, 1999]. However, this record is long (396 year) and relatively detailed.

In the tropical part of the Andes, several very long glacier length records are available from the lichenometric dating of moraines [*Rabatel et al.*, 2005, 2006]. In the other tropical regions the information on length changes does not extend this far back in time. The records in Africa all start around the beginning of the 20th century [*Hastenrath*, 1983; *Taylor et al.*, 2006]. The two records in Indonesia start both in 1825 when they where described in an expedition report [*Williams Jr. and Ferrigno*, 1989].

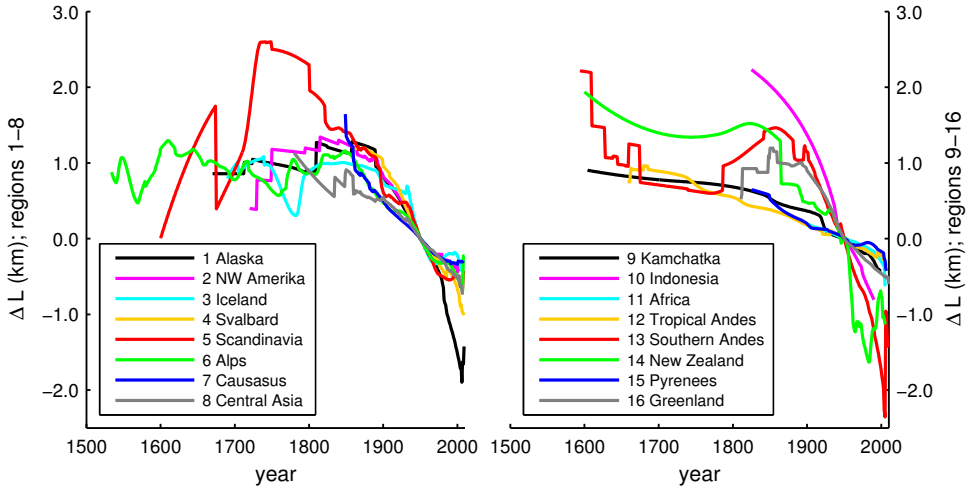

Figure 2.10: *Regional glacier length change in time. For each region, the length change relative to L_{1950} is averaged over the available records. Frequently, the averages have jumps when a new record starts. In the 20$^{\text{th}}$ century most regional averages are smooth because the number of available records is larger (cf. Figure 2.9).*

Reconstructions of glacier length fluctuations have led to several long records in the southern Andes [e.g. *Villalba et al.*, 1990; *Koch and Kilian*, 2005; *Araneda et al.*, 2007; *Masiokas et al.*, 2009a]. This region even has the largest number of available records around 1700. However, the reconstructions are generally not very detailed. The number of records in the southern Andes more than doubles in 1945. In this year, aerial photographs of the Patagonian Icefields were made [*López et al.*, 2010] and a great number of outlet glaciers of the Patagonian Icefields is included in the data set.

The majority of the records in Greenland come from south and west Greenland, where historical information from the 19th century is available [*Weidick*, 1968; *Yde and Knudsen*, 2007]. Nineteen records from *Weidick* [1968] have been extended with Landsat images. In addition, there are two records from the eastern part of Greenland [*Hynek et al.*, 2009; *Mernild et al.*, 2011]. In Svalbard, less historical information is available. The longest record of Svalbard starts in 1861. Most of the records start around 1900, when the end of the Little Ice Age is timed for this region [e.g. *Rachlewicz et al.*, 2007].

In Figure 2.10 the regional averages of the glacier length records are given. As could be expected from the variety of glaciers in the data set, there is a large variability in the historical length changes. Before 1850 there are frequent jumps in the regional length change when a new record enters the regional sample. After 1850 the samples are larger and the average length curves are rather smooth. The regions Alaska, South America and New Zealand show

	region	number of records	# data points per record	start year average (range)	end year average (range)
1	Alaska	16	9	1842 (1670-1910)	1997 (1965-2009)
2	Rocky Mountains	33	20	1873 (1720-1935)	1988 (1965-2004)
3	Iceland	6	65	1822 (1690-1932)	2004 (1995-2007)
4	Svalbard	16	7	1899 (1861-1936)	1999 (1975-2009)
5	Scandinavia	20	70	1846 (1600-1917)	2006 (2002-2009)
6	Alps	87	93	1856 (1534-1942)	2005 (1978-2009)
7	Causasus	38	22	1882 (1849-1905)	1999 (1987-2008)
8	Central Asia	48	13	1889 (1780-1943)	1998 (1962-2007)
9	Kamchatka	1	17	1604 (1604-1604)	2000 (2000-2000)
10	Indonesia	2	8	1825 (1825-1825)	1990 (1990-1990)
11	Africa	7	10	1898 (1893-1906)	2004 (2003-2005)
12	Tropical Andes	10	13	1746 (1658-1932)	1998 (1994-2008)
13	Southern Andes	59	7	1882 (1594-1945)	2004 (1983-2009)
14	New Zealand	3	68	1786 (1600-1894)	2003 (2001-2005)
15	Pyrenees	4	26	1844 (1825-1850)	2004 (2003-2007)
16	Greenland	24	10	1860 (1811-1939)	2009 (2005-2010)
	Global	374	36	1865 (1534-1945)	2001 (1962-2010)

Table 2.1: *Characteristics of the glacier length records per region. The numbers of the regions correspond to the numbers in Figure 2.2. Given are: the total number of length records in the region, the regional average number of data points per record, the average year in which the records start (with the range of years in which the records of the region start) and the year the records of the region on average end (again with the range).*

a large retreat compared with the other regions since 1950. Alaska and South America include several large tidewater glaciers that have shown a pronounced retreat. The New Zealand average is dominated by the large fluctuations of Frans Jozef glacier. Furthermore, the two relatively small tropical glaciers in Indonesia have shown the largest retreat since the mid-19th century relative to their size. At present they have almost disappeared. Despite the regional characteristics, the regional averaged length changes show a remarkable coherency. A global glacier retreat started around the middle of the 19th century and continues up to the present.

2.4 Concluding summary

Records of historical glacier length fluctuations can provide insight in long-term glacier dynamics and the relation between glacier fluctuations and climate change. However, it is not straightforward to get an overview of the global signal before the start of the measurement era in the late 19th century. We have presented a data set of world-wide glacier length fluctuations, which combines measurements with all kinds of glacier length reconstructions. The data set contains the glacier length records of 374 glaciers and it covers the period 1534–2010.

Only records starting prior to 1950 and covering several decades are included. Records of glacier length changes that are known to be strongly influenced by other causes than climate change, such as glacier surges, are excluded. However, some calving glaciers are included. The data set has global coverage. There are glacier length records from all continents, except for Antarctica, and on virtually all latitudes. Unfortunately, there are no records from the Russian and Canadian Arctic, where a large fraction of the global ice-covered area is found. The number of available records is strongly time-dependent. The number of available records is very limited in the early 17th century and there is no rapid increase until the mid-19th century.

Besides glacier length change, information on the method of data acquisition of each data point is added to the dataset. There is a large variety in measurement and reconstruction methods, divided in 4 categories: *i)* measurements, *ii)* reconstruction on historical evidence, *iii)* reconstruction with dendrochronological dating, *iv)* reconstruction based on other methods. Furthermore, the location and geometrical characteristics of the glacier are included: latitude; longitude; maximum, median and minimum altitude; length; area; and annual precipitation.

The glacier length records show a coherent global glacier signal, with, in general, little length change in the 17th to mid-19th century, followed by a general retreat, that continued throughout the 20th century. The observed retreat over the 20th century confirms that steep glaciers are less sensitive to climatic change than glaciers with a gentle slope.

The data set is available online (www.staff.science.uu.nl/∼lecle102/data) and data will be submitted to the WGMS.

3

Climate reconstruction from the glacier length record of Glaciar Frías, North Patagonia

Summary

We explore the climatic information contained in the record of length fluctuations of Glaciar Frías, in the north Patagonian Andes of Argentina. This record is one of the longest and most detailed glacier records in southern South America, starting in 1639. In order to interpret the length variations of Glaciar Frías since the maximum Little Ice Age extent in 1639, we use a combination of a simplified surface energy-balance model to calculate the glacier mass balance, and a flow-line model to account for the dynamical response of the glacier to changes in the climatic forcing. The overall retreat of the glacier observed over 1639–2009 is best explained by an annual mean temperature increase of 1.16 °C or a decrease in annual precipitation of 34%, most of which would have occurred during the 20th century. The glacier model is also forced with independent proxy-based reconstructions of precipitation and temperature, based on tree rings and a composition of documentary evidence, tree rings, sediments, corals, and ice cores. The uncertainties in the presently available proxy reconstructions are rather large, leading to a wide range in the modelled glacier length. Most of the observations lie within this range. However, in these reconstructions, the mid-17th century is too cold and the early 19th century ca. 0.7 °C too warm to explain the observed glacier lengths.

This Chapter is based on P.W. Leclercq, P. Pitte, R. H. Giesen, M. H. Masiokas, J. Oerlemans, Climatic interpretation of the length fluctuations of Glaciar Frías, North Patagonia, Argentina, *submitted to* Climate of the Past.

3.1 Introduction

To understand current climate variability and make reliable predictions of future climate change, knowledge of the past climate is needed. As instrumental measurement series have limited length, this requires the use of proxy-based information. This is especially the case in southern South America, where long instrumental records of good quality are scarce and mostly limited to lowland, populated areas in Chile and Argentina [*Rosenblüth et al.*, 1997]. Most of the available proxies in southern South America are based on dendrochronological records, where the climate-dependent rate of growth is measured from annual tree ring properties (e.g. ring width and density, see *Boninsegna et al.* [2009] for an overview). There are, however, other climate proxies. Exploiting as many independent sources as possible, increases the reliability of the resulting climate reconstructions. Recently, *Neukom et al.* [2010] and *Neukom et al.* [2011] have developed a gridded dataset of precipitation and temperature anomalies in southern South America, using a combination of different climate proxies. In addition to reconstructions based on Andean tree rings, they include a variety of other proxies, such as documentary evidence, ice-cores, and corals. However, the climatic information that can be derived from observed glacier length fluctuations in South America has not yet been fully exploited. So far, this information of glacier fluctuations in southern South America has only been used qualitatively [e.g. *Harrison et al.*, 2007; *Neukom et al.*, 2011].

Usually, the high-resolution, proxy-based climate reconstructions depend on transfer functions derived from correlations with observational data. One of the benefits of this approach is that the records allow for a proper statistical calibration and verification of the models used to develop the climate reconstructions. However, this type of reconstructions has various limitations inherent to the series available. For example, for tree-ring chronologies the capacity of capturing long-term (i.e. centennial scale) climate variability, is limited by the length of the original tree-ring series and by the process of standardisation intended to remove the biological trends in the records [*Cook and Kairiukstis*, 1990]. Uncertainty in the validity of the transfer function over the entire period of reconstruction and the decrease of low frequency variability, lead to increasing uncertainties in the long term trends of reconstructed temperature and precipitation records [e.g. *Briffa et al.*, 1998, 2001; *Esper et al.*, 2002].

Information of glacier fluctuations can provide valuable complementary climatic information over the past centuries. Fluctuations in climate cause changes in the accumulation (snowfall) and ablation (melt) of a glacier, and thus affect the glacier mass budget. In turn, fluctuations in a glacier's mass budget lead to dynamical adjustment of the glacier geometry. The interaction between glaciers and climate is well understood, and can be described using physical relations [e.g. *Oerlemans*, 2001; *Cook et al.*, 2003; *Hock and Holmgren*, 2005; *Rye et al.*, 2010; *Giesen and Oerlemans*, 2010]. Therefore, we are not dependent on empirical transfer functions when we use glacier fluctuations as a climate proxy. Despite the lower temporal resolution inherent to the response time of glaciers to climate change, past glacier fluctuations

thus form a valuable climate proxy to complement existing temperature and precipitation reconstructions.

On centennial timescales, length fluctuations are generally the only known glacier variable. Combinations of documentary and geomorphological information has lead to high resolution glacier length records [e.g. *Zumbühl and Holzhauser*, 1988; *Nussbaumer et al.*, 2011]. However, the historical evidence available for the southern part of the Andes is far less extensive than for Europe. In this context, the length record of Glaciar Frías, in the Monte Tronador area in northern Patagonia is a fairly detailed, long glacier length record [*Villalba et al.*, 1990; *Masiokas et al.*, 2009b]. In this study, we exploit this glacier length record by extracting information of the North Patagonian climate over the past four centuries.

Glacier length changes have been used previously to reconstruct large-scale temperature fluctuations, by analysing a large sample of glacier length records with a simple glacier model [*Oerlemans*, 2005; *Leclercq and Oerlemans*, 2011]. This approach cannot be used for individual glaciers. The influence of precipitation variations cannot be neglected locally, and the simple model, although valid for the mean of a larger sample, is likely to perform poorly for an individual glacier. In order to study the response of Glaciar Frías to climatic changes during the last four centuries, we have modelled its dynamic response using a coupled glacier mass balance – ice dynamical model.

In the next Section, we will describe the general setting of Glaciar Frías and the available information for driving and calibrating the glacier model. This model has two components: the first one calculating the surface mass balance from temperature and precipitation, and the second describing the ice-flow dynamics of the glacier. Section 3.3 gives a description of both components. In Section 3.4, we discuss the characteristics of Glaciar Frías derived from a steady-state run with modern climate. We then use the glacier model to extract the climatic information from the historical length record. First directly, by using dynamic calibration of the mass balance [*Oerlemans*, 1997a]. Secondly, we force the glacier model with existing proxy climate records from this region. Comparing the resulting modelled glacier length with the observed glacier fluctuations gives an idea of the accuracy of the existing proxies. To conclude, we study the behaviour of Glaciar Frías under the projected climate change of the 21st century.

3.2 Data

3.2.1 Study site

Glaciar Frías (41.15 °S, 71.83 °W) is located on the north east face of Monte Tronador, a 3448 m high peak on the Chilean–Argentinean border in the north Patagonian Andes (Figure 3.1). The climate of Glaciar Frías is temperate maritime, with prevailing westerlies and large amounts of precipitation, predominantly in winter [*Villalba et al.*, 1990; *Brock et al.*, 2007].

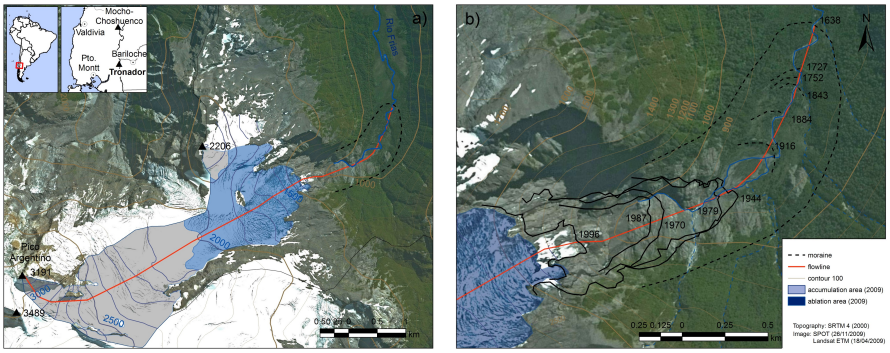

Figure 3.1: ***a)*** *Topography of Glaciar Frías, flowing from the Argentinean summit on the northern slopes of Monte Tronador. The accumulation and ablation area of Glaciar Frías (2009) are indicated with grey and blue shading, repectively. The central flowline is given in red, and altitude in 100 m contour lines. The location of Monte Tronador is shown in the insets.* ***b)*** *Close-up of the glacier forefield with the observed and reconstructed glacier terminus positions. For clarity, not all observations are included.*

The Patagonian Andes form an effective north–south barrier to the westerlies. Hence, the region is characterized by a large east–west precipitation gradient, with over 2 m of precipitation on the western side and less than 1 m on the eastern side [*Villalba et al.*, 2003].

Monte Tronador has several glaciers on the Chilean as well as on the Argentinean side. These glaciers have shown a general pattern of recession since the Little Ice Age (LIA) maximum, identified in this area between the 17th and the 19th centuries [*Villalba et al.*, 1990; *Masiokas et al.*, 2010]. Glaciar Casa Pangue has retreated 1938 m in the period 1911–2000 [*WGMS*, 2008 and earlier volumes] and the surface of its lower ablation area has thinned with 2.3 $\pm$ 0.6 m a^{-1} on average between 1961 and 1998 [*Bown and Rivera*, 2007]. Likewise, the regenerated portions of Glaciar Castaño Overo and the Glaciar Río Manso have retreated noticeably over the last decades [*WGMS*, 2008 and earlier volumes; *Masiokas et al.*, 2010].

Glaciar Frías has also substantially retreated over the 20th century (Figure 3.9). Between 1916 and 2009 the glacier terminus retreated 1.9 km. The fluctuations of Glaciar Frías have been reconstructed for the last four centuries from dendro-geomorphological, historical and field evidence [*Villalba et al.*, 1990]. The glacier flows into the Frías valley, and the historical position of the tongue was well below the tree line. This made it possible to reconstruct the length variations back to 1639, by dendrochronological dating of moraines [*Villalba et al.*, 1990]. In addition, there exist several historical sources since the mid-19th century, and field measurements from 1976 to 1985. For this study, the existing length record was revised and the length record has been extended using aerial photography and satellite images (Figure 3.9, Table 3.2). At present, the length record of Glaciar Frías is the most detailed long record of South America [see *Masiokas et al.*, 2009b, for an overview of glacier length observations

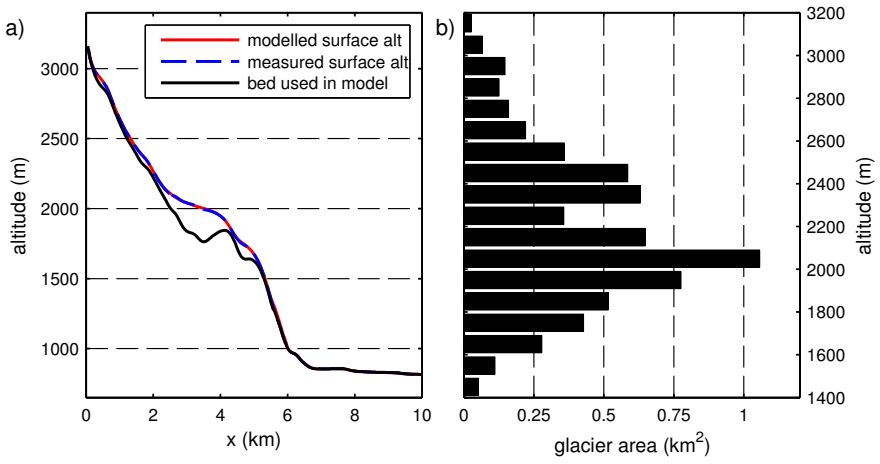

Figure 3.2: ***a)*** *Bed altitude along the glacier flow line (black) from the DEM. For* $0 < x < 5.7$ *km the DEM gives the ice surface altitude instead of the bed altitude. Here, the bed profile is determined with the ice flow model. The modelled glacier surface (red) differs less than 10 m from the measured surface altitude (dashed blue) (except for* $5.7<x<6.00$ *km, where there is ice in the model run, whereas in 2000 the terminus was at* $x \approx 5.7$ *km).* ***b)*** *Elevation distribution of the present-day glacier area in 100 m intervals.*

in South America]. In addition, Frías glacier has no extensive debris cover, calving at the terminus, or surges. This makes the Frías glacier well suited for climate reconstruction, as it is free of glaciological processes that may complicate the interpretation of the length fluctuations in terms of climatic change.

Because of the diversity of methods used in the determination of the glacier length changes, the length record has a variety of uncertainties. The glacier outlines from satellite images and aerial photos have an exact date, and an uncertainty in derived glacier length is estimated to be 10–50 m, i.e. 2 pixels, to account for rectification and interpretation errors. The field measurements were carried out yearly at unspecified dates, and are considered to be accurate within 10 m. They are connected to the record with the frontal position in 1979 taken from a Corona satellite image. The dates of the historical sources are also well known, up to the year, but the spatial uncertainty can be large, especially of the 1856 etch (accuracy taken to be $\pm$ 150 m). The positions of the dated moraines are well known (within 50 m) but the dating has an uncertainty in the determined age of the trees and in the estimated time of seedling establishment [*Luckman*, 2000]. *Villalba et al.* [1990] give an uncertainty of 20 years for the dating in the Frías valley.

The geometry of Glaciar Frías has been derived from a 2009 SPOT 5 image (Table 3.2), in combination with the SRTM v.4 digital elevation model (DEM) from 2000. In 2009, the

glacier had an area of 6.54 km^2 and was 5.55 km long, flowing from the Argentinean summit of Monte Tronador at 3191 m down to 1450 m. The glacier surface is rather steep, with a mean slope of 0.32, but it has a more gentle slope around 2000 m (Figure 3.2a). The glacier hypsometry is shown in Figure 3.2b. A large part of the area is in the 2000–2200 m range, with a much narrower accumulation area above 2600 m. The present-day glacier tongue as well as the historical glacier tongue are also relatively narrow (Figure 3.1).

In our dynamical model (section 3.3.2) we use the central flowline and we parameterise the lateral glacier geometry with a trapezoidal cross section. The central flowline is determined from the DEM and corrected by visual inspection. The width of the valley floor and the slope of the valley walls are derived from 25 cross sections.

3.2.2 Meteorological and glacier mass balance data

Unfortunately, the amount of glaciological and meteorological information available for the Glaciar Frías area is scarce. No mass balance measurements are available for Tronador glaciers and meteorological records are either short, low resolution, or distant from the study site. Based on short term precipitation measurements made in the late 1950's, *Gallopin* [1978] estimated that annual precipitation in the accumulation area of Monte Tronador is between 4.5 and 7 ma^{-1}.

For two other glaciers in the Chilean Lake District, with a climate comparable to Glaciar Frías, glacier mass balances have been measured. *Rivera et al.* [2005] and *Bown et al.* [2007] describe glaciological mass balance measurements (stakes and snow density measurements) collected during the two hydrological years 2003/2004 and 2004/2005 on the southeastern glacier at Volcán Mocho-Choshuenco. This volcano is inactive since 1864 and lies 130 km north of Glaciar Frías (Figure 3.1). The ELA of this glacier lies between 1950 and 2000 m. The winter balance at 2000 m varied between 2.9 and 4 m w.e. a^{-1}, and a large mass balance gradient of 0.015 m w.e. $a^{-1}m^{-1}$ was measured. *Brock et al.* [2007] have operated an automatic weather station (AWS) during several periods in 2004 and 2005 on the Pichillancahue-Turbio glacier on the active Volcán Villarica, 190 km north of Glaciar Frías (Figure 3.1). Due to the volcanic activity of Volcán Villarica, the mass balance of this glacier is strongly influenced by tephra covering the surface. Therefore, these measurements of the surface energy balance are not directly applicable to the mass balance of Frías glacier. However, *Brock et al.* [2007] present several results of interest for this study: they measured significant melt events at the ELA during the accumulation season caused by high air temperatures, and they confirm the high accumulation and melt rates found by *Rivera et al.* [2005] and *Bown et al.* [2007]. In a reconstruction of the ELA of glaciers along the Andes of South America from a compilation of 0 °C isotherm altitude and precipitation, *Condom et al.* [2007] give an ELA between 1800 and 2200 m for the region of Glaciar Frías. *Carrasco et al.* [2008] also give a similar value from improvements of the relations used by *Condom et al.* [2007] for the southern Andes.

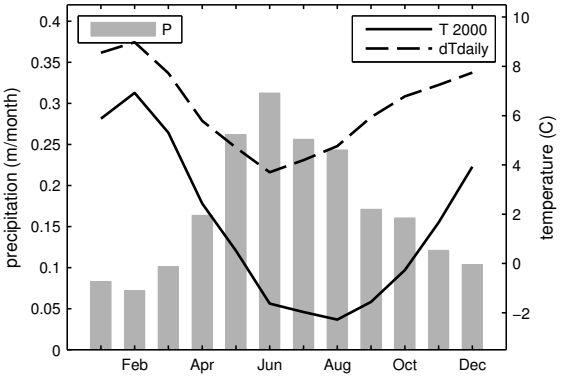

Figure 3.3: *1980-2009 climatology of Glaciar Frías, from a combination of ERA-40 and ERA-interim data. Shown are the meteorological parameters needed for the mass balance model: monthly average temperature at 2000 m (black), and amplitude of the daily cycle (dashed black), and average monthly sum of precipitation at 850 m (grey bars).*

The meteorological stations nearest to Glaciar Frías with long, complete, temperature data are Bariloche at 55 km to the east and Puerto Montt at 100 km to the west (Figure 3.1). At Puerto Montt, radio-sonde measurements are performed once or twice a day, but the record has a considerable amount of missing data. Long, complete precipitation measurements from sites close to the Glaciar Frías are also not available. The existing precipitation measurements show a very large precipitation gradient over the Andes [*Villalba et al.*, 2003]. The station of Punta Huano, located 35 km west of Glaciar Frías at 200m altitude, has an average of 3.2 ma^{-1} over the 10 years of precipitation measurements in the period 1969–1980, whereas at Bariloche, on the eastern side of the Andes, an average annual precipitation of 0.88 m is measured over the period 1931–2009.

Because of the lack of nearby weather stations with long and detailed records, we use ERA-interim reanalysis data (1 January 1989 – 18 December 2010; 0.75° resolution) [*Simmons et al.*, 2006] to force the mass balance model. The ERA-interim data are extended with ERA-40 reanalysis data (ECMWF Re-Analysis, 1 September 1957 – 1 September 2002; 1.125° resolution) for the period 1 January 1980 – 31 December 1988. Although ERA-40 is available from 1957, data for the mid and high latitudes on the Southern Hemisphere are not reliable in the presatellite era [*Bromwich and Fogt*, 2004]. The spatial resolution of the ERA reanalysis data is too low to adequately resolve the local weather on an individual mountain. Therefore, we are limited to a mass balance that is based on the climatology of the reanalysis. We calculate monthly averages of temperature at 2000 m, the lapse rate, and the amplitude of the daily cycle from the 6 hourly temperature values at the 4 grid points surrounding Glaciar

Frías. The lapse rate and 2000 m temperature are derived from a linear fit through the pressure levels between 900 hPa and 500 hPa (10 levels for ERA-interim, 4 for ERA-40). The precipitation is calculated from the sum of convective and large-scale precipitation given at the surface-level. For each month of the year, the climatological averages over the 1980–2009 period are calculated for each grid point and bilinearly interpolated to the location of Glaciar Frías (Figure 3.3).

The temperature climatologies at the four grid points are very similar, but the calculation of precipitation is more difficult. Because two of the four grid points used in the temperature calculation are located on the eastern side of the Andes, these give lower precipitation totals. As the glacier of our interest is on the water divide, where we expect the maximum precipitation, we only take the western grid points into account. Still, the ERA reanalysis precipitation of 2.05 ma^{-1} is much lower than is measured at Punta Huano station. This is probably due to the relatively low resolution of the ERA topography, as also the gradient in the ERA precipitation across the Andes is not as strong as derived from the measurements. For the input of the glacier mass balance model, described in the next section, we have increased the ERA precipitation with a factor 2.2, such that the modelled winter accumulation at 2000 m is in agreement with the measured winter accumulation of Mocho-Choshuenco. The relative distribution of the annual precipitation over the months in the ERA data is assumed to be correct.

3.2.3 Climate reconstructions for southern South America

For North Patagonia, several reconstructions of temperature [e.g. *Villalba et al.*, 1997, 2003] and precipitation [e.g. *Villalba et al.*, 1998; *Lara et al.*, 2008; *Boucher et al.*, 2011] exist. *Neukom et al.* [2010, 2011] have compiled a temperature and precipitation reconstruction for southern South America on a 0.5°x 0.5°grid from a selection of the available proxy records. In this study, we use the *Neukom et al.* [2010, 2011] and the *Villalba et al.* [2003] reconstructions to drive the glacier model, and then examine how well the observed glacier lengths are reproduced.

Neukom et al. [2011] provide gridded summer (DJF) and winter (JJA) temperature anomalies at yearly resolution for the periods 900–1995 and 1706–1995, respectively. As with the ERA reanalysis data, we use the values of the four grid points surrounding Glaciar Frías to compute the temperature anomalies with bilinear interpolation. Since the mass balance of Frías is sensitive to temperature perturbations in every month of the year (see Section 3.4.1), we apply the summer anomaly not only to the three summer months DJF, but to the summer half year November–April. Likewise, the winter anomaly is applied to May–October. In the period before 1706, when no winter temperatures are available, we apply the summer anomaly to the entire year. Winter and summer precipitation anomalies [*Neukom et al.*, 2010] are available for the period 1590–1995 and 1498–1995, respectively. Like with temperature, the precipitation anomalies of DJF are extended to the summer half year, and JJA precipitation anomalies to the winter half year, to get anomalies for every month of the year.

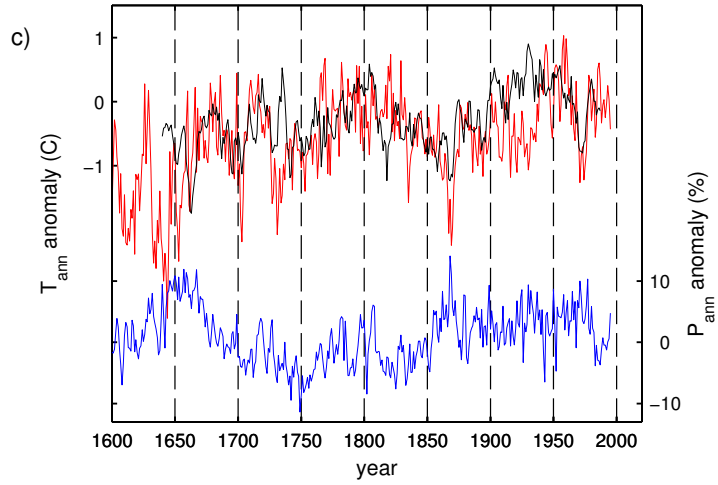

Figure 3.4: *Annual mean temperature anomaly of Neukom et al. [2011] (red) and Villalba et al. [2003] (black) w.r.t. 1980-2009 mean, and annual mean precipitation anomaly of Neukom et al. [2010] w.r.t. the 1600–1995 mean (blue).*

For additional comparison, we also drive the model with 1640–1987 tree-ring based annual temperature anomalies as reconstructed by *Villalba et al.* [2003] for the Monte Tronador region. The reconstructed temperature anomalies reflect the annual temperature anomalies [*Villalba et al.*, 2003]. These records are not used in the temperature reconstruction of *Neukom et al.* [2011]; the two temperature reconstructions are independent. For precipitation we again use the *Neukom et al.* [2010] reconstruction. Annual average temperature anomalies of both reconstructions and precipitation anomalies are shown in Figure 3.4.

3.3 Methods

3.3.1 Mass balance

The lack of mass balance and detailed meteorological measurements in the direct vicinity of Glaciar Frías makes it impossible to drive and validate a detailed surface energy balance model. In this study, a simple surface mass balance model is used to calculate the annual surface mass balance, following the approach of *Oerlemans* [2010], further extended in *Giesen and Oerlemans* [2011]. The model is driven with monthly averaged temperatures and monthly precipitation totals of the ERA reanalysis (Section 3.2.2). A concise description of the model is given below, for details we refer to *Giesen and Oerlemans* [2011].

The annual surface mass balance at a certain point on the glacier is given by

$$B = \int_{\text{year}} P_{\text{snow}} + (1-r)\min\left(0; -\frac{Q}{\rho_{\text{w}} L_{\text{f}}}\right) dt, \tag{3.1}$$

where P_{snow} (m w.e.) is the mass gained from solid precipitation and the mass loss is determined from the surface energy balance Q. Melt is assumed to occur when the surface energy balance is positive. Part r of the meltwater is allowed to refreeze in the snowpack. The constants ρ_{w} and L_{f} are the water density and latent heat of melt, respectively. The mass balance is calculated at hourly time steps.

Precipitation is assumed to increase linearly with altitude with lapse rate p (Table 3.1). Hourly precipitation is obtained by equally distributing the monthly total over all hourly timesteps of the month. Temperature is determined from the monthly mean temperatures and an additional daily cycle, with a monthly amplitude. Both the precipitation and the temperature lapse rate are constant throughout the year. Precipitation that falls at air temperatures below 1.5 °C is assumed to be solid P_{snow}.

Because humidity, cloudiness, and wind speed data are not available for the Frías glacier surface, the energy available for melt is calculated from a simplified representation of the surface energy balance that only requires temperature and solid precipitation as input. The surface energy is divided into the net solar radiative flux and a second term $\psi(T_{\text{a}})$, that represents all other atmospheric fluxes as a function of air temperature only:

$$Q = (1-\alpha)\tau S_{\text{in}} + \psi. \tag{3.2}$$

The net incoming short-wave radiation is calculated by multiplying the incoming solar radiation at the top of the atmosphere on a plane with the mean slope and aspect of Glaciar Frías (S_{in}), with the (constant) atmospheric transmissivity τ (Table 3.1). S_{in} is calculated from standard astronomical relations [e.g. *Iqbal*, 1983]. Subsequently, the part of the incoming solar radiation that is reflected by the surface with albedo α is subtracted. When no snow is present, we use a constant ice albedo α_{ice}. After fresh snow has fallen, α decreases exponentially in time from the fresh snow albedo α_{frsnow} to the firn albedo α_{firn} with a time-scale t^* [*Oerlemans and Knap*, 1998]. For snowfall around the melting point, α_{frsnow} is dependent on air temperature. For small snow depths, α is a function of both the snow albedo and the ice albedo, according to a depth-scale d^* [*Giesen and Oerlemans*, 2010].

The remaining atmospheric fluxes (net long-wave radiation, latent and sensible heat) are parameterized by ψ as a function of air temperature only. The parameterization is based on in-situ measurements of these fluxes with automatic weather stations on several glaciers [*Giesen and Oerlemans*, 2011]. A threshold temperature T_{thresh} is defined, below which ψ has the

constant value ψ_{min} and above which ψ increases linearly with air temperature.

$$\psi = \begin{cases} \psi_{\text{min}} & \text{for } T_{\text{a}} < T_{\text{thresh}} \\ \psi_{\text{min}} + cT_{\text{a}} & \text{for } T_{\text{a}} \geq T_{\text{thresh}} \end{cases} \tag{3.3}$$

The best choice for the parameters T_{thresh}, c, and ψ_{min} depends on the climatic setting of the glacier. Here, the values that suit a wet climate, comparable to the maritime glaciers of Norway, are chosen. See Table 3.1 for the values of all model parameters.

If snow is present, part of the meltwater that is formed when Q is positive is allowed to refreeze. Following *Oerlemans* [1991], this part r is dependent on the temperature of the subsurface layer T_{sub} (°C):

$$r = 1 - e^{T_{\text{sub}}}. \tag{3.4}$$

The refreezing of meltwater heats the snowpack, leading to a change in the subsurface temperature T_{sub}, calculated as

$$\frac{\mathrm{d}T_{\text{sub}}}{\mathrm{d}t} = \frac{rQ}{C}, \tag{3.5}$$

where C is the heat capacity of the subsurface layer, taken equivalent to a 2 m thick layer of ice. At the end of the ablation season (the 30th of April), T_{sub} is reset to the annual mean air temperature. If this temperature is higher than 0 °C, T_{sub} is set to 0 °C, and no refreezing will occur. This means that for present-day climate refreezing occurs above 2350 m.

For the steady-state run with 1980–2009 climate, the mass balance model is run at 50 m intervals between 700 and 3400 m a.s.l. to calculate the climatic mass balance profile as a function of height. The dynamical model, described below, is forced with this profile, until a steady-state is reached. When the reconstructed monthly precipitation and temperature anomalies are used as input for the glacier mass-balance model, a mass-balance profile is calculated for each year in the period covered by the reconstruction (1600–1995 for *Neukom et al.* [2011] and 1640–1987 for *Villalba et al.* [2003]), again from 50 m intervals between 700 and 3400 m. This mass balance record is then used to force the dynamical model for the same period, after a spin-up time of 100 years with the mean mass balance profile of the first 30 years of the reconstruction.

In order to infer climatic information directly from the historical length record of Glaciar Frías, the mass balance history is reconstructed by dynamic calibration [*Oerlemans*, 1997a]. In this method, it is assumed that at all times the mass balance profile $B(z,t)$ can be described by an altitude-independent balance perturbation $\delta B(t)$ added to a reference profile $B_{\text{ref}}(z)$:

$$B(z,t) = B_{\text{ref}}(z) + \delta B(t) \tag{3.6}$$

The mass balance profile from the 1980-2009 climate is taken as the reference profile B_{ref}. The values for δB are taken such, that the difference between the modelled glacier length record and the observed glacier lengths is minimised. An optimised sequence of step func-

tions is generally sufficient to describe δB. The model has a spin-up period of 100 years with δB_{start}, such that the glacier has the steady-state length of the first observation when the record starts. The dynamical glacier model is run for the period of the observed length record, forced by the reconstructed mass balance history. If the dynamical model reproduces the observed lengths, the mass balance history is assumed to be correct.

Table 3.1: *Model parameter values of the surface mass balance model and the ice-dynamical model.*

Parameter	Symbol	Value	Unit
Temperature lapse rate	γ	0.0048	K m^{-1}
Precipitation vertical gradient	p	0.0015	m a^{-1} m^{-1}
Threshold temperature for snow	T_{snow}	1.5	°C
Atmospheric transmissivity	τ	0.5	–
Water density	ρ_{w}	1000	kg m^{-3}
Ice density	ρ_{ice}	900	kg m^{-3}
Latent heat of melt	L_{f}	3.34 10^5	J kg^{-1}
Fresh snow albedo	α_{frsnow}	0.69–0.90	–
Firn albedo	α_{firn}	0.53	–
Ice albedo	α_{ice}	0.35	–
Albedo time-scale	t^*	21.9	days
Albedo depth-scale	d^*	0.001	m w.e.
Heat capacity of subsurface layer	C	3.76 10^6	Jm^{-2}K^{-1}
Threshold temperature $\psi(T_{\text{a}})$	T_{thresh}	0.44	°C
Minimum $\psi(T_{\text{a}})$	ψ_{min}	-30	W m^{-2}
Slope $\psi(T_{\text{a}})$	c_1	9	W m^{-2} K^{-1}
Sliding constant	f_s	5.7 10^{-20}	Pa^{-3} m^2 s^{-1}
Deformation constant	f_d	1.9 10^{-24}	Pa^{-3} s^{-1}

3.3.2 Glacier dynamics

We use a one-dimensional flowline model to describe the ice dynamics. This model has been used earlier in the study of several other glaciers [e.g. *Stroeven et al.*, 1989; *Greuell*, 1992; *Oerlemans*, 1997a,b], so here we only give a brief description.

Starting from conservation of mass, we can define for each vertical cross sectional area S along the flowline:

$$\frac{\partial S}{\partial t} = \frac{\partial (US)}{\partial x} + wB, \tag{3.7}$$

where U is the vertical mean ice velocity of a cross section, w is the width at the glacier surface and B is the specific mass balance. We parameterise the cross section with a trapezoid. Thus, surface width w is given by:

$$w = w_0 + \lambda H, \tag{3.8}$$

where H is the glacier thickness and λ is the effective slope of the valley wall. The area of the cross section S is given by:

$$S = H(w_0 + \frac{1}{2}\lambda H). \tag{3.9}$$

Combining these three equations gives the time evolution of the ice thickness:

$$\frac{\partial H}{\partial t} = \frac{-1}{w_0 + \lambda H}\frac{\partial}{\partial x}\left\{HU(w_0 + \frac{1}{2}\lambda H)\right\} + B. \tag{3.10}$$

We use the shallow ice approximation (SIA), such that the mean vertical ice velocity is entirely determined by the local driving stress σ (Budd et al. 1979). We separate the vertical mean ice velocity in a component due to sliding and a component due to ice deformation, given by:

$$U = U_d + U_s = f_d H\sigma^3 + f_s\frac{\sigma^3}{H}, \tag{3.11}$$

with σ given by the ice thickness H and surface slope $\frac{\partial h}{\partial x}$ (h is the surface altitude):

$$\sigma = -\rho_{\text{ice}} g H \frac{\partial h}{\partial x}. \tag{3.12}$$

Substituting this expression for U into eq (3.10) gives the expression for the evolution of the ice thickness:

$$\frac{\partial H}{\partial t} = \frac{-1}{w_0 + \lambda H}\frac{\partial}{\partial x}\left\{D\frac{\partial h}{\partial x}\right\} + B, \tag{3.13}$$

with D:

$$D = \left(w_0 + \frac{1}{2}\lambda H\right)\rho_{\text{ice}}^3 g^3 H^3 \left\{f_d H^2\left(\frac{\partial h}{\partial x}\right)^2 + f_s\left(\frac{\partial h}{\partial x}\right)^2\right\}. \tag{3.14}$$

Eq (3.13) is solved on a staggered grid, with a grid size of 25 m. Time integration is done with a forward explicit scheme, in time steps of 0.00025 year (approx. 2 hour). The specific mass balance B is a function of surface altitude h and taken from the balance profile calculated with the mass balance model. For time-dependent simulations, B is recalculated every year.

The topography of the glacier bed of Glaciar Frías is unknown, except for that part of the valley that is currently deglaciated. The bed topography of the part that is currently covered by ice is derived from the model forced with the climatological mass balance (section 3.3.1,

Figure 3.5). Following an iterative procedure, the bed altitude along the flow line and the glacier width at the bed are adjusted such that the modelled surface width and altitude in equilibrium state match the observed surface width and surface altitude along the flow line. The bed profile that reproduces the present-day surface best (Figure 3.2a) has an overdeepening around x = 3500 m, followed by a bump that is at the same location as the ridge that is currently emerging from the ice at ca. 1800 m (Figure 3.1).

3.4 Results and discussion

3.4.1 Steady state

Before using the coupled mass balance – glacier model for climate reconstruction, we examine the model's performance and sensitivities with a steady-state solution. The climatological conditions of the period 1980–2009 are used as input for the mass-balance model to calculate the present-day climatological mass balance profile (Figure 3.5). The calculated profile is almost linear below the ELA at 2090 m, and the gradient becomes smaller for higher elevations. This is in line with mass balance profiles observed elsewhere [e.g. *Andreassen et al.*, 2005]. The calculated mass balance gradient of 0.0011 mw.e. m^{-1} a^{-1} is large, but smaller than measured at Mocho-Choshuenco. This could be caused by the less pronounced seasonality in the precipitation at the higher latitude of Glaciar Frías. The calculated ELA at Glaciar Frías is a bit higher than the ELA at the Mocho-Choshuenco. This is reasonable, as the Glaciar Frías flows to the north-east and thus receives more incoming short-wave radiation than the Mocho-Choshuenco, that flows towards the south-east. For a selected number of altitudes, the evolution of the cumulative mass balance throughout the hydrological year is shown in Figure 3.6. The winter accumulation at 2000 m is 3.0 m w.e., but this all melts during the ablation season. The winter accumulation is in line with the accumulation at Mocho-Choshuenco. The annual precipitation at 2000 m that is needed for this amount of accumulation is 7.3 mw.e.a^{-1}, which is at the high end of the observations of *Gallopin* [1978]. As shown by the mass balance at 2500 m, ablation is still substantial above the equilibrium line, but this is outpaced by the accumulation. The model shows that at 1000 m there is hardly any accumulation, so in the present-day climate the glacier tongue would sustain year-round melting when it reaches the bottom of the Frías valley.

If we force the ice-dynamical model with the calculated climatological mass balance of the period 1980–2009, the calculated equilibrium glacier length is 6025 m. This is in good agreement with the observed glacier lengths in this period (cf. Figure 3.9, Table 3.2), indicating that the calculated mass balance is fairly accurate. The length of Frías glacier is very sensitive to small changes in the mass balance profile, due to the present-day geometry (the ELA is in the altitude range where the glacier has a large part of its area, while the terminus is narrow

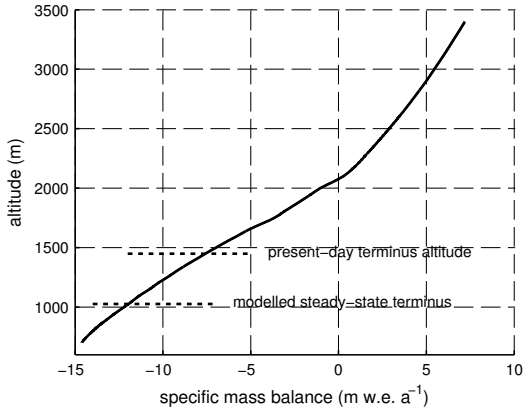

Figure 3.5: *Mass balance profile $B(z)$ calculated from present-day forcing. NB: the profile is given for the entire model domain, the present-day terminus is at 1450 m (glacier length = 5550 m), the modelled steady-state terminus is at 1027 m altitude (glacier length = 6025 m).*

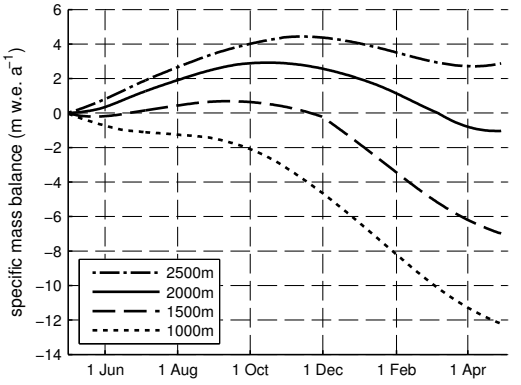

Figure 3.6: *Temporal evolution of the annual cumulative mass balance, shown in Figure 3.5, at selected altitudes. The time evolution is shown during one mass balance year, that starts on May 1 and ends on April 30.*

in the steep part, see Figure 3.1, 3.2). However, because no measurements of the individual components of the energy budget are available, compensating errors can not be excluded.

In Figure 3.7, the seasonal sensitivity characteristic (SSC) [*Oerlemans and Reichert*, 2000] of the mass balance of Glaciar Frías in equilibrium state is shown. The SSC consists of 24 numbers that give the sensitivity of the annual mass balance to monthly perturbations

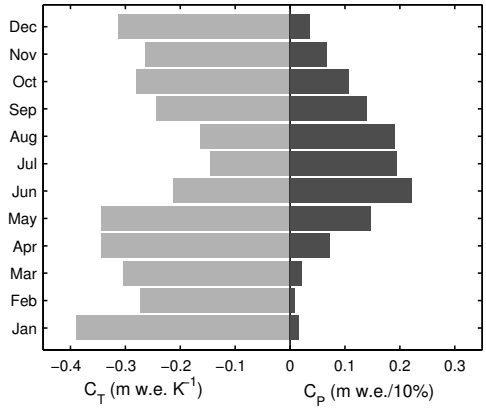

Figure 3.7: *Seasonal sensitivity characteristic, showing the sensitivity of the mass balance to changes in temperature (C_T) and precipitation (C_P) in a specific month. Changes in precipitation are relative, shown is the change in mass balance after a 10% change in monthly precipitation. Mass balance is calculated for the glacier geometry of the equilibrium state.*

in precipitation and temperature. The temperature sensitivities indicate that Glaciar Frías is in a very maritime climate. The SSC values are large and the mass balance is sensitive to temperature changes in every month of the year. Even temperature anomalies in the winter season lead to a significant changes in the mass balance. Furthermore, variations in winter precipitation are more important for the mass balance than variations in summer precipitation. Most of the precipitation falls in winter, and summer precipitation falls as rain on a large part of the glacier.

To conclude we calculate the response time and climate sensitivity of the glacier in equilibrium state. This is done by imposing a stepwise perturbation in the climatic forcing that is kept constant until the glacier has reached a new equilibrium. The climate sensitivity indicates the difference between the two equilibria. The response time is a measure for the time needed to reach the new equilibrium, defined as the time needed to reach $(1-e^{-1})$ of the final change. As the mass balance is sensitive to temperature change in all months of the year, the perturbations consist of changes in the annual mean temperature, of -1.0, -0.5, 0.5 and 1.0 K. The resulting changes in glacier length and glacier volume are shown in Figure 3.8. Frías has a response time of 14 a, for both volume and length changes. This is short compared with other alpine glaciers [cf. *Jóhannesson et al.*, 1989; *Greuell*, 1992; *Oerlemans*, 1997a,b; *Brugger*, 2007; *Laumann and Nesje*, 2009], indicating that Glaciar Frías reacts rather directly to changes in climate. The climate sensitivity is dependent on the size of the perturbation, it varies between 1850 – 2950 m K^{-1} in terms of length change, and 0.22 – 0.38 km^3 K^{-1} in terms of volume change for the four perturbations used here. The large spread is caused

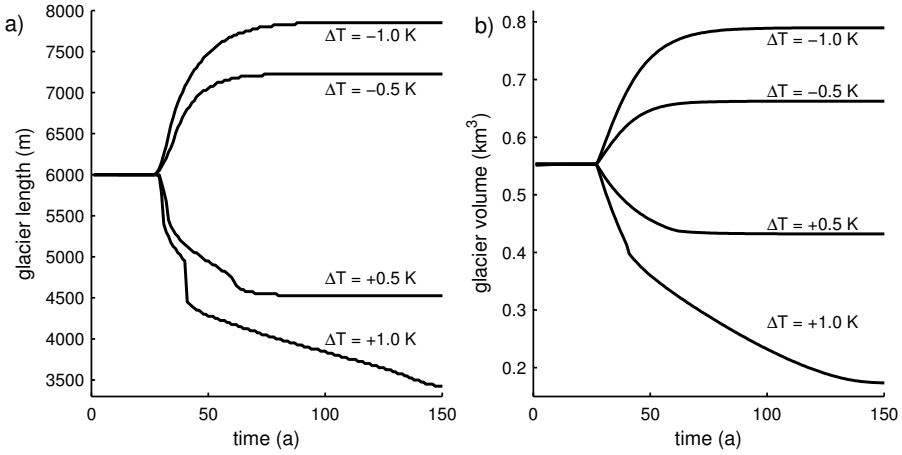

Figure 3.8: ***a)*** *Length and* ***b)*** *volumes changes of Glaciar Frías after perturbation of the present-day climate with +1.0, +0.5, -0.5 and -1.0 K at t = 25 a. It shows the response of Glaciar Frías to perturbations in climate. For T +1K, the glacier retreats over the overdeepening in the bed, which causes a drastic decrease in both volume and length.*

by the strong dependence of the climate sensitivity on surface geometry and the bed topography at the glacier terminus. For limited perturbations, the terminus remains in the steep part between 5–7 km. For the temperature decrease of 1 K the terminus advances over the flat valley floor, whereas for a temperature increase of 1 K the glacier is forced to retreat into the overdeepening, which implies a major mass loss. For the limited perturbations of +/- 0.5 K, the climate sensitivity is 2700 m K^{-1} and 0.23 km^3 K^{-1}.

3.4.2 Historical fluctuations

Climatic information from dynamic calibration

As shown in Figure 3.9, the observed length record can be reproduced very well using dynamic calibration of the mass balance profile with a sequence of 13 step functions. To explain the maximum glacier length in 1639, the mass balance profile must have been 1.5 mw.e. a^{-1} higher than the 1980-2009 mean profile. This maximum of δB is followed by a slight decline over the following two centuries, until the mass balance makes a significant drop at the end of the 19th century. In the 20th century, more length observations are available and thus the reconstructed δB then shows more fluctuations. The most striking fluctuation is around 1970, prior to the significant and well documented re-advance of the glacier, that culminated in 1977. Overall, there is a negative trend in the mass balance over the 20th century of -0.0077

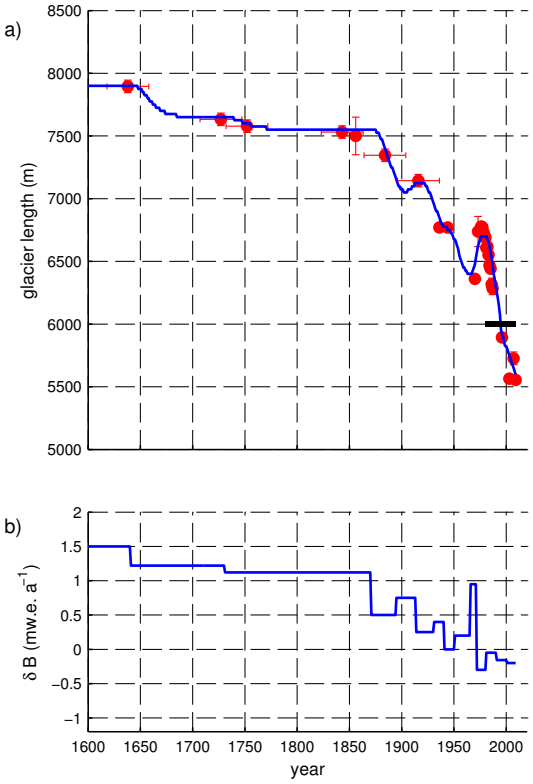

Figure 3.9: ***a)*** *Measured glacier length of Frías (red dots) with bars indicating the uncertainty in both time (dated moraines) and length (most of the times smaller than the dots); modelled equilibrium length for the 1980–2009 climate (black); and modelled glacier length reconstructed with dynamical calibration (blue).* ***b)*** *Mass balance perturbations δB that reproduce the observed glacier length.*

m w.e. a^{-2}. The current retreat is best explained by $\delta B = -0.2$ mw.e. a^{-1} in the period 2001–2009. Hence, the glacier retreat over the entire period of the length record, 1639–2009, is best explained by a decrease in δB of 1.7 m w.e. a^{-1}.

Changes in the mass balance are in general due to changes in both precipitation and temperature. Although the influence of these two climate components can not be disentangled from the mass balance reconstruction, it is possible to give a quantitative indication of the change in temperature or precipitation needed to arrive at the reconstructed mass balance changes. The sensitivity of the mass balance profile to changes in annual temperature and precipitation is determined based on least squares fit of the mass balance profiles calculated with the temperature perturbations of ± 0.5 and ± 1 K and precipitation perturbations of ± 10

and ±20%. The mass balance sensitivity to changes in temperature is -1.46 mw.e. a^{-1} K^{-1}, and 0.51 mw.e. a^{-1} per 10% increase in precipitation. The observed retreat of Glaciar Frías over the period 1639–2009 is thus best explained by a temperature increase of 1.16 K, or a precipitation decrease of 34% (meaning that the precipitation in the 17th century must have been 134% of present-day precipitation). Or, most likely, the observed glacier retreat is a combination of both.

Trenberth et al. [2007, Fig 3.9] show a negative trend in measured surface temperature of -0.2 to -0.5 °C per century over the period 1901–2005 for the region of Tronador, in apparent contradiction to the decrease of the reconstructed mass balance. However, based on analyses of radiosonde data, *Carrasco et al.* [2008] conclude that the cooling in this region is restricted to the near-surface troposphere. At the 850 hPa level the temperature trend is positive for summer and winter (for 1958–2006: 0.013 and 0.014 Ka^{-1}, respectively). In addition, *Rivera et al.* [2002] attribute the retreat of glaciers in southern Chile for a large part to a decrease in precipitation. Indeed at Puerto Montt, precipitation has decreased by 20% in the period 1958–2006. Simply adding these trends in precipitation and free atmosphere temperature gives a trend in δB of -0.03 m w.e. a^{-2} for 1958–2006. This is even larger than the trend in the reconstructed δB, which is -0.015 m w.e. a^{-2} over the same period.

Forcing the glacier model with climate reconstructions

Instead of deriving a mass balance reconstruction based on dynamical calibration, we can also calculate the historical mass balance using the temperature and precipitation records based on other proxy reconstructions. In this way the observed glacier length can serve as a constraint on the proxy-based climate reconstructions. This could in addition provide information on the relative contributions of fluctuations in precipitation and temperature to the glacier length changes. We force the glacier model with the reconstructions of *Neukom et al.* [2010, 2011] and *Villalba et al.* [2003]. The calculated glacier length for the period 1600–1995 and 1640–1987, respectively, is shown together with the observed glacier length in Figure 3.10a.

When we first focus on the results calculated from the *Neukom et al.* [2010, 2011] reconstructions, the modelled length is promising in a qualitative sense: maximum extents before 1800, in 1884 and in 1916 are reproduced (although the timing does not exactly match the dating of the moraines) together with the large retreat between 1880 and 1960, and the re-advance in the 70's that is followed by the retreat that continues up to present day. However, when the results are examined in more detail, the agreement is rather poor. The length variations in the 20th century are too large: the modelled glacier length in 1940 is 500 m larger than the observed length, while in 1970 it is 700 m shorter than observed, and the subsequent re-advance is again larger than observed. In the beginning of the 19th century the glacier is too small to reach the 1843 moraine, and the maximum extent in the 17th century is about 1 km too large. Only the 1727 and 1756 moraines are well reproduced.

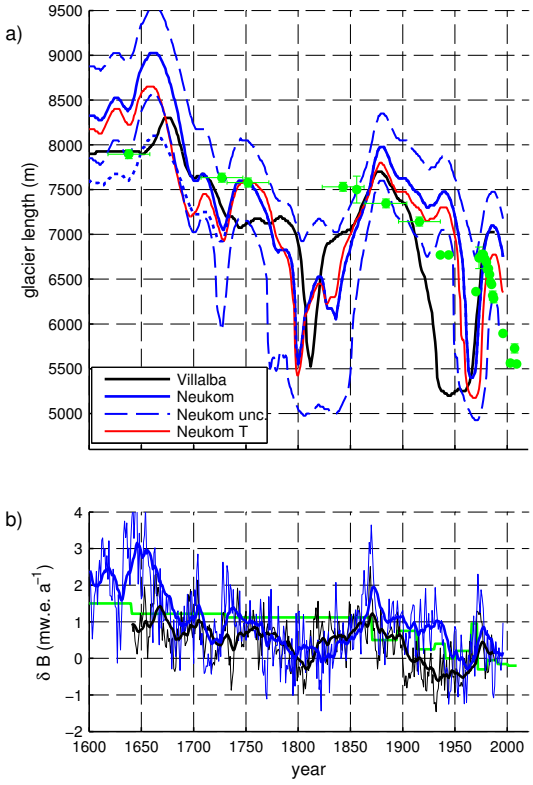

Figure 3.10: *Results of model forced with the available precipitation [Neukom et al., 2010] and temperature [Neukom et al., 2011; Villalba et al., 2003] reconstructions.* ***a)*** *Glacier length for the period 1600–1995 based on: Neukom et al. [2011, 2010] (blue), with upper and lower estimate (dashed blue) indicating the uncertainty, and the DJF anomaly only applied to summer half year prior to 1706, keeping winter temperatures at 1980-2009 average (blue dotted); Villalba et al. [2003] temperature, Neukom et al. [2010] precipitation (black); Neukom et al. [2011] temperature, precipitation kept constant at the 1980–2009 reference (red); observations (green dots), with uncertainty intervals.* ***b)*** *δB calculated from the annual mass-balance profiles from the reconstructions by Neukom et al. (blue), Villalba et al. (black), with 21-year exponential smoothing, and δB obtained from dynamical calibration (green) (cf. Figure 3.9).*

We have also calculated the length record from perturbations in temperature only, leaving the precipitation constant at the 1980–2009 mean. The resulting length record closely resembles the length record of the model run with perturbations in both temperature and precipitation (Figure 3.10a). This indicates that the fluctuations in precipitation are in general of minor importance for the observed glacier fluctuations over the last four centuries. The only significant difference between the two modelled length records is in the mid-17th century. In this

period, a positive precipitation anomaly contributes to the glacier advance, accounting for an additional advance of 0.4 km (Figure 3.4, 3.10a).

The large fluctuations in the modelled length during the 20th century could be an indication that the modelled response of the glacier is too large. The length record could be smoother if the glacier response is reduced by changing the ice dynamics. However, adjusting the sliding and deformation velocities of the glacier with a different parameter choice for f_d and f_s (equation 3.11, Table 3.1) does not improve the modelled length record. Also the parameter choice in the mass balance model, where especially the parametrisation of ψ is uncertain, cannot explain the overestimated variations. Variation of these parameters lead to a more positive, or negative, mass balance for the entire period of reconstruction. Other parameter values thus lead to a constantly larger or smaller glacier, not to smaller or larger length fluctuations.

While the uncertainties in the glacier model cannot account for the discrepancies between the observed glacier length fluctuations and the modelled length from the climate reconstruction, the differences can to a large extent be explained by the uncertainties in the climate reconstructions. Using the decadal-scale uncertainties in the reconstructions of *Neukom et al.* [2010, 2011], we have estimated upper and lower limits for the modelled glacier length (dashed blue lines in Figure 3.10a). For the upper limit we calculated maximum mass balance from the precipitation plus 1SE uncertainty and the temperature minus the 1 SE uncertainty. Likewise, we calculated the lower limit in modelled glacier length from the minimal precipitation and maximal temperatures within the 1SE uncertainty margin. The uncertainty in the reconstruction is fairly large, when translated into glacier length. Almost all glacier length observations fall within the range that is derived from uncertainty in the prescribed forcing. Only the constraints set by the maximum glacier length in the 1600–2009 period, as determined by the 1639 moraine, and the length measurements in 1843, 1936 and 1944 are not met. As the modelled maximum extent is reached in the period prior to 1706, when no winter temperature anomalies are available, this result should be interpreted with care. This is illustrated by the 900 m smaller extent when the summer anomaly prior to 1706 is only applied to the summer half of the year, keeping the winter temperatures at the 1980-2009 mean (dotted blue line in Figure 3.10a). Furthermore, it is evident that the glacier is particularly sensitive to climatic forcing when the length is in the range of 5000–7000 m. When the terminus is in this range, the uncertainty band is much wider, without the uncertainties in precipitation or temperature being larger.

With the *Villalba et al.* [2003] reconstruction as temperature forcing, the modelled glacier length is comparable to the previous reconstruction (Figure 3.10a). Again, the modelled length qualitatively shows the same characteristics as the observed record, but the reconstruction fails to reproduce the length observations on more or less the same points in time as the reconstruction forced with the *Neukom et al.* [2011] temperature anomalies. However, in this second reconstruction the maximum extent is smaller, more in line with the observations

(but timed later). And, in contradiction to the other reconstruction, the glacier extent is much smaller than observed throughout the entire first half of the 20th century.

We have calculated δB from the mass-balance profiles of both reconstructions (Figure 3.10b), to compare the differences in mass balance profiles between the results of the dynamical calibration and those obtained when the model is forced with reconstructed temperature and precipitation anomalies from North Patagonia. As the calibrated mass-balance record only reproduces the observations in the simplest way, the mass-balance based on the reconstructed temperature and precipitation can not be expected to be identical. The glacier has likely experienced unobserved retreat in the periods between two maximum stands that are indicated by the moraines. With this in mind still three discrepancies between the observed and modelled glacier lengths can be identified: i) The δB based on *Neukom et al.* [2011] is more than 1 mw.e.a^{-1} too high in the period 1640–1660. ii) Both reconstruction-based δBs are too low to reproduce the observed length in 1843. An increase of 1 mw.e. a^{-1} in δB would reproduce the local maximum in glacier length, as indicated by the 1843 moraine. This modelled maximum is timed 15 years before the dated age of the moraine, which is within the uncertainty range of the dating. iii) There is a striking difference between the two reconstruction-based mass balances in the first half of the 20th century. The *Neukom et al.* [2011] reconstruction results in a too high mass balance with a too large glacier extent, while the *Villalba et al.* [2003] gives a much lower δB, which results in a too small glacier extent during this period.

As the past glacier fluctuations appear to be mainly temperature driven, we express the differences in terms of temperature anomaly. It is difficult to draw firm conclusions for the period before 1706, as the uncertainties in the reconstructed mass balance are large due to the missing winter temperatures. If the summer anomaly is applicable to the winter anomaly, the best estimate of the reconstructed temperature of *Neukom et al.* [2011] for the middle of 17th century is in the order of 0.7–1.0 °C too low. The temperature reconstruction of *Villalba et al.* [2003] is compatible with the observed glacier length in this period, although the timing of the advance deviates from the dating of the moraine. Both reconstructions give too high temperatures around 1800. According to the modelled glacier length, the best estimate of the temperature anomaly should be 0.7 °C lower in the period 1790–1820. The disagreement between the two reconstructions in the first half of the 20th century is remarkable, as for both reconstructions this period is part of the calibration period. The mass balance obtained from the dynamical calibration suggests that, for this period, the mean of the two temperature reconstructions would explain the observed glacier length.

These results arguably have a substantial uncertainty, which is difficult to quantify. The glacier mass balance model for this glacier is only validated with the steady-state length from reanalysis climatology. The reliability of the model would greatly improve from mass-balance measurements at the Glaciar Frías. Local weather observations on the Glaciar Frías could help to determine the uncertainty that originates from using coarse resolution meteorological and climatological information as input [*Hofer et al.*, 2010]. Furthermore, the glacier is shown to be sensitive to temperature variations throughout the entire year, while in the case

of *Neukom et al.* [2010, 2011] only values for the summer and winter months are given. Still, in view of the uncertainties associated with the climate reconstructions used in this study, the additional climatic information provided by glacier length fluctuations can be of great value. The modelled glacier length gives an extra constraint within the relatively large uncertainty range of the climate reconstructions, and in addition suggests to adjust the decadal average of certain periods in the reconstructions.

3.4.3 Future of Glaciar Frías

Regional climate projections for South America predict a warming trend and decrease in precipitation over the next century for North Patagonia [*Vera et al.*, 2006; *Christensen et al.*, 2007]. According to the A1B scenario, by the end of the 21th century the annual precipitation will have decreased by 15%, compared to the 1980–1999 average. Winter (JJA) precipitation will decrease by 5–10%, while the projected summer (DJF) precipitation loss is predicted to go up to 30%. For the period 2080–2099, annual mean temperature is projected to be 2 °C higher than in the reference period 1980–1999, with the changes in summer temperature (+2.5 °C) being stronger than in winter (+1.5 °C).

Figure 3.11 shows the future response of Glaciar Frías to the projected changes in north Patagonian climate. For simplicity, the coupled model was forced with a linear increase in annual temperature and a linear decrease in annual precipitation, such that in 2100 the annual temperature is 2 °C higher than the 1980–2009 average, and annual precipitation has decreased with 10 % in 2100 (in the annual mean we have given the projected change in winter precipitation more weight than the change in summer precipitation, as the mass balance is hardly sensitive to summer precipitation, cf. Figure 3.7). Based on this scenario, the projected retreat of Glaciar Frías is quite dramatic. Under the conditions of a 2 °C temperature rise and a 10% decrease in annual precipitation, the glacier will retreat 3400 m to a length of 2175 m in 2100. This projected retreat in length is larger than the retreat since the maximum stand in 1639. The terminus will retreat to an elevation of 2150 m, while it currently is at 1450 m. In terms of volume, the shrinkage is even more pronounced: the glacier is projected to loose more than 80% of its volume during the 21st century. A simple sensitivity test, in which the precipitation is kept at the 1980–2009 level (dashed black in Figure 3.11), shows that the glacier retreat is mainly due to the increase in temperature. The extra precipitation slows down the retreat, but the eventual mass loss is very similar.

3.5 Conclusion

In this study we have presented a model for Glaciar Frías in the north Patagonian Andes of Argentina. This glacier, which has the most detailed, long record of LIA and post-LIA fluctuations in southern South America (currently spanning the period 1639-2009), has a land-

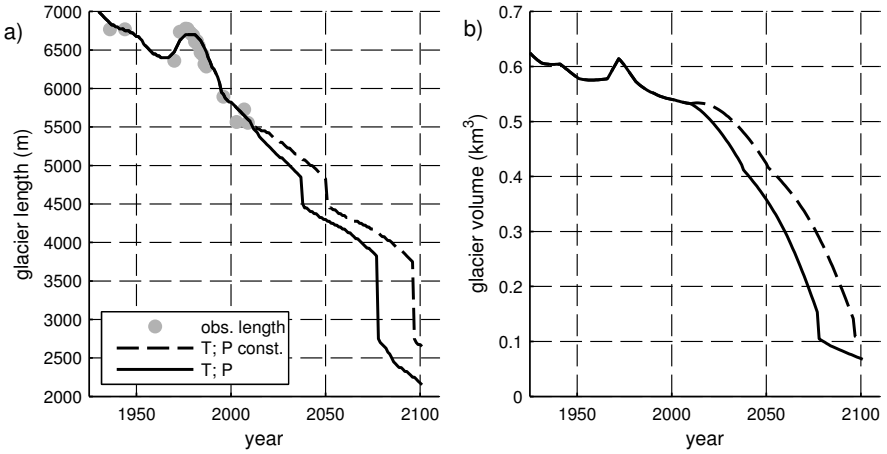

Figure 3.11: *Modelled **a)** glacier length and **b)** glacier volume of Glaciar Frías for the period 1925–2100. Glacier length and volume for the period 1925–2009 are calculated from the reconstructed mass balance profiles, for 2010–2100 the mass balance is calculated from the future scenario. The full scenario (increase in T of 2 °C and decrease in P of 10% over the 21th century) is given by the solid black line. The length and volume change with precipitation kept at the 1980–2009 level is given in dashed black. In **a)** also glacier length observations are included (grey dots).*

based tongue, and is free from extensive debris cover. Therefore, Glaciar Frías is well suited for the study of past climate of the northern Patagonian Andes. Given the lack of detailed meteorological information near Glaciar Frías, we forced a simplified surface-energy balance model with climatological monthly temperature and precipitation values derived from ERA reanalysis. The results provided interesting new information regarding the climate sensitivity of this glacier and offered for the first time in Patagonia the possibility of comparing modelled glacier mass balance changes with those obtained from independent, proxy-based climate reconstructions.

Glaciar Frías is located in a temperate maritime climate. It is very sensitive temperature changes throughout the entire mass-balance year, with a stronger sensitivity to changes in summer than to changes in winter temperature. The mass balance is to a lesser extent sensitive to variations in precipitation, mainly to changes in winter precipitation. Glaciar Frías has a response time of only 14 a, and therefore follows fluctuations in climate quite closely. The calculated present-day mass balance corresponds well with the little information that is available in the north Patagonian Andes. Moreover, the equilibrium length with present-day climate (6025 m) is within the range expected from the glacier length observations. This indicates that the model is performing well and gives confidence in the deduced sensitivity of the glacier to changes in regional climate.

The reconstructed mass balance history indicates that the overall retreat of Glaciar Frías during the period 1639–2009 can be best explained by a decrease of 1.7 m w.e. a^{-1} of the specific mass balance profile. This change in climatic conditions can be caused by an increase in temperature as well as, or in combination with, a decrease in precipitation. If it would only be attributed to changing precipitation, the precipitation in the mid-17th century must have been 134% of the 1980–2009 average. If attributed to temperature, the mass balance decrease implies a temperature increase of 1.16 °C. Until the mid of the 19th century, North Patagonian climate was in a relatively stable state, with only minor warming/drying. At the end of the 19th century, mass balance dropped substantially and continued to decrease until the 21st century, with some fluctuations of which the most striking was around 1970.

Driving the glacier model with independently reconstructed temperature and precipitation shows that the fluctuations of Glaciar Frías over the last four centuries were predominantly temperature-driven. Glacier length records can, in combination with a glacier model, also be used to validate or constrain high resolution proxies. In the case of North Patagonia, existing proxy-based reconstructions of precipitation and temperature seem to reconstruct the interdecadal variability well. The glacier model forced with these reconstructions produces glacier advances and retreats that in timing agree well with the dated moraines and observations. However, in quantitative sense, the reconstructed anomalies have a relatively high level of uncertainty. This is reflected in the large range of possible glacier lengths. In addition, to explain the observed glacier lengths of Glaciar Frías, temperature around 1800 must have been 0.7 °C lower than the best estimate of the reconstructed temperatures by *Neukom et al.* [2011] and *Villalba et al.* [2003], and up to 1 °C higher around 1640 than reconstructed by *Neukom et al.* [2011]. Error margins in these results might be substantial, due to uncertainties in the climate reconstructions and in the glacier model, but are difficult to quantify. The uncertainties in the glacier model could be reduced substantially by performing mass-balance measurements and weather observations on Glaciar Frías.

Following the IPCC A1B scenario for North Patagonia, Glaciar Frías is projected to continue its rapid retreat in the near future. By 2100, the glacier will likely have lost more than 80% of its present-day volume and the terminus will have retreated high up the Monte Tronador. Like with the past fluctuations, this expected retreat is mostly due to the projected increase in temperature.

Table 3.2: *Glacier length record of Glaciar Frías used in this study, including year of measurement (or reconstructed date of maximum extent), total length along the flowline (km), cumulative length change (m), method of observation (*moraine *indicates a moraine dated with dendrochronology,* historical *are historical sketches and photos,* field *denotes field measurements of terminus position, and* Landsat, Corona, SPOT *and* ASTER *are positions measured from satellite images), data source, and estimate of accuracy of the length measurement (m).*

year	L (km)	dL (m)	type	source	accuracy (m)
1639	7.90	0	moraine	*Villalba et al.* [1990]	50
1727	7.63	-262	moraine	*Villalba et al.* [1990]	50
1752	7.58	-316	moraine	*Villalba et al.* [1990]	50
1843	7.53	-364	moraine	*Villalba et al.* [1990]	50
1856	7.50	-400	historical	*Fonk* [1886]	150
1884	7.35	-549	moraine	*Villalba et al.* [1990]	50
1916	7.14	-752	moraine	*Villalba et al.* [1990]	50
1936	6.77	-1125	historical	*Agostini* [1949]	20
1944	6.77	-1125	aerial	SHN	10
1970	6.36	-1534	aerial	IGM	10
1973	6.74	-1157	Landsat MSS	GLCF	120
1976	6.78	-1141	field	S. Rubulis	10
1977	6.77	-1121	field	S. Rubulis	10
1978	6.74	-1159	field	S. Rubulis	10
1979	6.71	-1181	field / Corona	S. Rubulis / EROS	10
1980	6.69	-1207	field	S. Rubulis	10
1981	6.61	-1231	field	S. Rubulis	10
1982	6.62	-1277	field	S. Rubulis	10
1983	6.55	-1343	field	S. Rubulis	10
1984	6.47	-1427	field	S. Rubulis	10
1985	6.44	-1453	field	S. Rubulis	10
1986	6.32	-1463	Landsat TM	GLCF	50
1987	6.29	-1495	Landsat TM	GLCF	50
1996	5.89	-1886	field	S. Rubulis	20
2003	5.56	-2607	ASTER	GLIMS	30
2007	5.73	-2444	Landsat ETM	CONAE	50
2009	5.55	-2617	SPOT	Spot image	10

SHN	Servicio de Hidrografía Naval, Argentina
IGM	Instituto Geográfico Nacional, Argentina
GLCF	Global Land Cover Facility, University of Maryland, U.S.
S. Rubulis	field measurements of S. Rubulis, reported in *Villalba et al.* [1990]
EROS	Earth Resources Observation and Science Center, U.S. Geological Survey
GLIMS	Global Land Ice Measurements from Space
CONAE	Comisión Nacional de Actividades Espaciales, Argentina

4

Global and hemispheric temperature reconstruction from glacier length fluctuations

Summary

Temperature reconstructions for recent centuries provide a historical context for the warming over the twentieth century. We reconstruct annual averaged surface temperatures of the past 400 years on hemispherical and global scale from glacier length fluctuations. We use the glacier length records of 308 glaciers. The reconstruction is a temperature proxy with decadal resolution that is completely independent of other temperature records. Temperatures are derived from glacier length changes using a linear response equation and an analytical glacier model that is calibrated on numerical model results. The global and hemispherical temperatures reconstructed from glacier length fluctuations are in good agreement with the instrumental record of the last century. Furthermore, our results agree with existing multi-proxy reconstructions of temperature in the pre-instrumental period. The temperature record obtained from glacier fluctuations confirms the pronounced warming of the twentieth century, giving a global cumulative warming of 0.94 ± 0.31 K over the period 1830–2000 and a cumulative warming of 0.84 ± 0.35 K over the period 1600–2000.

This Chapter is based on P.W. Leclercq, J. Oerlemans, Global and hemispheric temperature reconstruction from glacier length fluctuations, Climate Dynamics, *in press*.

4.1 Introduction

Knowledge of the climate variability over the last centuries forms the key to understanding present day climate change. For recent times this information is provided by instrumental records [*Jones and Moberg*, 2003; *Brohan et al.*, 2006]. However, before the mid 19th century, such instrumental records are mostly lacking. Temperature reconstruction then demands the use of natural climate archives, proxies, to reconstruct past climates on longer timescales. Focusing on temperature changes, many proxies have been used in studies made in the last decades. These proxies include those of biogenic nature, e.g. the widely used tree-rings [*Briffa et al.*, 2001; *Esper et al.*, 2002; *Mann and Jones*, 2003] and corals [*Lough*, 2004], reconstructions based on historical evidence [*Pfister et al.*, 1999; *Brázdil et al.*, 2005; *Jones et al.*, 2009], as well as pure physical methods such as temperature reconstructions from ice cores [*Mosley-Thompson et al.*, 2006; *Overpeck et al.*, 1997], borehole temperatures [*Huang et al.*, 2000] and groundwater composition [*Alvarado et al.*, 2009]. Biogenic and historical records mostly have a high resolution, resolving annual or even monthly variations, whereas the physical proxies have the advantage that they do not need a calibration on the instrumental record [*Jones et al.*, 2009; *Juckes et al.*, 2007]. Recently multi-proxy composites were made by combining the results of different proxies [*Mann et al.*, 2008; *Huang*, 2004], which creates a more reliable temperature reconstruction. From this perspective it is useful to explore as many independent and reliable proxies as possible.

The observed worldwide glacier retreat over the 20th century is a strong indication for global warming [e.g. *Dyurgerov and Meier*, 2000]. Here we present a quantitative reconstruction of global and hemispheric temperatures from glacier length fluctuations for the period 1600 to 2000. Glacier length fluctuations constitute a physical proxy for variations in temperature; they do not need calibration on the instrumental temperature record, and are fully independent of other reconstructions. Glaciers can be found on all continents and at virtual all latitudes, even in the tropics, and therefore the information on glacier length fluctuations potentially has good global coverage. However, as with other proxies [*Huang et al.*, 2000; *Mann et al.*, 2008], information on glacier fluctuations is more abundant in the Northern Hemisphere (NH) than in the Southern Hemisphere (SH). Glaciers respond slowly to changes in climate so they are a proxy with decadal resolution at best. The response of glaciers to changes in climate is dependent on the glacier geometry and its climatic setting [*Oerlemans*, 2001]. These differences have to be taken into account for each glacier individually when the variations in glacier length are interpreted.

First we discuss the improvements of the data set on glacier length fluctuations compared to the set used in the temperature reconstruction by *Oerlemans* [2005] (section 4.2). In section 4.3 the adjustments to the methods for calculating an average temperature record from the glacier fluctuations are explained. In the next sections we present the reconstructed global (section 4.4.1) and hemispheric (section 4.4.2) temperatures. We compare them with the multi-proxy composite temperature reconstruction of *Mann et al.* [2008] . In addition, we

reconstruct regional European temperatures of the past four centuries. We compare the reconstructed temperatures to instrumental records and the temperature reconstruction based on the multi-proxy temperature reconstruction of *Luterbacher et al.* [2007] to test our assumption that variations in precipitation can be neglected on global and hemispherical scale (section 4.4.3).

4.2 Data

4.2.1 Glacier length changes

For this study we have used an extension of the data on glacier length fluctuations as described in *Oerlemans* [2005]. Where possible, we have revised and extended the previously used records. Moreover, we have added new records. More than half of the 169 records used in *Oerlemans* [2005] were of glaciers located in the European Alps. In the present data set, the number of glacier length records of glaciers outside the Alps has significantly increased: from 73 to 222. Only records that start prior to 1950 and extend over at least several decades were used. All records with less than five data points were excluded, as well as records of glacier length changes that are known to be strongly influenced by other causes than climate change, e.g. surges. However, some calving glaciers were included. The data of the frontal position measurements available from the WGMS (www.wgms.ch) [*WGMS*, 2008 and earlier volumes] form the basis of our data set. Furthermore, there is a wealth of data on reconstructed glacier lengths in the literature. The measurements (often done by volunteers) and reconstructions of length changes involve time-consuming work for each of the glaciers individually. Complete references and glacier characteristics are given in Appendix A.

Figure 4.1 shows the global distribution of the 308 glacier length records. Records can be found on all continents and are, not surprisingly, strongly clustered in the major mountainous regions. There is a striking paucity in data from glaciers in the Canadian and Russian Arctic, as well as from glaciers near the Antarctic Ice Sheet. On the other hand, there is a wealth of information on the glaciers in the Alps, Norway, and Iceland. For many glaciers, yearly measurements were available since the early 20th century or even since the end of the 19th century. In addition, there are historical sources, some of which go back to the 16th century [e.g. *Zumbühl*, 1980; *Zumbühl and Holzhauser*, 1988; *Nussbaumer et al.*, 2007; *Nesje et al.*, 2008]. Continuous measurements are also available of glaciers in North West America, especially in the Canadian Rockies and Coast Mountains. Unfortunately, half of these records are not continued until the present day, but end between 1965 and 1985. In North America, additional historical documentation is less abundant than in Europe. In the Caucasus and Central Asia most records start in the second half of the 19th century, from first historical documents or the dating of Little Ice Age (LIA) moraines. Glaciers in mountain areas in the former Soviet Union, such as the Caucasus, Pamirs and Altai, are relatively well documented [e.g.

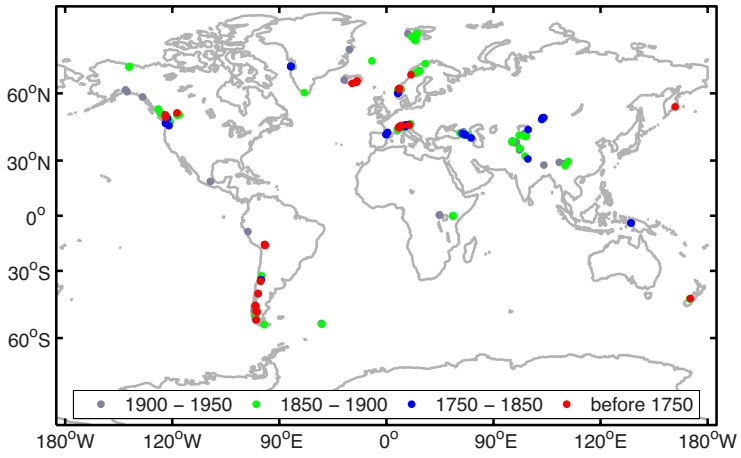

Figure 4.1: *Distribution of records over the world; colours indicate the period of the first data point of the record. In many cases the distance between glaciers is so small that the dots overlap.*

Panov, 1993; *Kutuzov and Shahgedanova*, 2009]. There is far less information of glaciers in the Himalayas, despite its large glacierization. The information on the arctic glaciers in Alaska, Greenland and Svalbard in the 19th century is a combination of historical sources and geological evidence [e.g. *Yde and Knudsen*, 2007; *Rachlewicz et al.*, 2007]. Also the tropics are represented in our data set, with records in the tropical Andes, central Africa, Himalayas and Indonesia. However, it should be noted that in central Africa no data prior to 1850 are available. Further south, the records are limited to the Central and Southern Andes and New Zealand. All three regions have a few detailed and long records as shown by the examples in Figure 2.1. On the SH, almost all the data prior to 1850 rely on proxy-based dating of geomorphological features [*Masiokas et al.*, 2009b; *Rabatel et al.*, 2008].

The maximum of 308 available records occurs between 1945 and 1965 (Figure 4.2). In 1945 the first aerial photographs of the Patagonian Icefields are made [*López et al.*, 2010], resulting in a marked increase in the number of available records from that year on. Going back in time, the number of available records shows a strong decrease in the period 1850-1900. In 1900 there are 230 records available, 156 of which are located outside the European Alps and 32 are on the SH. Only 70 records extend to 1850, of which 52 lie outside the Alps and 19 are located in the SH. In 1750 there are 34 records available (26 outside the Alps, 15 in SH). In 1650 these numbers are reduced to 14 records in total (7 outside the Alps, 5 on SH). In 1600 there are 9 remaining, of which 6 are in the Alps, 1 in Norway 1 in Southern Patagonia and 1 in New Zealand. After 1965 the number of records decreases as well. A few times the end of a record is due to the disappearance of the glacier, but more often more recent data are not available because measurements are not continued or not reported. In 1990 many of the

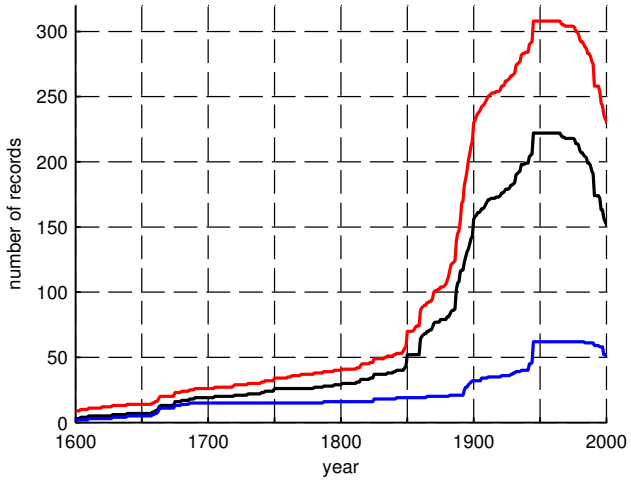

Figure 4.2: *The total number of records in time (red), the number of records outside the European Alps (black) and the number of records on the Southern Hemisphere (blue).*

records located in the former Soviet Union end, which leads to a notable drop of the available records. Of the 308 records, 231 continue up to at least 2000, and 181 records continue up to 2005.

Going back in time, not only the number of records decreases, but also the data points of the remaining records become scarce, as the examples in Figure 2.1 show. Some length records have annual resolution in the 20th century, but before 1880 no record has annual data. This does not mean we do not have any information on the glacier length in between two measurements. Glacier advances usually leave marks in the landscape such as trim lines and moraines. In addition, glacier retreats or advances are limited to tens of metres per year (Figure 2.7). This limits the possible glacier stands between two measurements. The decrease in the number of data points going back in time leads nevertheless to a decrease in the resolution of the reconstructed temperature from decadal in the 20th century to about half a century in the 17th century (Appendix 4.7.2). In order to be able to use the records for a temperature reconstruction, data points are connected using Stineman interpolation [*Stineman*, 1980; *Johannesson et al.*, 2009] to get yearly values for the entire record. Stineman interpolation creates no more maxima or minima than is required by the data. Moreover, the method performs very well when the density of data points varies strongly in time, as is the case with most glacier length records.

4.2.2 Additional glacier data

In order to assess the accuracy of the data on glacier length fluctuations, we include the method of data acquisition of each data point in the data set. Because of the large variety in methods, we use a bulk method of 4 categories: 1) direct measurements, 2) historical sources, 3) dendrochronological dating and 4) other dating methods. The category of direct measurements of the glacier terminus position includes field measurements, with or without GPS, (aerial) photography when designed for the purpose and satellite observations. The category of historical sources contains all data points derived from historical documents such as sketched maps from pioneers, pictures, paintings, written descriptions, etc.. Glacier stands derived from geomorphological evidence, dated with dendrochronology are put in the third category. The fourth category includes geomorphological evidence dated with other, less accurate, methods, e.g. lichenometry and radiocarbon dating. All data points for which the method is unknown are assumed to have the same accuracy as the fourth category.

As a glacier front is at least several hundreds of metres wide, even the most accurate measurement method inherently has an uncertainty of several metres in the denoted glacier length change. Larger uncertainties result from debris cover and limited resolution of observations, making it difficult to indentify the position of the glacier front accurately. We assign a maximum uncertainty of 50 m to the direct measurements (first category) [*Hall et al.*, 2003]. For the reconstruction of glacier fronts from historical documents one has to relate the glacier front to features in the landscape mentioned in the documents or depicted in paintings, sketches etc.. The maximum error of the thus determined front positions is 150 m. Measurement methods of the third and fourth category not only have an inaccuracy in the position, but have an additional uncertainty in the timing of the measured frontal position [e.g. *Villalba et al.*, 1990]. We translate the uncertainty in the timing into an uncertainty in position. Taking into account a typical retreat rate of 10 m per year (Figure 2.7), we arrive at an uncertainty of 300 m for the third category and an uncertainty of 500 m for the fourth category.

Besides the length record, we need additional information on the glacier geometry and climatic setting to reconstruct the temperature anomalies (section 4.3). Included are: the maximum, minimum and, if available, the median elevations; the length of the main flow line in the reference year 1950; the glacier area and position; and the average annual precipitation on the glacier. The data on the glacier geometry are mostly available from either the same source as the length changes, or from the World Glacier Inventory [*National Snow and Ice Data Center*, 1999, update 2009] (http://nsidc.org/data/g01130.html) and WGMS databases. The length of the flow line in 1950 is calculated from the difference in glacier length between the year of measurement and 1950. If there is no measurement in 1950, the interpolated value is used. For the precipitation, we use the climatological annual precipitation at the mean altitude of the glacier. When in situ measurements are lacking, values are estimated from climatologies [e.g. *Zuo and Oerlemans*, 1997a] or nearby weather stations. The majority of the weather sta-

tions are situated at lower elevations than the elevation of the glacier. Therefore, an estimate of the surplus precipitation at the glacier altitude is added to the measurements.

4.2.3 Temperature data for comparison

We compare our results with the University of East Anglia (Norwich, UK) Cimatic Research Unit instrumental surface-air temperature data from 1850 to 2009 [*Brohan et al.*, 2006] (http://www.cru.uea.ac.uk/cru/data/temperature), the combined proxy records of *Mann et al.* [2008], and the reconstruction of European surface temperatures of *Luterbacher et al.* [2004, 2007]; *Xoplaki et al.* [2005] (hereafter referred to as *Luterbacher et al.* [2007]). In both reconstructions data on glacier fluctuations have not been included.

From the available instrumental temperature records, we use the combined land ocean HADCRUT3 global and hemispheric annual mean series. These series give the temperature anomaly relative to the mean temperature of the 1961–1990 reference period. Using the KNMI climate explorer (www.climexp.knmi.nl) we calculated the mean annual temperature anomaly over 25°W to 40°E and 35°N to 70°N for comparison with the reconstructed European temperature. In addition, we have calculated Scandinavian temperatures from the grid points between 5–20°E and 60–70°N and the average temperature over the Alps using the grid points between 5-15°E and 45-50 °N.

Mann et al. [2008] reconstruct global and hemispheric temperature anomalies for the last two millennia from a multi-proxy composite. The majority of the records are tree-ring proxies, and in addition records from marine sediment, speleothem, lacustrine, ice core, coral and historical documentary series are used. *Mann et al.* [2008] thus combine most of the presently available temperature proxies. They describe the results of various proxy reconstructions resulting from different methods in averaging and the exclusions of a part of the available records. Here we use the "error-in-variables" (EIV) composite of all land and ocean records.

Luterbacher et al. [2007] reconstructed European seasonal temperatures for the period 1500 to 2000 on a 0.5° latitude/longitude grid extending from 25°W to 40°E and from 35°N to 70°N. The reconstruction is based on instrumental series, documentary records of sea-ice and temperature and a few tree-ring records. From 1901 to 2000 the land-only CRU temperatures are used. We calculate European annual temperature anomalies by calculating seasonal temperature anomalies relative to the 1961–1990 seasonal mean and subsequently averaging over the 4 seasons per year and over the entire grid. In addition we have calculated Scandinavian temperatures from the grid points between 5–20°E and 60–70°N and the average temperature over the Alps using the grid points between 5–15°E and 45–50°N.

To conclude, we use the HISTALP temperature record for comparison of the temperature reconstructed from the records in the Alps. The HISTALP project (www.zamg.ac.at/histalp/) provides temperature, precipitation, pressure, sunshine and cloudiness for the Greater Alpine Region (GAR) 4–19°E, 43–49°N [*Auer et al.*, 2007]. The GAR temperature record goes back

to 1760 and consists of homogenized (historical) instrumental measurements in and around the European Alps [*Böhm et al.*, 2010].

4.3 Theory and methods

4.3.1 Glaciers and climate

The response of glaciers to a changing climate is dependent on the climate setting of the glacier and on its geometry. To describe the response, two main characteristics of a glacier are needed: its response time and its climate sensitivity. These are both conceptual quantities, derived from the response of a glacier in equilibrium state to a stepwise change in climatic forcing [*Jóhannesson et al.*, 1989]. As we are dealing with glacier length changes, the response time and climate sensitivity are defined in terms of change in glacier length and temperature. The climate sensitivity is a measure for the size of glacier length change going from one equilibrium state to another as a result of a change in the climatic conditions. The response time is a measure for the time needed to approach the new equilibrium length. It is defined as the time the glacier requires to reach $(1-e^{-1})$ of the final length change after a stepwise perturbation of the climatic forcing.

The most relevant meteorological parameters for changes in the climatic forcing are changes in temperature and precipitation [*Oerlemans et al.*, 1999; *Greuell and Smeets*, 2001]. In principle, glacier length variations reflect fluctuations in both temperature and precipitation. However, experiments with mass balance models show that glaciers are far more sensitive to typical changes in temperature than to typical changes in precipitation [*Giesen and Oerlemans*, 2010; *Adhikari and Huybrechts*, 2009; *Mackintosh et al.*, 2002; *Oerlemans*, 2001]. We neglect fluctuations in precipitation and assume that fluctuations in glacier length are caused by fluctuations in temperature only (see sections 4.4.3 and 4.5 for discussion). Furthermore, we assume that the temperature signal extracted from the glacier length fluctuations represents fluctuations in the annual averaged temperature. Glaciers in a cold and dry continental climate are mostly sensitive to changes in summer temperature, but for more maritime and tropical glaciers the melt season is longer, sometimes all year round. Those glaciers are thus more sensitive to fluctuations in the annual averaged temperature [*Oerlemans and Reichert*, 2000].

To relate the glacier length fluctuations to fluctuations in temperature, we follow the approach of *Oerlemans* [2005], who uses a linear first-order response equation:

$$\frac{dL'(t)}{dt} = -\frac{1}{\tau}\left(cT'(t) + L'(t)\right) \tag{4.1}$$

Here, t is time (a), τ (a) is the response time of the glacier, c (m/K) the climate sensitivity, L' is length change (m) and T' is a temperature perturbation (K) (annual mean) with respect

to a reference state. *Oerlemans* [2007] shows that for suitable values for τ and c this relation performs very well. Rearranging the terms and replacing $\frac{1}{c}$ by γ gives an expression for the temperature relative to the reference state in terms of glacier length change, response time and the inverse climate sensitivity γ:

$$T'(t) = -\gamma \left(L'(t) + \tau \frac{dL'(t)}{dt} \right). \tag{4.2}$$

4.3.2 Calculation of γ and τ

Each glacier has a specific γ and τ that characterize the response to changes in annual average temperature. In general, γ and τ are dependent on the geometry of the glacier and its climatic setting. We calculate these values for each glacier using the expressions of *Oerlemans* [2001] that are based on the simple glacier model discussed in Chapter 1.2.6:

$$\gamma = c_1 \frac{s}{\sqrt{P}} \tag{4.3}$$

and

$$\tau = c_2 \frac{1}{\beta s \sqrt{1 + 20 s} \sqrt{L}} \tag{4.4}$$

Here, P (ma^{-1}) is the mean yearly precipitation at the glacier, s is the mean slope of the glacier surface, β (mwe $\mathrm{a}^{-1}\mathrm{m}^{-1}$) is the balance gradient, parametrized as $\beta = 0.006\sqrt{P}$ [*Oerlemans*, 2005], and L (m) is the length of the flow line. The constants c_1 and c_2 are calibrated by comparing the results of numerical ice flow models with the results of the expressions derived from the analytical model (Eq. 4.3, 4.4). We have to take the results of numerical models as 'true values' for the response time and climate sensitivity. The response time and climate sensitivity are defined in terms of response from one equilibrium state to another, due to a stepwise change in the climatic forcing. In reality climate is never constant. Therefore glaciers hardly ever reach an equilibrium with the current climate. Moreover, climate changes not in a stepwise fashion from one constant state to another. This makes it impossible to derive the response time and the climate sensitivity of a glacier directly from observations [*Oerlemans*, 2007].

For the calibration of the response time τ we use the results of fifteen numerical models (Table 4.1). The calibration based on least squares gives a optimal value of 19.4 $\mathrm{m}^{\frac{1}{2}}$ for c_2. The analytical model corresponds well with the results of the numerical models and there is a significant correlation of 0.83 between the response times calculated with the minimal model and the response times derived from the numerical models.

For the calibration of c_1 we have the climate sensitivities ($\frac{1}{\gamma}$) of fourteen glaciers, obtained with numerical models (table 4.1). The best results, again based on least squares, are obtained with a value of 0.00204 K a^{-1} for c_1. For γ there is a correlation between the values of

glacier	response time (a)	climate sens. (m/K)	reference
Gr Aletsch	83	5436	Oerlemans [unpublished]
Argentière	27-45 (38)	4200	*Huybrechts et al.* [1989]
AX010	50-84 (60)	3616	*Adhikari and Huybrechts* [2009]
Brikdalsbreen	52-60 (56)	-	*Laumann and Nesje* [2009]
Franz Josef	20-27 (24)	3200	*Oerlemans* [1997b]
Hintereis	94 ± 15	4200	*Greuell* [1992]
Muragl	-	1700	*Jouvet et al.* [2008]
Nigardsbreen	63-73 (68)	6100	*Oerlemans* [1997a]
Pasterze	70-137 (80)	-	*Zuo and Oerlemans* [1997b]
Rhone	58	2600	*Wallinga and van de Wal* [1998]
Sofiyskiy	73-84 (77)	2000	*De Smedt and Pattyn* [2003]
Solheima	69	5500	*Mackintosh* [2000]
Storglaciären	125	3300-5400 (4500)	*Brugger* [2007]
Rabots	165-197 (179)	2600-4600 (3400)	*Brugger* [2007]
Untere Grindelwald	34-45 (38)	4500	*Schmeits and Oerlemans* [1997]
Vernagt	50	4667	*Smith and Budd* [1980]

Table 4.1: *Values of climate sensitivity and response time obtained from the literature; if a range is given the number between brackets is used for calibration.*

numerical models and the values of the analytical model of 0.50. This correlation is only significant at the 90% confidence level (see section 4.5 for discussion). We get different values for τ and γ than *Oerlemans* [2005], who used the results of only 6 numerical models for the calibration of c_1 and c_2.

4.3.3 Temperature reconstruction

Provided we know the precipitation, the average slope, and the absolute length of the glacier, we can reconstruct a temperature anomaly record from a glacier length record using Eq. 4.2 - 4.4. We take the glacier state in 1950 as the reference state, because all records cover the year 1950.

Besides the length changes, equation (4.2) also contains the derivative of the length change. Our method, based on a simplified analytical glacier model, can not account for year-to-year variations in the rate of length change. It does not resolve glaciological details such as irregularities in the bed topography at the glacier tongue. To be able to apply the linear response equation (4.2) all records are smoothed [*Oerlemans*, 2005; *Oerlemans et al.*, 2007]. For the smoothing we use the following weighted running average: for the calculation of the ith smoothed value, the weights w_j of the neighbouring values are given by

$$w_j = 10^{-\frac{|i-j|}{width}} \tag{4.5}$$

resulting in a smoothed value s_i

$$s_i = \frac{\sum_{j=i-width}^{i+width} w_j v_j}{\sum_{j=i-width}^{i+width} w_j} \tag{4.6}$$

where v_j is the jth value of the record and *width* is the filter width. This width is set to 10 points (years), but it is decreasing when the beginning or end of the record is less then 10 points away. In this way the full record can still be used at the cost of less smoothing near its ends. The first and last point are not affected by the smoothing procedure, so the total length change remains the same after smoothing. We have tried different filter widths and different smoothing procedures, e.g. Gaussian filter, but the above mentioned method yields the optimal results in combination with the Stineman interpolation. From the interpolated and smoothed record we get a temperature anomaly $T'(t)$ for each glacier length record using (4.2). As the length of the temperature reconstruction is the same as the length of the glacier length record, there is a wide variety in reconstruction length and covered period. To be able to compare the reconstructions from different records, the temperature anomaly of each record is expressed relative to the 1945–1965 mean, the period that is covered by all records.

4.3.4 Average of temperature records

As can be seen in Figure 4.1, the records are clustered and thus do not cover large portions of the Earth's surface. Furthermore, the number of records varies in time (Figure 4.2). This requires an averaging method that on the one hand takes the spatial distribution into consideration when assigning the temperature records of individual glaciers a certain weight, and, on the other hand, is flexible so it can change the assigned weights in time. For our method of estimating the uncertainty it is convenient to consider glaciers on an individual basis. We opt for a method that assigns a weight to each record based on the mutual distances between glaciers. For each year the mutual distances R_{ij} between the glaciers that have a record in that year are calculated. The weight of a particular record W_i in a year with N records is given by the ratio of the total of the squared distances of this glacier to the other $(N-1)$ glaciers, to the total of the squared mutual distances for all N glaciers

$$W_i = \frac{\sum_{j=1}^{N} R_{ij}^2}{\sum_{k=1}^{N} \sum_{l=1}^{N} R_{kl}^2} \tag{4.7}$$

We have compared the global average of the reconstructed temperature with the results obtained with other weight functions. It appears that the temperature reconstruction is not sensitive to the weight function (see Appendix 4.7.1 for details).

4.3.5 Estimate of uncertainty

The reconstructed temperatures from individual glacier length records have an uncertainty due to uncertainties in the data on length change, gaps is the glacier length records, and uncertainties in the calculated response time τ and (inverse) climate sensitivity γ. We use a smooth bootstrapping procedure [*Hesterberg et al.*, 2005] to evaluate the resulting uncertainty in the spatially averaged temperature reconstructions. We calculate the average of N reconstructed temperature records (N is 308 for the global average, 246 for the NH average, etc.). From these N records we then randomly draw with replacement 100 samples of again N records. For each of these samples the average is calculated and recalculated 10 times with perturbed values for each of the glacier length change data points, the response times and the climate sensitivities. In addition, interpolated gaps in the glacier lengths records are perturbed by adding autoregressive noise. Thus we have an ensemble of 1100 temperature reconstructions. Twice the standard deviation of this ensemble, smoothed over 20 years, is taken to be the 95% confidence interval.

The uncertainty of the data points is related to the method of measurement, given by the categories described in Section 4.2.2. The perturbation of a glacier length change data point is a number randomly drawn for a normal distribution times a factor ε given by the data accuracy category of that measurement. Hence the perturbed glacier length change L'_{pertb} is given by:

$$L'_{\text{pert}} = L' + r_d * \varepsilon \tag{4.8}$$

where for each data point of the record a new random number r_d is drawn. The errors of the measurements are with 99% certainty (3 standard deviations) within the limits given in section 2.2. The factors ε give the standard deviation of the perturbations, and should thus be one third of the estimated maximum error.

The uncertainty in the response time τ calculated with the analytical glacier model is derived from the goodness of fit of the calibrated results (Eq. 4.4) to the results of the numerical models (Table 4.1). We divide the values obtained with the numerical model by those of the corresponding analytical model. We get 15 numbers spread around the ideal value 1. The standard deviation of these numbers is $\sigma_\tau = 0.28$. We perturb τ calculated with the analytical model by multiplying it with a random factor. As τ can not have negative values, we draw the factors from the gamma distribution instead of a normal distribution. The perturbed values τ_{pert} are thus given by:

$$\tau_{\text{pert}} = r_\tau * \tau \tag{4.9}$$

where r_τ is a random number drawn from the gamma distribution with mean 1 and standard deviation σ_τ. The random number is redrawn for each time a temperature is reconstructed from a glacier length record.

The uncertainty in the inverse climate sensitivity γ (Eq. 4.3 is treated in the same way as the uncertainty in the response time. For the 14 glaciers, we divide the results from numerical

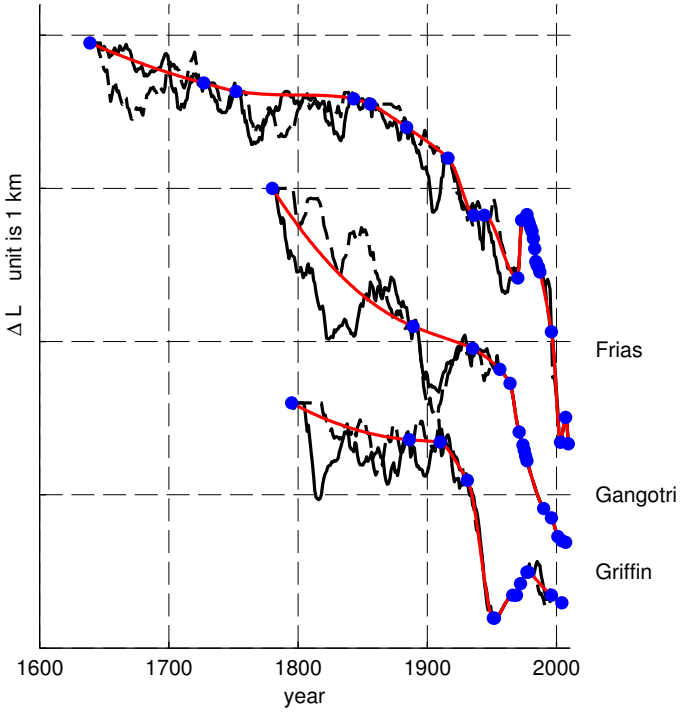

Figure 4.3: *Examples of sparse records (see Appendix A for references) with AR noise added to gaps. The measured length changes are indicated by blue dots; the interpolated record (red) with added AR noise is given in black lines. For each record, two independent perturbations of the record are shown.*

models in Table 1 by the result of the analytical model. The standard deviation σ_γ of these numbers is 0.50. We perturb γ by multiplying it with a random factor. Like τ, γ cannot be negative (that would imply the glacier advances when temperature increases), hence we draw the factors from the gamma distribution as well. The perturbed values γ_{pert} are thus given by:

$$\gamma_{\text{pert}} = r_\gamma * \gamma \tag{4.10}$$

where r_γ is a random number drawn from the gamma distribution with mean 1 and standard deviation σ_γ. The random numbers are redrawn for each time a temperature is reconstructed from a glacier length record.

If a record does not have annual data, as most records do for at least some period, the gaps are filled by interpolation (see Section 4.2). If the period without length measurements is in the order of the response time of the glacier or larger, information on climatic variations is lost. Autoregressive (AR) noise is added to the parts of the length records that are interpolated for

a period longer than 0.3 times the response time, to estimate the magnitude of the error in the temperature reconstruction that is caused by the use of sparse glacier length records. That means that for every year in the gap of the record, we have recalculated $L(t)$:

$$L(t) = L_{\text{interp}}(t) + L^*(t), \tag{4.11}$$

where $L(t)$ is the new perturbed length record, L_{interp} is the record obtained from the Stineman interpolation of the data points, and $L^*(t)$ is the AR noise perturbation. The perturbation term $L^*(t)$ is calculated with an autoregressive model (AR model) [e.g. *Box and Jenkins*, 1976; *Fisher*, 2002]:

$$\sum_{k=0}^{p} \phi(k) L^*(t-k) = \sigma_L \varepsilon(t), \tag{4.12}$$

where ε is zero-mean white noise, $\phi(k)$ are the order-p autoregressive model coefficients, and σ_L is the noise variance. The values of $\phi(k)$ and σ_L are calculated using the Yule–Walker method from eight detrended, detailed, long records: Bergsetbreen, Bondhusbreen, Glacier des Bossons, Brikdalsbreen, Buerbreen, Mer de Glace, Rosenlauigletscher and Untere Grindelwaldgletscher.

The AR model is run both forward and backward, starting from both sides of the gap. A linear transition from the forward to the backward noise signal is made, such that the perturbed record starts and ends at a data point without abrupt length changes. If end moraines are present (measurements category 3 or 4), the AR model is maximised to the glacier length at these moraines. In Figure 4.3 examples of perturbed interpolations are shown.

4.4 Results

4.4.1 Global temperature anomaly

In Figure 4.4a, we show the global temperature reconstructions from glacier length records, the multi-proxy global land and ocean temperature reconstruction from *Mann et al.* [2008] for the period 1600–2000, and the instrumental land and ocean record for the period 1850–2000. All records shown are temperature anomalies with respect to their 1961–1990 mean. The uncertainty bands give a 95% confidence interval. *Mann et al.* [2008] have calibrated their temperature reconstruction with the instrumental record. Therefore, this reconstruction has no uncertainty indicated for the period of the instrumental record (1850 to 2000). The temperature reconstruction from glacier length fluctuations has no annual resolution, inherent to the slow response of a glacier to perturbations of its mass balance. For the first period (1600–1700), the temperature record has a lower than decadal resolution, due to the lower resolution of the length records (Appendix 4.7.2). Hence the temperature signal of an individual glacier length record is rather smooth in this period. The small irregularities in the global average

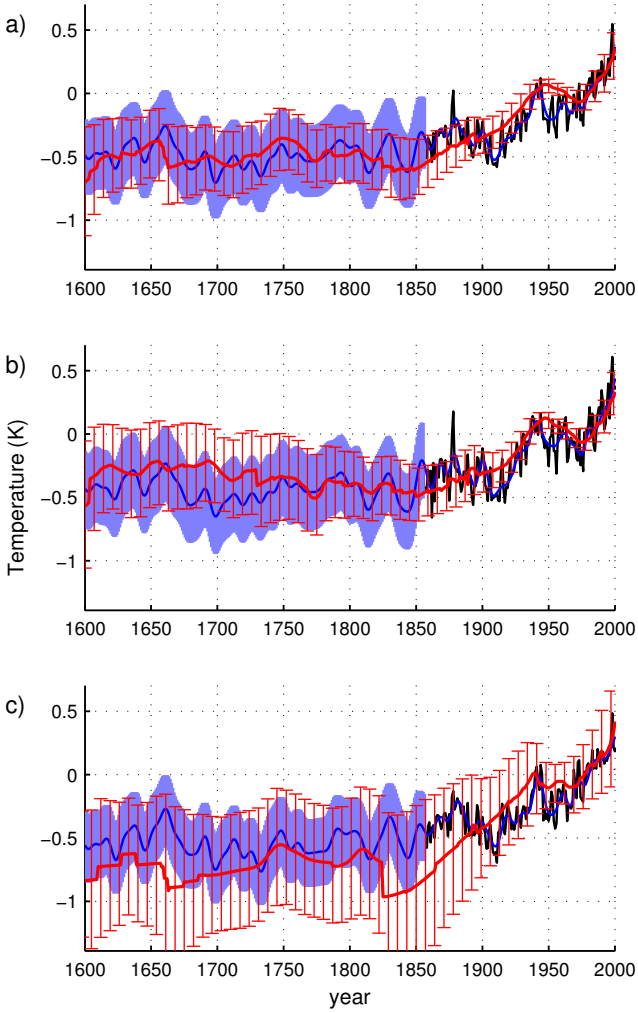

Figure 4.4: ***a)*** *Global,* ***b)*** *NH, and* ***c)*** *SH, temperature anomaly w.r.t. 1961–1990 mean from: HADCRUT3 instrumental record (black); Mann et al. [2008] multi-proxy with land and ocean records, shaded uncertainty (blue); glacier reconstruction of this study with 95% confidence interval bars (red).*

before 1900 result from the addition to the sample of records that deviate from the average temperature. After 1900, these irregularities disappear because of the increase in the number of available records.

Our reconstruction shows a fairly constant global mean temperature for the period 1600-1830. From 1830 until 1940, temperatures continuously increased by 0.61 $\pm$ 0.26 K. From 1940 to

1970, there is a temporal decrease of the global mean temperature of 0.07 $\pm$ 0.12 K. After 1970, temperature is increasing leading to a cumulative warming from 1830 to 2000 of 0.94 $\pm$ 0.31 K and of 0.84 $\pm$ 0.35 K for the period 1600-2000. The rate of temperature change over the period 1980–2000, with a linear trend of 0.16 K per decade, is the highest over the last 400 years. It is comparable with the temperature change over the period 1920-1940, which has a linear trend of 0.12 K per decade. Our reconstruction supports the conclusion of *Mann et al.* [2008] that the high global average temperatures of the 1990–2000 decade are unprecedented in at least the last four centuries.

For the period 1920 to 2000, the reconstructed temperature corresponds well with the instrumental land and ocean record, as both show the same amount of warming. However, in the reconstruction the temporal maximum in the 1940's is timed a few years later and the cooling afterwards is less abrupt than in the instrumental record. For the 19th century, there is a difference between the reconstruction and the instrumental record. The glacier records show a warming trend which starts between 1830–1840 and continues uninterrupted into the 20th century. The instrumental record shows a cooling trend at the end of the 19th century and the start of the 20th century. Consequently, the instrumental record shows higher temperatures at the end of the 19th century and lower temperatures at the beginning of the 20th century. Before 1850, the reconstruction from the glacier records agrees very well with the multi-proxy record. Before 1650, the uncertainties of the glacier reconstruction increase rapidly as the number of available records becomes very small.

4.4.2 Northern and Southern Hemisphere temperature anomaly

The reconstructed NH temperature anomalies (Figure 4.4b) show results that are similar to the global reconstruction. The glacier reconstruction shows constant temperatures for the period 1600–1700, followed by a gradual cooling from 1700 to 1850. From 1850 to 1945, the NH mean temperature rises by 0.61 $\pm$ 0.26 K. After a decline in temperature from 1945 to 1975 of 0.18 $\pm$ 0.11 K, temperature rises until 2000. The cumulative temperature increase for the period 1850 to 2000 given by the reconstruction from glaciers is 0.82 $\pm$ 0.27 K.

From 1600 to 1850, the temperature reconstruction from glacier length agrees very well with *Mann et al.* [2008] land and ocean NH reconstruction. Both *Mann et al.* [2008] and the instrumental record show a slight warming in the second half of the 19th century, followed by a cooling in the early 20th century. This fluctuation is not present in our reconstruction, that shows a constant warming since 1850 as in the global temperature reconstruction. In the instrumental record as well as in our reconstruction, the cooling in the middle of the 20th century is more pronounced on the NH than in the global average. To conclude, the recent strong warming is well reproduced by the temperature reconstruction from glacier length fluctuations up to 2000.

The reconstruction of SH temperature anomalies is shown in Figure 4.4c. The reconstruction gives a SH temperature increase of 1.27 $\pm$ 0.76 for the period 1850–2000. Despite of the much smaller number of records on the SH compared to the NH, is our SH temperature reconstruction in good agreement with the instrumental record between 1900 and 2000. Both the instrumental records and our reconstruction show a less pronounced cooling in the middle of the 20th century than is observed on the NH, and strong warming over the last two decades of 0.13 K per decade. Between 1600 and 1825 our results are in good agreement with *Mann et al.* [2008]. The larger error compared to the error in the NH temperature reconstruction in the period 1850–2000 is due to the smaller number of records (Figure 4.2). Prior to 1850, the number of available records on the SH is comparable to that of the NH. The larger uncertainty in the reconstructed temperature of the SH for the period 1600–1850 results from larger uncertainty in glacier length data and sparser records. The clear jumps of the temperature in 1825 and around 1660 result from the addition of records to the sample.

4.4.3 European temperature anomaly

Europe is very well represented in our data set, with ample records from different parts of the continent. Within the boundaries of 25°W to 40°E and 35°N to 70°N used in *Luterbacher et al.* [2007] we have 115 records. Most of the records (86) originate from the Alps in central Europe, but we also have records throughout Scandinavia (20), on Iceland (6) and in the Pyrenees (4) (Figure 4.1). We use these records to test our assumption that the influence of variations in precipitation is of secondary importance for large-scale temperature reconstructions. In Figure 4.5, we show the reconstructed temperature from two regions (Alps and Scandinavia) and the continental average. Along with our reconstruction, we have plotted the instrumental record HADCRUT3, the instrumental HISTALP record and the documentary reconstruction of *Luterbacher et al.* [2007].

The reconstructed temperature of the Alps (Figure 4.5b) is in the second half of the 19th century higher than the instrumental records. This is probably due to glacier retreat that is attributed to a decrease in winter precipitation at the end of the LIA [*Vincent et al.*, 2005]. From the beginning of the 20th century until 1985 the reconstructed temperature is in agreement with the instrumental records. In the last two decennia the reconstructed temperature from glacier length changes does not reproduce the observed strong warming. The response in glacier length change could be delayed due to downwasting and consequent dynamical decoupling of the glacier tongue observed in the Alps [e.g. *Paul et al.*, 2004]. Prior to the start of the instrumental records, the temperature reconstructed from glaciers is in broad agreement with the reconstruction of *Luterbacher et al.* [2007].

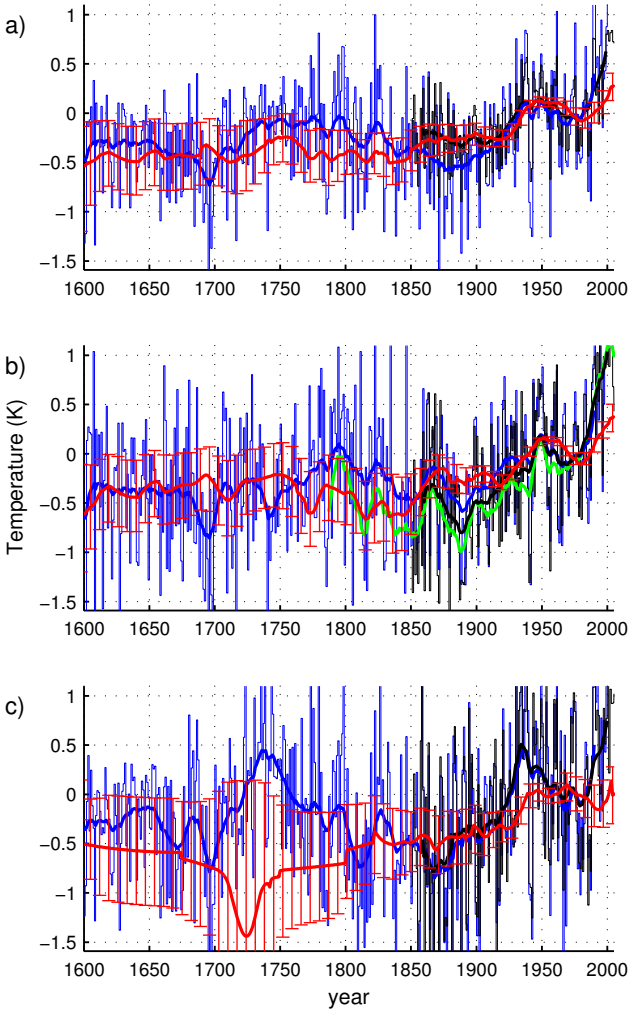

Figure 4.5: *Annual average **a)** European, **b)** European Alps, and **c)** Scandinavian temperature w.r.t. 1961–1990 mean from: HADCRUT3 measurements with 15 year smoothed series (black); Luterbacher et al. [2007] with 15 year smoothed time series (blue); glacier reconstruction, with uncertainty bars (red). For the European Alps (**b**), also the 15 year smoothed HISTALP instrumental temperature record is shown (green).*

The temperature reconstruction from Scandinavian glaciers (Figure 4.5c) is also influenced by fluctuations in precipitation that are relatively large, due to the maritime climate of most of the glaciers in the data set. We reconstruct a cooling in the 1990's due to glacier advances. The advances are explained by an increase in precipitation rather than a decrease in temperature [*Andreassen et al.*, 2005]. The strong warming in the 1930's is underestimated by the reconstruction from glaciers. The slight increase in precipitation during that period is likely to play only a minor role in this [*Giesen*, 2009]. The reconstruction of *Luterbacher et al.* [2007] and the temperature reconstructed from the glacier length variations widely diverge in the 18th century.

The reconstructed temperatures for the separate regions do not match the instrumental records. This is at least partly due to unaccounted variations in precipitation. The continental average over the temperature reconstructions from all European glacier length records is in good agreement with the European instrumental record (Figure 4.5a). However, there seems to be a lag of 7 years in the warming period 1915-1940 and the cooling period around 1960. The warming in the last two decades 1980 - 2000 as reconstructed from the glacier lengths is not as strong as in the instrumental record.

4.5 Discussion

4.5.1 The influence of precipitation

The present glacier retreat is observed worldwide [*WGMS*, 2008]. All the temperature reconstructions presented in this article show a warming trend since the mid-19th century, resulting in a warming in the order of 0.5–1.0 K. Only a strong drying on a global scale could explain a worldwide retreat of the same magnitude. There is no independent evidence at all of such drying [*Trenberth et al.*, 2007; *Smith et al.*, 2009]. Thus, only an increase in global temperature can explain the observed glacier retreat. In this study we have calculated the global and hemispherical temperature records that best explain the observed glacier fluctuations.

As argued in section 4.3.1, the mass balance of glaciers is more sensitive to changes in temperature than to variations in (winter) precipitation. The yearly variations in mass balance are explained by variations in precipitation as well as temperature, but the decadal variations in glacier mass balance result essentially from changes in temperature and the related dynamic adjustment of the glacier size. The glacier length signal reflects the integrated mass balance over decadal timescales. Hence we believe that variations in precipitation only have a limited contribution to the glacier length variations. Furthermore, in their estimate of the contribution of glaciers to global sea level rise over a period of 70 years, *Van de Wal and Wild* [2001] show that the projected variations in precipitation have virtually no influence on the calculated global glacier volume changes. Nevertheless, for individual glaciers and mountain regions, variations in precipitation contribute to the explanation of the observed glacier

fluctuations [e.g. *Steiner et al.*, 2008; *Fischer*, 2010; *Andreassen et al.*, 2005; *Vincent*, 2002]. Hence, on a regional scale, fluctuations in precipitation cannot be neglected in the climate reconstruction from glacier fluctations. This is evident when we compare the reconstructed temperature of the European Alps and Scandinavia to the corresponding instrumental records (section 4.4.3).

The reconstruction of European annual temperature anomalies from glacier length is in far better agreement with the instrumental temperature record than the reconstructions of the individual regions (Figure 4.5). In the pre-instrumental period the continental average is also in better agreement with the temperature reconstruction of *Luterbacher et al.* [2007] than the regional reconstructions. It appears that on a continental scale, there is only a small influence of variations in precipitation on the derived climate signal. We expect that this is caused by the incoherency of variations of precipitation on a large spatial scale. The average correlation distance of annual precipitation anomalies is about four times as small as the average correlation distance of temperature anomalies [*Krajewski et al.*, 2000; *Hansen and Lebedeff*, 1987]. We believe this justifies our assumption that we can neglect the fluctuations of precipitation in the hemispheric and global climate reconstructions from observed glacier fluctuations.

4.5.2 Contributions to the uncertainty

The uncertainty calculations account for several causes in the uncertainty of the reconstructed temperature. In order to estimate the magnitude of the contribution of the different causes, the uncertainties in the average temperature reconstruction are calculated separately for each contribution. The results for the global temperature reconstruction is shown as an example (Figure 4.6). The separate contributions are calculated by taking ensembles with 100 members of the global average temperature change, with only one of the four perturbations mentioned in Section 4.3.5 (Figure 4.6a–d). In addition, we have calculated the global average from random samples of all records (Figure 4.6e). The ensembles are shown along with the best estimate of the global temperature change. The magnitude of the uncertainties is given by the spread of the members in the ensemble calculated from random perturbation of the originally used values. By comparing the Figures 4.6a–e it becomes clear that the uncertainty in the climate sensitivity, gaps in the records, and the variability in the individual reconstructions are the major contributors to the total uncertainty of the global average temperature. The smallest contributor is the uncertainty in the response time. In Figure 4.6f, the ensemble, consisting of 1100 members, of the complete uncertainty estimate is shown along with the ensemble average and the best estimate with its uncertainty (cf. Figure 4.4a). The ensemble average and the best estimate are almost identical.

To reduce the uncertainty, more data could be added to the glacier length data set. More records in the data set could reduce the sample uncertainty. Adding data to existing records, giving them a higher resolution, would reduce the uncertainty due to gaps. It is not very likely

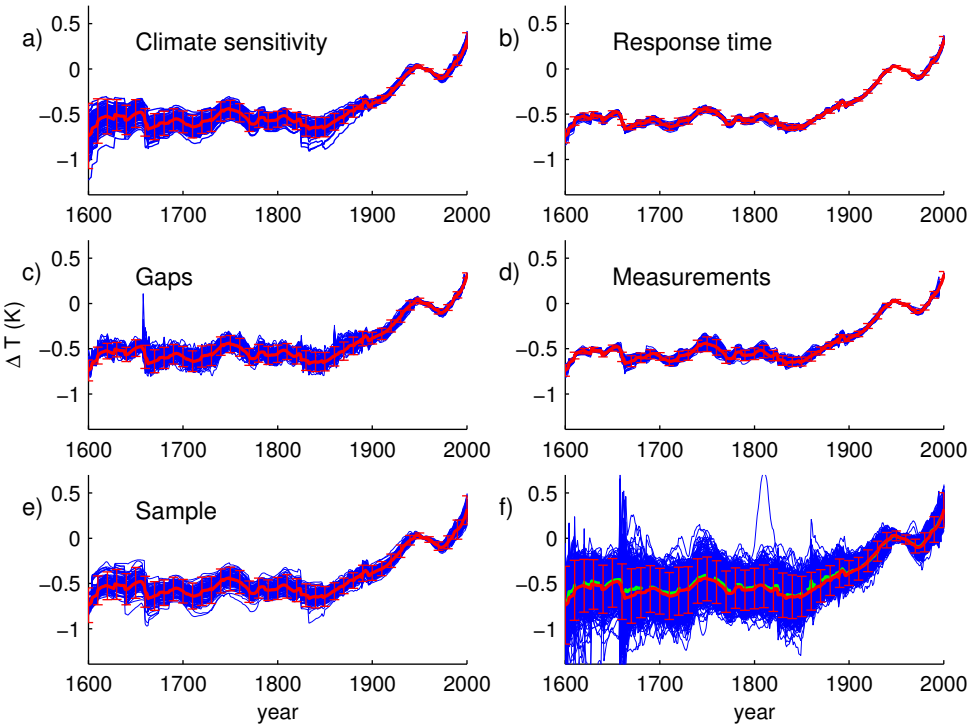

Figure 4.6: *The uncertainty in the global average reconstructed temperature for each of the 5 separate causes, based on the spread of the 100-member ensemble caused by uncertainty in:* ***a)*** *the inverse climate sensitivity* γ*;* ***b)*** *response time* τ*;* ***c)*** *gaps in sparse records;* ***d)*** *measured length change; and* ***e)*** *sampling of the 308 available records. In* ***f)****, the 1100-member ensemble including all uncertainties of the global average is shown (cf. Figure 4.4a). The ensemble average (dashed green) is very close to the best estimate (red). The uncertainty bars give twice the standard deviation of the ensemble.*

that on these points major improvements are possible on the short term. However, a significant reduction of the uncertainty in the reconstructions could be obtained by improving the climate sensitivity calculation. The poor fit of calibrated climate sensitivity of the analytical model to the results of numerical models suggests that for a good estimate of the climate sensitivity more details of the glacier geometry should be taken into account. The only geometric factor included in the analytical glacier model is the average slope, while assuming a constant glacier width. Detailed information on the glacier geometry is currently lacking for most of the glaciers used in this study. However, the climate sensitivity of a glacier is strongly dependent on its geometry [*Oerlemans*, 2001; *Brugger*, 2007]. Furthermore, we assume a climate sensitivity that is constant in time, but in reality the climate sensitivity of a glacier changes with glacier advance or retreat [e.g. *Mackintosh*, 2000]. We expect that including a more de-

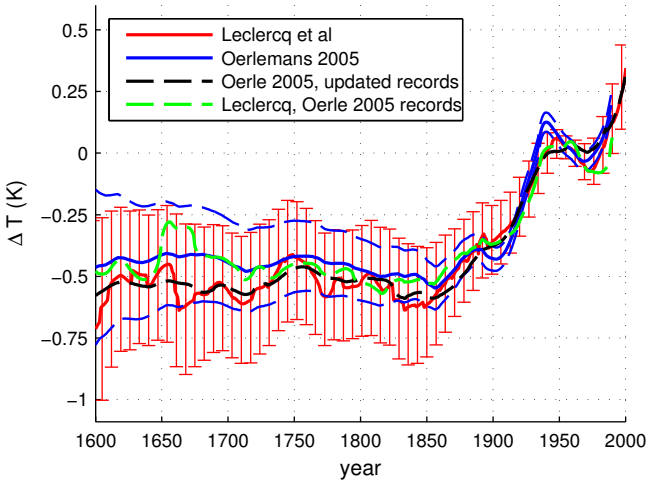

Figure 4.7: *Reconstructed global temperature from: this study (red, with uncertainty bars); the study of Oerlemans [2005] (blue, uncertainty range in dashed blue); the method as used in Oerlemans [2005] on the revised 169 records (dashed black); and calculated from the original 169 records of Oerlemans [2005] with the methods of this study (dashed green).*

tailed glacier geometry could greatly improve the accuracy of the reconstructed temperature from individual records. This could be achieved in the near future, as more and more glacier outlines become available through projects like the GLIMS initiative.

As described in section 4.3.3, the amount of smoothing decreases towards the end of the records. This can result in overestimation of temperature changes near the ends of the record. This effect is most important for the glaciers with a large response time (see equation 4.2). For most records, this effect of less smoothing is less strong at the start of the records. About 80% of the records have more than one year between the first two length measurements. The interpolated values between the first and the second measurement give a smooth record. Near present time measurements are more abundant and less than 50% of the records have more than one year between the last two data points. So the overestimation of the temperature anomalies of individual records occurs mostly from 1968, when the first record ends, on to 2000, when 77 records have ended. This is represented by an increasing uncertainty from 1968 to 2000 (Figure 4.4, 4.5). To prevent this we should cut off the ends of the smoothed record. However, we think there is more to gain from the information of the entire records than we loose in noise resulting from lack of smoothing near the ends.

4.5.3 Comparison with the earlier reconstruction

Comparison with the results of *Oerlemans* [2005] shows that the present reconstruction with more data has a less pronounced warming in the period up to 1940, more in line with the instrumental record. In addition, the best estimate of the present reconstruction shows a cooler period in the mid-19th century than the best estimate of *Oerlemans* [2005]. These differences are not caused by the difference in averaging method (compare the blue line with the dashed green line in Figure 4.7). The differences are the result from the additional data, as is clear from the difference between the earlier results of *Oerlemans* [2005] and the results from the updated records with the methods of *Oerlemans* [2005] (Figure 4.7). The estimated uncertainty of the present reconstruction is larger, despite the increased number of records. We have attributed larger uncertainties to the values of the response time and climate sensitivity of each glacier, as calculated with the analytical glacier model. And we have included the uncertainty due to missing data and an estimate of the uncertainty in the data on glacier length change.

4.6 Conclusion

We have shown that glacier length records can provide very useful information on past temperature fluctuations. They form a reliable proxy for fluctuations of the annual temperature on decadal time scales and on hemispherical, or larger, spatial scales, reproducing the instrumental record over the last century very well. Furthermore, the reconstruction of temperature fluctuations based on glacier length changes is fully independent of other proxies. Thus, it forms a valuable addition to existing proxies.

The reconstructed temperature shows a spatially coherent signal. This makes the global average insensitive to the method of averaging. Our reconstruction shows that the global mean temperature rose by 0.94 ± 0.31 K over the period 1830–2000. The warming over the period 1850–2000 is 0.82 ± 0.27 K and 1.27 ± 0.76 K on the NH and SH, respectively. The high global averaged temperatures of the period between 1980 and 2000 are unprecedented in at least the last 400 years. In addition, the rate of temperature increase over the period 1980–2000 is the highest of the period 1600–2000. In these respects our reconstruction supports existing proxy-reconstructions. However, compared to the multi-proxy composite of *Mann et al.* [2008] and the instrumental record, the glacier records show a slightly colder second half of the nineteenth century. According to our reconstruction, the rise of the global temperature and the temperatures on both hemispheres started between 1830 and 1850 and continued uninterrupted into the 20th century.

4.7 Appendix

4.7.1 Average weight function

We test the sensitivity of the temperature reconstruction to the chosen spatial averaging method. Therefore, we calculate the reconstructed global average temperature with three different weight methods:

1. equal weights for all records
2. the weights of *Oerlemans* [2005]
3. weights of individual records based of the distance between the glaciers instead of the squared distance

and compare these results with the average obtained from the method as described in section 4.3.4. The resulting global average temperature anomalies (relative to 1950) are shown in Figure 4.8.

In the case of equal weights for all records, the average temperature anomaly in a certain year is the arithmetic mean of all available records in that year.

Oerlemans [2005] defined 4 regions on the Northern Hemisphere:

- North America, containing the glaciers of the North-western USA, the Canadian Rockies and Alaska,
- North Atlantic, including the glaciers of Greenland, Iceland, Scandinavia and Svalbard,
- the Alps and Pyrenees,
- Asia, including the Caucasus, Tien Shan, Himalyas, Altai and Kamchatka.

For each region the average temperature is calculated without further weighting of individual records. To calculate the Northern Hemisphere average, the regions 1 to 4 are given different weights: 0.2, 0.3, 0.2, and 0.3, respectively. The Southern Hemisphere is not subdivided in regions, the average is the arithmetic mean of the available records. The global mean is given by the arithmetic mean of both hemispheres.

The last weighting procedure considered is similar to that used in the reconstruction (as described in section 4.3.4). The difference is that the weight is not depended on the squared distance between the glaciers, but on the distance itself. Hence, the influence of the spatial distribution on the attributed weights is less strong.

The different averaging procedures result in a different weight for specific regions. For example, the cumulative weight of the records on the Southern Hemisphere is 50% in the method of *Oerlemans* [2005], independent on the number of records. It varies between a 32% and 53%

in the average of the mutual distance methods. When we give equal weights to all records, it is less than 25% for the period 1850–2000, but more than 60% for the period 1660–1700.

The differences between the temperature reconstructions resulting from different weights methods are small, much smaller than the uncertainty in the reconstruction due to the causes discussed in 4.3.5 and shown in Figure 4.4a. Thus, the temperature reconstruction is not sensitive to the kind of average taken, which suggests a strongly coherent temperature signal over the globe.

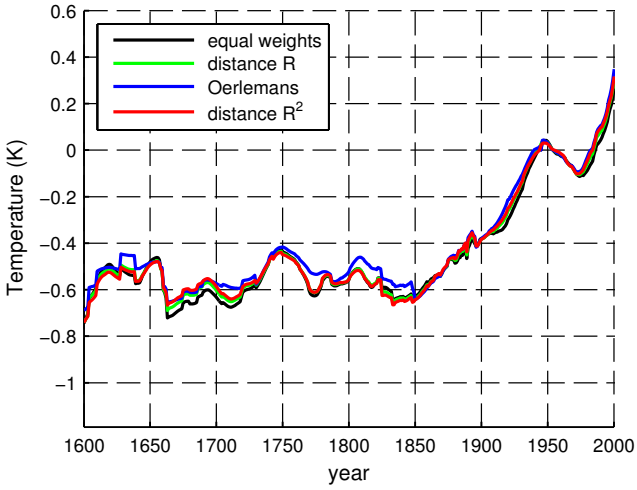

Figure 4.8: *Average global temperature calculated with different weights: equal weights to all records (black); 5 weighted samples as in Oerlemans [2005] (blue); the weights based on R (green); the weights based on R^2 as used in this study (red).*

4.7.2 Records with sparse data

As shown in Figure 2.1, most of the records have sparse data points before 1900 (if any data points at all). Very often these points are maximum stands derived from dated end moraines. This obviously influences the resolution of the temperature reconstruction and could cause a bias to lower temperatures. Here we have included an experiment with the two high resolution records of Mer de Glace [*Nussbaumer et al.*, 2007] and Untere Grindelwald [*Zumbühl*, 1980] (Figure 4.9) to get a qualitative idea of the influence of sparse data on the temperature reconstruction. We have plotted the original record and two stripped versions: one using only the data points of maximum and minimum glacier stands (min-max record) and one using only the maximum glacier stands before 1900 (max-only record). The number of data points decreases correspondingly. For Mer de Glace the original record has 153 data

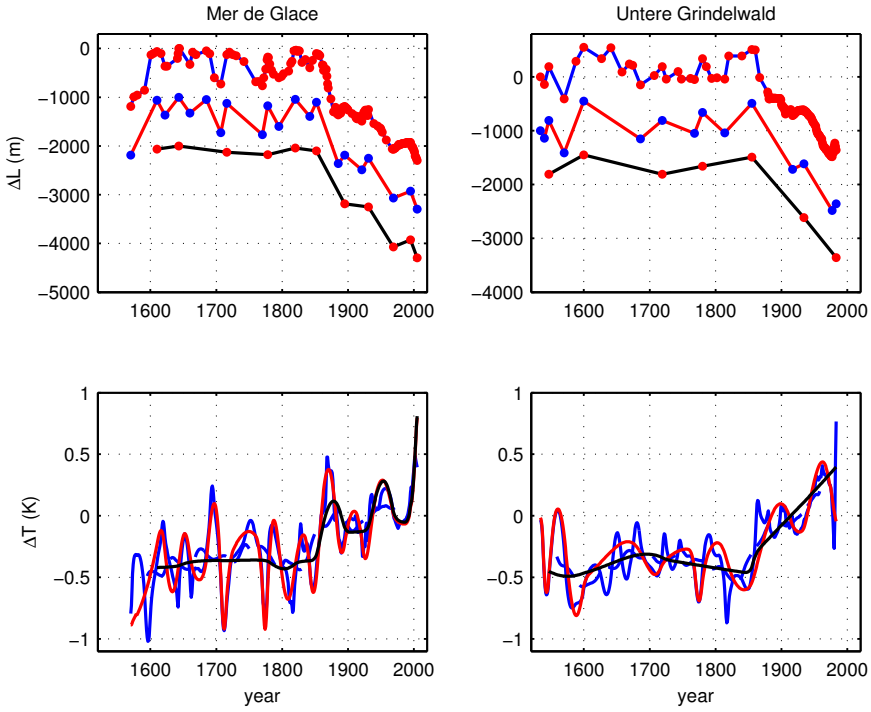

Figure 4.9: *Length fluctuation records of Mer de Glace [Nussbaumer et al., 2007] and Untere Grindelwald [Zumbühl, 1980] and the reconstructed temperatures. The upper panel shows the original length record (blue) and 2 derived low resolution records: 1) when only the minimum and maximum stands are taken into account (red) and 2) when only maximum stands are taken into account (black). The derived records have been shifted for better visibility. In the lower panel the reconstructed temperatures from the original record (blue) with 51 year running average (dashed blue), the record with minimum and maximum stands (red) and the record with only maximum glacier stands (black) are shown.*

points covering the period from 1570 to 2005, the record with only minimum and maximum glacier stands has 21 data points and the maximum-only record has 12 data points. The length record of Untere Grindelwald glacier has 128 data points in the period from 1534 to 1983, the minimum–maximum record has 15 data points and the maximum-only record has 7 data points covering the period 1547–1983.

The reconstructed temperatures of these 6 records are also shown. In the case of Mer de Glace, the temperature reconstructed from the min–max record is very similar to the original temperature reconstruction. In the min–max record of Untere Grindelwald glacier not all minimum and maximum glacier stands are used, because then the min–max record would resemble the original very much. It only has 7 points from 1600 to $\pm$1850. Therefore, the reconstructed temperature misses some of the variations. After 1850 it is again very similar

to the temperature reconstructed from the original record with almost annual resolution. The temperature reconstructed from the max-only record is in both cases close to the 51 year running average of the temperature reconstruction from original record.

These experiments show that we do not need glacier length records with annual resolution to reconstruct temperatures with a decadal resolution. Gaps of several decades can be bridged with interpolation as long as the extremes are known. The temperature derived from records that exist of maximum glacier stands does not necessarily have a cold bias. Records that are based on dated moraines are similar to this maximum-only records. In general, records with large gaps (up to 100 years) give us relevant climatic information, but with a low ($\pm$50–year) resolution.

5

The glacier contribution to sea-level rise for the period 1800-2005

Summary

In this Chapter, a new estimate of the contribution of glaciers and ice caps to the sea-level rise over the period 1800-2005 is calculated from the available information on changes in glacier length. At present, length records form the only direct evidence of glacier change that has potential global coverage before 1950. We calculate a globally representative signal from 349 glacier length records. By means of scaling, a global glacier volume signal is deduced, that is calibrated on the mass-balance and geodetic observations of the period 1950-2005. We find that the glacier contribution to sea-level rise was 8.4 ± 2.1 cm for the period 1800-2005 and 9.1 ± 2.3 cm for the period 1850-2005.

This Chapter is based on P.W. Leclercq, J. Oerlemans, J.G. Cogley, Estimating the glacier contribution to sea-level rise for the period 1800-2005, Reviews in Geophysics, **32**, 4/5, 519-535, 2011

5.1 Introduction

There is abundant evidence that eustatic sea level has been rising for at least the past two centuries [e.g. *Church and White*, 2006; *Jevrejeva et al.*, 2008; *Cabanes et al.*, 2001; *Warrick and Oerlemans*, 1990; *Barnett*, 1983]. Although the uncertainties are significant, the general view is that this rise has been between 15 and 25 cm for the period 1850-2000. This number is based on the analysis of tide gauge data, which do not provide a very good coverage of the oceans. Nevertheless, it appears that tide gauge and satellite data are broadly in agreement [e.g. *Nicholls and Cazenave*, 2010], lending some credibility to the use of tide gauge data to infer sea levels further back in time. For the period 1993 to 2009, high precision altimetry from satellites shows that sea level rose by 3.3 ± 0.4 mm yr^{-1} [*Nerem et al.*, 2010]. This suggests that sea level rise is accelerating.

Finding the causes for the current sea-level rise is crucial. Thermal expansion of ocean water, changes in terrestrial storage of water, mass loss of ice caps and glaciers, and possible long-term imbalances of the mass budgets of the Greenland and Antarctic ice sheets have been listed as the most important processes contributing to the observed sea-level rise. The pressure, both scientific and political, to make estimates of future sea-level change has led to the use of so-called semi-empirical approaches in which a simple relation between past sea-level rate and temperature or radiative forcing is determined, and then extrapolated through the 21st century [e.g. *Rahmstorf*, 2007; *Grinsted et al.*, 2009; *Vermeer and Rahmstorf*, 2009]. The uncertainties in such an approach are large and the resulting potential errors in projections enormous. For instance, if a long-term contribution from the Antarctic ice sheet to sea-level rise were to be erroneously attributed to the melt of glaciers and ice caps, an empirically determined sensitivity parameter could be very inaccurate. To constrain models in a better way, the processes that cause sea-level change have to be quantified in the best possible way. In this paper we attempt to estimate the contribution of glaciers and ice caps since 1800 AD. Throughout this paper we mean by glacier contribution the contribution to sea-level change from all glaciers and ice caps outside the large ice sheets of Greenland and Antarctica. Included are the glaciers and ice caps on Greenland and Antarctica which are not part of or attached to the main ice sheets.

There are basically two approaches to estimate the loss of glacier ice over longer periods of time. The first approach is to use modelled climate sensitivity of glacier mass balance in combination with instrumental meteorological records of temperature and/or precipitation. It is assumed that the glacierised area does not change, and that the effect of climate change can simply be calculated by the combination of mass-balance sensitivity and climate perturbations. This approach was applied by *Zuo and Oerlemans* [1997a] to 100 glacierized regions, allowing for the fact that glaciers in different climatic settings have different sensitivities. A major problem in this procedure is the definition of an initial state. One cannot just assume that at a certain point in time the state of any glacier is in balance with the prevailing climate. *Zuo and Oerlemans* [1997a] showed that a difference of only 0.3 K between the real climate

and the climate in which glaciers would have been in equilibrium (climatic imbalance) has a large effect on the calculated contribution to sea-level change.

In the second approach one uses data on geometric changes of glaciers directly. This is attractive, because climate data are not needed as input and the problem of defining an initial state does not exist. However, other difficulties have to be handled. When going back in time over a few centuries, the only available geometric parameter is glacier length. The step from glacier length to glacier volume is not a trivial one and depends on the geographic setting. *Lüthi et al.* [2010] showed for 12 Swiss glaciers that with the use of a simple glacier model, information on glacier length change can be used to calculate glacier volume changes. They also showed strong coherence of recorded length changes across the Swiss Alps. However, this method requires an equilibrium line altitude history and at least two volume measurements for each of the glaciers used in the study. A different solution is to calibrate volume changes calculated from length records by in situ mass-balance observations over the past 50 years. This method was exploited by *Oerlemans et al.* [2007] and will be extended in the current paper, by using a significantly larger number of glacier length records, and by involving more extensive in-situ mass balance and geodetic measurements [*Cogley*, 2009a].

In section 2 the data sets used in this study are presented. In section 3 we discuss some basic statistics of the glacier length records, consider the significance of regional variability, and discuss methods of normalisation. In section 4 we discuss the method to obtain a proxy for global glacier volume. In section 5 the glacier contribution to sea-level change is then presented. Section 6 provides a discussion about uncertainties, a comparison to other estimates, and a summary of the results.

5.2 Data

5.2.1 Glacier length variations

The dataset on glacier length used in this study is an extension of the one used in *Oerlemans et al.* [2007]. A number of records has been updated, and 152 records were added, mostly from remote areas like Greenland, Alaska, Central Asia and the southern Andes. The total number of records is 349. Although there is a reasonable coverage of the land masses (Figure 6.1), there are relatively few records from regions where much ice is found (Alaska, islands of the Arctic Ocean, Antarctica). There are no records from Antarctica or the arctic part of Canada and Russia, and only 8 from Greenland. In contrast, southern Europe (Pyrenees, Alps, Caucasus) has many records. Although there is an appreciable number of records from the Rocky Mountains, they are far from up-to-date: half of them have their last data points before 1990. Unlike North American records, most of the records in Patagonia continue up to 2005 at least, but 35 of the 54 records only start in 1945. The mean starting date of the 349 records is 1867, the mean end date 2001 (varying from 1534 to 1945 and from 1962 to

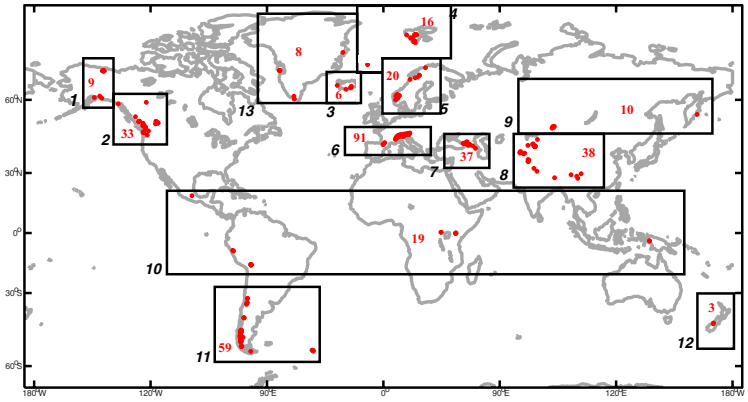

Figure 5.1: *Distribution of the glacier length records over the globe. In many cases the distance between glaciers is so small that the red dots overlap. The boxes depict the regions; the red number inside the boxes gives the number of records in the region; the number outside the box (in italics) gives the number of the region (cf. Table 6.1).*

2009, respectively). The set of length records is divided into 13 regional subsets, following the division into regions by *Radić and Hock* [2010] (Figure 6.1, Table 6.1). These subsets will be used to calculate a globally representative glacier signal.

The backbone of the data set is formed by Fluctuations of Glaciers data of the World Glacier Monitoring Service [*WGMS*, 2008 and earlier volumes]. Other sources are regular scientific publications, expedition reports, websites of glacier monitoring programs, and data supplied as personal communication. See the Supplementary Materials for details of the individual records and references. Only records that start prior to 1945 are included in the data set. There are many more records available that start after 1950, but these were not included, because the main purpose of this study is to reconstruct the variations on a centennial time scale. Furthermore, records of glaciers that are known to be surging were excluded. The proportion of glaciers that surge is small, implying that their exclusion will hardly affect the representativeness of the data set.

Most of the records have data points with varying spacing in time, as shown by the examples of glacier length records (Figure 2.1). Before 1900 most data points are reconstructed on the basis of geomorphological or historical evidence, e.g. paintings, drawings, and descriptions. For European glaciers there is plenty of historical information, resulting in some detailed records [e.g. *Zumbühl*, 1980; *Nussbaumer et al.*, 2007], but mostly, records have sparse data prior to 1900. From 1900 onwards, there is more information available worldwide, even annually for regions like Iceland, Norway, the Alps, and New Zealand. All records are interpolated with Stineman interpolation [*Stineman*, 1980; *Johannesson et al.*, 2009] to get annual values for the entire period covered by the record.

With Stineman interpolation the interpolated values are calculated from the values of the data points and the slopes at the gives points. The slope at a point is calculated from the circle passing through the point itself, the point before and the point after it. This method works well for series with uneven spacing between the data points, as is the case with the glacier length records. Moreover, it has the advantage that it produces no spurious minima or maxima not prescribed by the data.

In this paper we consider glacier length changes relative to the glacier length in 1950 (L_{1950}), and we use normalised glacier length changes, defined as:

$$L^*(t) = \frac{L(t) - L_{1950}}{L_{1950}}. \tag{5.1}$$

The length of the glacier is taken from the WGMS, the World Glacier Inventory [*National Snow and Ice Data Center*, 1999, update 2009], or the same source as the length record of the glacier. These glacier length measurements are made in different years for different glaciers. For all glaciers, L_{1950} is calculated from the measured glacier length and the length change between 1950 and the year of measurement. If the record has no data point in 1950, the length change is calculated from the interpolated length record. As we will show, the normalised length change can be used to reconstruct a globally coherent glacier length signal. Thus it will play a key role in the reconstruction of the volume change of all glaciers and small ice caps.

5.2.2 Global glacier mass balance

Global averages of measured mass balances for 1950/51 to 2008/09 are taken from an update of the compilation of *Cogley* [2009a]. The dataset includes 2905 balance-years of measurements by glaciological methods on 355 glaciers, and 13 671 balance-years of measurements by geodetic methods on 359 glaciers. Most of the glaciological measurements are of annual mass balance, while most of the geodetic measurements cover several to many years. The joint analysis of these disparate data, including a procedure for generating annual pseudo-series of geodetic mass balance with estimates of uncertainty, is explained by *Cogley* [2009a].

The annual glaciological time series are serially uncorrelated. This finding is exploited by calculating pentadal averages of the annual estimates, which reduces uncertainty by a factor of $1/\sqrt{5} = 0.45$. To address the problem of spatial bias, with some ice-covered regions well represented while others have no measurements at all, the pentadal averages are interpolated to the centres of the 1301 glacierized cells of a 1°x 1°grid.

The interpolation algorithm is explained in more detail by *Cogley* [2004]. Briefly, the interpolation function is a polynomial, fitted by least squares, in the two horizontal coordinates of an azimuthal equidistant projection centred at each cell in turn. During the interpolation, the pentadal averages of the measurements are weighted by a suitable distance-decay function,

which is derived from an analysis of the spatial autocorrelation of annual glaciological time series. The distance scale for loss of correlation between these time series is close to 600 km, as shown by *Cogley and Adams* [1998]. For each cell, the interpolated estimate is the first coefficient of the polynomial (its ÒinterceptÓ on the mass-balance axis) and its uncertainty is the standard error of that coefficient as estimated by the least-squares procedure. The global average for each pentad is the sum of the 1°x 1°cell estimates, and its uncertainty is the root-sum-square of the cell uncertainties, each weighted by the glacierized area of each cell. The uncertainty of the glacierized areas is allowed for by conventional propagation of errors. Glacierized cells around the periphery of Antarctica are not included in the interpolation, and their contribution to the global average is obtained by upscaling the estimate for the rest of the world, following *Kaser et al.* [2006].

The total of the global glacierized area used in this paper amounts to 704,000 km^2 and is the glacierized area contained in the grid cells plus the glacierized area around the periphery of Antarctica. This total area is smaller than the 741,000 km^2 used in *Radić and Hock* [2010], who relied on an older estimate of the glacierized area in Antarctica outside the ice sheet proper.

5.3 Regional and global length records

5.3.1 Regional glacier length changes

The glacier records display a consistent signal over the globe (e.g. Figure 2.1). The curves differ in details like amplitude of the signal and fluctuations on decadal time scale, but the overall picture is rather uniform. There is a clear world-wide retreat of glaciers that started in the middle of the 19th century. The general retreat since this time is further illustrated by Figure 5.2. Here the average rate of length change of the available records is shown for four different periods: 1801-1850, 1851-1900, 1901-1950, and 1951-2000. From 1801-1850, the majority of the glaciers had a small to moderate retreat, but a substantial proportion, 28%, of the glaciers advanced. Therefore the median retreat rate for this period is just slightly negative, namely -0.9 ma^{-1}. For all three periods after 1851, the median rate of change is more negative: -5.8, -10.3, and -8.9 ma^{-1} for the periods 1851-1900, 1901-1950, and 1951-2000, respectively. In these periods the number of average advances is very small, namely less than 5%.

For each of the 13 regions, we have calculated the average length change from the records within the region. Figure 5.3a shows these regional glacier length records after smoothing with a weighted running average filter, with 21-year width. This smoothing is necessary because jumps in the stacked record are created when a record enters the stack or when a record in the stack ends. The stacked records of the regions start at different years, varying from 1534 (Alps, region 6) to 1861 (Svalbard & Jan Mayen, region 4), but all stacked records

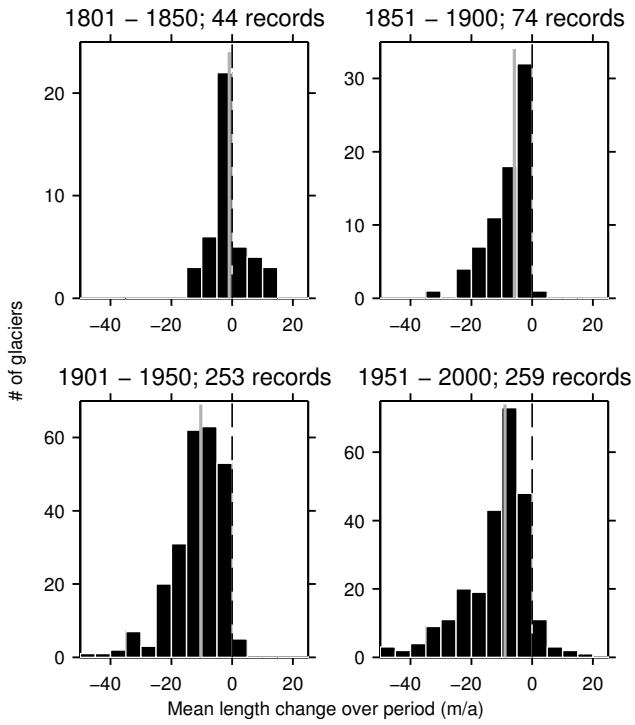

Figure 5.2: *Averaged rate of length change for four different periods. The vertical grey line indicates the median rate of length change. Note the changing number of records for each period.*

continue to 2004 at least. Furthermore, the glacier retreat since the middle of the 19th century in all regions is clearly visible. However, the amount of length change over the covered period is variable.

We have also calculated the average normalised length change for each region, using eq. (5.1). The resulting stacked records are shown in Figure 5.3b, again smoothed with a 21-year weighted running average filter. The tropical glaciers (region 10) are a clear outlier, with a large relative change. In general, the tropical glaciers are rather small, and they have significantly retreated over the past centuries. Especially the glaciers on Irian Jaya (Carstenz and Meren) have very large relative retreats (and have now almost disappeared), but also the glaciers in Central Africa and Bolivia have become much smaller. The smallest relative length changes have occurred in regions 3, 6, and 8 (Iceland, Alps, and Central Asia). In general the variability in the normalised stacked records is smaller than the variability in the stacked records, shown in Fig 5.3a. This can be explained by the fact that larger glaciers

are flatter and therefore more sensitive to climate change [*Oerlemans*, 2005]; the length and climate sensitivity compensate each other when we use the relative length change.

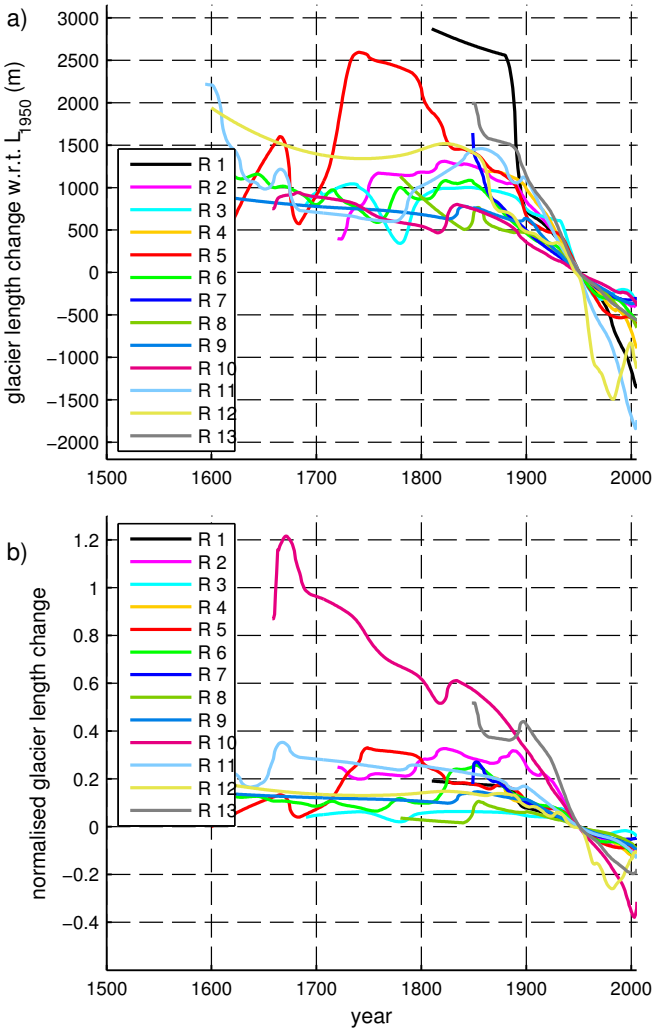

Figure 5.3: ***a)*** *Stacked glacier length records for the different regions. The length change is with respect to the length in 1950. In* ***b)*** *the* normalised *length records are shown. The clear outlier is the average of the tropical glaciers, region 10. See Table 6.1 and Figure 6.1 for the further corresponding regions.*

Table 5.1: *The 13 regions from which the glacier length records are available.* Area *is the total of ice-covered area within the region [Radić and Hock, 2010],* Addition *is the area that is added to this region, when we calculate the weight of the region. The total of added area is the area of glaciers and ice caps in regions in which we have no information on glacier length fluctuations.*

	region	# of records	area (km^2)	addition (km^2)	weight	comments
1	Alaska	9	79 260	-	0.1385	
2	Rocky Mountains	33	21 480	73 345	0.1656	incl. half of Canadian arctic
3	Iceland	6	11 005	-	0.0192	
4	Jan Mayen, Svalbard	16	36 506	37 384	0.1291	incl. Novaya Zemlya & Franz Josef Land
5	Scandinavia	20	3 057	-	0.0053	
6	Alps and Pyrenees	91	3 045	-	0.0053	
7	Caucasus	37	1 397	-	0.0024	
8	Central Asia	38	114 330	-	0.1997	
9	N. & E. Asia	10	2 902	19 397	0.0390	incl. Severnaya Zemlya
10	Tropics	19	7 069	-	0.0123	
11	Southern Andes	59	29 640	1 870	0.0550	incl. half of sub-Antarctic Islands
12	New Zealand	3	1 156	1 870	0.0053	incl. half of sub-Antarctic Islands
13	Greenland	8	54 400	73 345	0.2232	incl. half of Canadian arctic
	Total	349	362 193	210 265	1	glaciers and ice-caps on Antarctica not incl.

5.3.2 The global signal

The goal of this study is to develop a globally representative proxy for ice volume from the available glacier length records. This is done following the method of *Oerlemans et al.* [2007]. As discussed above, the normalised length records have more coherency than the length records. Therefore, we use the normalised length records to construct a proxy for global ice volume. Moreover, most of the records come from regions where the ice cover is relatively small (notably the Alps and Caucasus). To obtain a globally representative length signal we have to apply a weighting procedure that reduces the effect of overrepresentation of regions with many records. We achieve this by averaging the stacked records of the 13 regions. The result is shown in Figure 5.4a.

The black line is the average normalised length record of all available records ($\bar{L}^*$). In this average the large relative retreat of the tropical glaciers (see Figure 5.3b) is clearly visible. The mean of all regions, with equal weights, ($\bar{L}^*_{13}$) then yields the red curve in Figure 5.4a. After 1860, the two different averages are very similar, although $\bar{L}^*_{13}$ reveals a larger glacier retreat during the period 1960-2000. Before 1850, the records differ significantly due to the suppression of the tropical signal in the regional average.

A third approach ($\bar{L}^*_{w13}$) is to give the regions different weights, proportional to the area covered by glaciers in the regions. In principle, this is the best method to construct a proxy from the glacier length records that is representative for the ice volume. It removes the bias generated by the fact that we have more regions with smaller glaciers. The ice-covered area of the regions is taken from *Radić and Hock* [2010] (Table 6.1). To obtain weights, the ice-covered area not covered by the 13 regions is distributed over the regions that could plausibly represent the regions devoid of records (column labelled “addition" in Table 6.1). We have not included the area of Antarctic glaciers; we have no representative region with glacier length records. We have to assume that their behaviour is similar to the behaviour of the global signal we deduce from the other regions. In fact, this procedure reveals the weakness of the data set on glacier length fluctuations; little to nothing is known in regions with large amounts of ice, like the Canadian arctic and the Russian arctic islands. From Table 6.1 it is clear that the average is mainly determined by regions 1, 2, 4, 8, and 13. It only makes sense to construct $\bar{L}^*_{w13}$ for the period in which the sum of the represented area equals the total area, or is at least close to it. The fraction of the represented area, which equals the cumulative weight of the regions with records available in that year, is given in Fig 5.4b. We have calculated $\bar{L}^*_{w13}$ for the entire period 1600–2005 (blue line in Figure 5.4a), but the fraction of represented area does not reach 80% until the 1850's. Furthermore, we should keep in mind that the number of records in the dominating regions is limited until the beginning of the 20th century.

$\bar{L}^*$, $\bar{L}^*_{13}$, and $\bar{L}^*_{w13}$ appear to be remarkably similar throughout the 20th century. This finding reflects that (i) the relative change in glacier length has been comparable for smaller and larger glaciers and (ii) the behaviour of glaciers over the past century has been coherent over the globe. Before 1900, the similarity between the different averages is smaller, but we should

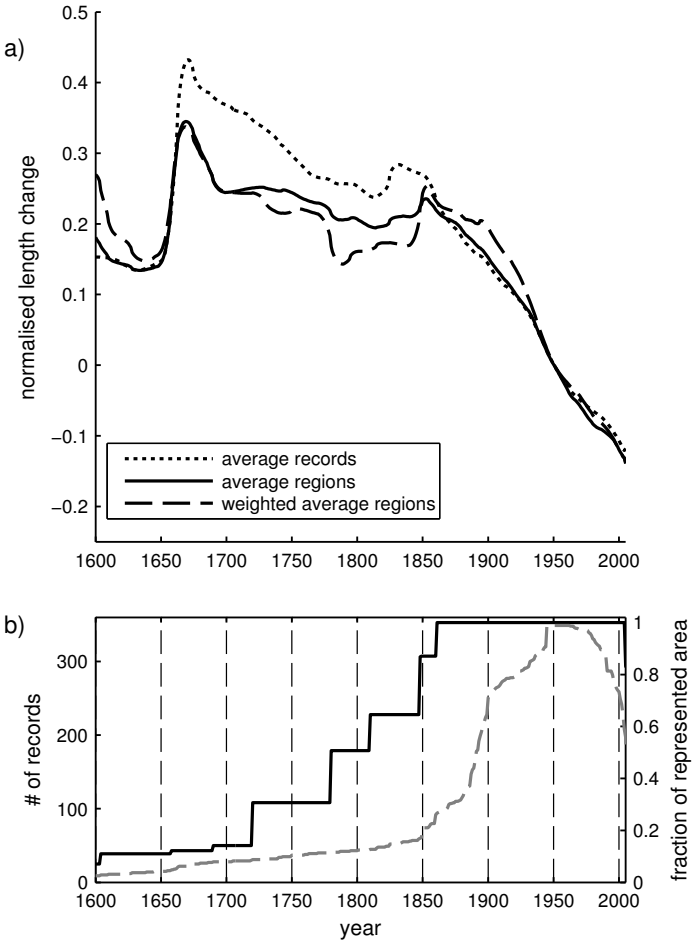

Figure 5.4: ***a)*** *The stacked global length signal from normalised glacier length records for three different averaging methods: mean of all records $\bar{L}^*$ (solid), mean of the 13 regions $\bar{L}^*_{13}$ (dotted), and the weighted average of the 13 regions $\bar{L}^*_{w13}$ (dashed).* ***b)*** *Total number of available records (dashed grey), and cumulative weight of the regions that have at least one record (black line); the weights of the individual regions are given in Table 6.1.*

keep in mind that here the number of records is limited, especially for the regions with a large weight. It would be most appropriate to base the proxy for world-wide glacier volume on $\bar{L}^*_{w13}$. However, this would limit the period of the reconstruction, and, in the second half of the 19th century, the reconstruction would rely heavily on just a few records. As $\bar{L}^*_{w13}$ and

$\bar{L}^*_{13}$ are very similar, we base the glacier volume proxy on $\bar{L}^*_{13}$. This will be worked out in the next section.

5.4 Proxy for glacier volume

5.4.1 Scaling glacier volume to glacier length

To use the global glacier length signal to deduce the changes of glacier volume, we have to relate glacier length to glacier volume. There exist scaling theories relating the length of a single glacier to its volume [e.g. *Bahr et al.*, 1997], but it is not entirely evident how this scaling of individual glaciers should be translated to a global average. Here, we follow the approach of *Oerlemans et al.* [2007]. The ice volume scales with the ice thickness, the length and the width of a glacier [cf. *Bahr et al.*, 1997]:

$$[V] = [H][L][W]. \tag{5.2}$$

Based on results from analytical and numerical glacier modeling, we can assume a scaling relation between the normalised ice thickness and the glacier length:

$$\frac{H}{H_{ref}} = \left(\frac{L}{L_{ref}}\right)^{\alpha}, \tag{5.3}$$

where H is the mean ice thickness, L the glacier length or ice-cap radius and the subscript "ref" indicates a reference state. For a glacier on a flat bed with ice that deforms perfectly plastically the mean ice thickness is proportional to the square root of the glacier length, i.e. $\alpha = 0.5$ [*Weertman*, 1961]. From numerical models, using the shallow ice approximation, values in the range 0.40 to 0.44 are found, depending on the slope of the bed [*Oerlemans*, 2001]. Next we assume that the length and the width of a glacier are also related through a power law, with exponent β. Then it follows for the normalised volume:

$$\frac{V}{V_{ref}} = \left(\frac{L}{L_{ref}}\right)^{1+\alpha+\beta}. \tag{5.4}$$

We use L_{1950} as reference length, such that the normalised glacier volume can be written in terms of normalised length change L^* using eq. (5.1):

$$\frac{V}{V_{1950}} = \left(\frac{L}{L_{1950}}\right)^{1+\alpha+\beta} = (1+L^*)^{1+\alpha+\beta}. \tag{5.5}$$

We assume a similar scaling as for individual glaciers can be used for the normalised global glacier length signal $\bar{L}^*_{13}$. Thus, the normalised global ice volume V^* can be expressed as:

$$V^* = (1+\bar{L}^*_{13})^{\eta}\,, \tag{5.6}$$

where $\eta = 1+\alpha+\beta$, and ranges from 1.4, for glaciers for which a change in volume does not affect the glacier width ($\beta = 0$), to 2.5, for ice caps that can expand freely in all directions ($\beta = 1$). Based on the analysis of the geometry of more than 300 glaciers by *Bahr et al.* [1997], the most likely average value for η is 2.0 to 2.1. Note that according to expressions 5.1 and 5.6 the non-dimensional volume equals unity in 1950, the reference year for the length changes. We consider V^* to be the best possible glacier volume proxy derived from the set of glacier length records, with η within the 1.4 to 2.5 rage, but probably close to 2.0. V^* is again smoothed with a 21-year filter to smooth out jumps created in the volume when new regions enter the $\bar{L}^*_{13}$ average.

5.4.2 Calibration of glacier volume proxy

To estimate the glacier contribution to sea-level rise, we need to translate the normalised glacier volume V^* into actual glacier volume change. Therefore, we calibrate the reconstructed glacier volume change on the compilation of mass balance data of *Cogley* [2009a], that gives the changes in global ice mass for the period 1951-2009 (see section 5.2.2). We denote the cumulative contribution to sea-level change as determined from the mass balance measurements by S_C. The calibration of V^* on S_C is simply done with a linear regression (least squares) such that:

$$\Delta V = a + bV^* = -S_C, \tag{5.7}$$

where ΔV is expressed in terms of sea-level equivalent. The regression is calculated for the period 1951-2005, because after 2005 the numbers of glacier length and mass-balance records are considered to be too small.

As explained in section 5.2.2, the uncertainty in the total mass balance is calculated from the variance of the available measurements. However, although formally correct, this calculation underestimates the true uncertainty. Uncertainties due to the fact that not all regions are represented in the mass balance measurements, and in particular the uncertainty in the upscaling to Antarctica, are not taken into account. Furthermore, in the conversion of specific mass balance to ice volume change, the total ice-covered area is kept constant. In order to get a more realistic estimate of the uncertainty in the reconstructed contribution of glaciers to sea-level change, we have calculated upper and lower bounds of S_C by assuming that:

1. In 1950 about half of the ice-covered area is represented in the mass balance series, this fraction increases linearly to 75% in 1980, and stays constant after 1980.

2. The unrepresented ice has on average experienced half of the measured loss, which gives the lower bound, or,

3. the unrepresented area has experienced an average mass balance of 1.5 times that of the measured record, which gives the upper bound.

The resulting upper and lower bounds of the cumulative total mass balance are shown as dashed black lines in Figure 5.5. The range in the cumulative total mass balance series is used to estimate an uncertainty band for ΔV. We recalculate ΔV, by calibrating it on the upper and lower estimate of S_C. The differences between ΔV_{upper} and ΔV_{lower} on the one hand and ΔV on the other (calculated while setting the difference in 2005 to zero), give an uncertainty range for the contribution of glaciers to sea-level change reconstructed from glacier length changes.

5.5 Results

After the calibration of ΔV on S_C, the glacier contribution to sea-level change can be extended backwards in time (Figure 5.5). Since the number of records before 1800 and after 2005 is very limited (Figure 5.4b), the reconstruction is only shown for the period 1800-2005. We have found the contribution of glaciers to be 8.4 $\pm$ 2.1 for the period 1800-2005, with a maximum of 9.1 $\pm$ 2.3 cm between 1850 and 2005. The uncertainties in these estimates are derived from the result we obtain when we calibrate to the lower and upper estimate of the mass balance series. These uncertainties are substantial, following from the assumed range in the mass balance measurements. The cumulative total mass balance of all glaciers and ice-caps is calculated to be 3.2 $\pm$ 0.8 cm sea-level equivalent for the period 1950 - 2005.

As shown earlier by *Oerlemans et al.* [2007], the reconstructed contribution is hardly dependent on the choice of the scaling parameter η, as can be seen in Figure 5.6a. The estimates of sea-level rise over the period 1850-2005 differ by about 1 cm for a range η from 1.4 to 2.5. This is a wide range, covering the range of assumptions from the width of all glaciers being constant for any change of volume, to all glaciers being unbounded ice caps. Hence, the choice of the scaling parameter is not critical. It should be noted that for every choice of η the regression constants a and b in eq. (5.7) are different.

The reconstructed sea-level change is more sensitive to the calculation of the global length signal (Figure 5.6b) and the mass balance data (Figure 5.6c). For the two global length signals derived from regional averages, $\bar{L}^*_{13}$ and $\bar{L}^*_{w13}$, the results are almost the same. If we use $\bar{L}^*_{w13}$ for the reconstruction of ΔV, the decrease in the ice volume seems to start later, at the end of the 19th century. Of course, this result is not conclusive as this record does not go far back in time and the number of records in the regions with large weight is limited (as was already stressed in section 5.3.2, this is the reason we use $\bar{L}^*_{13}$). Using $\bar{L}^*$ gives a much larger

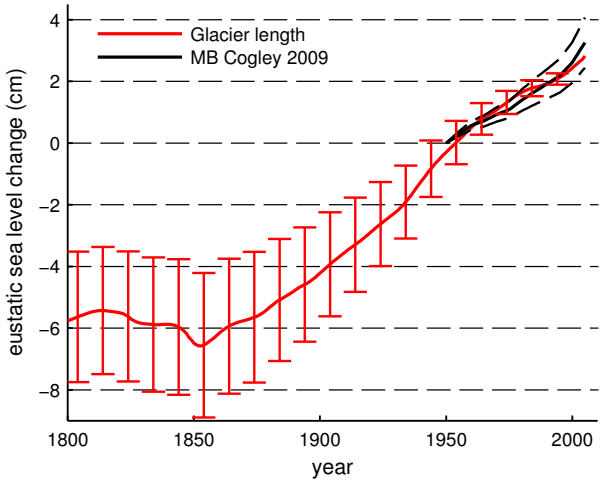

Figure 5.5: *Reconstructed contribution of glaciers and ice-caps to sea-level rise. The cumulative mass balance record is given in black [Cogley, 2009a]; the reconstructed sea-level change from the glacier length records is shown in red. The range of the upper and lower estimates is indicated with dashed black lines for the mass balance record and with red uncertainty bars for the reconstruction from glacier lengths.*

contribution to sea-level change. Before the marked increase in the number of records in the second half of the 19th century, the relative contribution of the tropical glaciers to this global signal is much higher than in the other two averages. As the tropical glaciers are outliers in the normalised length change signal (see Figure 5.3b), this results in an increased sea-level change.

If we calibrate ΔV on the mass balance data set compiled by *Dyurgerov and Meier* [2005], we get a substantially smaller estimate of the contribution of glaciers to sea-level change. The result is then very close to the 5 to 6 cm for the period 1850-1900 found by *Oerlemans et al.* [2007], who used this data set. This shows that our result is sensitive to the uncertainties in the global mass balance record on which ΔV is calibrated.

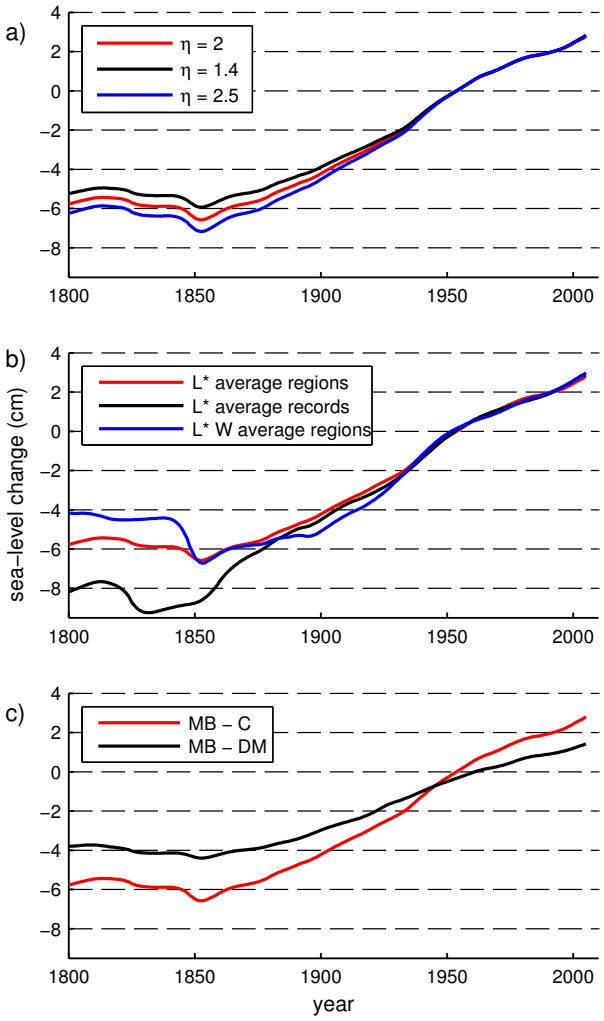

Figure 5.6: *Sensitivity of the reconstructed sea-level change to the choice of parameters; in each figure the best estimate shown in Figure 5.5 is displayed in red.* ***a)*** *Sensitivity to different values of the scaling constant* η*;* ***b)*** *Global ice volume change (sea-level equivalent) calculated from the different global length signals shown in Figure 5.4a;* ***c)*** *The global ice volume calibrated on the mass balance record of Cogley [2009a] (MB-C, as used in this study) and of Dyurgerov and Meier [2005] (MB-DM, as used in Oerlemans et al. [2007])*

5.6 Conclusion and discussion

5.6.1 Uncertainty

The data on glacier area, as summarized in Table 6.1, do not directly affect our estimate of the glacier contribution to sea-level rise. This information was only used to verify that L^*_{13} can be used as a proxy for global ice volume variations. The fact that the regional averages of normalised length change present a rather homogeneous picture, with the notable exception of the tropical glaciers, is a consequence of the coherent behaviour of glaciers over the globe on a centennial time scale.

This also explains the fact that, if we use the mass balance record of *Dyurgerov and Meier* [2005] (Figure 5.6c), the reconstructed contribution based on the current data set of 349 glaciers is very similar to the results of *Oerlemans et al.* [2007], who used only 197 records. The difference between the results of this study and of *Oerlemans et al.* [2007] can thus mainly be attributed to the extended mass balance series of *Cogley* [2009a], who noted that the newly-assimilated geodetic mass balances in this compilation were on average more negative than those in earlier compilations. However, this total mass balance, and thus the reconstruction of glacier sea-level contribution, is sensitive to the distribution of the global ice cover. In this study, the calculation of the total mass balance and the corresponding total ice-volume change is based on the gridded data set of *Hock et al.* [2009], with a total glacier area of 704 000 km^2, instead of the regional data set of *Radić and Hock* [2010] used for the weighted average of the global length signal.

As shown in Figure 5.6a, our result is not very sensitive to the value of η used in the volume-length scaling. The difference in the calculated sea-level contribution is within 1 cm, for values of η ranging from 1.4 to 2.5. This is a very wide range. Therefore, we expect that taking the geometries of individual glaciers into account by differentiation of η and applying the volume scaling (eq. 5.6) to individual glaciers instead of to the global average, will not substantially reduce the uncertainty in the reconstructed contribution. This would in addition require information on the geometry of all glaciers in the length data set. This information is not available at present.

Fundamental to our approach is the assumption that both the global length signal L^*_{13} and the global cumulative mass balance record S_C are truly globally representative. Several regions with large amounts of ice are not represented in the glacier length data set (Figure 6.1 and Table 6.1). This introduces an uncertainty in the global length signal, although we think that the glacier length signal is spatially rather coherent. The same holds for the mass balance measurements. The relative error in the reconstructed contribution of glaciers to sea-level change is approximately proportional to the error in the glacier contribution calculated from the mass balance series for the period 1950-2005. It is difficult to quantify these uncertainties, so we have shown (Figure 5.5) the results with rather large uncertainty range of 25%. This

gives a best estimate for the contribution of glaciers to sea-level change for the period 1850-2005 of 9.1 $\pm$ 2.3 cm eustatic sea-level equivalent. The best estimate shows a minimum in 1850, but as the uncertainty bars indicate, the significance of this minimum should not be overestimated. The number of length records as well as their global coverage is limited in the first half of the 19th century.

5.6.2 Comparison to earlier results

Earlier studies of the contribution of glaciers to sea-level change on a centennial timescale [*Meier*, 1984; *Zuo and Oerlemans*, 1997a; *Gregory and Oerlemans*, 1998; *Oerlemans et al.*, 2007] all give smaller estimates than our results. Except for *Oerlemans et al.* [2007], all estimates are based on calculated mass balances. *Meier* [1984] calculated the contribution for the period 1900-1961. Based on very few measured volume changes and mass balance series he arrived at a contribution of 2.8 $\pm$ 1.6 cm, whereas we have calculated a contribution to sea-level rise of 4.7 $\pm$ 1.8 cm for the same period.

Zuo and Oerlemans [1997a] and *Gregory and Oerlemans* [1998] calculated mass balance sensitivities for glaciers distributed over 100 different regions; the sensitivity was dependent on the characteristic precipitation (mean annual precipitation on the glaciers) in the region and a distinction was made between sensitivity to changes in summer temperatures and non-summer temperatures. Based on measured temperature data, *Zuo and Oerlemans* [1997a] found a contribution of glaciers to sea-level rise of 2.7 $\pm$ 0.9 cm for the period 1865-1990. Based on the same mass balance sensitivities but using temperatures calculated with a general circulation model, *Gregory and Oerlemans* [1998] found a contribution of 1.9 or 3.3 cm for the period 1860-1990, depending on the climate scenario. These estimates are significantly lower than the estimate presented in this study; we have calculated a contribution to sea-level rise of 8.0 $\pm$ 2.2 cm for the period 1860-1990. Our two- to four-fold greater estimate can partly be explained by the difference in the total area of all glaciers: *Zuo and Oerlemans* [1997a] used 527 900 km^2, excluding the glaciers around Greenland (those were included in the contribution of the Greenland ice sheet) and Antarctica. Instead, we use the more recent estimate of 704 000 km^2, used in *Cogley* [2009a], which includes glaciers in Greenland and Antarctica. Secondly, and more importantly, *Zuo and Oerlemans* [1997a] have underestimated the characteristic precipitation in most of the 100 regions. This leads to lower values for the mass balance sensitivity, and thus to a too low estimate of the volume loss of glaciers. Slangen et al. (manuscript in preparation) show with the use of the precipitation from an ensemble of twelve climate models and accounting for the difference in total glacier area, that the results of the mass balance sensitivity approach are comparable to the results presented in this study.

Compared to our results, *Oerlemans et al.* [2007] estimated a smaller contribution for the period 1850-2000, and their best estimate showed a more pronounced minimum in the contribution around 1850. The difference in the reconstructed contribution for the period 1850-

2000 is almost entirely due to the training data set S_C (see section 5.5 and Figure 5.6c). The disappearance of the pronounced maximum is due to the additional glacier length data.

5.6.3 Concluding summary

In this study we have calculated the contribution of glaciers and ice caps to sea-level change of the last two centuries from geometric changes of glaciers. Length change is the only glacier property for which information goes far back in time. Hence, we have reconstructed a global volume signal from glacier length using a scaling relation. The global length signal is derived from the average of 13 regions. This can be done, because glaciers show a worldwide coherent signal. We have calibrated the thus derived glacier volume changes on the total mass balance of the period 1950-2005. This gives a maximum sea-level contribution for the period 1850-2005 of 9.1 $\pm$ 2.3 cm and a best estimate for the contribution over the period 1800-2005 of 8.4 $\pm$ 2.1 cm. This contribution is larger than previously estimated. According to our estimate, 35-50% of the observed sea-level rise since 1800 is due to melt of glaciers and ice caps.

6

The influence of glacier retreat on mass balance, estimated from length changes

Summary

The paper by Huss et al. [2010] presents a comprehensive set of 100-year conventional mass balance series for 30 Swiss glaciers. They conclude that these 30 glaciers have lost 14 km^3 of ice during these 100 years. In the second part of the paper, the authors relate the fluctuations in alpine glacier conventional mass balance to climatic changes attributed to the Atlantic Multidecadal Oscillation (AMO). In this Chapter it is argued that the conventional mass balance is not the appropriate measure to interpret climatic fluctuations. Reference-surface mass balances should be used instead. Due to the dynamic response of glaciers to changes in their climatic forcing, the importance of short-term climatic oscillations is overestimated. Taking the changes in glacier geometry into account, the AMO related climate variations are significantly less important to the recent mass loss than the trend caused by the gradual warming over the past century.

This Chapter is based on P.W. Leclercq, R.S.W. van de Wal, J. Oerlemans, Comment on "100-year mass changes in the Swiss Alps linked to the Atlantic Multidecadal Oscillation" by Matthias Huss et al., GRL 37, 2010, The Cryosphere Discussions 4, pp. 2475-2481, 2010.

6.1 Introduction

Huss et al. [2010a] base the modeled mass-balance series for the 100-year period 1908-2008 on in-situ measurements and ice volume changes derived from sequential Digital Elevation Models (DEMs) of the studied glaciers (with a total of 3 to 9 DEMs per glacier). These measurements constrain a degree-day mass balance model that is used to compute daily mass balance values for the studied glaciers on a 25 x 25 m grid. For each year *Huss et al.* [2010a] calculate the specific mass balance by dividing the total mass balance of the glacier surface by the glacier area of that year. They show that the conventional mass balance of the Swiss glaciers was mostly negative for the last century, leading to a total ice volume loss of 14 km^3 for the 30 glaciers from 1908 to 2008.

In the second part of the paper, the authors link the conventional mass balance anomalies to climatic fluctuations and show a statistical correspondence between the AMO and the mean mass balance anomalies of the 30 glaciers. They fit a combination of a sinusoidal and a linear trend to the conventional mass balance anomaly and conclude that about half of the loss of ice mass over the most recent decade can be attributed to the 65-year period variation that is superimposed on the negative linear trend.

6.2 Climatic interpretation of mass balance

The conventional mass balance calculated by *Huss et al.* [2010a] is the measure of the actual ice volume change in a year. This mass balance is not only dependent on the climate but also on the changing configuration of the glacier surface. Hence the variations in the mass balance do not reflect only climate variations [e.g. *Oerlemans*, 2008, section 3.4]. To use the variations in mass balance for a climatic interpretation, the mass balance should be calculated for a *constant glacier surface*, the so-called reference-surface mass balance [*Elsberg et al.*, 2001; *Harrison et al.*, 2009]. Over the last century, the glaciers used in the study of *Huss et al.* [2010a] have significantly retreated, losing part of their ablation area [*Zemp et al.*, 2006]. Loss of ablation area leads to a more positive mass balance, bringing a glacier closer to equilibrium (see Figure 6.1). A part of the climate change over the last century is thus not visible in the mass balance but hidden in the change of glacier geometry [e.g. *Nemec et al.*, 2009; *Paul*, 2010].

The change of glacier geometry as a consequence of changes in climate is a slow process with a response time of typically a few decades [e.g. *Jóhannesson et al.*, 1989; *Oerlemans*, 1997b; *Brugger*, 2007; *Adhikari and Huybrechts*, 2009]. Therefore short-term climate variations are less damped by geometric adjustment of the glacier than long-term climate variations (Figure 6.1). To estimate the relative importance of short-term climate variability for the state of glaciers, variations of the reference-surface mass balance should be used.

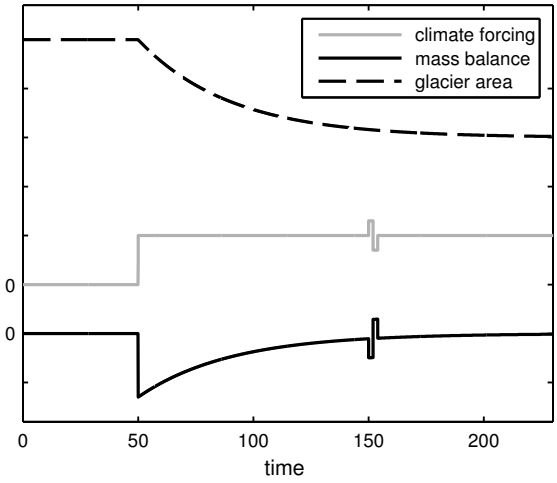

Figure 6.1: *Schematic response of the mass balance (solid black) and glacier area (dashed black) to an idealized climate change (grey). Due to the slow change in glacier area the mass balance acts as a high-pass filter [cf. Oerlemans, 2001, section 9.7].*

6.3 Reference-surface versus conventional mass balance

We estimate the minimum difference between the reference-surface mass balance and the conventional mass balance of the last decade for the glaciers used in the study of *Huss et al.* [2010a]. The mass balance relative to the 1908 glacier surface is calculated using data on glacier length change [*Swiss glacier monitoring network*, 1881-2009]. Most of the area loss is at the glacier tongue [*Paul*, 2007] and is thus related to the change of the frontal position of the glacier. Twelve of the 30 glaciers used in the study of *Huss et al.* [2010a] have a length change record covering most of the 1908-2008 period (Table 6.1). The length change ΔL times the width of the glacier tongue W provides a minimum estimate of the area loss $\Delta A = W\Delta L$ (Figure 6.2). If we assume that ΔA is much smaller than the present-day surface area A_{pd}, the difference between the average conventional mass balance and the average reference-surface mass balance is given by:

$$\Delta b = \frac{\dot{b}\Delta A}{A_{pd}} \tag{6.1}$$

where $\dot{b}$ the specific mass balance for the lost ablation area ΔA. We calculate $\dot{b}$ at the altitude of the present day tongue from the average ablation on the tongue of the Swiss Morteratsch

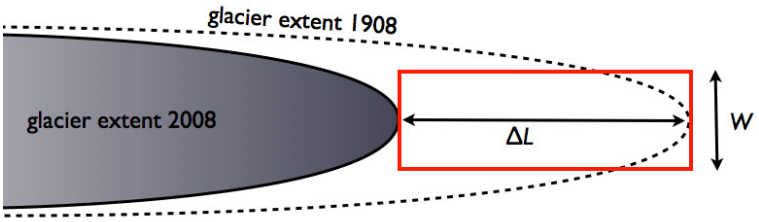

Figure 6.2: *Schematic illustration of the estimated area loss from length change ΔL and glacier width W. Shown are the former glacier extent in 1908 (dashed) and the present day glacier extent (shaded). The red rectangle indicates the minimum estimated area loss.*

glacier of -6 m w.e. a^{-1} [*Oerlemans et al.*, 2009] and a balance gradient of 0.006 m w.e $a^{-1}m^{-1}$. The width of the glacier tongue is measured from Swiss Topo maps, scale 1:25000. For A_{pd} we take the values given by *Huss et al.* [2010a]. If we assign equal weights to large, medium-large and small glaciers as in *Huss et al.* [2010a], the weighted average of Δb is -0.36 m w.e a^{-1}. The Δb of Pizol is excluded from the average, as this value (-3.00 m w.e.a^{-1}) clearly is an outlier. The mean conventional mass balance over the last decade is -0.87 m w.e a^{-1} [*Huss et al.*, 2010a]. Thus the minimal estimate of the mean reference-surface mass balance for the last decade is -1.23 m w.e a^{-1}. Δb only contributes to the negative trend and not to the amplitude of the sinusoid fitted through the mass balance anomaly. Hence, the contribution to the recent glacier wastage of natural variability related by *Huss et al.* [2010a] to the AMO is 33% at most. This is clearly lower than the 50% estimate calculated by *Huss et al.* [2010a].

In a recent article, *Paul* [2010] quantified the influence of changes in glacier extent and elevation on the mass balance of a part of the Swiss Alps, but for a different period (1850-1970/80). He performed experiments with a physical mass-balance model [*Machgut et al.*, 2006; *Paul et al.*, 2009] and measured or reconstructed glacier surface topographies of the Great Aletsch Glacier region in Switzerland. Based on these calculations *Paul* [2010] concluded that only 30-50% of the climate change over the period 1850-1970/80 can be observed in the conventional mass balance and 70-50% of the climate change is 'hidden' in the geometrical change of the glacier surface. A similar strong effect of the geometrical change on the mass balance (nearly 50%) has been found by *Nemec et al.* [2009] for the Morteratsch glacier, also located in Switzerland.

6.4 Conclusion

As stated by *Huss et al.* [2010a], the conventional mass balance is mainly and increasingly negative despite the geometric adjustment of the glaciers. This implies that there is a strong

Table 6.1: *Glaciers used for minimum estimate, their observed length changes, estimated minimum loss of ablation area, present day ablation at the tongue and calculated difference between reference-surface mass balance and specific balance. Following Huss et al. [2010a] the glaciers are divided in three groups: large >15 km^2 (5), medium 3-15 km^2 (4) and small <3 km^2 (3).*
* *The Δb of Pizol is not included in the average Δb of -0.36.*

glacier	ΔL (period) m	ΔA_{min} km^2	$\dot{b}$ m w.e. a^{-1}	Δb m w.e. a^{-1}	
Aletsch	-2430 (1908-2007)	1.51	-9	-0.16	LARGE
Gorner	-1998 (1908-2007)	1.20	-5.5	-0.17	
Unteraar	-1765 (1908-2001)	0.90	-7	-0.28	
Unterer Grindelwald	-714 (1908-1983)	0.48	-10	-0.25	
Rhone	-740 (1908-2007)	0.53	-5.5	-0.18	
Allalin	-1190 (1908-2005)	0.47	-3	-0.15	MEDIUM
Gries	-1732 (1908-2006	0.78	-4	-0.15	
Trient	-848 (1908-2007)	0.51	-7	-0.61	
Zinal	-1102 (1908-2007)	0.33	-6	-0.64	
Basodino	-495 (1908-2008)	0.37	-3	-0.51	SMALL
Pizol*	-338 (1908-2008)	0.08	-3	-3.00*	
Verstancla	-439 (1926-2008)	0.11	-4	-0.48	

negative trend in the reference-surface mass balance, the mass balance that truly reflects climatic change. Using the conventional mass balance this trend is underestimated: by a factor 1.5 according to the simplified minimum estimate presented here, and by up to a factor 3 by detailed calculations [*Paul*, 2010; *Nemec et al.*, 2009]. The underestimate of this negative trend goes together with an overestimate of the importance of the short-term climate variability visible in the conventional mass balance anomaly. It is this short-term variability that is related to the AMO in Figure 3 of *Huss et al.* [2010a] (see Figure 1.14). Thus the influence of the AMO on glacier behaviour is overestimated by *Huss et al.* [2010a].

In addition, Huss et al. [2010a] argue that a negative phase in the mass balance anomaly is caused by a positive phase in the AMO index. A positive phase in the AMO is associated with higher temperatures in Europe. In this causal relation, we would expect the change in AMO before, or simultaneously with, the change in mass balance anomaly. However, the phase difference between the mass balance anomaly and the AMO index is such that first the mass balance become more negative followed several years later by a positive AMO index. At first sight the causal relation between AMO and mass balance anomaly is opposite. This further indicates that the significance of the AMO with respect to glacier shrinkage in the Swiss Alps over the past century is small compared to the gradual warming over this period. The 100-year mass changes in the Swiss Alps are dominated by the long-term trend rather than the AMO.

A

Appendix: Overview of glacier length records with references

Table contents

This Chapter includes a table with metadata of the glacier length record data set that is used for the studies presented in this thesis. Given are the name of the glacier; its position in latitude-longitude; the year of the first and the last data point of the record; the total number of data points in the record; the glacier length in 1950; and, last but not least, references to the sources of the data. Some often returning references (like WGMS) are abbreviated, full name and reference is given at the end of the table. For a description of the data set, the reader is referred to Chapter 2.

Table A.1: *Glacier length records*

name	location		record period		# data	L1950	references
	lat	lon	first	last		km	
211	42.01	77.96	1860	2006	7	4.85	*Kutuzov and Shahgedanova* [2009]
324	42.04	78.18	1860	2006	6	5.89	*Kutuzov and Shahgedanova* [2009]
392	42.00	77.97	1860	2006	7	3.88	*Kutuzov and Shahgedanova* [2009]
393	41.99	77.97	1860	2006	6	4.97	*Kutuzov and Shahgedanova* [2009]
394	41.98	77.96	1860	2006	6	2.64	*Kutuzov and Shahgedanova* [2009]
Abano	42.70	44.52	1860	1990	34	4.30	WGMS, ID 767
							Panov and Pisareva [1973]
Aksu-Vostochniy	42.85	77.10	1921	1990	25	4.99	WGMS, ID 784
							G.B. Osipova, pers. com.
Akugdlit	69.64	-54.50	1813	2010	11	3.41	*Weidick* [1968]
							Weidick et al. [1992]
							Citterio et al. [2009]
							Ettema et al. [2009]
							M. Citterio pers. com
							Landsat 2001 2010
Aldegonda	77.97	14.08	1900	2006	7	4.30	*Glazovsky et al.*
							I. Solovjanova - pers. com. 2006
							Lavrentiev [2008]
Alibekskiy	43.28	41.53	1875	1990	38	4.67	*Panov* [1993]
							WGI
Allalin	46.05	7.93	1881	2005	113	6.70	WGMS, ID 394
Alpeiner	47.05	11.13	1881	2001	72	4.90	WGMS, ID 497
Amalia	-50.92	-73.53	1945	2005	5	29.47	WGMS, ID 1633
							López et al. [2010]
Ape	52.08	-126.22	1900	1984	7	7.10	*Williams Jr. and Ferrigno* [2002]
Argentière	45.97	6.93	1600	2005	51	9.40	WGMS, ID 354
							Huybrechts et al. [1989]
							Bouverot [1958]
							Vivian [1975]
Arolla	45.98	7.50	1856	2007	116	5.10	WGMS, ID 377
							Swiss glacier monitoring network [1881-2009]
Artesonraju	-8.92	-77.60	1932	1994	5	3.40	*Kaser and Osmaston* [2002]
Ashu-Tor south (326)	42.04	78.16	1860	2006	6	6.04	*Kutuzov and Shahgedanova* [2009]
Asia	-50.82	-73.61	1945	2005	4	17.74	WGMS, ID 1652
							López et al. [2010]
Assakiat	70.52	-52.07	1850	2010	12	8.14	*Weidick* [1968]
							Weidick et al. [1992]
							Citterio et al. [2009]
							Ettema et al. [2009]
							M. Citterio pers. com
							Landsat 2001 2010
Athabasca	52.20	-117.25	1730	1995	31	7.00	WGMS, ID 7
							Luckman [1988]
Atlante	-9.25	-77.20	1932	1994	4	2.40	*Kaser and Osmaston* [2002]

Table A.1: *Glacier length records (continued)*

name	location		record period		# data	L1950	references
	lat	lon	first	last		km	
Azha	29.13	96.82	1933	1998	5	21.25	*Rai and K* [2005] *Liu et al.* [2006] *Yuanqing et al.* [2003]
Azufre	-35.29	-70.55	1894	2005	7	3.31	*Espizúa and Pitte* [2009] *Leiva et al.* [2008]
B Abyl-Oyuk	50.12	87.48	1850	1962	3	5.20	WGMS, ID 1082
Bachfall	47.08	11.08	1892	1996	56	3.10	WGMS, ID 500
Baishui No. 1	27.40	100.15	1900	2002	5	3.00	*Yuanqing et al.*
Bara Shigri	32.15	77.69	1863	1995	6	28.18	*Raina and Srivastava* [2008] *Kumar et al.* [2007]
Basòdino	46.42	8.47	1899	2009	85	2.42	WGMS, ID 463 *Swiss glacier monitoring network* [1881-2009]
Benito	-47.05	-73.69	1945	2005	5	32.73	WGMS, ID 1040 *López et al.* [2010]
Berglas	47.07	11.12	1891	2007	76	2.60	WGMS, ID 496 Gletscherberichte
Bergset	61.65	7.03	1743	2006	72	4.66	WGMS, ID 2290 *Nussbaumer et al.* [2011]
Bernardo	-48.68	-73.57	1945	2005	5	54.87	WGMS, ID 1634 *López et al.* [2010]
Bertilbreen	78.68	16.27	1900	2002	4	5.49	*Rachlewicz et al.* [2007] *Hagen et al.* [1993]
Betrambreen	78.75	16.82	1900	2002	4	5.65	*Rachlewicz et al.* [2007] *Hagen et al.* [1993]
Bezengi	43.05	43.07	1888	1998	40	18.00	WGMS, ID 703 *Panov* [1993]
Birdzhalychiran	43.37	42.53	1887	2007	5	7.48	WGMS,ID 756 D. Petrakov, pers. com.
Bituktube	43.37	42.40	1887	2007	7	3.13	WGMS,ID 764 D. Petrakov, pers. com.
Blanc	44.95	6.22	1921	2005	55	6.30	WGMS, ID 351
Blue	47.83	-123.67	1815	1999	60	4.20	WGMS, ID 210 *Koutnik* [2009]
Bluemlisalp	46.50	7.77	1893	2007	102	3.20	WGMS, ID 436 *Swiss glacier monitoring network* [1881-2009]
Bolshoy Azau	43.28	42.43	1849	2007	42	9.20	WGMS, ID 701 *Laverov* [2004] *Panov* [1993] *Zolotarev* [2009]
Bolshoy Chontor	41.97	77.90	1860	2006	6	4.38	*Kutuzov and Shahgedanova* [2009]
Bolshoy M	50.12	87.58	1924	1990	17	9.00	WGMS, ID 792
Bondhusbreen	60.03	6.33	1801	2009	101	7.80	WGMS, ID 318 NVE reports *Bogen et al.* [1989] *Nussbaumer et al.* [2011]

Table A.1: *Glacier length records (continued)*

name	location		record period		# data	L1950	references
	lat	lon	first	last		km	
Bordoo	41.80	78.17	1943	2003	4	5.10	*Aizen et al.* [2006] *Aizen et al.* [2007]
Bossons	45.87	6.78	1580	2005	166	7.20	WGMS, ID 355 *Bouverot* [1958] *Nussbaumer* [2010] *Nussbaumer and Zumbühl* [2011]
Briksdals	61.65	6.92	1869	2009	119	5.70	WGMS, ID 314 NVE-reports *Bogen et al.* [1989] *Nussbaumer et al.* [2011]
Brunni	46.73	8.78	1882	2003	117	3.20	WGMS, ID 427 *Swiss glacier monitoring network* [1881-2009]
Buerbreen	60.03	6.43	1822	2009	87	7.50	H. Elvehoy (NVE), pers. com. *Nussbaumer et al.* [2011]
Bøya	61.30	6.46	1867	2009	67	5.05	WGMS, ID 2297 *Nussbaumer et al.* [2011] *Østrem et al.* [1988]
Cachet	-47.10	-73.20	1945	2005	5	10.00	WGMS, ID 1026 *Aniya* [2001] *López et al.* [2010]
Caltha lake	59.15	-122.28	1914	1985	6	0.33	WGMS, ID 40
Calvo	-50.70	-73.29	1945	2005	4	15.26	WGMS, ID 1650 *López et al.* [2010]
Carstensz	-4.10	137.17	1825	1990	7	1.80	WGMS, ID 1051 *Williams Jr. and Ferrigno* [2002] *Williams Jr. and Ferrigno* [1989]
Casa pangue	-41.13	-71.87	1911	2000	7	6.89	WGMS, ID 2010
Castano overo	-41.18	-71.83	1944	1983	6	5.40	WGMS, ID 918
Cesar	-0.13	37.30	1899	2004	7	0.40	WGMS, ID 694 *Hastenrath* [1983]
Chalaat	43.13	42.70	1890	1988	25	7.56	WGMS, ID 1110 *Panov* [1993] WGI
Chamberlin	69.32	-53.53	1848	2005	10	3.85	*Yde and Knudsen* [2007]
Chamberlin	69.28	-144.93	1900	1981	4	2.94	*Evison et al.* [1996]
Charquini Norte	-16.36	-68.12	1663	1997	16	0.60	*Rabatel et al.* [2006] *Rabatel et al.* [2008]
Charquini Oeste	-16.28	-68.19	1663	1997	16	0.51	*Rabatel et al.* [2006] *Rabatel et al.* [2008]
Charquini Sur	-16.18	-68.14	1686	1997	15	1.36	*Rabatel et al.* [2006] *Rabatel et al.* [2008]
Charquini Sureste	-16.30	-68.15	1664	1997	13	1.60	*Rabatel et al.* [2006] *Rabatel et al.* [2008]
Chogo Lumgma	36.00	75.00	1902	1989	6	46.00	WGMS, ID 972
Chungpar-tash.	35.23	74.72	1856	1987	4	12.02	WGMS, ID 985

Table A.1: *Glacier length records (continued)*

name	location		record period		# data	L1950	references
	lat	lon	first	last		km	
Chungurchatchiran	43.37	42.55	1887	2007	5	9.39	WGMS,ID 857
							D. Petrakov, pers. com.
Cipreses	-34.55	-70.37	1842	2007	12	11.88	WGMS, ID 2008
							Araneda et al. [2009]
							Le Quesne et al. [2009]
Clendenning	50.87	-123.90	1883	1979	7	11.10	*Williams Jr. and Ferrigno* [2002]
							WGMS, ID 17
Colonia	-47.17	-73.43	1945	2005	5	39.80	WGMS, ID 1027
							López et al. [2010]
Cook	-54.48	-36.20	1882	2003	5	8.62	WGMS, ID 2870
							Gordon et al. [2008]
							Hogg et al. [1982]
Coronas	43.63	0.65	1825	2005	11	0.40	*Chueca et al.* [2003]
Daunkogel	47.00	11.10	1891	2007	89	3.20	WGMS, ID 604
							Gletscherberichte
Davidova	41.83	78.18	1932	2003	6	6.56	*Aizen et al.* [2006]
							Aizen et al. [2007]
Dich-Su	42.98	43.18	1850	2000	11	14.35	*Panov and Pisareva* [1973]
							I. Bushueva, pers. com.
Dickson	-50.77	-73.22	1897	2003	9	14.80	WGMS, ID 1660
							López et al. [2010]
							Rivera and Casassa [2004]
Diem	46.82	10.95	1893	2007	99	3.60	WGMS, ID 513
							Gletscherberichte
Djankuat	43.20	42.77	1887	2005	23	4.40	WGMS, ID 726
							Panov and Pisareva [1973]
Dolonata	42.83	77.05	1927	1990	24	4.06	WGMS, ID 798
							G.B. Osipova, pers. com.
Dorfer	47.10	12.33	1896	1997	64	4.20	WGMS, ID 577
Drummond	51.60	-116.10	1884	1965	7	1.20	*Williams Jr. and Ferrigno* [2002]
							WGMS, ID 1398
Dvoinoi Levyi	41.92	78.25	1943	2003	3	3.05	*Aizen et al.* [2006]
							Aizen et al. [2007]
E. Gruebl	46.98	11.23	1897	1994	53	3.40	WGMS, ID 597
Ebbabreen	78.73	16.95	1900	2005	7	8.41	*Rachlewicz et al.* [2007]
							Hagen et al. [1993]
Eel	48.22	-123.55	1920	1976	12	2.00	WGMS, ID 188
Elena	0.38	29.70	1906	2005	6	0.75	*Kaser and Osmaston* [2002]
							Taylor et al. [2006]
Elsabreen	78.68	16.38	1900	2002	4	1.72	*Rachlewicz et al.* [2007]
							Hagen et al. [1993]
Engabreen	66.65	13.85	1600	2007	77	12.00	WGMS, ID 298
							NVE reports
							Bogen et al. [1989]
Erciyes	38.88	35.75	1902	2008	8	0.55	*Sarikaya et al.* [2009]
Esetuk	69.30	-144.33	1910	1981	4	6.63	*Evison et al.* [1996]

Table A.1: *Glacier length records (continued)*

name	location		record period		# data	L1950	references
	lat	lon	first	last		km	
Excelsior	60.00	-148.77	1797	2006	8	25.33	*Weeks* [2011] *Le Bris et al.* [2011]
Exit	60.17	-149.78	1825	2006	12	11.20	*Weeks* [2011] *Wiles and Calkin* [1994] *Le Bris et al.* [2011]
Exploradores	-46.50	-73.17	1945	1990	4	20.40	WGMS, ID 1011 *Aniya* [2001]
Fåbergstølbreen	61.43	7.14	1899	2007	103	7.00	H. Elvehoy (NVE), pers. com.
Fedchenko	38.71	72.33	1928	1990	11	77.27	*Barbat et al.* [1977] G.B. Osipova, pers. com.
Fee	46.08	7.88	1883	2007	99	5.70	WGMS, ID 392 *Swiss glacier monitoring network* [1881-2009]
Ferdinandbreen	78.70	16.33	1900	2002	4	3.67	*Rachlewicz et al.* [2007] *Hagen et al.* [1993]
Fernau	46.98	11.13	1902	2007	82	2.70	WGMS, ID 601 Gletscherberichte
Ferpecle	46.02	7.58	1891	2005	113	6.50	WGMS, ID 379 *Swiss glacier monitoring network* [1881-2009]
Fiero	-46.70	-73.20	1945	1990	4	18.00	*Aniya* [2001]
Fiescher	46.05	8.15	1891	2007	113	16.40	WGMS, ID 471 *Swiss glacier monitoring network* [1881-2009]
Fisht	43.95	43.18	1905	1990	15	1.29	*Barbat et al.* [1977] *Panov* [1993] I. Bushueva, pers. com.
Fleur de Neige	49.83	-122.60	1895	1978	9	1.30	WGMS, ID 20 *Williams Jr. and Ferrigno* [2002]
Forni	46.40	10.57	1833	2005	72	5.40	WGMS, ID 670
Forno	46.30	9.70	1857	2007	98	5.70	WGMS, ID 396 *Swiss glacier monitoring network* [1881-2009]
Fox	-43.53	170.15	1894	2002	41	13.20	WGMS, ID 1536 B. Fitzharris, pers. com. 1993 *Williams Jr. and Ferrigno* [1989]
Franz Josef	-43.50	170.22	1600	2005	113	10.25	*McKinzey et al.* [2004] B. Fitzharris, pers. com. 1993 *Williams Jr. and Ferrigno* [1989] WGMS WGMS_ID 899
Freya	74.38	-20.83	1939	2008	5	6.70	*Hynek et al.* [2009] *Ahlmann* [1953] *Ettema et al.* [2009]
Frias	-41.15	-71.83	1639	2009	27	6.59	*Villalba et al.* [1990] *Leiva et al.* [2008] *Masiokas et al.* [2009b]

Table A.1: *Glacier length records (continued)*

name	location		record period		# data	L1950	references
	lat	lon	first	last		km	
Fyles	52.10	-126.23	1900	1985	6	9.20	WGMS, ID 27 *Williams Jr. and Ferrigno* [2002]
Güssfeldt	-32.61	-70.03	1896	2005	11	8.39	*Espizúa and Pitte* [2009] *Leiva et al.* [2008]
Gaissberg	46.83	11.07	1891	2007	111	3.50	WGMS, ID 508 Gletscherberichte
Gangotri	30.80	79.20	1780	2007	15	31.20	*Naithani et al.* [2001] *Intute* [2009] *Raina and Srivastava* [2008]
Garabashi	43.30	42.47	1887	2007	7	3.90	WGMS, ID 761 D. Petrakov, pers. com.
Geblera	50.13	87.58	1835	1989	22	5.20	WGMS, ID 1083 *Galakhov and Mukhamedov* [1999]
Gebroulaz	45.28	6.63	1907	2001	54	4.00	WGMS, ID 352
Gepatsch	46.85	10.77	1763	2007	91	9.00	WGMS, ID 522 Gletscherberichte *Nicolussi and Patzelt* [2000]
Gergeti	42.65	44.57	1860	1990	43	8.50	WGMS, ID 768 *Panov and Pisareva* [1973] *Panov* [1993]
Golubina	42.45	74.48	1861	2003	10	5.48	*Aizen et al.* [2006] *Aizen et al.* [2007]
Gorner	45.97	7.80	1882	2007	111	14.70	WGMS, ID 391 *Swiss glacier monitoring network* [1881-2009]
Gr Aletsch	46.50	8.03	1870	2007	117	25.40	WGMS, ID 360 *Swiss glacier monitoring network* [1881-2009]
Gr Gosau	47.48	13.60	1905	2007	68	2.60	WGMS, ID 536 Gletscherberichte
Gregoriev	41.96	77.92	1860	2006	5	3.76	*Kutuzov and Shahgedanova* [2009]
Gregory	-0.15	37.32	1893	2004	11	0.60	WGMS, ID 693 *Hastenrath* [1983]
Greve	-48.89	-73.91	1945	2005	7	45.86	WGMS, ID 1637 *López et al.* [2010]
Grewingk	59.58	-150.98	1858	2006	9	18.59	*Wiles and Calkin* [1994] *Weeks* [2011] *Le Bris et al.* [2011]
Grey	-50.86	-73.34	1936	2005	7	34.22	WGMS, ID 1659 *López et al.* [2010] *Rivera and Casassa* [2004]
Gries	46.43	8.33	1847	2006	49	6.80	WGMS, ID 359 *Swiss glacier monitoring network* [1881-2009]
Griffin	49.85	-122.63	1795	2004	13	2.60	WGMS, ID 21 *Koch et al.* [2009]
Grosse	-46.45	-73.30	1945	1990	4	18.00	WGMS, ID 1044

Table A.1: *Glacier length records (continued)*

name	location		record period		# data	L1950	references
	lat	lon	first	last		km	
Grosselend	47.03	13.32	1898	2006	89	2.70	WGMS, ID 542 Gletscherberichte
Gruenau	46.98	11.20	1891	2007	89	2.50	WGMS, ID 599 Gletscherberichte
Gualas	-46.59	-73.52	1945	2005	5	31.94	WGMS, ID 1019 *López et al.* [2010]
Gurgler	46.80	10.98	1850	2006	62	8.80	WGMS, ID 511
HPN-1	-47.15	-73.73	1945	2005	5	26.16	WGMS, ID 1039 *López et al.* [2010]
HPN-3	-47.24	-73.69	1945	2005	5	44.47	WGMS, ID 1037 *López et al.* [2010]
HPS-15	-49.84	-73.65	1945	2005	4	13.87	WGMS, ID 1643 *López et al.* [2010]
HPS-29	-50.50	-73.46	1945	2005	4	17.26	WGMS, ID 1649 *López et al.* [2010]
HPS-38	-51.03	-73.61	1945	2005	4	15.64	WGMS, ID 1654 *López et al.* [2010]
Hüfi	46.82	8.85	1882	2007	115	7.30	WGMS, ID 426 *Swiss glacier monitoring network* [1881-2009]
Hailuogou	29.57	101.92	1900	2007	13	13.19	WGMS, ID 849 *Lui et al.* [2010] *Rai and K* [2005]
Hallstaetter	47.48	13.62	1883	2007	76	2.40	WGMS, ID 535 Gletscherberichte
Hans	77.08	15.67	1900	2009	28	17.00	WGMS, ID 306 J. Jania - pers. com. 2005 J. Jania and L. Kolondra - pers. com. 2010
Harker	-54.37	-36.53	1902	2003	9	8.24	WGMS, ID 2868 *Gordon et al.* [2008] *Hogg et al.* [1982]
Havoc	50.52	-123.88	1750	1979	8	7.00	WGMS, ID 12 *Williams Jr. and Ferrigno* [2002]
Heaney	-54.45	-36.27	1928	2003	5	10.42	WGMS, ID 2871 *Gordon et al.* [2008] *Hogg et al.* [1982]
Hellstugubreen	61.34	8.26	1901	2007	68	3.40	H. Elvehoy (NVE), pers. com.
Helm	49.97	-123.00	1865	2003	20	2.50	WGMS, ID 45 Canadian Ministry of Water, Land and Air Protection *Koch et al.* [2009]
Hintereis	46.80	10.77	1770	2007	102	8.00	WGMS, ID 491 Gletscherberichte
Hochjoch	46.78	10.82	1937	2007	70	4.50	WGMS, ID 492 Gletscherberichte

Table A.1: *Glacier length records (continued)*

name	location		record period		# data	L1950	references
	lat	lon	first	last		km	
Hodges	-54.27	-36.54	1930	2003	5	1.21	WGMS, ID 28 *Gordon et al.* [2008] *Hogg et al.* [1982]
Horn	47.00	11.82	1895	2007	100	3.40	WGMS,WGMS_ID 589 Gletscherberichte
Hubert	47.78	-123.70	1924	1977	7	-0.20	WGMS, ID 213
Humo	-34.55	-70.13	1787	2007	12	7.00	*Cobos* [1998] *Le Quesne et al.* [2009]
Hyrningsjökull	64.80	-23.77	1931	2007	65	2.05	WGMS, ID 3092 O. Sigurdsson, pers. com.
Ice river	47.82	-123.67	1924	1976	7	1.08	WGMS, ID 209
Illecillewaet	51.23	-117.47	1887	1995	34	3.00	WGMS, ID 1400 Canadian Ministry of Water, Land and Air Protection
Irik	43.33	42.50	1887	2007	5	9.06	WGMS, 759 D. Petrakov, pers. com.
Irikchat	43.33	42.53	1887	2007	5	3.47	WGMS, ID 758 D. Petrakov, pers. com.
Isfalls	67.92	18.57	1897	2005	55	2.20	WGMS, ID 333
Jamtal	46.87	10.17	1902	2007	83	3.60	WGMS, ID 480 Gletscherberichte
Jankhu Uyu	-16.05	-68.32	1658	1997	10	0.86	*Rabatel et al.* [2008]
Jorge Montt	-48.46	-73.52	1945	2005	4	47.61	WGMS, ID 1016 *López et al.* [2010]
Kangiussaq	65.85	-52.09	1860	2009	9	5.25	*Weidick* [1968] *Weidick et al.* [1992] *Ettema et al.* [2009] M. Citterio pers. com Landsat 2000 2009
Karachaul	43.38	42.45	1887	2007	5	6.35	WGMS, ID 3022 D. Petrakov, pers. com.
Karlinger	47.13	12.70	1896	1994	58	3.80	WGMS, ID 568
Kehlen	46.68	8.42	1893	2007	107	3.40	WGMS, ID 431 *Swiss glacier monitoring network* [1881-2009]
Kesselwand	46.83	10.80	1914	2007	54	4.25	WGMS, ID 507 Gletscherberichte
Khakel	43.23	41.85	1888	1994	39	3.98	WGMS, ID 700 *Panov* [1993] WGI
Kirtisho	42.50	43.50	1890	1988	22	5.31	WGMS, ID 1112 *Panov* [1993]
Kleinelend	47.07	13.25	1898	2007	82	2.70	WGMS, ID 541 Gletscherberichte
Klujev	39.25	70.45	1936	1990	34	4.20	WGMS, ID 739 G.B. Osipova, pers. com.
Kolpakovsky	42.08	78.28	1860	2006	6	13.04	*Kutuzov and Shahgedanova* [2009]

Table A.1: *Glacier length records (continued)*

name	location		record period		# data	L1950	references
	lat	lon	first	last		km	
Korumdu	50.13	87.68	1936	2005	39	4.00	WGMS, ID 793
Koryto	54.78	161.80	1604	2000	17	6.40	Y. Muravyev, pers. com. *Sawaguchi et al.* [1999]
Kozitsiti	42.63	43.72	1888	2000	27	3.02	WGMS, ID 706 *Panov* [1993] WGI
Krapf	-0.13	37.32	1893	2004	8	0.40	*Williams Jr. and Ferrigno* [1991] *Hastenrath* [1983]
Krimmler	47.08	12.25	1896	2006	74	3.60	WGMS, ID 584 Gletscherberichte
Kukurtly	43.35	42.38	1887	2007	6	7.30	WGMS, ID 763 D. Petrakov, pers. com.
La Mare	46.43	10.60	1895	2005	64	3.50	WGMS, ID 636
Lago del Desierto 1	-49.01	-72.90	1740	2007	6	2.12	*Masiokas et al.* [2009a]
Lago del Desierto 2	-49.07	-72.90	1645	2007	8	2.37	*Masiokas et al.* [2009a]
Lago del Desierto 3	-49.08	-72.92	1655	2007	8	1.48	*Masiokas et al.* [2009a]
Langfjordjøkulen	70.14	21.75	1900	2005	10	4.60	NVE Reports
Langgletscher	46.47	7.93	1888	2005	118	8.00	WGMS, ID 386 *Swiss glacier monitoring network* [1881-2009]
Langtaler	46.80	11.02	1850	2007	110	5.50	WGMS, ID 510 Gletscherberichte addition from unknown source
Lazg-Tsiti	42.55	44.37	1850	1987	23	2.29	*Panov* [1993]
Leffingwell	69.29	-144.18	1890	1981	4	6.26	*Evison et al.* [1996]
Leirbreen	61.34	8.06	1909	2007	49	3.80	H. Elvehoy (NVE), pers. com.
Lengua	-52.80	-72.98	1628	2007	8	6.83	*Koch and Kilian* [2005] *Schneider et al.* [2007] *Dickmann* [2008] C. Schneider, pers. com.
Leones	-46.80	-73.26	1945	2005	5	12.86	WGMS, ID 1022 *López et al.* [2010]
Leviy Karagemsk	50.23	88.17	1850	2005	28	3.50	WGMS, ID 1084
Lewis	-0.15	37.26	1893	2004	16	1.00	*Williams Jr. and Ferrigno* [1991] *Hastenrath* [1983]
Lodal	61.78	7.24	1750	2005	76	8.82	*Nussbaumer et al.* [2011]
Lyngmarksbræ	69.28	-53.55	1812	2005	12	2.19	*Yde and Knudsen* [2007]
Lys	45.90	7.83	1904	2005	92	5.60	WGMS, ID 620
Maliy Aktru	50.08	87.75	1911	2005	53	4.50	WGMS, ID 795 additions from unknown source
Malyi Azau	43.28	42.45	1887	2007	7	7.04	WGMS, ID 762 D. Petrakov, pers. com.
Mandrone	46.17	10.53	1942	2005	47	5.50	WGMS, ID 664
Martial	-54.78	-68.42	1898	2003	6	0.86	WGMS, ID 917
Marukhskiy	43.33	41.17	1888	2000	35	4.10	WGMS, ID 727 *Panov* [1993]

Table A.1: *Glacier length records (continued)*

name	location		record period		# data	L1950	references
	lat	lon	first	last		km	
Marzell	46.78	10.88	1891	2006	104	4.40	WGMS, ID 515 Gletscherberichte
Mc Whaebreen	78.77	16.67	1900	2002	4	4.73	*Rachlewicz et al.* [2007] *Hagen et al.* [1993]
McCall	69.28	-143.83	1895	2005	12	8.20	WGMS, ID 1388 *Rabus and Echelmeyer* [1998] M. Nolan, pers. com. *Delcourt et al.* [2008]
Melang	28.45	99.73	1932	2002	6	10.85	*Rai and K* [2005] *Yuanqing et al.* [2003]
Mer de Glace	45.88	6.93	1570	2005	153	12.00	WGMS, ID 353 *Nussbaumer et al.* [2007]
Meren	-4.08	137.17	1825	1990	8	2.10	WGMS, ID 1050 *Williams Jr. and Ferrigno* [1989]
Mikelchiran	43.37	42.50	1887	2007	5	5.08	WGMS, ID 755 D. Petrakov, pers. com.
Mikkajekna	67.40	17.70	1897	2002	44	4.70	WGMS, ID 338 additions from unknown source
Milam	30.43	80.05	1849	2006	11	18.07	*Bhambri and Bolch* [2009] *Raj* [2011]
Minapin	36.18	74.58	1889	1987	8	19.50	WGMS, ID 994
Mittivakkat	65.68	-37.08	1900	2010	8	8.33	*Mernild et al.* [2011]
Mizhirgichiran	43.05	43.17	1888	1998	20	8.81	WGMS, ID 1509 *Panov and Pisareva* [1973]
Moiry	46.08	7.60	1924	2007	82	5.80	WGMS, ID 380 *Swiss glacier monitoring network* [1881-2009]
Morsárjökull	64.12	-16.88	1932	2006	70	10.54	WGMS, ID 3104 O. Sigurdsson, personal communnication
Morteratsch	46.40	9.93	1878	2007	130	7.60	WGMS, ID 1673 *Swiss glacier monitoring network* [1881-2009]
Motzfeldt SnøV	61.15	-45.03	1855	2008	8	4.78	*Weidick* [1988] *Ettema et al.* [2009] M. Citterio pers. com Landsat 1992, 2002, 2008
Motzfeldt SnøØ	61.15	-45.03	1855	2008	7	2.90	*Weidick* [1988] *Ettema et al.* [2009] M. Citterio pers. com Landsat 1992 2002 2008

Table A.1: *Glacier length records (continued)*

name	location		record period		# data	L1950	references
	lat	lon	first	last		km	
Napassorssuaq	60.30	-45.27	1894	2010	6	3.09	*Weidick* [1968] *Weidick et al.* [1992] *Weidick* [1988] *Ettema et al.* [2009] T. Bolch pers. com. M. Citterio pers. com Landsat 2010
Narssaq	60.99	-45.90	1900	2008	12	3.11	*Weidick* [1968] *Weidick et al.* [1992] *Weidick* [1988] *Ettema et al.* [2009] M. Citterio pers. com Landsat 1992 2000 2008
Nef	-46.98	-73.32	1945	2005	5	32.76	WGMS, ID 1024 *López et al.* [2010]
New Moon	53.92	-127.77	1875	2003	83	1.60	WGMS, ID 5 *Williams Jr. and Ferrigno* [2002]
Niederjoch	46.78	10.87	1891	2007	112	3.40	WGMS, ID 516 Gletscherberichte
Nigardsbreen	61.72	7.13	1675	2009	116	9.60	WGMS, ID 290 NVE reports *Østrem et al.* [1977] *Nesje et al.* [2008] *Nussbaumer et al.* [2011]
Nisqually	46.78	-121.75	1840	2001	75	7.60	WGMS WGMS_ID 201 *Heliker et al.* [1984] *Granshaw and Fountain*
Noeick	52.30	-125.72	1900	1978	4	5.30	WGMS, ID 28 additions from unknown source
Nordenskiöldbreen	78.70	17.18	1880	2004	10	29.23	*Rachlewicz et al.* [2007] *Hagen et al.* [1993] *Kuipers Munneke* [2005]
Noroeste	-52.73	-73.12	1942	2007	6	13.90	*Schneider et al.* [2007] C. Schneider, pers. com. *Dickmann* [2008]
Nuka	59.66	-150.73	1724	2006	12	7.57	*Weeks* [2011] *Wiles and Calkin* [1994] *Le Bris et al.* [2011]
O'Higgins	-48.92	-73.36	1945	2005	4	54.47	WGMS, ID 1015 *López et al.* [2010]
Ob Grindelwald	46.62	8.10	1593	2000	129	5.50	WGMS, ID 444 *Swiss glacier monitoring network* [1881-2009] *Zumbühl* [1980]
Obersulzbach	47.12	12.30	1870	2007	83	6.30	WGMS, ID 583 Gletscherberichte

Table A.1: *Glacier length records (continued)*

name	location		record period		# data	L1950	references
	lat	lon	first	last		km	
Occidental	-48.83	-73.76	1945	2005	5	56.21	WGMS, ID 1636 *López et al.* [2010]
Oedenwinkel	47.12	12.65	1816	2007	52	4.20	WGMS, ID 559 Gletscherberichte additions from unknown source
Oeste M	-52.82	-73.17	1942	2007	5	3.01	*Schneider et al.* [2007] *Dickmann* [2008] *Schneider et al.* [2003]
Oeste N	-52.80	-73.15	1942	2007	5	11.09	*Schneider et al.* [2007] *Dickmann* [2008] *Schneider et al.* [2003]
Oeste S L	-52.83	-73.23	1942	2007	5	9.51	*Schneider et al.* [2007] *Dickmann* [2008] *Schneider et al.* [2003]
Oeste S R	-52.83	-73.20	1942	2007	5	8.39	*Schneider et al.* [2007] *Dickmann* [2008] *Schneider et al.* [2003]
Ofhidro	-48.50	-73.68	1945	2005	5	26.39	WGMS, ID 1633 *López et al.* [2010]
Okpilak	69.15	-144.18	1890	2006	7	8.76	*Evison et al.* [1996]
Okpilak-6	69.17	-144.15	1890	1981	4	1.58	*Evison et al.* [1996]
Ossoue	42.78	-0.13	1850	2007	42	1.70	WGMS, ID 2867 *Réné* [2003]
Oulettes	42.78	-0.14	1850	2003	32	0.80	*Réné* [2003]
Overlord	50.02	-122.83	1893	2002	17	2.70	WGMS, ID 43 *Williams Jr. and Ferrigno* [2002] *Koch et al.* [2009] addition from unknown source
Paierl	77.22	16.25	1900	1985	7	27.00	WGMS, ID 294
Palue	46.37	9.98	1894	2007	75	4.30	WGMS, ID 398 *Swiss glacier monitoring network* [1881-2009]
Paradies	46.50	9.07	1873	2007	98	4.10	WGMS, ID 412 *Swiss glacier monitoring network* [1881-2009]
Pared Norte	-47.37	-73.35	1945	2005	5	26.12	WGMS, ID 1030 *López et al.* [2010]
Pasterze	47.10	12.70	1620	2007	130	9.80	WGMS, ID 566 *Lang and Lieb* [1993] *Williams Jr. and Ferrigno* [1993] *Nicolussi and Patzelt* [2000] Gletscherberichte
Peñon	-35.27	-70.56	1660	2007	10	2.98	*Espizúa and Pitte* [2009] *Leiva et al.* [2008]
Petersen	69.30	-53.55	1894	2005	10	2.11	*Yde and Knudsen* [2007]
Petrova	41.87	78.27	1869	2003	6	12.82	*Aizen et al.* [2006] *Aizen et al.* [2007]

Table A.1: *Glacier length records (continued)*

name	location		record period		# data	L1950	references
	lat	lon	first	last		km	
Peyto	51.67	-116.55	1897	2004	19	5.80	WGMS, ID 57 S. Munro, pers. com.
Piedras Blancas	-49.27	-72.97	1610	2007	10	5.72	*Masiokas et al.* [2009a]
Piscis	-47.45	-73.43	1945	2005	5	9.24	WGMS, ID 1032 *López et al.* [2010]
Pizol	46.95	9.38	1893	2009	96	0.63	WGMS, ID 417 *Swiss glacier monitoring network* [1881-2009]
Pjetursson	69.30	-53.42	1894	2005	8	1.95	*Yde and Knudsen* [2007]
Pollockbreen	78.70	16.02	1900	2002	4	3.11	*Rachlewicz et al.* [2007] *Hagen et al.* [1993]
Popov	41.99	77.93	1860	2006	6	6.07	*Kutuzov and Shahgedanova* [2009]
Portage	60.83	-148.97	1810	2004	13	15.00	*Crossen* [1992] G. Braasch (2004), aerial photograph (interpretation by J.Oerlemans)
Praviy Aktru	50.05	87.44	1936	1980	15	5.35	WGMS, ID 831 G.B. Osipova, pers. com.
Qingua Kujatdleq	65.95	-51.92	1860	2009	9	15.42	*Weidick* [1968] *Weidick et al.* [1992] *Ettema et al.* [2009] M. Citterio pers. com Landsat 2000 2009
Queets	47.77	-123.60	1913	1976	16	1.44	WGMS, ID 215
Rabots	67.90	18.48	1910	2003	26	4.53	*Brugger* [2007] *Brugger et al.* [2005]
Ragnarbreen	78.75	16.73	1900	2002	4	6.03	*Rachlewicz et al.* [2007] *Hagen et al.* [1993]
Raigorodskiy	39.67	70.75	1908	1990	29	6.20	WGMS, ID 743
Raikot	35.33	74.59	1934	2007	10	14.83	*Schmidt and Nüsser* [2009]
Rama	39.17	70.45	1870	1990	14	5.64	WGMS, ID 744 G.B. Osipova, pers. com.
Rembesdalsskåka	60.53	7.36	1917	2007	35	8.10	H. Elvehoy (NVE), pers. com.
Rhone	46.62	8.40	1600	2009	159	10.50	WGMS, ID 473 *Swiss glacier monitoring network* [1881-2009] *Aellen* [1981] *Zumbühl and Holzhauser* [1988]
Rodzevicha	49.50	87.00	1850	1995	17	5.30	*Galakhov and Mukhamedov* [1999] WGMS, ID 1086
Roseg	46.38	9.83	1855	2007	102	5.80	WGMS, ID 406 *Swiss glacier monitoring network* [1881-2009]
Rosenlaui	46.65	8.15	1760	1978	62	5.21	WGMS,ID 445 *Zumbühl and Holzhauser* [1988] *Swiss glacier monitoring network* [1881-2009]

Table A.1: *Glacier length records (continued)*

name	location		record period		# data	L1950	references
	lat	lon	first	last		km	
Ross	-54.56	-36.18	1882	2003	8	11.50	WGMS, ID 2869 *Gordon et al.* [2008] *Hogg et al.* [1982]
Rotmoos	46.82	11.05	1847	2007	113	3.50	WGMS, ID 509 Gletscherberichte
Sólheima	63.58	-19.28	1705	2007	83	15.00	WGMS, ID 3122 *Sigurðsson* [1998] *Mackintosh et al.* [2002] O. Siggurdsson, pers. com.
Saint Sorlin	45.18	6.17	1893	1996	43	3.20	WGMS, ID 356
Salajekna	67.12	16.38	1898	2002	24	9.40	WGMS, ID 341
Saleina	45.98	7.07	1891	2007	113	6.50	WGMS, ID 458 *Swiss glacier monitoring network* [1881-2009]
Samarin	76.83	16.42	1900	1985	6	18.00	WGMS, ID 311
San Quintin	-46.90	-73.62	1945	2005	5	68.19	WGMS, ID 1041 *López et al.* [2010]
San Rafael	-46.72	-73.51	1675	2005	9	57.12	WGMS, ID 1042 *López et al.* [2010] *Araneda et al.* [2007]
Sapozhniikova	44.90	79.45	1850	1995	14	5.40	WGMS, ID 1087 *Galakhov and Mukhamedov* [1999]
Sardloq	65.87	-52.61	1860	2009	8	3.85	*Weidick* [1968] *Weidick et al.* [1992] *Ettema et al.* [2009] M. Citterio pers. com Landsat 2000 2009
Sari Tor	41.82	78.20	1932	2003	6	4.50	*Aizen et al.* [2006] *Aizen et al.* [2007]
Sarqaq	70.08	-51.70	1849	2010	11	6.78	*Weidick* [1968] *Weidick et al.* [1992] *Citterio et al.* [2009] *Ettema et al.* [2009] M. Citterio pers. com Landsat 2001 2010
Saskatchewan	52.20	-117.13	1895	1995	28	14.50	WGMS, ID 8 *Williams Jr. and Ferrigno* [1989]
Schlaten	47.12	12.38	1912	2007	66	6.40	WGMS, ID 580 Gletscherberichte
Schwarzenstein	47.02	11.85	1891	2007	99	2.80	WGMS, ID 588 Gletscherberichte
Sentinel	58.67	-136.58	1935	1985	24	3.31	WGMS, ID 44
Sermiarssuit	70.52	-52.15	1811	2010	12	11.55	*Weidick* [1968] *Weidick et al.* [1992] *Citterio et al.* [2009] *Ettema et al.* [2009] Landsat 2001 2010

Table A.1: *Glacier length records (continued)*

name	location		record period		# data	L1950	references
	lat	lon	first	last		km	
Sermikavsak	71.22	-53.96	1850	2010	12	14.99	*Weidick* [1968]
							Weidick et al. [1992]
							Møller [1959]
							Gribbon [1970]
							Citterio et al. [2009]
							Ettema et al. [2009]
							Landsat 2001 2010
Serminguaq	66.28	-52.40	1860	2010	12	20.85	*Weidick* [1968]
							Weidick et al. [1992]
							Ettema et al. [2009]
							M. Citterio pers. com
							Landsat 1988 2000 2010
Sermitsiaq	60.54	-44.16	1833	2010	9	12.47	*Weidick* [1968]
							Weidick et al. [1992]
							Weidick [1988]
							Ettema et al. [2009]
							T. Bolch pers. com.
							M. Citterio pers. com
							Landsat 2010
Sherman	60.60	-145.20	1910	1965	5	13.00	*Kienholz* [2010]
Shurovskiy	39.62	70.58	1871	1968	14	11.63	*Petrov and Shetinnikov* [1977]
							G.B Osipova, pers. com.
Sigssarigsut	66.37	-52.38	1860	2010	10	8.58	*Weidick* [1968]
							Weidick et al. [1992]
							Ettema et al. [2009]
							M. Citterio pers. com
							Landsat 2000 2010
Simony	47.07	12.27	1900	2007	73	3.80	WGMS, ID 575
							Gletscherberichte
Skaftafells	64.08	-16.80	1932	2006	72	18.38	WGMS, ID 3113
							Sigurðsson [1998]
							O. Sigurdsson, pers. com.
Skazka	42.83	43.67	1890	2000	59	3.30	WGMS, ID 705
							Panov [1993]
							Panov and Pisareva [1973]
Sofiyskiy	49.78	87.77	1898	2001	5	7.40	*De Smedt and Pattyn* [2003]
Soler	-46.90	-73.18	1675	2005	10	8.30	*Aniya* [2001]
							López et al. [2010]
Sorbreen	71.03	-8.18	1861	1975	8	5.80	*Anda et al.* [1985]
							Aerial photos / Norsk Polarinstitutt

Table A.1: *Glacier length records (continued)*

name	location		record period		# data	L1950	references
	lat	lon	first	last		km	
Sorqaup	70.47	-51.88	1850	2010	11	9.64	*Weidick* [1968] *Weidick et al.* [1992] *Citterio et al.* [2009] *Ettema et al.* [2009] M. Citterio pers. com Landsat 2010
South Cascade	48.37	-121.05	1890	2000	45	3.70	WGMS, ID 205 A. Rasmussen, pers. com.
Speke	0.40	29.86	1906	2003	5	1.00	*Kaser and Osmaston* [2002] *Taylor et al.* [2006]
Staircase	49.83	-122.61	1895	2004	11	2.20	WGMS, ID 18 *Koch et al.* [2009]
Steffen	-47.33	-73.60	1945	2005	5	50.22	WGMS, ID 1036 *López et al.* [2010]
Stegaholtbreen	61.48	7.19	1903	2007	102	7.70	H. Elvehoy (NVE), pers. com.
Stein	46.70	8.43	1893	2007	112	4.70	WGMS, ID 448 *Swiss glacier monitoring network* [1881-2009]
Stocking	-43.67	170.07	1865	2001	50	1.25	*Salinger et al.* [1983] *Burrows* [2005] *Chinn* [1996] WGI
Storbreen	61.57	8.13	1870	2005	59	3.30	WGMS, ID 302 NVE Reports *Matthews* [1979]
Storglaciären	67.90	18.57	1891	2002	108	3.80	WGMS, ID 332
Suatisi Sredniy	42.70	44.42	1882	1990	23	4.70	WGMS_ID 770
Sulzenau	46.98	11.15	1850	2007	83	3.70	WGMS, ID 600 Gletscherberichte
Surf	50.50	-123.97	1893	1979	8	1.40	WGMS 2008, WGMS_ID 13 addition from unknown source
Svinafell	64.03	-16.75	1740	2006	77	12.00	WGMS_ID 3123&3124 O. Siggurdsson, pers. com. additions from unknown source
Taillon	42.70	-0.06	1850	2003	21	0.70	WGMS, ID 963 *Réné* [2003]
Taschach	46.90	10.87	1856	2007	88	5.80	WGMS, ID 519 Gletscherberichte
Tavlebreen	77.95	15.05	1936	2006	5	5.97	*Lavrentiev* [2008]
Tbilisa	43.13	42.47	1870	1988	18	3.21	WGMS, ID 724 *Panov* [1993]
Tchaikazan	51.02	-123.78	1900	1982	6	8.90	WGMS, ID 60
Tebenkopf	60.67	-148.55	1670	2009	12	13.50	*Wiles et al.* [1999] *Barclay et al.* [2009] *Le Bris et al.* [2011]
Terrific	50.43	-123.43	1883	1979	8	3.70	WGMS, ID 15

Table A.1: *Glacier length records (continued)*

name	location		record period		# data	L1950	references
	lat	lon	first	last		km	
Terskol	43.30	42.48	1887	2007	4	6.47	WGMS, ID 760 D. Petrakov, pers. com.
Thunderclap	49.85	-122.65	1886	2004	10	2.80	WGMS, ID 22 *Koch et al.* [2009]
Tikhitsi	41.14	47.47	1850	1988	23	2.07	WGMS, ID 777 *Panov* [1993]
Torre	-49.35	-72.33	1594	2007	10	6.78	*Masiokas et al.* [2009a]
Trient	46.00	7.03	1879	2007	127	5.00	WGMS, ID 457 *Swiss glacier monitoring network* [1881-2009]
Ts. Tuyuksuyskiy	43.05	77.08	1923	2005	41	3.40	WGMS, ID 817
Tsanfleuron	46.32	7.23	1892	2005	114	3.80	WGMS, ID 371 *Swiss glacier monitoring network* [1881-2009]
Tseya	42.92	43.67	1890	2000	73	8.80	WGMS, ID 704 *Panov* [1993] *Panov and Borovik* [1976]
Tsidjore Nouve	46.00	7.45	1880	2007	118	4.90	WGMS, ID 376 *Swiss glacier monitoring network* [1881-2009]
Tsoloss	51.38	-123.87	1720	1982	5	1.60	WGMS, ID 63 addition from unknown source
Tunorssuaq	69.32	-53.36	1848	2010	13	2.00	*Yde and Knudsen* [2007]
Turtmann	46.13	7.68	1885	2005	115	6.10	WGMS, ID 385
Tyndall	-0.15	37.30	1893	2004	16	0.60	WGMS, ID 697 *Hastenrath* [1983]
Tyndall	-51.12	-73.43	1945	2005	4	41.71	WGMS, ID 1013 *López et al.* [2010]
U Grindelwald	46.58	8.07	1534	1983	128	9.00	WGMS, ID 443 *Swiss glacier monitoring network* [1881-2009] *Zumbühl* [1980]
Uilpata	42.77	43.82	1890	1990	48	2.30	*Panov* [1993] *Panov and Pisareva* [1976]
Ulluchiran	43.38	42.43	1887	2007	5	6.30	WGMS, ID 836 D. Petrakov, pers. com.
Ullukol	43.38	42.47	1887	2007	5	5.32	WGMS, ID 834 D. Petrakov, pers. com.
Ullumalienderku	43.38	42.48	1887	2007	5	5.88	WGMS, ID 833 D. Petrakov, pers. com.
Umbal	47.05	12.25	1896	2007	76	5.00	WGMS, ID 574 Gletscherberichte

Table A.1: *Glacier length records (continued)*

name	location		record period		# data	L1950	references
	lat	lon	first	last		km	
Umiartopfiup	70.47	-51.98	1850	2010	11	15.82	*Weidick* [1968] *Weidick et al.* [1992] *Citterio et al.* [2009] *Ettema et al.* [2009] M. Citterio pers. com Landsat 2010
Unteraar	46.57	8.22	1719	2005	128	14.00	WGMS, ID 450 *Swiss glacier monitoring network* [1881-2009]
Untersulzbach	47.13	12.35	1896	2007	73	6.40	WGMS, ID 582 Gletscherberichte
Upsala	-49.74	-73.38	1945	2005	10	62.17	WGMS, ID 921 *López et al.* [2010]
Vacas	-32.55	-69.99	1896	2005	11	6.84	*Espizúa and Pitte* [2009] *Leiva et al.* [2008]
Valdez	61.30	-146.20	1901	2008	18	35.20	*Millett* [1964] *Kienholz* [2010]
Valsorey	45.90	7.27	1889	2007	112	4.30	WGMS, ID 365 *Swiss glacier monitoring network* [1881-2009]
Vatnajökull	64.50	-16.50	1690	1995	23	20.00	*Sigurðsson* [1998] *Thorarinsson* [1943]
Ventina	46.27	9.77	1899	2005	78	3.80	WGMS, ID 629 *Zumbühl and Holzhauser* [1988]
Ventorrillo	19.02	-98.62	1921	1999	10	0.99	WGMS, ID 914
Verstancla	46.84	10.07	1926	2009	72	2.18	WGMS, ID 409 *Swiss glacier monitoring network* [1881-2009]
Victoria	51.38	-116.27	1898	1966	15	4.20	WGMS, ID 1399 *Williams Jr. and Ferrigno* [1989]
Viltragen	47.13	12.37	1891	2007	72	4.60	WGMS, ID 581 Gletscherberichte
Vostostochniy Klukhorskiy	43.23	41.87	1890	1990	16	1.52	*Panov* [1993] *Borovik and Kravcova* [1977]
Waldemarbreen	78.67	12.00	1909	1995	8	3.83	WGMS, ID 2307
Waxegg	47.00	11.80	1881	2007	103	2.40	WGMS, ID 590 Gletscherberichte
Wedgemount	50.15	-122.78	1900	1995	26	3.00	WGMS, ID 42 *Williams Jr. and Ferrigno* [1989]
White (USA)	47.87	-123.70	1815	2001	14	3.50	WGMS, ID 212
Wila Lluxita	-16.05	-68.30	1662	1997	11	0.85	*Rabatel et al.* [2008]
Wolverine	60.42	-148.90	1713	2006	8	8.02	*Wiles et al.* [1999] *Weeks* [2011]
Wurten	47.03	13.00	1834	2007	159	4.10	WGMS, ID 545 Gletscherberichte

Table A.1: *Glacier length records (continued)*

name	location		record period		# data	L1950	references
	lat	lon	first	last		km	
Yalik	59.48	-150.73	1889	2006	10	15.14	*Weeks* [2011] *Wiles and Calkin* [1994] *Le Bris et al.* [2011]
Yuzhniy	42.17	46.15	1862	2000	43	2.01	WGMS, ID 779 *Panov* [1993]
Zemu	27.71	88.23	1903	2005	6	28.63	*Raina and Srivastava* [2008] *Krishna* [2005]
Zeravshanskiy	39.52	70.67	1880	1990	15	28.50	WGMS, ID 745
Zettalunitz	47.08	12.38	1896	2007	70	4.90	WGMS, ID 578 Gletscherberichte
Zinal	46.07	7.63	1891	2007	114	8.60	WGMS, ID 382 *Swiss glacier monitoring network* [1881-2009]
Zongo	-16.30	-68.14	1680	2008	29	3.22	*Rabatel et al.* [2008]
Zulumart	39.10	72.83	1943	2001	5	21.00	WGMS, ID 2100 *Osipova et al.* [2005]

WGMS:	World Glacier Monitoring Service, Fluctuations of Glaciers ISSN 1997-910X (print)/ISSN 1997-9118 (online), ID number corresponds with the glacier identification number in the WGMS database
WGI:	National Snow and Ice Data Center. 1999, updated 2009. World glacier inventory. World Glacier Monitoring Service and National Snow and Ice Data Center/World Data Center for Glaciology. Boulder, CO. Digital media
Gletscherberichte:	Glacier monitoring of Austrian glaciers by volunteers of the OEAV, published annually in *Bergauf*
NVE reports:	Annual reports of the Norwegian Water Resources and Energy Directorate
pers. com.	personal communication

Bibliography

Adhikari, S., and P. Huybrechts (2009), Numerical modelling of historical front variations and the 21st-century evolution of Glacier AX010, Nepal Himalaya, *Annals of Glaciology*, *50*(52), 27–34.

Aellen, M. (1981), *Die Schweiz und ihre Gletscher*, Kümmerly and Frey, Schweizerischen Verkehrszentrale.

Agostini, A. (1949), *Nahuel-Huapí - Bellezas Naturales de los Andes en la Patagonia Septentrional*, Estudios Fotográficos, Buenos Aires, Argentina.

Ahlmann, H. W. (1953), *Glacier Variations and Climatic Fluctuations*, vol. series three, The American Geographical Society, New York.

Aizen, V. B., V. A. Kuzmichenok, A. B. Surazakov, and E. M. Aizen (2006), Glacier changes in the central and northern Tien Shan during the last 140 years based on surface and remote-sensing data, *Annals of Glaciology*, *43*, 202–213.

Aizen, V. B., E. M. Aizen, and V. A. Kuzmichonok (2007), Glaciers and hydrological changes in the Tien Shan: simulation and prediction, *Environmental Research Letters*, *2*.

Alvarado, J. A. C., F. Barbecot, R. Purtchert, M. Gillon, W. Aeschbach-Hertig, and R. Kipfer (2009), European climate variations over the past half-millennium reconstructed from groundwater, *Geophysical Research Letters*, *36*(L15703), doi:10.1029/2009GL038826.

Anda, E., O. Orheim, and J. Mangerud (1985), Late Holocene glacier variations and climate at Jan Mayen, *Polar Research*, *3*(2), 129–140.

Andreassen, L. M., H. Elvehøy, B. Kjøllmoen, R. V. Engeset, and N. Haakensen (2005), Glacier mass-balance and length variation in Norway, *Annals of Glaciology*, *42*, 317–325.

Aniya, M. (2001), Glacier variations of Hielo Patagónico Norte, Chilean Patagonia, since 1944/1945, with special reference to variations between 1995/1996 and 1999/2000, *Bulletin of Glacier Research*, *18*, 55–63.

Araneda, A., F. Terrejón, M. Aguayo, L. Torres, F. Cruces, M. Cisternas, and R. Urrutia (2007), Historical records of San Rafael glacier advances (North Patagonian Icefield): another clue to 'Little Ice Age' timing in southern Chile?, *The Holocene*, *17*(7), 2007.

Araneda, A., F. Torrejón, M. Aguayo, I. Alvial, C. Mendoza, and R. Urrutia (2009), Historical records of Cipreses glacier (34 °S): combining documentary-inferred 'Little Ice Age' evidence from Southern and Central Chile, *The Holocene*, *19*(8), 1173–1183.

Auer, I., et al. (2007), HISTALP - historical instrumental climatological surface time series of the Greater Alpine Region, *International Journal of Climatology*, *27*, 17–46, doi:10.1002/joc.1377.

Bahr, D. B., M. F. Meier, and S. D. Peckham (1997), The physical basis of glacier volume-area scaling, *Journal of Geophysical Research*, *102*(B9), 20,355–20,362.

Barbat, U. P., A. D. Svyatec, and L. G. Cherkasov (1977), *Catalogue of Glaciers of the USSR*, vol. 14, Gidrometeoizdat, Leningrad.

Barclay, D. J., G. C. Wiles, and P. E. Calkin (2009), Tree-ring crossdates for a First Millennium AD advance of Tebenkopf Glacier, southern Alaska, *Quaternary Research*, *71*, 22–26, doi:10.1016/j.yqres.2008.09.005.

Barnett, T. P. (1983), Recent changes in sea level and their possible causes, *Climate Change*, *5*, 15–38.

Bhambri, R., and T. Bolch (2009), Glacier mapping: a review with special reference to the Indian Himalays, *Progress in Physical Geography*, *33*(5), 672–704.

Bindoff, N. L., et al. (2007), Observations: Oceanic Climate Change and Sea Level, in *Climate Change 2007: The Physical Science Basis. Contribution of Working Group I to the fourth Assessment Report of the Intergovernmental Panel on Climate Change*, edited by S. Solomon, D. Qin, M. Manning, Z. Chen, M. Marquis, K. B. Averyt, M. Tignor, and H. L. Miller, Camebridge University Press, Camebridge, United Kingdom and New York, NY, USA.

Bogen, J., B. Wold, and G. Østrem (1989), Historic glacier variations in Scandinavia, in *Glacier fluctuations and climate change*, edited by J. Oerlemans, pp. 109–128, Kluwer Academic Publishers.

Böhm, R., P. D. Jones, J. Hiebl, D. Frank, M. Brunetti, and M. Maugeri (2010), The early instrumental warm-bias: a solution for long central European temperature series 1760-2007, *Climatic Change*, *101*, 41–67, doi: 10.1007/s10584-009-9649-4.

Boninsegna, J. A., et al. (2009), Dendroclimatological reconstructions in South America: a review, *Palaeogeography, Palaeoclimatology, Palaeoecology*, *281*, 210–228, doi:10.1016/j.palaeo.2009.07.020.

Borovik, E. S., and V. I. Kravcova (1977), *Catalogue of Glaciers of the USSR*, vol. 8, Gidrometeoizdat, Leningrad.

Boucher, E., J. Guiot, and E. Chapron (2011), A millennial multi-proxy reconstruction of summer pdsi for southern south america, *Climate of the Past*, *7*(3), 957–974, doi:10.5194/cp-7-957-2011.

Bouverot, M. (1958), Notice sur les variations des glaciers du Mont Blanc, *unknown*.

Bown, F., and A. Rivera (2007), Climate changes and recent glacier behaviour in the Chilean Lake District, *Global and Planetary Change*, *59*, 76–86.

Bown, F., A. Rivera, C. Acuña, and G. Casassa (2007), *Recent glacier mass balance calculations at Volcán Mocho-Choshuenco (40°S), Chilean Lake District*, vol. 318, pp. 143–152, IAHS Publ., Wallingford, UK.

Box, G. E. P., and G. M. Jenkins (1976), *Time series analysis forecasting and control*, Holden-day.

Brázdil, R., C. Pfister, H. Wanner, H. von Storch, and J. Luterbacher (2005), Historical climatology in Europe - the state of the art, *Climatic Change*, *70*, 362–430, doi:10.1007/s10584-005-5924-1.

Briffa, K. R. (2000), Annual climate variability in the Holocence: interpreting the message of ancient trees, *Quaternary Science Reviews*, *19*, 87–105.

Briffa, K. R., F. H. Schweingruber, P. D. Jones, T. J. Osborn, S. G. Shiyatov, and E. A. Vaganov (1998), Reduced sensitivity of recent tree-growth to temperature at high northern latitudes, *Nature*, *391*, 678–682.

Briffa, K. R., T. J. Osborn, F. H. Schweingruber, I. C. Harris, P. D. Jones, S. G. Shiyatov, and E. A. Vaganov (2001), Low-frequency temperature variations from a northern tree ring density network, *Journal of Geophysical Research*, *106*.

Brock, B., A. Rivera, G. Casassa, F. Bown, and C. Acuña (2007), The surface energy balance model of an active ice-covered volcano: Villarrica Volcano, southern Chile, *Annals of Glaciology*, *45*, 104–114.

Brohan, P., J. Kennedy, I. Harris, S. Tett, and P. Jones (2006), Uncertainty estimates in regional and global observed temperature changes: a new dataset from 1850, *Journal of Geophysical Research*, *111*(D12106), doi: 10.1029/2005JD006548.

Bromwich, D. H., and R. L. Fogt (2004), Strong trends in the skill of the ERA-40 and NCEP-NCAR reanalyses in the high and midlatitudes of the Southern Hemisphere, 1958-2001, *Journal of Climate*, *17*, 4603–4619.

Brugger, K. A. (2007), The non-synchronous response of Rabots Glaciär and Storglaciären, northern Sweden, to recent climate change: a comparative study, *Annals of Glaciology*, *46*, 275–282.

Brugger, K. A., K. A. Refsnider, and M. F. Whitehill (2005), Variation in glacier length and ice volume of Rabots Glaciär, Sweden, in response to climate change, 1910-2003, *Annals of Glaciology*, *42*, 180–188.

Burrows, C. J. (2005), *Julius Haast in the Southern Alps*, Canterbury University Press.

Cabanes, C., A. Cazenave, and C. L. Provost (2001), Sea level rise during past 40 years determined from satellite and in situ observations, *Science*, *294*(5543), 840–842, doi:10.1126/science.1063556.

Carrasco, J. F., R. Osorio, and G. Casassa (2008), Secular trend of the equilibrium-line altitude on the western side of the southern Andes, derived from radiosonde and surface observations, *Journal of Glaciology*, *54*(186), 538.

Chinn, T. J. (1996), New Zealand glacier responses to climate change of the past century, *New Zealand Journal of Science*, *39*, 415–428.

Christensen, J. H., et al. (2007), Regional climate projections, in *Climate Change 2007: The Physical Science Basis. Contribution of Working Group I to the fourth Assessment Report of the Intergovernmental Panel on Climate Change*, edited by S. Solomon, D. Qin, M. Manning, Z. Chen, M. Marquis, K. B. Averyt, M. Tignor, and H. L. Miller, Camebridge University Press, Camebridge, United Kingdom and New York, NY, USA.

Chueca, J., A. Julián, and I. López (2003), Variations of Glaciar Coronas, Pyrenees, Spain, during the 20th century, *Journal of Glaciology*, *49*(166), 449–455.

Church, J. A., and N. J. White (2006), A 20th century acceleration in global sea-level rise, *Geophysical Research Letters*, *33*(L01602), doi:10.1029/2005GL024826.

Church, J. A., and N. J. White (2011), Sea-level rise from the late 19th to the early 21st century, *Surveys in Geophysics*, pp. 1–18, doi:10.1007/s10712-011-9119-1.

Church, J. A., et al. (2001), Changes in sea level, in *Climate Change 2001: The Physical Science Basis. Contribution of Working Group I to the third Assessment Report of the Intergovernmental Panel on Climate Change*, edited by J. T. Houghton, D. J. Griggs, M. Noguer, P. J. van der Linden, X. Dai, K. Maskell, and C. A. Johnson, Camebridge University Press, Camebridge, United Kingdom and New York, NY, USA.

Church, J. A., N. J. White, L. F. Konikow, C. M. Moningues, J. G. Cogley, E. Rignot, J. M. Gregory, A. J. M. Michiel R. van den Broeke, and I. Velicogna (2011), Revisiting the Earth's sea-level and energy budgets from 1961 to 2008, *Geophysical Research Letters*, *38*(L18601), doi:10.1029/2011GL048794.

Citterio, M., F. Paul, A. P. Ahlstrøm, H. F. Jepsen, and A. Weidick (2009), Remote sensing of glacier change in West Greenland: accounting for the occurence of surg-type glaciers, *Annals of Glaciology*, *50*(53), 70.

Cobos, D. R. (1998), Glacier fluctuations in the upper Atuel river basin, Mendoza, Argentina, *Nivoglaciologa - Glaciology and Snow Studies*.

Cogley, J. G. (2003), Gghydro – global hydrographic data, release 2.3, Trent Technical Note. Revised January 2007, Department of Geography, Trent University, Peterborough, Ontario, Canada.

Cogley, J. G. (2004), Greenland accumulation: An error model, *Journal of Geophysical Research*, *109*(D18101), doi:10.1029/2003JD004449.

Cogley, J. G. (2009a), Geodetic and direct mass-balance measurements: comparison and joint analysis, *Annals of Glaciology*, *50*(50), 96–100.

Cogley, J. G. (2009b), A more complete version of the World Glacier Inventory, *Annals of Glaciology*, *50*(53), 32–38.

Cogley, J. G., and W. P. Adams (1998), Mass balance of glaciers other than the ice sheets, *Journal of Glaciology*, *44*(147), 315–325.

Condom, T., A. Coudrain, J. E. Sicart, and S. Théry (2007), Computation of the space and time evolution of equilibrium-line altitudes on Andean glaciers (10°N-55°S), *Global and Planetary Change*, *59*, 189–202.

Cook, E. R., and L. A. Kairiukstis (Eds.) (1990), *Methods of dendrochronology, applications in the environmental sciences*, Kluwer Academic Publishers, Dordrecht, The Netherlands.

Cook, K. H., X. Yang, C. M. Carter, and B. N. Belcher (2003), A modeling system for studying climate controls on mountains glaciers with application to the Patagonian Icefields, *Climatic Change*, *56*, 339–367.

Crossen, K. J. (1992), *Guide to the Little Ice Age Landforms and Glacial Dynamics in Portage Valley and Portage Pass*, Alaska Geological Society, International Conference on Arctic Margins (1992: Anchorage, Alaska).

D' Arrigo, R., R. Wilson, and G. Jacoby (2006), On the long-term context for late twentieth century warming, *Journal of Geophysical Research*, *111*(D03103), doi:10.1029/2005JD006352.

De Smedt, B., and F. Pattyn (2003), Numerical modelling of historical front variations and dynamic response of Sofiyskiy glacier, Altai mountains, Russia, *Annals of Glaciology*, *37*, 143–149.

Delcourt, C., F. Pattyn, and M. Nolan (2008), Modelling historical and recent mass loss of McCall Glacier, Alaska, USA, *The Cryosphere*, *2*, 23–31, doi:10.5194/tc-2-23-2008.

Dickmann, N. (2008), GIS-basiertes Gletscherinventar des Gran Campo Nevado, Patagonien, im internationalen Projekt GLIMS, Master's thesis, Department of Geography, RWTH Aachen University.

Dyurgerov, M., and M. F. Meier (2005), Glaciers and the changing earth system: a 2004 snapshot, *Occasional Paper No. 58, INSTAAR, University of Colorado*.

Dyurgerov, M. B., and M. F. Meier (2000), Twentieth century climate change: evidence from small glaciers, *PNAS*, *97*(4), 1406–1411.

Elsberg, D. H., W. D. Harrison, K. A. Echelmeyer, and R. M. Krimmel (2001), Quantifying the effects of climate and surface change on glacier mass balance, *Journal of Glaciology*, *47*(159), 649–658.

Enfield, D. B., A. M. Mestas-Nuez, and P. J. Trimble (2001), The Atlantic Mulitdecadal Oscillation and its relation to rainfall and river flows in the continental U.S., *Geophysical Research Letters*, *28*(10), 2070–2080, doi: 10.1029/2000GL012745.

Esper, J., E. R. Cook, and F. H. Schweingruber (2002), Low-frequency signals in long tree-ring chronologies for reconstructing past temperature variability, *Science*, *295*, 2250–2253.

Espizúa, L. E., and P. Pitte (2009), The Little Ice Age glacier advance in the Central Andes (35°S), Argentina, *Palaeogeography, Palaeoclimatology, Palaeoecology*, *281*, 345–350.

Ettema, J., M. R. van den Broeke, E. van Meijgaard, W. J. van de Berg, J. L. Bamber, J. E. Box, and R. C. Bales (2009), Higher surface mass balance of the Greenland ice sheet revealed by high-resolution climate modeling, *Geophysical Research Letters*, *36*(L12501), doi:10.1029/2009GL038110.

Evison, L. H., P. E. Calkin, and J. M. Ellis (1996), Late-holocene glaciation and twentieth-century retreat, northeastern Brooks Range, Alaska, *The Holocene*, *6*(1), 17–24.

Fettweis, X., E. Hanna, H. Gallée, P. Huybrechts, and M. Erpicum (2008), Estimation of the greenland ice sheet surface mass balance for the 20th and 21th centuries, *The Cryosphere*, *2*, 117–129, doi:10.5194/tc-2-117-2008.

Fischer, A. (2010), Glaciers and climate change: Interpretation of 50 years of direct mass balance of hintereisferner, *Global and Planetary Change*, *71*, 13–26, doi:10.1016/j.gloplacha.2009.11.014.

Fisher, D. A. (2002), High-resolution multiproxy climatic records from ice cores, tree-rings, corals and documentary sources using eigenvector techniques and maps: assessment of recovered signal and errors, *The Holocene*, *12*, 401–419, doi:10.1191/0959683602hl546rp.

Fonk, F. (1886), *Diario del Fray Fransisco Menéndez a la Cordillera*, Colección Biblioteca National, Valparaiso, Chile.

Galakhov, V., and Mukhamedov (1999), Glaciers of Altay, Novosibirsk (in Russian).

Gallopin, G. C. (1978), Estudio ecológico integrado de la cuenca del Río Manso Superior, (Río Negro, Argentina). part i. descripción general de la cuenca, in *Anales de Parques Nacionales*, vol. XIV, pp. 161–230, Servicio Nacional de Parques Nacionales, Buenos Aires, Argentina.

Giesen, R. H. (2009), The ice cap Hardangerjøkulen in the past, present and future climate, Ph.D. thesis, IMAU, Utrecht University.

Giesen, R. H., and J. Oerlemans (2010), Response of the ice cap Hardangerjøkulen in southern Norway to the 20th and 21st century climates, *The Cryosphere*, *4*, 191–213, doi:10.5194/tc-4-191-2010.

Giesen, R. H., and J. Oerlemans (2011), A simple surface mass balance model, *in preparation*.

Giesen, R. H., M. R. van den Broeke, J. Oerlemans, and L. M. Andreassen (2008), Surface energy balance in the ablation zone of Midtdalsbreen, a glacier in southern Norway: Interannual variability and the effect of clouds, *Journal of Geophysical Research*, *113*(D2 1111 doi: 10.1029/2008JD10390).

Glazovsky, A., Y. Macheret, F. Navarro, and E. Vasilenko (), Aldegondabreen, Svalbard, website.

Gordon, J. E., V. M. Haynes, and A. Hubbard (2008), Recent glacier changes and climate trends on South Georgia, *Global and Planetary Change*, *60*(1-2), 73–84, doi:10.1016/j.gloplacha.2006.07.037.

Granshaw, F. D., and A. G. Fountain (), Gateway to the glaciers of Mount Rainier, website.

Gregory, J. M., and J. Oerlemans (1998), Simulated future sea-level rise due to glacier melt based on regionally and seasonally resolved temperature changes, *Nature*, *391*, 474–476.

Greuell, W. (1992), Hintereisferner, Austria: mass-balance reconstruction and numerical modelling of the historical length variations, *Journal of Glaciology*, *38*, 233–244.

Greuell, W., and C. J. J. P. Smeets (2001), Variations with the elevation in the surface energy balance on the Pasterze (Austria), *Journal of Geophysical Research*, *106*(D23), 31,717–727.

Gribbon, P. W. F. (1970), Frontal recession of Sermikavask, West Greenland, *Journal of Glaciology*, *9*(56).

Grinsted, A., J. C. Moore, and S. Jevrejeva (2009), Reconstructing sea level from paleo and projected temperatures 200 to 2100 ad, *Climate Dynamics*, *34*(4), 461–472, doi:10.1007/s00382-008-0507-2.

Hagen, J. O., O. Liestøl, E. Roland, and T. Jørgensen (1993), *Glacier atlas of Svalbard and Jan Mayen*, Nor. Polarinst. Medd.

Hall, D. K., K. J. Bayr, W. Schöner, R. A. Bindschadler, and J. Y. L. Chien (2003), Consideration of the errors inherent in mapping historical glacier positions in Austria from ground and space (1893-2001), *Remote Sensing of the Environment*, *86*, 566–577, doi:10.1016/S0034-4257(03)00134-2.

Hansen, J., and S. Lebedeff (1987), Global trends of measured surface air temperature, *Journal of Geophysical Research*, *92*(D11), 13,345–13,372.

Harrison, S., V. Winchester, and N. Glasser (2007), The timing and nature of recession of outlet glaciers of Hielo Patagonico Norte, Chile, from their Neoglacial IV (Little Ice Age) maximum positions, *Global and Planetary Change*, *59*, 67–78, doi:10.1016/j.gloplacha.2006.11.020.

Harrison, W. D., L. H. Cox, R. Hock, R. S. March, and E. C. Pettit (2009), Implications for the dynamic health of a glacier from comparison of conventional and reference-surface balances, *Annals of Glaciology*, *50*(50), 25–30.

Hastenrath, S. (1983), *The Glaciers of Equatorial East Africa*, D. Reidel Publishing Company, P.O.Box 17 3300 AA Dordrecht.

Hegerl, G. C., T. J. Crowley, W. T. Hyde, and D. J. Frame (2006), Climate sensitivity constrained by temperature reconstructions over the past seven centuries, *Nature*, *440*, 1029–1032, doi:10.1038/nature04679.

Heliker, C. C., A. Johnson, and S. M. Hodge (1984), The Nisqually glacier, Mount Rainier, Washington, 1857-1979: A summary of the long-term observations and a comprehensive bibliography, *U.S geological survey*, *open-file report 83-541*.

Hesterberg, T., D. S. Moore, S. Monaghan, A. Clipson, and R. Epstein (2005), Bootstrap methods and permutation tests, in *Introduction to the practice of statistics*, edited by D. S. Moor and G. P. McCabe, W.H. Freeman, New York.

Hock, R. (2003), Temperature index melt modelling in mountain areas, *Journal of Hydrology*, *282*, 104–115.

Hock, R. (2005), Glacier melt: a review of processes and their modelling, *Progress in Physical Geography*, *29*(3), 362–391.

Hock, R., and B. Holmgren (2005), A distributed surface energy-balance model for complex topography and its application to Storglaciären, Sweden, *Journal of Glaciology*, *51*(172), 25–36.

Hock, R., M. de Woul, V. Radic, and M. Dyurgerov (2009), Mountain glaciers and ice caps around Antarctica make large sea-level rise contribution, *Geophysical Research Letters*, *36*, doi:10.1029/2008GL037020.

Hofer, M., T. Mölg, B. Marzeion, and G. Kaser (2010), Empirical-statistical downscaling of reanalysis data to high-resolution air temperature and specific humidity above a glacier surface (Cordillera Blance, Peru), *Journal of Geophysical Research*, *115*(D12120), doi:10.1029/2009JD012556.

Hogg, I. G. G., J. G. Paren, and R. J. Timmis (1982), Summer heat and ice balances on Hodges Glacier, South Georgia, Falkland Islands Dependencies, *Journal of Glaciology*, *28*(99), 221–237.

Huang, S. (2004), Merging information from different resources for new insights into climate change in the past and future, *Geophysical Research Letters*, *31*(L13205), doi:10.1029/2004GL019781.

Huang, S., H. N. Pollack, and P.-Y. Shen (2000), Temperature trends over the past five centuries reconstructed from borehole temperatures temperature trends over the past five centuries reconstructed from borehole temperatures, *Nature*, *403*(6771), 756–758.

Huitzing, W.-D. (2011), Closure of the global sea level rise budget for the 20^{th} century, Master's thesis, Utrecht University.

Huss, M., A. Bauder, M. Funk, and R. Hock (2008), Determination of the seasonal mass balance of four alpine glaciers since 1865, *Journal of Geophysical Research*, *113*(F01015,oi:10.1029/2007JF000803).

Huss, M., R. Hock, A. Bauder, and M. Funk (2010a), 100-year mass changes in the Swiss Alps linked to the Atlantic Multidecadal Oscillation, *Geophysical Research Letters*, *37*(L10501), doi:10.1029/2010GL042616.

Huss, M., R. Hock, A. Bauder, and M. Funk (2010b), Reply to the comment of leclercq et al. on "100-year mass changes in the Swiss Alps linked to the Atlantic Multidecadal Oscillation, *The Cryosphere Discussions*, *4*, 2587–2592, doi:10.5194/tcd-4-2587-2592.

Huybrechts, P., P. D. Nooze, and H. Decleir (1989), Numerical modelling of Glacier d' Argentière and its historic front variations, in *Glacier fluctuations and climate change*, edited by J. Oerlemans, Glaciology and quaternary geology, Kluwer Academic Publishers, P.O. box 17, 3300 AA Dordrecht, The Netherlands.

Huybrechts, P., J. Gregory, I. Janssens, and M. Wild (2004), Modelling Antarctic and Greenland volume changes during the 20th and 21st centuries forced by GCM time slice integrations, *Global and Planetary Change*, *42*(1-4), 83 – 105, doi:10.1016/j.gloplacha.2003.11.011.

Hynek, B., W. Schöner, G. Weys, J. Abermann, and M. Olefs (2009), Mass balance 07/08 freya glacier, NE-Greenland, poster (at IGS conference Newcastle).

Intute (2009), Retreat of the Gangotri glacier, Indian Himalayas, website.

Iqbal, M. (1983), *An Introduction to Solar Radiation*, Academic Press.

Jansen, E., et al. (2007), Palaeoclimate, in *Climate Change 2007: The Physical Science Basis. Contribution of Working Group I to the fourth Assessment Report of the Intergovernmental Panel on Climate Change*, edited by S. Solomon, D. Qin, M. Manning, Z. Chen, M. Marquis, K. B. Averyt, M. Tignor, and H. L. Miller, Camebridge

University Press, Camebridge, United Kingdom and New York, NY, USA.

Jevrejeva, S., A. Grinsted, J. C. Moore, and S. Holgate (2006), Nonlinear trend and multiyear cycles in sea level records, *Journal of Geophysical Research*, *111*(C09012).

Jevrejeva, S., J. Moore, A. Grinsted, and P. Woodworth (2008), Recent global sea level started over 200 years ago?, *Geophysical Research Letters*, *35*(L08715), doi:10.1029/2008GL033611.

Jóhannesson, T., C. Raymond, and E. Waddington (1989), Time-scale for adjustment of glaciers to changes in mass balance, *Journal of Glaciology*, *35*(121), 355 – 369.

Johannesson, T., H. Bjornsson, and G. Grothendieck (2009), Package 'stinepack', Icelandic Meteorological Office.

Jones, P., and A. Moberg (2003), Hemispheric and large-scale surface air temperature variations: an extensive revision and an update to 2001, *Journal of Climate*, *16*, 206–223.

Jones, P., et al. (2009), High-resolution palaeoclimatology of the last millennium: a review of current satus and future prospects, *The Holocene*, *19*(1), 3–49.

Jones, P. D., K. R. Briffa, T. P. Barnett, and S. F. B. Tett (1998), High-resolution palaeoclimatology of the last millennium: interpretation, integration and comparison with General Circulation Model control-run temperatures, *The Holocene*, *8*(4), 455–471.

Jouvet, G., M. Picasso, J. Rappaz, and H. Blatter (2008), A new algorithm to simulate the dynamics of a glacier: theory and applications, *Journal of Glaciology*, *54*(188), 801–811.

Juckes, M., M. Allen, K. Briffa, J. Esper, G. Hegerl, A. Moberg, T. Osborn, and S. L. Weber (2007), Millenial temperature reconstruction intercomparison and evaluation, *Climate of the Past*, *3*, 591–609.

Kamb, B., C. F. Raymond, W. D. Harrison, H. Engelhardt, K. A. Echelmeyer, N. Humphrey, M. M. Brugman, and T. Pfeffer (1985), Glacier surge mechanism: 1982-1983 surge of variegated glacier, alaska, *Science*, *227*(4686), pp. 469–479.

Kaser, G., and H. Osmaston (2002), *Tropical glaciers*, Camebridge University Press.

Kaser, G., J. G. Cogley, M. B. Dyugerov, M. F. Meier, and A. Ohmura (2006), Mass balance of glaciers and ice caps: Consensus estimates for 1961-2004, *Geophysical Research Letters*, *33*(L19501), doi:10.1029/2006GL027511.

Kienholz, C. (2010), Shrinkage of selected South-Central Alaskan glaciers. a spatio-temporal analysis applying photogrammetric, GIS-based and historical methods, Master's thesis, University of Bern.

Klok, E. J., and J. Oerlemans (2004), Climate reconstructions derived from global glacier length records, *Arctic, Antarctic and Alpine Research*, *36*(4), 575–583.

Koch, J., and R. Kilian (2005), 'Little Ice Age' glacier fluctuations, Gran Campo Nevado, southernmost Chile, *The Holocene*, *15*, 20–28.

Koch, J., B. Menounos, and J. G. Clague (2009), Glacier change in Garibaldi Provincial Park, southern Coast Mountains, British Columbia, since the Little Ice Age, *Global and Planetary Change*, *66*(3-4), 161–178, doi: 10.1016/j.gloplacha.2008.11.006.

Konikow, L. F. (2011), Contribution of global groundwater depletion since 1900 to seaâĂŘlevel rise, *Geophysical Research Letters*, *38*(L17401), doi:10.1029/2011GL048604.

Koutnik, M. (2009), University of Washington research on Blue Glacier, website.

Krajewski, W. F., G. J. Ciach, J. R. McCollum, and C. Bacotiu (2000), Initial validation of the Global Precipitation Climatology Project montly rainfall over the United States, *Journal of Applied Meteorology*, *39*, 1071–1086.

Krishna, A. P. (2005), Snow and glacier cover assessment in the high mountains of Sikkim Himalaya, *Hydrological Processes*, *19*, 2375–2383, doi:10.1002/hyp.5890.

Kuipers Munneke, P. (2005), Past and future of Nordenskioldbreen, Master's thesis, RUG.

Kuipers Munneke, P., C. H. Reijmer, M. R. van den Broeke, P. Stammes, G. König-Langlo, and W. H. Knap (2008), Analysis of clear-sky Antarctic snow albedo using observations and radiative transfer modeling, *J. Geophys. Res. (D)*, *113*, D17,118, doi:10.1029/2007JD009653.

Kumar, V., P. Singh, and V. Singh (2007), Snow and glacier melt contribution in the Beas River at Pandoh Dam, Himachal Pradesh India, *Hydrological Sciences Journal*, *52*(2), 376–388, doi:10.1623/hysj.52.2.376.

Kutuzov, S., and M. Shahgedanova (2009), Glacier retreat and climatic variability in the eastern Terskey-Alatoo, inner Tien Shan between the middle of the 19th century and beginning of the 21st century, *Global and Planetary Change*, *69*, 59–70, doi:10.1016/j.gloplacha.2008.11.006.

Lang, H., and K. Lieb (1993), *Die Gletscher Kärntens*, Verlag des Naturwissenschaftlichen Vereins Kärnten.

Lara, A., R. Villalba, and R. Urrutia (2008), A 400-year tree-ring record of the Puelo River summer–fall streamflow in the Valdivian Rainforest eco-region, Chile, *Climatic Change*, *86*, 331–356, doi:10.1007/s10584-007-9287-7.

Laumann, T., and A. Nesje (2009), The impact of climate change on future frontal variations of Brikdalsbreen, western Norway, *Journal of Glaciology*, *55*(193).

Laverov, N. P. (Ed.) (2004), *Modern methods of geological-geophysical monitoring over natural processes on the territory of Kabardino-Balkaria*, KBGU, Nalchik.

Lavrentiev, I. (2008), Structure and regime of Nordenskiold glaciers (Svalbard) from remote sensing data, Ph.D. thesis, Moscow State University.

Le Bris, R., F. Paul, H. Frey, and T. Bolch (2011), A new satellite derived glacier inventory for Western Alaska, *Annals of Glaciology*, *52*(59).

Le Quesne, C., C. Acuña, J. A. Boninsegna, A. Rivera, and J. Barichivich (2009), Long-term glacier variations in the Central Andes of Argentina and Chile, inferred from historical records and tree-ring reconstructed precipitation, *Palaeogeography, Palaeoclimatology, Palaeoecology*, *281*, 334–344.

Leclercq, P. W., and J. Oerlemans (2011), Global and hemispheric temperature reconstruction from glacier length fluctuations, *Climate Dynamics*, doi:10.1007/s00382-011-1145-7.

Leclercq, P. W., J. Oerlemans, and J. G. Cogley (2011), Estimating the glacier contribution to sea-level rise for the period 1800–2005, *Surveys in Geophysics*, *32*(4-5), 519–535, doi:10.1007/s10712-011-9121-7.

Leiva, J. C., L. E. Espizúa, R. J. Iturraspe, M. Masiokas, F. A. Norte, and R. Villalba (2008), The response of the Argentinian glaciers to the climate of the XX and XXI centuries, in *Terra glacialis, special issue; Mountain glaciers and climate changes in the last century*, edited by L. Bonardi, pp. 179–192, Servizio Glaciologico Lombardo.

Lemke, P., et al. (2007), Observations: Changes in snow, ice, and frozen ground, in *Climate Change 2007: Physical Science Basis. Contribution of Working Group I to the Forth Assessment Report of the Intergovernmental Panel on Climate Change*, edited by S. Solomon, M. Manning, Z. Chen, M. Marquis, K. B. Averyt, M. Tignor, and H. L. Miller, Cambridge University Press, Cambridge, United Kingdom and New York, NY, USA.

Ligtenberg, S. R. M., M. M. Helsen, and M. R. van den Broeke (2011), An improved semi-empirical model for the densification of antarctic firn, *The Cryosphere Discussions*, *5*(4), 1921–1948, doi:10.5194/tcd-5-1921-2011.

Liu, S., D. Shangguan, Y. Ding, H. Han, C. Xie, Y. Zhang, J. Li, J. Wang, and G. Li (2006), Glacier changes during the past century in the Gangrigabu mountains, southeast Qinghai-Xizang (Tibetan) Plateau, China, *Annals of Glaciology*, *43*, 187–193.

López, P., P. Chevallier, V. Favier, B. Pouyaud, F. Ordenes, and J. Oerlemans (2010), A regional view of fluctuations of glacier length in southern South America, *Global and Planetary Change*, *71*, 85–108, doi: 10.1016/j.gloplacha.2009.12.009.

Lough, J. M. (2004), A strategy to improve the contribution of coral data to high-resolution paleoclimatology, *Palaeogeography, Palaeoclimatology, Palaeoecology*, *204*(1-2), 115 – 143, doi:10.1016/S0031-0182(03)00727-2.

Luckman, B. H. (1988), Dating the moraines and the recession of Athabasca and Dome glaciers, Alberta, Canada, *Arctic and Alpine Research*, *20*, 40–54.

Luckman, B. H. (2000), The little ice age in the canadian rockies, *Geomorphology*, *32*(3-4), 357 – 384, doi:DOI: 10.1016/S0169-555X(99)00104-X.

Lui, Q., S. Liu, Y. Zhang, X. Wang, Y. Zhang, W. Guo, and J. Xu (2010), Recent shrinkage and hydrological response of Hailuogou glacier, a monsoon temperate glacier on the east slope of Mont Gongga, China, *Journal of Glaciology*, *56*(196), 215.

Luterbacher, J., D. Dietrich, E. Xoplaki, M. Grosjean, and H. Wanner (2004), European seasonal and annual temperature variability, trends, and extremes since 1500, *Science*, *303*, 1499–1503.

Luterbacher, J., M. A. Liniger, A. Menzel, N. Estrella, P. M. Della-Marta, C. Pfister, T. Rutishauser, and E. Xoplaki (2007), Exceptional European warmth of autumn 2006 and winter 2007: Historical context, underlying dynamics, and its phenological impacts, *Geophysical Research Letters*, *34*(L12704), doi:10.1029/2007GL029951.

Lüthi, M. P., A. Bauder, and M. Funk (2010), Volume change reconstruction of Swiss glaciers from length change data, *Journal of Geophysical Research*, *115*(F0402), doi:10.1029/2010JF001695.

Machgut, H., F. Paul, M. Hoelzle, and W. Haeberli (2006), Distributed glacier mass balance modelling as an important component of modern multi-level glacier monitoring, *Annals of Glaciology*, *43*, 335–343.

Mackintosh, A. N. (2000), Glacier fluctuations and climatic change in Iceland, Ph.D. thesis, University of Edinburgh.

Mackintosh, A. N., A. J. Dugmore, and A. L. Hubbard (2002), Holocene climatic changes in Iceland: evidence from modelling glacier length fluctuations at Sólheimajökull, *Quarternary International*, *91*, 39–52.

Mann, M. E., and R. S. Bradley (1999), Northern hemisphere temperature during the past millenium: Inferences, uncertainties, and limitations, *Geophysical Research Letters*, *26*(6), 759–762.

Mann, M. E., and P. Jones (2003), Global surface temperatures over the past millenium, *Geophysical Research Letters*, *30*(15), doi:10.1029/2003GL017814.

Mann, M. E., Z. Zhang, M. K. Hughes, R. S. Bradley, S. K. Miller, S. Rutherford, and F. Ni (2008), Proxy-based reconstructions of hemispheric and global surface temperature variations over the past two millennia, *PNAS*, *105*(36), 13,252 – 13,257.

Masiokas, M., B. Luckman, R. Villalba, S. Delgado, P. Skvarca, and A. Ripalta (2009a), Little Ice Age fluctuations of small glaciers in Monte Fitz Roy and Lago del Desierto areas, south Patagonian Andes, Argentina, *Palaeogeography, Palaeoclimatology, Palaeoecology*, *281*, 351–362, doi:10.1016/j.palaeo.2007.10.031.

Masiokas, M. H., A. Rivera, L. E. Espizúa, R. Villalba, S. Delgado, and J. C. Aravena (2009b), Glacier fluctuations in extratropical South America during the past 1000 years, *Palaeogeography, Palaeoclimatology, Palaeoecology*, *281*(3-4), 242–268, doi:10.1016/j.palaeo.2009.08.006.

Masiokas, M. H., B. H. Luckman, R. Villalba, A. Ripalta, and J. Rabassa (2010), Little Ice Age fluctuations of Glaciar Río Manso in the north Patagonian Andes of Argentina, *Quaternary Research*, *73*, 96–106, doi: 10.1016/j.yqres.2009.08.004.

Matthews, J. A. (1979), The vegetation of the Storbreen gletschervorfeld, Jotunheimen, Norway, I. Introduction and approaches involving classification, *Journal of Biogeography*, *6*(1), 17–47.

McKinzey, K. M., W. Lawson, D. Keller, and A. Hubbard (2004), A revised Little Ice Age chronology of the Franz Josef Glacier, Westland, New Zealand, *Journal of the Royal Society of New Zealand*, *34*(4), 381–394.

Meier, M. F. (1984), Contribution of small glaciers to global sea level, *Science*, *226*(4681), 1418–1421.

Meier, M. F., M. B. Dyurgerov, U. K. Rick, S. O'Neel, W. T. Pfeffer, R. S. Anderson, S. P. Anderson, and A. F. Glazovsky (2007), Glaciers dominate eustatic sea-level rise in the 21st century, *Science*, *317*, 1064–1067, doi: 10.1126/science.1143906.

Mernild, S. H., N. T. Knudsen, W. H. Lipscomb, J. C. Yde, J. K. Malmros, B. Hasholt, and B. H. Jakobsen (2011), Increasing mass loss from greenland's mittivakkat gletscher, *The Cryosphere*, *5*, 341–348, doi:10.5194/tc-5-341-2011.

Millett, M. T. (1964), Observations of glacier termini in the Prince William Sound Area, Alaska, Ph.D. thesis, Department of Geography, McGill University, Montreal.

Moberg, A., D. M. Sonechkin, K. Holmgren, N. M. Datsenko, and W. Karlén (2005), Highly variable Northern Hemisphere temperatures reconstructed from low- and high-resolution proxy data, *Nature*, *433*.

Møller, J. T. (1959), Glaciers in Upernivik Ø, *Geografisk Tidsskrift*, *58*.

Mosley-Thompson, E., L. G. Thompson, and P.-N. Lin (2006), A multi-century ice-core perspective on 20th-century climate change with new contribution from high-Arctic and Greenland (PARCA) cores, *Annals of Glaciology*, *43*, 42.

Naithani, A. K., H. C. Nainwal, K. K. Sati, and C. Prasad (2001), Geomorphological evidences of retreat of the Gangotri glacier and its characteristics, *Current Science*, *80*(1), 87–93.

National Snow and Ice Data Center (1999, update 2009), *World Glacier Inventory*, World Glacier Monitoring Service and National Snow and Ice Data Center/World Data Center for Glaciology, Boulder, CO, USA.

Nemec, J., P. Huybrechts, O. Rybak, and J. Oerlemans (2009), Reconstruction of the annual balance of Vadret da Morteratsch, Switzerland, since 1865, *Annals of Glaciology*, *50*(50), 126.

Nerem, R. S., D. P. Chambers, C. Choe, and G. T. Mitchum (2010), Estimating mean sea level change from the TOPEX and Jason altimeter missions, *Marine Geodesy*, *33*(1), 435–446, doi:10.1080/0190419.2010.491031.

Nesje, A., S. O. Dahl, T. Thun, and Ø. Nordli (2008), The 'Little Ice Age' glacial expansion in western Scandinavia: summer temperature or winter precipitation?, *Climate Dynamics*, *30*, 789–801, doi:10.1007/s00382-007-0324-z.

Neukom, R., et al. (2010), Multi-centennial summer and winter precipitation variability in southern South America, *Geophysical Research Letters*, *37*(L14708), doi:10.1029/2010GL043680.

Neukom, R., et al. (2011), Multiproxy summer and winter surface air temperature field reconstructions for southern South America covering the past centuries, *Climate Dynamics*, *37*, 35–51, doi:10.1007/s00382-010-0793-3.

Nicholls, R. J., and A. Cazenave (2010), Sea-level rise and its impact on coastal zones, *Science*, *328*, 1517, doi: 10.1126/science.1185782.

Nick, F. M. (2006), Modelling the behaviour of tidewater glaciers, Ph.D. thesis, IMAU.

Nicolussi, K., and G. Patzelt (2000), Untersuchungen zur holozänen Gletscherentwicklung von Pasterze und Gepatschferner (Ostalpen), *Zeitschrift für Gletscherkunde und Glazialgeologie*, *36*(1-2).

Nussbaumer, S. U. (2010), Continental-scale glacier variations in Europe (Alps, Scandinavia) and their connection to climate over the last centuries, Ph.D. thesis, University of Bern.

Nussbaumer, S. U., and H. J. Zumbühl (2011), The LIA history of the Glacier des Bossons (Mont Blanc area, France): a new high-resolution glacier length curve based on historical documents, *Climatic Change*, doi: 10.1007/s10584-011-0130-9.

Nussbaumer, S. U., H. J. Zumbühl, and D. Steiner (2007), Fluctuations of the "Mer de Glace" (Mont Blanc area, France) AD 1500-2050: an interdisciplinary approach using new historical data and neural network simulations, *Zeitschrift für Gletscherkunde und Glazialgeologie*, *40*, 1–183.

Nussbaumer, S. U., A. Nesje, and H. J. Zumbühl (2011), Historical glacier fluctuations of Jostedalsbreen and Folgefonna (southern Norway) reassessed by new pictorial and written evidence, *The Holocene*, *21*, 455–471, doi: 10.1177/095968361.

Oerlemans, J. (1991), The mass balance of the Greenland ice sheet: sensitivity to climate change as revealed by energy-balance modelling, *The Holocene*, *1*(1), 40–48.

Oerlemans, J. (1997a), A flow-line model for Nigardsbreen: projection of future glacier length based on dynamic calibration with the historic record, *Annals of Glaciology*, *24*(382-289).

Oerlemans, J. (1997b), Climate sensitivity of Franz Josef Glacier, New Zealand, as revealed by numerical modelling, *Arctic and Alpine Research*, *29*, 233–239.

Oerlemans, J. (2001), *Glaciers and Climate Change*, AA Balkema Publishers.

Oerlemans, J. (2005), Extracting a climate signal from 169 glacier records, *Science*, *308*, 675–677.

Oerlemans, J. (2007), Estimating response times of Vadret da Morteratsch, Vadret da Palü, Brikdalsbreen from their length records, *Journal of Glaciology*, *53*(182).

Oerlemans, J. (2008), *Minimal Glaciers Models*, Igitur, Utrecht Publishing & Archiving Services, Universiteitsbibliotheek Utrecht.

Oerlemans, J. (2010), *The microclimate of valley glaciers*, Igitur, Utrecht Publishing & Archiving Services, Universiteitsbibliotheek Utrecht.

Oerlemans, J., and J. P. F. Fortuin (1992), Sensitivity of glaciers and small ice caps to greenhouse warming, *Science*, *258*(5079), 115–117.

Oerlemans, J., and W. H. Knap (1998), A 1 year record of global radiation and albedo in the ablation zone of Morteratschgletscher, Switserland, *Journal of Glaciology*, *44*, 231–238.

Oerlemans, J., and B. K. Reichert (2000), Relating glacier mass balance to meteorological data using a Seasonal Sensitivity Characteristic (SSC), *Journal of Glaciology*, *46*(152), 1–6.

Oerlemans, J., H. Björnsson, M. Kuhn, F. Obleitner, F. Palsson, C. J. J. P. Smeets, H. F. Vugts, and J. de Wolde (1999), Glacio-meteorological investigations on Vatnajökull, Iceland, summer 1996: an overview, *Boundary-Layer Meteorology*, *92*(1), 3–26.

Oerlemans, J., M. Dyurgerov, and R. S. W. van de Wal (2007), Reconstructing the glacier contribution to sea-level rise back to 1850, *The Cryosphere*, *1*(1), 59–65.

Oerlemans, J., R. H. Giesen, and M. R. van den Broeke (2009), Retreating alpine glaciers: increased melt rates due to accumulation of dust (Vadret da Morteratsch, Swizerland), *Journal of Glaciology*, *55*(192), 729.

Osipova, G. B., T. Y. Khromova, and D. G. Tsvetkov (2005), Problems of the investigation of fluctuations of mountain glaciers using remote sensing data (in russian), in *Data of glaciological studies*, vol. 98, edited by V. M. Kotlyakov, pp. 129–134, Russian Academy of Science, Institute of Geography, Moscow.

Østrem, G., N. Haakensen, and O. Melander (1977), Glaciological investigations at Nigardsbreen, Norway, *Norsk Geografisk Tidsskrift*, *30*, 187–209.

Østrem, G., K. D. Selvig, and K. Tandberg (1988), *Atlas over breer i Sør-Norge (Atlas of glaciers in South Norway)*, vol. 61, Norges vassdragsog energiverk, Vassdagsdirektoretet.

Overpeck, J., et al. (1997), Arctic environmental change of the last four centuries, *Science*, *278*, 1251–1256.

Panov, V. D. (1993), *Evolution of present-day glacierization of the Caucasus (in Russian)*, Gidrometeoizdat, St. Petersburg.

Panov, V. D., and E. S. Borovik (1976), *Catalogue of Glaciers of the USSR*, vol. 8, Gidrometeoizdat, Leningrad.

Panov, V. D., and T. V. Pisareva (1973), *Catalogue of Glaciers of the USSR*, vol. 8, Gidrometeoizdat, Leningrad.

Panov, V. D., and T. V. Pisareva (1976), *Catalogue of Glaciers of the USSR*, vol. 8, Gidrometeoizdat, Leningrad.

Paterson, W. S. B. (1994), *The physics of glaciers*, 3rd ed., Pergamon press, Oxford.

Paul, F. (2007), The new Swiss glacier inventory 2000 - application of remote sensing and GIS, Ph.D. thesis, Department of Geography, University of Zürich.

Paul, F. (2010), The influence of changes in glacier extent and surface elevation on modeled mass balance, *The Cryosphere*, *4*, 569–581, doi:10.5194/tc-4-569-2010.

Paul, F., A. Kääb, M. Maisch, T. Kellenberger, and W. Haeberli (2004), Rapid disintegration of Alpine glaciers observed with satellite data, *Geophysical Research Letters*, *31*(L21402), doi:10.1029/2004GL020816.

Paul, F., H. Escher-Vetter, and H. Machgut (2009), Comparison of mass balances for Vernagtferner obtained from direct measurements and distributed modeling, *Annals of Glaciology*, *50*, 169–177.

Pelto, M. S., and C. R. Warren (1991), Relationship between tidewater glacier calving velocity and water depth at the calvinf front, *Annals of Glaciology*, *15*, 115–118.

Petrov, N. V., and A. S. Shetinnikov (1977), *Catalogue of Glaciers of the USSR*, vol. 14, Gidrometeoizdat, Leningrad.

Pfister, C., et al. (1999), Documentary evidence on climate in the sixteenth-century Europe, *Climatic Change*, *43*, 55–110.

Pollack, H. N., and J. E. Smerdon (2004), Borehole climate reconstructions: Spatial structure and hemispheric averages, *Journal of Geophysical Research*, *109*(D11106), doi:10.1029/2003JD004163.

Rabatel, A., V. Jomelli, P. Naveau, B. Francou, and D. Grancher (2005), Dating of Little Ice Age glacier fluctuations in the tropical Andes: Charquini glaciers, Bolivia, 16°S, *C. R. Geoscience*, *337*, 1311–1322.

Rabatel, A., A. Machaca, B. Francou, and V. Jomelli (2006), Glacier recession on Cerro Charquini (16°S), Bolivia, since te maximum of the Little Ice Age (17th century), *Journal of Glaciology*, *52*(176), 110.

Rabatel, A., B. Francou, V. Jomelli, P. Naveau, and D. Grancher (2008), A chronology of the Little Ice Age in the tropical Andes of Bolivia (16°s) and its implications for climate reconstruction, *Quaternary Research*, *70*, 198–212.

Rabus, B. T., and K. A. Echelmeyer (1998), The mass balance of McCall Glacier, Brooks Range, Alaska, U.S.A.; its regional relevance and implications for climate change in the Arctic, *Journal of Glaciology*, *44*(147), 333–351.

Rachlewicz, G., W. Szczucinski, and M. Ewertowski (2007), Post-"Little Ice Age" retreat rates of glaciers around Billefjorden in central Spitsbergen, Svalbard, *Polish Polar Research*, *28*(3), 159–186.

Radić, V., and R. Hock (2010), Regional and global volumes of glaciers derived from statistical upscaling of glacier inventory data, *Journal of Geophysical Research*, *115*(F01010), doi:10.1029/2009JF001373.

Radic, V., and R. Hock (2011), Regionally differentiated contribution of mountain glaciers and ice caps to future sea-level rise, *Nature Geoscience*, *4*(2), 91–94, doi:10.1038/ngeo1052.

Rahmstorf, S. (2007), A semi-empirical approach to projecting future sea-level rise, *Science*, *315*, 368, doi:10.1126/science.1135456.

Rai, S. C., and J. T. K (2005), An overview of glaciers, glacier retreat, and subsequent impact in Nepal, India and China, WWF Nepal Program.

Raina, V. K., and D. Srivastava (2008), *Glacier Atlas of India*, Geological Society of India.

Raj, K. B. G. (2011), Recession and reconstruction of Milam Glacier, Kumaon Himalaya, observed with satellite imagery, *Current Science*, *100*(9), 1420–1425.

Réné, P. (2003), Reconstittution des variations frontales de trois glaciers pyrénéens depuis la fin du Petit Age Glaciaire (1850), programme ECLIPSE, Laboratoire du CNRS - Université du Mirail.

Rignot, E., I. Velicogna, M. R. van den Broeke, A. Monaghan, and J. T. M. Lenaerts (2011), Acceleration of the contribution of the Greenland and Antarctic ice sheets to sea level rise, *Geophysical Research Letters*, *38*(L05503), doi:10.1029/2011GL046583.

Rivera, A., and G. Casassa (2004), Ice elevation, areal, and frontal changes of glaciers from National Park Torres del Paine, Southern Patagonia Icefield, *Arctic, Antarctic and Alpine Research*, *36*(4), 379–389.

Rivera, A., C. Acuña, G. Casassa, and F. Bown (2002), Use of remotely sensed and field data to estimate the contribution of Chilean glaciers to eustatic sea-level rise, *Annals of Glaciology*, *34*, 367–372.

Rivera, A., F. Bown, G. Casassa, C. Acuña, and J. Clavero (2005), Glacier shrinkage and negative mass balance in the Chilean Lake District (40°S), *Hydrological Sciences Journal*, *50*(6).

Rosenblüth, B., H. A. Fuenzaliba, and P. Aceituno (1997), Recent temperature variations in southern South America, *International Journal of Climatology*, *17*, 67–85.

Rutherford, S., M. E. Mann, T. J. Osborn, K. R. Briffa, P. Jones, R. S. Bradley, and M. K. Hughes (2005), Proxy-based northern hemisphere surface temperature reconstructions: Sensitivity to method, predictor network, target season, and target domain, *Journal of Climate*, *18*(13), 2308–2329, doi:10.1175/JC13351.1.

Rye, C. J., N. S. Arnold, I. C. Willis, and J. Kohler (2010), Modeling the surface mass balance of high Arctic glacier using the ERA-40 reanalysis, *Journal of Geophysical Research*, *115*(F02014), doi:10.1029/2009JF001364.

Salinger, M. J., M. J. Heine, and C. J. Burrows (1983), Variations of the Stocking (Te Wae Wae) Glacier, Mount Cook, and climatic relationships, *New Zealand Journal of Science*, *26*, 321–338.

Sarikaya, M. A., M. Zreda, and A. Ciner (2009), Glaciations and paleoclimate of Mount Erciyes, central Turkey, sinc the Last Glacial Maximum, inferred from ^{36}cl cosmogenic dating and glacier modeling, *Quaternary Science Reviews*, *28*, 2326–2341, doi:10.1016/j.quascirev.2009.04.015.

Sawaguchi, S., K. Yamagata, Y. D. Muravyev, and O. N. Solomina (1999), Holocene glacier advances in Koryto Glacier, Kamchatka, Russia, in *Cryospheric studies in Kamchatka II*, edited by R. Naruse, T. Hara, T. Shiraiwa, T. Sone, and T. Sawagaki, pp. 79–84, The Institute of Low Temperature Science, Hokkaido University.

Schmeits, M., and J. Oerlemans (1997), Simulation of the historical variations in length of the Unterer Grindelwald-gletscher, *Journal of Glaciology*, *43*, 152–164.

Schmidt, S., and M. Nüsser (2009), Fluctuations of Raikot Glacier during the last 70 years: a case study from the Nanga Parbat Massif, Northern Pakistan, *Journal of Glaciology*, *55*(194), 949–959.

Schneider, C., M. Glaser, R. Kilian, A. Santana, N. Butorovic, and G. Casassa (2003), Weather observations across the Southern Andes at 53°S, *Physical Geography*, *24*(2), 97–119.

Schneider, C., M. Schnirch, C. Acuña, G. Casassa, and R. Kilian (2007), Glacier inventory of the Gran Campo Nevado Ice Cap in the Southern Andes and glacier changes observed during recent decades, *Global and Planetary Change*, *59*, 87–100.

Sigurðsson, O. (1998), Glacier variations in Iceland 1930-1995, *Jökull*, *45*, 3–26.

Simmons, A., S. Uppala, D. Dee, and S. Kobayashi (2006), ERA-Interim: new ECMWF reanalysis products from 1989 onwards, *ECMWF Newsletter*, *110*, 25–35.

Slangen, A. B. A., and R. S. W. van de Wal (2011), An assessment of uncertainties in using volume-area modelling for computing the twenty-first century glacier contribution to sea-level change, *The Cryosphere*, *5*(3), 673–686, doi:10.5194/tc-5-673-2011.

Smith, I. N., and W. F. Budd (1980), The derivation of past climate changes from observed changes of glaciers, in *Sea level, ice and climatic change*, edited by I. Allison, 131, pp. 31–52, IAHS.

Smith, T. M., P. A. Arkin, and M. R. P. Sapiano (2009), Reconstruction of near-global annual precipitation using correlations with sea surface temperature and sea level pressure, *Journal of Geophysical Research*, *114*(D12107).

Solomina, O. N., M. Ivanov, and T. Bradwell (2010), Lichenometric studies on maraines in the polar Urals, *Geografiska Annaler*, *92A*(1), 81–99.

Steiner, D., A. Pauling, S. N. Nussbaumer, A. Nesje, J. Luterbacher, H. Wanner, and H. J. Zumbühl (2008), Sensitivity of European glaciers to precipitation and temperature - two case studies, *Climate Change*, *90*, 413–441, doi:10.1007/s10584-008-9393-1.

Stineman, R. W. (1980), A consistently well-behaved method of interpolation, *Creative Computing*, pp. 54–57.

Stroeven, A., R. Van de Wal, and J. Oerlemans (1989), Historic front variations of the Rhone Glacier: simulation with an ice flow model, in *Glacier fluctuations and climate change*, edited by J. Oerlemans, Glaciology and

quaternary geology, Kluwer Academic Publishers, P.O. box 17, 3300 AA Dordrecht, The Netherlands.

Swiss glacier monitoring network (1881-2009), *Glaciological reports: The Swiss Glaciers, 1880-2004/05. Yearbooks of the Cryospheric Commission of the Swiss Academy of Sciences (SCNAT)*, vol. 1-126, Labratory of Hydraulics, Hydrology and Glaciology (VAW), ETH Zürich.

Taylor, R. G., L. Mileham, C. Tindimugaya, A. Majugu, A. Muwanga, and B. Nakileza (2006), Recent glacial recession in the Rwenzori Mountains of East Africa due to rising air temperature, *Geophysical Review Letters*, *33*(L10402 doi:10.1029/2006GL025962).

Thompson, L. G., E. Mosley-Thompson, M. E. Davis, P. N. Lin, K. Henderson, and T. A. Mashiotta (2003), Tropical glacier and ice core evidence of climate change on annual to millennial time scales, *Climatic Change*, *59*, 137–155, doi:10.1029/2004JD004933.

Thorarinsson, S. (1943), Vatnajökull, scientific results of the Swedish-Icelandic investigations 1936-37-38, *Geografiska Annaler*, *25*, 1–54.

Trenberth, K. E., et al. (2007), *Climate change 2007: The physical science basis. Contribution of working groups I to the fourth assessment report of the Intergovernmental Panel on Climate Change*, chap. 3, Cambridge University Press, Cambridge, UK and New York, NY, USA.

Van de Wal, R. S. W., and M. Wild (2001), Modelling the response of glaciers to climate change by applying volume-area scaling in combination with high resolution GCM, *Climate Dynamics*, *18*, 359–366.

van der Veen, C. J. (1996), Tidewater calving, *Journal of Glaciology*, *42*(141), 375–385.

Vera, C., G. Silvestri, B. Liebmann, and P. González (2006), Climate change scenarios for seasonal precipitation in South America from IPCC-AR4 models, *Geophysical Research Letters*, *33*(L13707), doi:10.1029/2006GL025759.

Vermeer, M., and S. Rahmstorf (2009), Global sea level linked to global temperature, *PNAS*, *106*(51), 21,527–21,532, doi:10.1073/pnas.0907765106.

Vieli, A., and F. M. Nick (2011), Understanding and modelling rapid dynamic changes of tidewater outlet glaciers: issues and implications, *Surveys in Geophysics*, doi:10.1007/s10712-011-9132-4.

Villalba, R., J. C. Leiva, S. Rubulls, J. Suarez, and L. Lenzano (1990), Climate, tree-ring and glacial fluctuations in the Rio Frias Valley, Rio Negro, Argentina, *Arctic and Alpine Research*, *22*(3), 215–232.

Villalba, R., J. A. Boninsegna, T. T. Veblen, A. Schmelter, and S. Rubulis (1997), Recent trends in tree-ring records from high elevation sites in the andes of northern Patagonia, *Climatic Change*, *36*, 425–454.

Villalba, R., E. R. Cook, G. C. Jacoby, R. D. D'Arrigo, T. T. Veblen, and P. D. Jones (1998), Tree-ring based reconstructions of northern Patagonia precipitation since AD 1600, *The Holocene*, *8*(6), 659–674, doi:10.1191/095968398669095576.

Villalba, R., et al. (2003), Large-scale temperature changes across the southern Andes: 20th-century variations in the context of the past 400 years, *Climatic Change*, *59*, 177–232.

Vincent, C. (2002), Influence of climate change over the 20th Century on four French glacier mass balances, *Journal of Geophysical Research*, *107*(D19, 4375), doi:10.1029/2001JD000832.

Vincent, C., E. Le Meur, D. Six, and M. Funk (2005), Solving the paradox of the end of the Little Ice Age in the Alps, *Geophysical Research Letters*, *32*(L09706), doi:10.1029/2005GL022552.

Vivian, R. (1975), *Les glaciers des Alpes occidentales*, Allier, Grenoble.

Wada, Y., L. P. H. van Beek, C. M. van Kempen, J. W. T. M. Reckman, S. Vasak, and M. F. P. Bierkens (2010), Global depletion of groundwater resources, *Geophysical Research Letters*, *37*(L20402), doi:10.1029/2010GL044571.

Wallinga, J., and R. S. W. van de Wal (1998), Sensitivity of Rhone Glacier, Switzerland, to climate change: experiments with a one-dimensional flowline model, *Journal of Glaciology*, *44*(147), 383–393.

Warrick, R. A., and J. Oerlemans (1990), Sea level rise, in *Climate Change - IPCC Scientific Assessment*, pp. 257–281, Cambridge University Press.

Weeks, L. S. (2011), Tracking ice marginal changes in south central Alaska using remote sensing and glacial geology, Master's thesis, The College of Wooster.

Weertman, J. (1961), Stability of ice-age ice-sheets, *Journal of Geophysical Research*, *66*, 3783–3792.

Weidick, A. (1968), Observations on some Holocene glacier fluctuations in West Greenland, *Meddelelser om Grønland*, *165*(6).

Weidick, A. (1988), Gletschere i Sydgrønland, *Grønlands Geologiske Undersøgelse (Geologi I Grønland 2)*.

Weidick, A., C. E. Bøggild, and N. T. Knudsen (1992), *Glacier inventory and atlas of West Greenland*, vol. 158, Grønland Geologiske Undersøgelse.

WGMS (2008), *Global Glacier Changes: facts and figures*, World Glacier Monitoring Service, Zurich, Switzerland.

WGMS (2008 and earlier volumes), *Fluctuations of Glaciers*, vol. I-IX, ICSU (FAGS) / IUGG (IACS) / UNEP / UNESCO / WMO, World Glacier Monitoring Service, Zurich, Switzerland.

Wiles, G. C., and P. E. Calkin (1994), Late Holocene, high-resolution glacial chronologies and climate, Kenai Mountains, Alaska, *Geological Society of America Bulletin*, *106*, 281–303, doi:10.1130/0016-7606(1994)106<0281:LHHRGC>2.3.CO;2.

Wiles, G. C., D. J. Barclay, and P. E. Calkin (1999), Tree-ring-dated 'Little Ice Age' histories of maritime glaciers from western Prince William Sound, Alaska, *The Holocene*, *9*(2), 163–173.

Williams Jr., R. S., and J. G. Ferrigno (Eds.) (1989), *Satellite Image Atlas of Glaciers of the World, Irian Jaya, Indonesia and New Zealand*, vol. 1386-H, U.S. Geological Survey.

Williams Jr., R. S., and J. G. Ferrigno (Eds.) (1991), *Satellite Image Atlas of Glaciers of the World, Middle East and Africa*, vol. 1386-G, U.S. Geological Survey.

Williams Jr., R. S., and J. G. Ferrigno (Eds.) (1993), *Satellite Image Atlas of Glaciers of the World, Europe*, vol. 1386-E, U.S. Geological Survey.

Williams Jr., R. S., and J. G. Ferrigno (Eds.) (2002), *Satellite Image Atlas of Glaciers of the World, North America*, vol. 1386-J, U.S. Geological Survey.

Wiscombe, W. J., and S. G. Warren (1980), A model for the spectral albedo of snow. I: Pure snow, *J. Atmos. Sci.*, *37*, 2712–2733.

Xoplaki, E., J. Luterbacher, H. Paeth, D. Dietrich, N. Steiner, M. Grosjean, and H. Wanner (2005), European spring and autumn temperature variability and change of extremes over the last haf millennium, *Geophysical Research Letters*, *32*(L15713), doi:10.1029/2005GL023424.

Yde, J. C., and N. T. Knudsen (2005), Glaciological features in the initial quiescent phase of Kuannersuit glacier, Greenland, *Geografiska Annaler*, *87A*(3), 473–485.

Yde, J. C., and N. T. Knudsen (2007), 20th-century glacier fluctuations on Disko Island (Qeqertarsuaq), Greenland, *Annals of Glaciology*, *46*, 209–214.

Yuanqing, H., Y. Yongyuan, D. D. Z. Hang, Y. Tandong, Y. Meixue, Z. Zhonglin, P. Hongxi, G. Juan, and L. Aigang (), Recent progress of the studies on environmental information in the glacial system, Mt. Yulong, China, manuscript.

Yuanqing, H., Z. Zhonglin, W. H. Theakstone, C. Tuo, Y. Tandong, D. D. Zhang, and P. Hongxi (2003), Recent variability of the climate and glaciers in China's monsoon region, in *Water Resources Systems - Water availability and Global Change*, IAHS, IAHS Press, Wallingford.

Zemp, M., W. Haeberli, M. Hoelzle, and F. Paul (2006), Alpine glaciers to disappear within decades?, *Geophysical Research Letters*, *33*(L13504), doi:10.1029/2006GL026319.

Zemp, M., H. J. Zumbühl, S. U. Nussbaumer, M. H. Masiokas, L. E. Espizua, and P. Pitte (2011), Extending glacier monitoring into the Little Ice Age and beyond.

Zolotarev, E. A. (2009), *Evolution of glaciation of Elbrus*, Nauchnii mir, Moscow.

Zumbühl, H. J. (1980), *Die Schwankungen der Grindelwaldgletscher in den historischen Bild- und Schriftquellen des 12. bis 19. Jahrhunderts*, Birkhäuser, Basel.

Zumbühl, H. J., and H. Holzhauser (1988), *Alpengletscher in der Kleinen Eiszeit*, *Die Alpen*, vol. 3, Schweizerischen Alpen Club.

Zuo, Z., and J. Oerlemans (1997a), Contribution of glacier melt to sea-level rise since AD 1865: a regionally differentiated calculation, *Climate Dynamics*, *13*, 835–845.

Zuo, Z., and J. Oerlemans (1997b), Numerical modelling of the historic front variation and the future behavior of the Pasterze glacier, Austria, *Annals of Glaciology*, *24*, 234–241.

Samenvatting

Ongeveer tien procent van het totale landoppervlak op aarde is bedekt met landijs. Het overgrote deel van dit ijs bevindt zich in de polaire gebieden, met name in de twee poolkappen op Groenland en Antarctica. Gletsjers, het landijs buiten deze poolkappen, vertegenwoordigen een relatief klein deel van het landijs op aarde, maar ze zijn wijdverspreid. Op elk continent en op nagenoeg alle breedtegraden zijn gletsjers te vinden. In de afgelopen eeuw hebben gletsjers zich wereldwijd teruggetrokken. De mondiale opwarming van het klimaat ligt hieraan ten oorzaak. Een belangrijk gevolg is stijging van de zeespiegel.

Om verandering van het huidige klimaat in een breder perspectief te plaatsen is het nuttig de klimaatvariaties uit het verleden te bestuderen. Directe metingen van de klimaatvariabelen gaan zelden verder terug dan het midden van de negentiende eeuw. Voor de kennis van het klimaat voor die tijd zijn we aangewezen op de informatie die is vastgelegd in natuurlijke archieven, zoals boomringen, koralen, sedimentlagen, ijskernen en gletsjers. Gletsjers zijn zeer bruikbaar voor klimaatreconstructies. Gletsjers reageren namelijk dynamisch op veranderingen in het klimaat en klimaatschommelingen vertalen zich in duidelijk waarneembare fluctuaties in de grootte van gletsjers. Daarnaast is de informatie van gletsjers een aanvulling op de vroege instrumentele reeksen, aangezien veel gletsjers zich op grotere hoogte en in afgelegen gebieden bevinden waar instrumentele metingen schaars zijn. Ten slotte geven de gletsjerfluctuaties door natuurkundige modellen direct kwantitatieve informatie over de klimaatvariaties, zonder dat calibratie op instrumentele temperatuurreeksen nodig is.

De meeste historische informatie over gletsjerfluctuaties betreft variaties in gletsjerlengte. Sinds het eind van de 19de eeuw worden lengteveranderingen van gletsjers gemeten, soms zelfs op jaarlijkse basis. De World Glacier Monitoring Service (WGMS) verzamelt en publiceert deze informatie. Van een groot aantal gletsjers zijn de lengtefluctuaties in de periode voor de eerste metingen gereconstrueerd op basis van historische bronnen en geologische bronmateriaal, zoals schilderijen, expeditieverslagen, foto's, en gedateerde morenen. In tegenstelling tot de directe metingen zijn de reconstructies niet in één archief opgeslagen. Een deel van het onderzoek bestond derhalve uit het verzamelen van de beschikbare informatie.

In hoofdstuk 2 beschrijf ik de coherente dataset van wereldwijde gletsjerlengte veranderingen die is samengesteld uit een grote verscheidenheid aan wetenschappelijke artikelen, rapporten, websites en correspondentie (Appendix A geeft een overzicht van alle gletsjers en de gebruikte bronnen). De dataset bevat de lengtereeksen van 374 gletsjers. Alleen reeksen die voor 1950 beginnen en tenminste 40 jaar lang zijn, zijn in de dataset opgenomen. Het aantal beschikbare reeksen is tijdsafhankelijk. In de tweede helft van de 19de eeuw neemt het

aantal reeksen sterk toe. Na 1962 neemt het weer af. In een enkel geval is dat omdat gletsjers verdwenen, maar meestal zijn metingen niet gecontinueerd of niet gerapporteerd. Het gemiddelde startjaar is 1865 en het gemiddelde eindjaar is 2001, met een spreiding tussen respectievelijk 1534 tot 1945 en 1962 tot 2010. De dataset heeft wereldwijde dekking, met lengtereeksen van elk continent behalve Antarctica. De informatie over historische gletsjerlengteveranderingen in het arctisch gebied is echter beperkt, afgezet tegen de grote ijsbedekking van dit gebied. Behalve de lengtefluctuaties is de acquisitiemethode per datapunt, en basale informatie over de gletsjergeometrie en het lokale klimaat (in de vorm van jaarlijkse neerslag) in de dataset opgenomen.

Hoofdstuk 3 beschrijft de reconstructie van klimaatfluctuaties in Noord Patagonia met een modelstudie van Glaciar Frías. De lengtefluctuaties van Glaciar Frías zijn bekend van 1639 tot en met 2009. Het is de meest gedetailleerde lange reeks van zuidelijk Zuid Amerika. De respons van Glaciar Frías op klimaatvariaties is gemodelleerd door middel van een één-dimensionaal stroomlijnmodel, aangedreven met een gesimplificeerd oppervlakte-massabalansmodel. De oppervlakte-massabalans is de koppeling tussen klimaat- en gletsjerfluctuaties. Het gesimplificeerde massabalansmodel gebruikt slechts twee termen om de uitwisseling van energie tussen atmosfeer en gletsjeroppervlak te beschrijven: één voor de zonnestraling en één voor alle temperatuurafhankelijke fluxen. Het ijsstroommodel simuleert de geometrische aanpassing van de gletsjer op veranderingen in de oppervlakte-massabalans. De combinatie van beide modellen geeft zo de lengteverandering als gevolg van een klimaatverandering.

Gebruikmakend van het gletsjermodel is nu te bepalen welke verandering van temperatuur of neerslag de waargenomen lengteveranderingen het best reproduceert. De 2,6 km terugtrekking van Glaciar Frías tussen 1639 en 2009 kan het best worden verklaard met een toename van de jaargemiddelde temperatuur met 1.16 °C sinds het midden van de 17de eeuw, of een afname van de jaarlijkse neerslag met 34%, t.o.v. het gemiddelde over de periode 1980–2010. Daarnaast is het gletsjermodel aangedreven met de resultaten van twee onafhankelijke hogeresolutie klimaatreconstructies voor Noord Patagonia. Kwalitatief lijken de reconstructies de variaties op de middellange termijn goed te reproduceren. De timing van het gemodelleerde groeien en krimpen van de gletsjer komt overeen met de lengtereeks. De klimaatreconstructies hebben een tamelijk grote onzekerheid, wat resulteert in een grote bandbreedte in de gemodelleerde gletsjerlengten. De meeste observaties vallen in de gemodelleerde bandbreedte, alleen in het midden van de 17de is de gemodelleerde gletsjer te groot en in het begin van de 19de juist te klein. Verder blijkt uit de klimaatreconstructies dat de variaties in neerslag nauwelijks van invloed zijn geweest op de fluctuaties van Glaciar Frías. Tot slot hebben we het model aangedreven met het IPCC A1B scenario voor het klimaat van de 21ste eeuw in Noord Patagonië. In dit scenario verliest Glaciar Frías 80% van zijn volume in de komende eeuw.

Het is vanuit praktisch oogpunt onhaalbaar om voor elke gletsjer in de dataset een klimatologische interpretatie van de lengtefluctuatie te maken met een gekoppeld massabalans-

ijsstroommodel zoals hierboven beschreven. De benodigde gletsjergeometrie en meteorologische gegevens zijn voor de meeste gletsjers niet voorhanden. Dus is een versimpelde aanpak vereist om alle wereldwijd geobserveerde gletsjerlengtefluctuaties te gebruiken voor de reconstructie van mondiale klimaatfluctuaties. De gekozen methode wordt beschreven in hoofdstuk 4. We nemen aan dat de lengtefluctuaties klein zijn ten opzichte van de totale gletsjerlengte. De respons van gletsjers op klimaatverandering kan dan beschreven worden met een lineaire differentiaalvergelijking. Verder nemen we aan dat het wereldwijde gletsjersignaal voornamelijk afhankelijk is van de mondiale temperatuurfluctuaties. In dat geval koppelt de responsvergelijking temperatuurvariatie aan gletsjerlengteverandering met behulp van twee gletsjerspecifieke parameters: de responstijd en de klimaatgevoeligheid. Deze parameters worden voor elk van de gletsjers berekend met behulp van een simpel gletsjermodel, met een sterk vereenvoudigde gletsjergeometrie, dat is gecalibreerd op de resultaten van 15 numerieke gletsjermodellen.

Met behulp van de berekende responstijden en klimaatgevoeligheden is voor elke gletsjerlengtereeks een historische temperatuurreeks te reconstrueren. Uit het gewogen gemiddelde van deze reeksen is de mondiale temperatuurvariatie bepaald, die de mondiale gletsjerfluctuaties van 1600 tot 2000 het best verklaart. Uit deze reconstructie blijkt dat de mondiale temperatuur tussen 1600 en 1830 min of meer constant was. Sinds 1830 stijgt de gemiddelde mondiale temperatuur, met slechts een korte onderbreking in de periode tussen 1940 en 1970 waarin de temperatuur iets afnam. De berekende mondiale temperatuurstijging tussen 1830 en 2000 is $0{,}94 \pm 0{,}31$ °C. Bovendien zijn de laatste twee decennia de warmste uit de reconstructie, met tevens de snelste temperatuurtoename.

De berekende temperatuurveranderingen komen goed overeen met de temperatuurmetingen van de 20ste eeuw. Dat bewijst dat de gletsjerfluctuaties een betrouwbare bron voor temperatuurreconstructies zijn. De temperatuurreconstructie komt ook goed overeen met andere, onafhankelijke, temperatuurreconstructies. Maar in de reconstructie gebaseerd op gletsjers begint de huidige opwarming eerder. Naast het mondiale temperatuursignaal is ook het noordelijk en het zuidelijk halfrond gemiddelde bepaald. Deze laten een vergelijkbaar beeld zien. Halverwege de 19$^{\text{de}}$ eeuw begint een opwarming die zich voortzet tot in de 20$^{\text{ste}}$ eeuw. De tijdelijke afkoeling in het midden van de 20$^{\text{ste}}$ eeuw is minder uitgesproken op het zuidelijk halfrond dan op het noordelijk halfrond. In de periode 1850–2000 steeg op het noordelijk halfrond de gemiddelde temperatuur met $0{,}82 \pm 0{,}27$ °C en op het zuidelijk halfrond met $1{,}27 \pm 0{,}76$ °C.

Door het wereldwijde krimpen van gletsjers, vormen gletsjers een belangrijke bijdrage aan de verandering van de zeespiegel over de afgelopen eeuw. De zeespiegel is sinds het midden van de 19$^{\text{de}}$ eeuw met ongeveer 20 cm gestegen. Het is de verwachting dat hij in de komende eeuw verder zal stijgen. Voor een betrouwbare voorspelling van de toekomstige zeespiegelstijging is het van belang de veranderingen in de zeespiegel van de afgelopen eeuwen te begrijpen. Hiervoor moeten de verschillende processen die bijdragen aan zeespiegelverandering worden doorgrond en moet het budget uiteindelijk te sluiten zijn: de som van de bijdragen moet

uitkomen op de gemeten zeespiegel. In hoofdstuk 5 worden de mogelijkheden verkend om aan de hand van de waargenomen lengteveranderingen de bijdrage van gletsjers aan de zeespiegelstijging te berekenen. Directe metingen van volumeveranderingen (massabalans) van gletsjers gaan, enkele uitzonderingen daargelaten, niet verder terug dan 1945. Pas vanaf 1950 zijn er genoeg metingen om een representatief beeld te krijgen van de wereldwijde volumeafname van gletjsers. De lengtereeksen gaan verder terug in de tijd, en bieden de mogelijkheid de waargenomen gletsjerbijdrage over een grotere tijdspanne uit te breiden.

Met behulp van regionaal gemiddelde lengteverandering wordt een genormaliseerde mondiale gletsjerlengtereeks berekend. Dit mondiaal gemiddelde is een compromis tussen representativiteit van de mondiale reeks ten opzichte van de spreiding van het gletsjerijs over de wereld enerzijds, en anderzijds spreiding van het gewicht over de reeksen om te voorkomen dat het signaal gedomineerd wordt door slechts enkele lengtereeksen. Vervolgens reken ik de genormaliseerde lengtesignaal om in verandering van genormaliseerd gletsjervolume door middel van schaling. De aldus verkregen genormaliseerde volumeverandering van gletsjers kan door calibratie aan de reeks van gemeten massabalans van gletsjers omgezet worden in daadwerkelijke volumeverandering en dus zeespiegelbijdrage. De berekende totale gletsjerbijdrage aan zeespiegelstijging is 8,4 $\pm$ 2,1 cm tussen 1800 en 2005, en 9,1 $\pm$ 2,3 cm tussen 1850 en 2005.

Verrassend genoeg is deze schatting nauwelijks afhankelijk van de parameters die in de schaling van lengte naar volume gebruikt worden. Daarnaast is de berekende gletsjerbijdrage in de 20ste eeuw niet gevoelig voor de gemaakte keuzen in het middelen naar een mondiaal signaal. Voor 1900 lopen de resultaten van verschillende wegingen uiteen. Klaarblijkelijk is de genormaliseerde gletsjerlengte wereldwijd coherent vanaf het moment dat een groot aantal reeksen beschikbaar is per regio. De resultaten zijn wel sterk afhankelijk van de gekozen calibratieset. Gebruikmakend van een oudere dataset valt de zeespiegelbijdrage 2 cm lager uit.

In Hoofdstuk 6 worden de waargenomen gletsjerlengtefluctuaties gebruikt om de invloed van de verandering van de gletsjergeometrie op de gemeten massabalans te schatten. Na een verandering in het klimaat, met een bijbehorende verandering in de oppervlakte-massabalans, past de geometrie van de gletsjer zich aan in de richting van een evenwicht met een oppervlaktemassabalans van nul. Bij een klimatologische interpretatie van een massabalansserie moet de verandering in gletsjergeometrie in acht worden genomen. Dit hoofdstuk richt zich op de vraag hoe groot de invloed van dit effect is geweest in de massabalansseries van 30 gletsjers in Zwitserland, als reactie op een eerder gepubliceerd onderzoek. Op basis van de lengteverandering is de conclusie dat de verandering van de gletsjergeometrie niet veronachtzaamd mag worden in de klimatologische interpretatie van de massabalansanomaliën tussen 1908 en 2008.

Curriculum vitae

Paul Willem Leclercq

17-07-1979	geboren te Tilburg
1991–1997	VWO Odulphus Lyceum Tilburg
1997–2006	natuurkunde, Universiteit Utrecht afstudeerrichting *Grondslagen en geschiedenis van de natuurkunde* scriptie *De adiabatische hypothese, ontwikkeling en toepassing in de kwantumtheorie* begeleider prof. dr. F. van Lunteren
2007–2012	promotieonderzoek *Klimaatreconstructie uit gletsjerlengtereeksen*, IMAU, Universiteit Utrecht promotor prof. dr. J. Oerlemans
2011– huidig	postdoc IMAU, Universiteit Utrecht, onderzoek naar Himalaya gletsjers

Publications

P.W. Leclercq, J. Oerlemans, J.G. Cogley: Estimating the glacier contribution to sea-level rise over the period 1800–2005, *Surveys in Geophysics* **32** (4-5), pp. 519-535, 2011, doi: 10.1007/s10712-011-9121-7.

P.W. Leclercq, J. Oerlemans: Global and hemispheric temperature reconstructions from glacier length fluctuations, *Climate Dynamics*, doi: 10.1007/s00382-011-1145-7.

P.W. Leclercq, P. Pitte, R.H. Giesen, M.H. Masiokas, J. Oerlemans: Climatic interpretation of the length fluctuations of Glaciar Frías, North Patagonia, Argentina, *Climate of the Past Discussions* **7** (5), pp. 3653–3697, 2011, doi:10.5194/cpd-7-3653-2011.

P.W. Leclercq, R.S.W van de Wal, J. Oerlemans: Comment on "100-year mass changes in the Swiss Alps linked to the Atlantic Multidecadal Oscillation" by Matthias Huss et al. (2010), *The Cryosphere Discussions* **4**, pp. 2475-2481, 2010, doi: 10.5194/tcd-4-2475-2010.

Acknowledgements
Dankwoord

The thesis is based on observed and reconstructed glacier length fluctuations. I am greatly indebted to all colleagues and volunteers who have contributed with dedication and commitment to the data on glacier length fluctuations I have compiled in the data set. In particular I would like to thank H. Blatter, K. Brugger, I. Bushueva, C. Burrows, T. Chinn, M. Citterio, L. Espizua, H. Elvehøy, I. Gärtner–Roer, T. Kerr, S. Kutuzov, P. Lopez, A. Mackintosh, M. Masiokas, S. Nussbaumer, G. Osipova, D. Petrakov, P. Pitte, A. Rabatel, S. Schmidt, C. Schneider, O. Sigurðsson, O. Solomina, J. Yde, L. Weeks, A. Weidick, G. Wiles, M. Zemp and H.J. Zumbühl, who helped in collecting the available data and made their own data on glacier length changes available. I am grateful to J. Luterbacher, M. Mann, R. Neukom, S. Rutherford, and R. Villalba for providing the data and of their climate reconstructions. I also thank Malou for being my dedicated employee for categorizing the length data.

Hans, bedankt dat je deze afgestudeerd wetenschapshistoricus hebt aangenomen voor een promotietraject in de glaciologie. Het is een eer om door jou begeleid te worden. Behalve dat ik goed op de hoogte bleef van de sneeuwomstandigheden in het Engadin, heb ik er van opgestoken dat de simpele aanpak die de essentie van het dynamische systeem recht doet zeer vruchtbaar is. Ik heb je begeleidingsstijl met veel vrijheid en vertrouwen zeer prettig gevonden. Ik heb het de afgelopen vier jaar erg naar mijn zin gehad, en ben dan ook blij dat onze samenwerking verder gaat.

None of the research articles on which this thesis is based was the work of me alone. The work is also the result of the contributions of my co-authors. Graham, thanks for your contributions to the sea-level paper. I look forward to meeting you in person! I have had a long correspondence with Pierre and Mariano, after the kick-off of the Frías project in Valdivia, Chile. I am glad you are happy with the results so far, I am happily awaiting news on the so badly needed mass balance project at Frías. Rianne, het is altijd een genoegen om de mogelijkheden en moeilijkheden van gletsjermodellen met je te bediscussiëren. Dank voor je hulp. Tot slot bedank ik Roderik voor zijn inbreng bij het paper dat heeft geresulteerd in hoofdstuk 6 van dit proefschrift, en ook voor het delen van zijn expertise op het gebied van zeespiegelstijging.

Dear Olga, Irina, Natasha, Misha, Sacha, and Vladimir, thank you very much for your warm welcome in Moscow, helping me to find my way in the Russian archives with data on glacier fluctuations and showing me around in the city. I enjoyed my stay very much, despite the

lack of snow. Also from a scientific point of view it was very fruitful, thanks to your help! Спасибо большое

I thank Anker Weidick for his invitation to come to Copenhagen and visit him at GEUS. The knowledge of Greenland stored in his memory is impressive. I also thank Adam Herrington for directing me to the work of Anker Weidick, and Dirk van As for his efforts in the role of ambassador of Copenhagen.

Frank, thanks for letting me work in Zürich. Tobias, Holger, Philippe, and Yvonne, thanks for being my personal GIS and ENVI help desk, taking me out for playing football and kubb, and showing me Sächsilüüte and the local vibrating nightlife. Michael and Samuel, I appreciated your thoughts and expertise on the historical glacier length fluctuations, and thanks for showing me the best place in and around Zürich for a barbecue.

Thanks to Veijo, Jim, and Marianne for taking me on the trip to "amusement park Nordenskiöld". It was a great experience.

Tot slot wil ik graag mijn collega's op het IMAU bedanken, in het bijzonder de HOEMBA-club, Marcel en mijn kamergenoten Irene, Peter en Stefan. Wetenschap komt regelmatig neer op eenzaam ploeteren. Gelukkig is er op het IMAU iemand die ervoor zorgt dat je computer het doet en zijn er altijd mensen om frustraties en succesjes mee te delen, computercode van te gebruiken, te rennen, fietsen, badmintonnen, klaverjassen en borrelen.